DOCTOR OF PHILOSOPHY

Electrical conductance and gating of porin channels in lipid bilayers

Jones, Cheryl Mary

Award date:
1994

Awarding institution:
University of Wales, Bangor

ELECTRICAL CONDUCTANCE AND GATING OF PORIN CHANNELS IN LIPID BILAYERS

Thesis submitted in candidature for the degree of
Doctor of Philosophy

September 1994

Cheryl Mary Jones

School of Electronic Engineering and Computer Systems
University of Wales
Bangor
United Kingdom

ACKNOWLEDGEMENTS

I would like to thank my supervisor Dr D. Martin Taylor for his continuous support, enthusiasm and guidance throughout the duration of this research and in the preparation of this thesis.

I would also like to gratefully acknowledge the award of an SERC-CASE studentship in collaboration with SmithKline Beecham Pharmaceuticals. I would like to thank my industrial supervisors at SmithKline Beecham Pharmaceuticals, Dr R. Southgate and particularly Dr J.T Lonsdale for his help and advice on the extraction and purification of porin.

My thanks also go to my colleagues in the School of Electronic Engineering and Computer Science especially Dr H. Fukushima, Dr S. Bone, Dr J. Burt, Dr J. Phelps and Dr G. Mullen for their helpful advice and discussions. I am also grateful to the staff of the mechanical workshop and also Albert Rees and George Stevens for their technical assistance.

I am extremely grateful to Terry Williams at UCNW Bangor who performed the computer modelling of the porin channels.

Finally my thanks go to Peter, my husband, for his aid in the production of this thesis.

SUMMARY

The trimeric protein known as porin, found in the outer membrane of *Escherichia coli*, forms ion channels which have been reported to be voltage-gated. The aim of this investigation is to increase the understanding of the function of such channels, particularly with respect to voltage-gating. To achieve this, porin was first extracted from whole cells of *E. coli* and then it was incorporated into lipid bilayers, made using the Montal-Mueller method, for subsequent investigation.

The extraction of porin from *E. coli* exploited both its tight association with peptidoglycan and its high level of detergent resistance. Porin was extracted from two strains of *E. coli*, 0111:B4 and K12 (a rough mutant), with the resulting samples being rich in OmpF and OmpC porins respectively.

Measurement of ion flow through the porin channels was made with different transmembrane voltages and with a variety of salts and salt concentrations. Such measurements enabled the selectivity of the channels to specific ions to be determined and estimates of pore diameter to be made. Instantaneous I/V characteristics were asymmetrical and non-linear for both porins and were influenced by the salt concentration, pH of the electrolyte and the number of channels in the bilayer. Based on electrostatic models of gramicidin-like channels, coupled with the available structural information on porin, it was concluded that the porin/LPS complex inserts unidirectionally into the bilayer and has a net negative charge at the LPS end. The influence of the number of channels in the bilayer on the I/V characteristic, most marked for the 0111:B4 porin, was interpreted as being due to 'clusters' of channels in close association an idea supported by the results of voltage-gating experiments.

Voltage-gating in single channels was shown to occur in three well defined steps, consistent with the known trimeric structure of porin. Multi-channel membranes showed several different types of current relaxation in response to a sustained voltage application. The most common type was composed of two exponential decays, suggesting the presence of two populations of closing channels. The results from voltage-gating experiments were compared with the theoretical behaviour of a simple two-state channel. This model was also extended to include entropy changes and it was concluded that porin followed the general behaviour predicted by a simple two-state model.

ABBREVIATIONS

ATP	Adenosine triphosphate
BCA	Bicinchoninic acid
BLM	Planar bilayer lipid membrane
EDTA	Ethylenediamine tetra-acetic acid
EIM	Excitability inducing material
EMF	Electromotive force
GHK	Goldman-Hodgkin-Katz
IGFET	Insulated gate field effect transistor
ISFET	Ion selective field effect transistor
KDO	3 deoxy-D-manno-2-octulosonic acid
LDAO	Lauryl dimethylamine oxide
LPS	Lipopolysaccharide
PC	Phosphatidylcholine
PTFE	Polytetrafluoroethene
SDS	Sodium dodecyl sulphate
SDS-PAGE	SDS polyacrylamide gel electrophoresis
VDAC	Voltage-dependent anion channel
VLSI	Very large scale integrated circuit

CONTENTS

CHAPTER 1

INTRODUCTION

Aerospace technology, nuclear physics, medical image/signal processing, seismic, weather and computer vision applications have always exerted a significant market pull for the development of massive high speed computational facilities (Kung, 1988). The miniaturisation and integration of electronic devices based on silicon technology is, however, being pushed to its physical limits. The size of VLSI electronic components is now such that only a further small reduction in size is necessary before they reach the dimensions of molecules. Although improvements in lithographic techniques may enable device sizes to be further miniaturised, eventually the bulk properties of the silicon wafer may be lost so that electron currents will no longer behave in their accustomed manner (Pethig, 1987). In consequence, there has been much speculation in recent years concerning the use of molecules instead of silicon to fabricate circuit elements. Much of the stimulus for Molecular Electronics came from the workshops organised by Forest Carter in 1981 and 1983.

Molecular electronic devices of commercial importance have already been produced e.g. liquid crystal displays, piezoelectric polymers and chemical sensors. Improved electronic devices have also been made by coupling existing integrated circuit technology with electroactive materials. Novel sensors have been developed which offer distinct advantages over conventional sensors, including small size, robustness and potential for low cost fabrication. The insulated gate field effect transistor (IGFET) is the most widely used device in this application. It has been modified by substituting an electrochemically active material for the gate metal (Esashi and Matsuo, 1978).

Recently biological materials have gained the interest of electronic engineers and physicists and in 1985 the International Symposium on Molecular Electronic Devices included a new subject area: Bio-molecular Electronic Devices. Biological systems are capable of performing with great efficiency many functions such as image analysis and learning that cannot easily be achieved with current technology. The living organism can be thought of as an energy and information processing apparatus with the ability to self-replicate.

Biological systems store and process information using individual molecules or sub-components of molecules as the storage medium. Biological systems are particularly impressive in areas where parallel processing of input signals is necessary

e.g. pattern and image processing. The parallel processing capabilities of neural systems are being emulated in both hardware and software in neural networks e.g. recognition of hand-written digits (Boser *et al.*, 1992) and spoken letters of the alphabet (Myers, 1992).

Biological systems also have their own analogues of solid state devices assembled from individual electroactive materials. Examples are:

(i) Molecular conductors where electrons hop or tunnel between redox centres (Bone and Zaba, 1992).

(ii) Biological amplifiers e.g. chemical amplification where a single odourant molecule results in the liberation of one hundred thousand cyclic-AMP molecules (Pethig, 1987).

(iii) Molecular batteries e.g. ion pumps which move ions against prevailing electrochemical gradients converting chemical energy (ATP) into electrical energy (Bone and Zaba, 1992).

(iv) Molecular switches e.g. voltage-gated ion channels in which the passage of ions through aqueous or semi-aqueous channels is regulated by the voltage across the cell membrane in which the ion channel resides.

It is this latter example of a biological 'solid-state' device, the voltage-gated ion channel, which is the subject of investigation in this research. The channel forming protein chosen for study is known as porin and is found in the outer membrane of *Escherichia coli*, a Gram-negative bacterium. The Gram-negative bacteria are extremely resistant to antibiotics and as a result Gram-negative infections are prevalent in modern hospitals. Antibiotics act at precise sites within the bacterial cell e.g. on the protein synthesising machinery (Singleton and Sainsbury, 1984). To reach the target site the antibiotic must first enter the bacterial cell. Entry and exit of solutes through the outer membrane of Gram-negative bacteria takes place through the aqueous channels formed by the porins (Benz and Bauer, 1988). Defence mechanisms exist to inactivate the penetrating antibiotic e.g. the bacterium produces β-lactamase, an enzyme which hydrolyses β-lactam antibiotics such as penicillins. Initially porin channels were thought to be simple 'sieves' but some authors have reported them to be voltage-gated (Schindler and Rosenbush, 1981). This finding is of great importance to the pharmaceutical industry, as it may provide a means of controlling the entry of antibiotic into the bacterial cell. Increasing the influx of antibiotic would be advantageous, since it would increase the probability of the antibiotic reaching its target site before being inactivated by the enzyme.

The study of the function of cellular components can be made in two ways:

(i) The components of interest may be studied in their original complex cellular environment or
(ii) the components may be purified to homogeneity and re-incorporated into some structure mimicking the original environment.

In the former it may not be possible to separate the effects of many different cell components. The latter has the disadvantage that the component being studied may not behave in the same manner as in the original cell because the cell component needs to be extracted from the original cell and purified. The production of proteins in sufficiently large quantities in active form and high purity is not trivial (Harris and Angal, 1989). Correlations between the results obtained from both approaches provide important clues as to the true nature and function of the cellular components.

The cell membrane in which most of the components of interest reside is mainly composed of lipids and proteins, the latter forming the active components. Lipids are amphipathic and spontaneously arrange themselves in the form of a bilayer when in aqueous media. This outstanding characteristic has led to two important experimental bilayer lipid membrane systems, namely planar bilayer lipid membranes (BLMs) and spherical liposomes (Tien *et al.*, 1989). As well as being useful in the study of the function of biological molecules, the planar bilayer technique also provides a possible method for exploiting the potential of biological molecules in practical applications.

Over the last decade the results of experiments on BLMs with suitably incorporated biological molecules have indicated that this technique holds much promise in the field of chemical/biosensors. BLM based sensors have been fabricated by depositing BLMs onto a polyacrylamide gel using the Langmuir-Blodgett technique (Tien *et al.*, 1989). Ion-selective sensors have been developed with incorporated ion channels such as valinomycin and gramicidin, chloroplast extracts and also auxin receptors (Tien *et al.*, 1989, Thompson *et al.*, 1983 and Krull, 1987). With incorporated valinomycin, K^+ concentrations of only 10^{-6} M can decrease the BLM resistance 10^4 to 10^8 fold.

Another class of biological molecules, the enzymes, can also be immobilised in a matrix such as starch or polyacrylamide. In combination with ion-selective electrode based sensors they provide highly selective and sensitive methods for the detection of given substrates and are available commercially. The substrate reacts with the enzyme and the product of the enzymatic reaction is measured by the ion-selective electrode. Examples of enzyme electrodes are given in the review by Kuan and Guilbault (1987) and include urea, creatinine, amino acid and glucose electrodes.

Ion channels selective for calcium and potassium have been employed in the fabrication of ion-selective field effect transistors (ISFETs). These are IGFETs where the gate metal has been substituted by a polymer matrix with incorporated ion channels such as valinomycin (Blackburn, 1987). Thin layers of gel containing enzymes have also been incorporated into ISFETs, in order to detect molecules such as urea (Daniellson *et al.*, 1979)

There is no guarantee, however, that the function of all biological molecules can be successfully exploited for future electronic devices. Biological materials (largely proteins) are designed to function within the protected and highly controlled environment of the cell. Once removed from the cell, often by an elaborate and lengthy purification technique, a protein may no longer behave in the same way as it did in the original cell. Even if the protein retains its functionality it will not have an indefinite shelf life. High temperature, extremes of pH, hydrolytic enzymes, metal ions and many other chemical and physical factors can adversely affect protein stability (Bone and Zaba, 1992).

Although the structure of many proteins which could be of use in electronic device applications, is still unknown there are some proteins which have been extensively studied and for which a detailed body of information exists e.g. bacteriorhodopsin and porin. The basic functions of voltage-gating and selectivity of the *Shaker* potassium channel have now been attributed to a particular region of the protein and new discoveries about its structure are constantly being made (Sigworth, 1993). Based on such knowledge, it may be possible in the future to synthesise peptides of predesigned structure to carry out desired functions, ultimately proteins may also be modified so that they are more suitable for use in bio-devices. Potential targets for protein engineering would include improved stability during storage and operation, widening or narrowing of substrate specificity and shift in or removal of pH dependence.

It is envisaged that biological molecules will play an important role in molecular electronics as constituents in well-assembled aggregates, with properties of the single molecules, such as shape, symmetry and electron affinity determining the overall nature of the molecular aggregate. A new field has recently emerged which is interested in the replication of molecular systems, namely 'supramolecular chemistry'. One possible route to form molecular systems is to use the natural ability of biological molecules to self-assemble. This ability has already been successfully exploited e.g. Fukushima (1994) has produced linear polymers of avidin and streptavidin in which the proteins were interlinked with bisbiotin ligands. A tetrabiotin ligand was also synthesised by Fukushima and preliminary experiments were carried out to investigate the possibility of extending the methodology to 2-D networks (Figure 1.1).

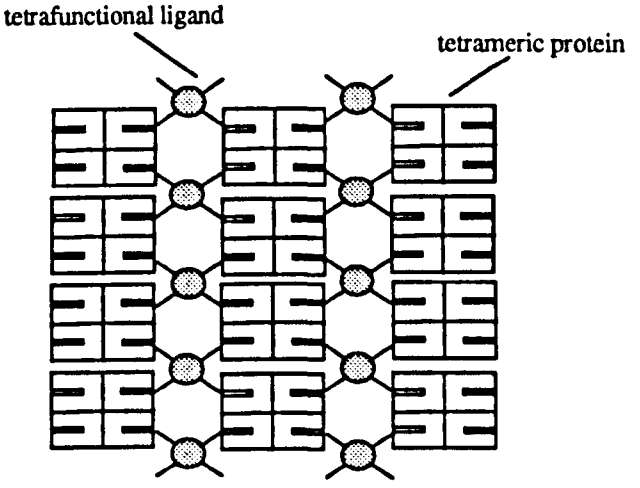

FIGURE 1.1 Schematic diagram of a 2-D network formed by the specific binding of a tetrameric protein such as streptavidin with a tetrabiotin ligand. (Adapted from Fukushima, 1994).

A network such as that depicted in Figure 1.1 assembled from proteins and artificial ligands with specific switching or optical properties, could form the basis of a true biodevice. Clearly, the study of individual molecules with properties of interest to the engineer is complementary to the study of such molecular assemblies.

The motivation for studying porin was, consequently two fold. Firstly, it is a switch of molecular dimensions and could provide important clues for the development of molecular switching elements. Secondly, an understanding of the mechanism of voltage-gating could lead to a means of overcoming the restricted flow of β-lactam antibiotics across the outer membrane of Gram-negative bacteria. The planar lipid bilayer method was the environment chosen in which to study porin, which was extracted and purified with the expert advice of SmithKline Beecham Pharmaceuticals.

CHAPTER 2

MODELS OF ION FLOW THROUGH CHANNELS

2.1 INTRODUCTION

A fundamental aim in the study of lipid membranes containing ion channels is to interpret the experimentally obtained current-voltage (I-V) relationships in terms of the structure of the ion channels. The magnitude of the current through a channel at any given voltage will depend on the molarity of the bathing electrolyte, the geometry of the channel and on the presence of charged residues or dipoles, either in or near the channel. If the application of voltage causes a change in the structure of the protein leading to a change in channel conductance, the effect is known as voltage gating. The time scale of these changes can be between 10^{-4} and 10^{2} seconds (Attwell and Jack, 1978) depending upon the channel concerned. The time taken for individual porin channels to change from the open to the closed state is rapid ($< 10^{-3}$s) but an ensemble of channels may take several hundreds of seconds or more to equilibrate. The concentration profile of ions in an 'open' channel reaches steady state in $< 10^{-6}$s (Attwell and Jack, 1978) so that this instantaneous ion flow can be dissociated experimentally from the slower voltage-dependent changes associated with gating. Instantaneous ion flow and voltage gating are usually modelled separately.

2.2 OHMIC EQUIVALENT CIRCUITS

One of the simplest and oldest models used to describe ion flow through channels uses ohmic equivalent circuits to represent the properties of the membranes and channels. The lipid bilayer or membrane separates two conducting solutions by an extremely thin insulating layer, in the order of nm, and therefore behaves as a significant electrical capacitor. An ion channel can be regarded as an elementary conductor spanning the insulating membrane and this, in parallel with the membrane capacitance, is shown in Figure 2.1a. The current-voltage relationship for this equivalent circuit is defined by Ohm's Law:

$$I = gV \tag{2.1}$$

where I is the current, V is the voltage applied across the membrane and g is the membrane conductance.

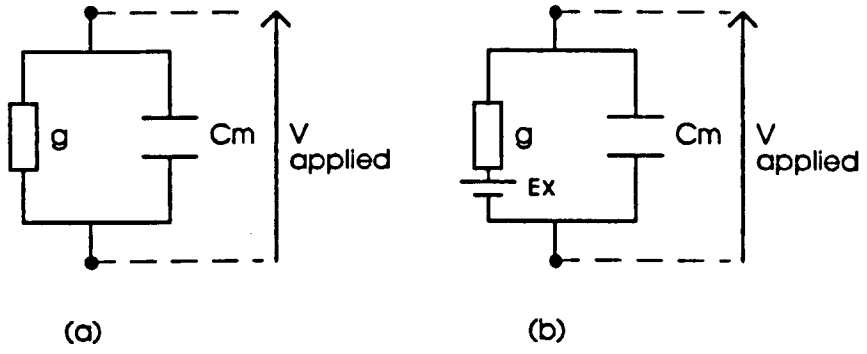

FIGURE 2.1 (a) Equivalent circuit of a channel in a bilayer membrane. g is the channel conductance, Cm the bilayer capacitance. (b) Modified equivalent circuit for a selective channel in a membrane with a concentration gradient of the permeant ion across it. An emf, Ex, means that at zero applied potential there is a current flowing through the channel.

An ion selective channel in a membrane which separates solutions with different concentrations of the permeant ion would not obey the simple Ohm's Law. At zero applied potential there will be a potential across the membrane known as an equilibrium potential. The bulk solutions on either side of the membrane, although of different concentrations, are initially electrically neutral. A channel allowing passage of one ion species only, say the cation, will allow this ion to diffuse from the more concentrated to the less concentrated solution. The preferential diffusion of cations will lead to an excess of cations on one side of the membrane and a depletion on the other. An electrical potential will develop to oppose the flow of cations so that eventually an equilibrium situation is reached where diffusion of cations in one direction is balanced by an opposing flow of cations driven by the electric potential. If the channel is permeable to one ion species only, the equilibrium potential is given by the Nernst potential (Nernst, 1888):

$$E_x = \frac{RT}{zF} \ln \frac{[x_1]}{[x_2]} \qquad (2.2)$$

where E_X is the potential, $[x_1]$ and $[x_2]$ are the concentrations of the permeant ion on the two sides of the membrane, F is Faraday's constant, R is the gas constant, z the valence of the ion species and T the absolute temperature. For the case of a channel

permeable to more than one ion species the equilibrium potential is a weighted mean of all the Nernst potentials for each ion species. The equivalent circuit (Figure 2.1b) now has an e.m.f. E_x in series with the resistor so that the modified Ohm's Law becomes

$$I = g(V - E_x). \tag{2.3}$$

Simple I-V measurements interpreted in terms of equivalent electrical circuits can give limited although useful information on ionic channels as illustrated by Figure 2.2. The number of channels in a membrane can easily be estimated by measuring the slope of the I-V relationship for the membrane (Figure 2.2a). The I-V characteristic does not pass through the origin when highly selective channels are in the membrane and there is a salt concentration gradient across them (Figure 2.2b). Voltage dependent conductance changes can also be clearly seen; the conductance changes may be discrete or gradual (Figure 2.2c).

The electrical circuit analogue does not of course describe how the ions actually move through the channel. In practice I-V relationships are often non-linear; for example when the concentrations of permeant ions is much higher on one side of a selective pore than the other. This non-linear behaviour can be predicted from theories of electrodiffusion as shown in section 2.4.1.1. In the following sections a theoretical description will also be given of models which attempt to describe ionic motion in terms of the structure of the permeable pathways.

2.3 ACCESS RESISTANCE

A measurement of channel conductance includes both the conductance of the channel interior and the access resistance at each end of the channel. An estimate of the access resistance can be made by considering the mouth of the channel to be approximated by a hemisphere of radius a, equal to the channel radius (Figure 2.3). The access resistance is then assumed to be the resistance of the bulk electrolyte outside this hemisphere and may be calculated as follows. Consider a hemispherical element of thickness dr and radius r. The resistance dR between opposite faces of this element is given by

$$dR = \rho \frac{dr}{2\pi r^2}.$$

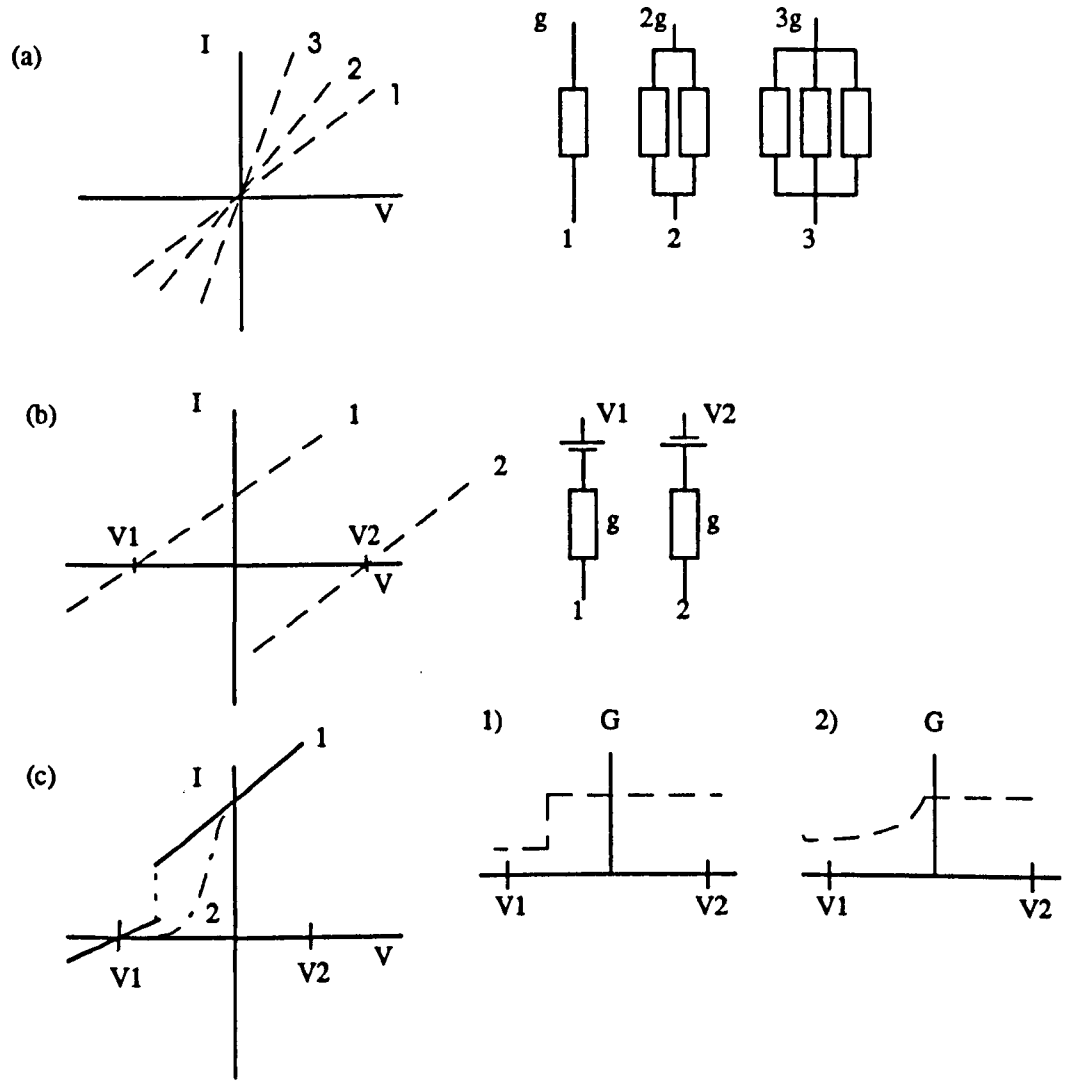

FIGURE 2.2 Current-voltage relationships of membranes a) 1,2 and 3 channels in a membrane with relative slopes of 1,2 and 3. b) Channels showing current flow at zero applied potential can be modelled with an emf in series c) Channels showing voltage dependent changes 1) discrete change and 2) gradual change (Hille, 1984).

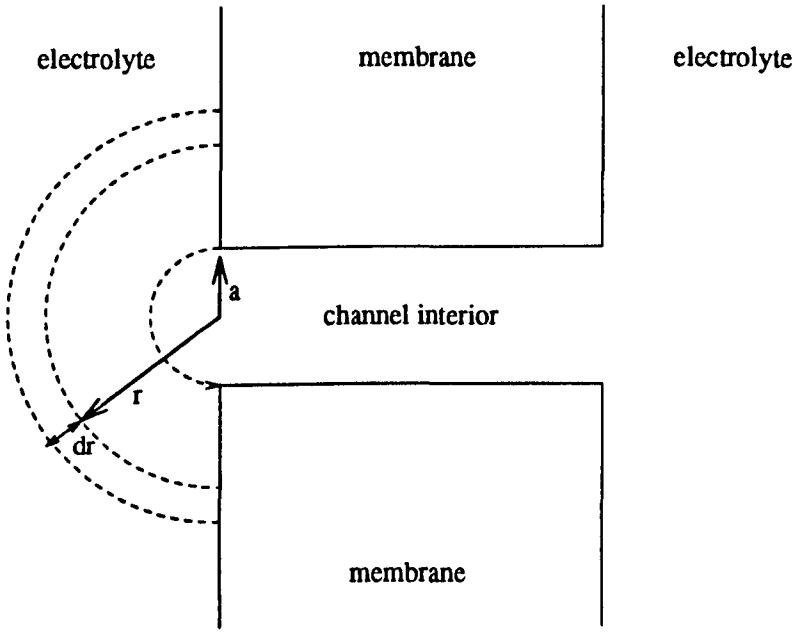

FIGURE 2.3 Model of channel used to calculate the access resistance.

where ρ is the resistivity of the electrolyte. The total resistance of the electrolyte is then given by

$$R = \frac{\rho}{2\pi}\int_a^{\infty}\frac{dr}{r^2} = \frac{\rho}{2\pi a}.$$

Taking account of the electrolyte on both sides of the channel, then the access resistance R_{acc} is given by

$$R_{acc} = \frac{\rho}{\pi a}. \tag{2.4}$$

Perskoff and Bers (1988) calculated the access resistance by solving the Nernst-Planck equation (see section 2.4.1) but ignoring any ion density gradients and assuming that only one species of ion is permeable. In their model the access resistance is given by

$$R_{acc} = \frac{kT}{2\pi q^2 a D n_{\infty}} \tag{2.5}$$

where D is the diffusion coefficient of the electrolyte ions, n_∞ the ion concentration in the bulk electrolyte, k is Boltzmann's constant, T the absolute temperature, q the unit of fundamental charge and a is the channel radius. Applying the Einstein equation

$$\frac{\mu}{D} = \frac{q}{kT}$$

where μ is the mobility of the ion species, and noting that the resistivity of monovalent electrolyte is given by

$$\rho = \frac{1}{\sigma} = \frac{1}{2n_\infty q\mu}$$

equation (2.5) reduces to equation (2.4).

Hall (1975) demonstrated, however, that the contribution of the hemisphere of electrolyte at the mouth of the channel was not negligible. In a more accurate calculation, he drew upon the well known formula for the capacitance, C, of an isolated disc of radius, a, residing in a material of permittivity $\varepsilon_0\varepsilon_r$, i.e.

$$C = 8\varepsilon_r\varepsilon_0 a.$$

Realising that

$$\varepsilon_r\varepsilon_o\rho = CR$$

for any dielectric material (Smythe, 1950) Hall arrived at an access resistance R_{acc} given by

$$R_{acc} = \frac{\rho}{2a}.$$

(2.6)

It should be remembered that even this result is an underestimate because it assumes that the planar disc defining the end of the channel is an isopotential, which is only approximately true. The total measured resistance will be the sum of the access and channel resistance i.e.

$$R_{total} = \frac{\rho}{2a} + \frac{\rho l}{\pi a^2} = \frac{\rho}{a}\left(\frac{1}{2} + \frac{l}{\pi a}\right)$$

(2.7)

where l is the channel length. From equation (2.7) it can be seen that so long as the condition

$$\frac{l}{\pi a} >> \frac{1}{2}$$
$$i.e. \quad a << \frac{2l}{\pi} \tag{2.8}$$

is met then the channel resistance dominates the total resistance. The current density, J, in the channel can be calculated using the relationship

$$J = \frac{I}{\pi a^2} = \frac{V}{\pi a^2 R_{total}} = \frac{V}{\rho\left(\frac{\pi a}{2} + l\right)}. \tag{2.9}$$

Figure 2.4a shows that as the channel radius increases the apparent current density in the channel decreases owing to the increasing influence of the access resistance. For comparison the current density has also been calculated using the equation

$$J = \sigma E \tag{2.10}$$

where the electric field, E, for the model channel in Figure 2.4b has been found numerically by a finite difference method.

Figure 2.4a clearly illustrates that the value of R_{acc} based on equation (2.4) is an underestimate compared to that proposed by Hall (1975) The numerical calculation suggests that even the Hall approach leads to an underestimate of R_{acc}. At large channel diameters the current densities calculated by the finite difference method decrease more slowly than expected. This is because the channel radius approaches the dimensions of the boundary of the mesh and the computation loses accuracy.

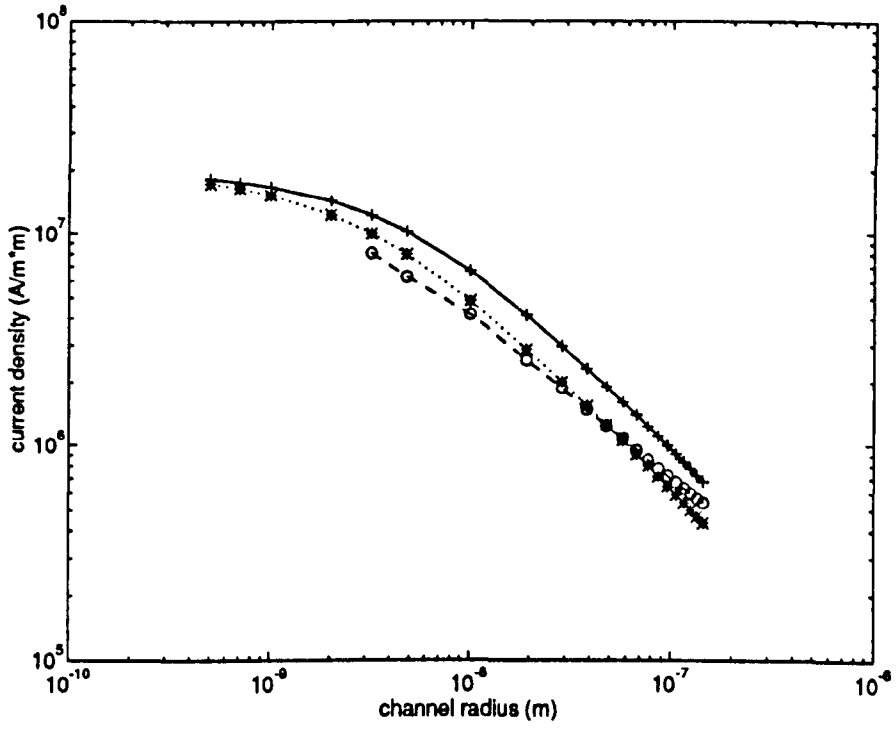

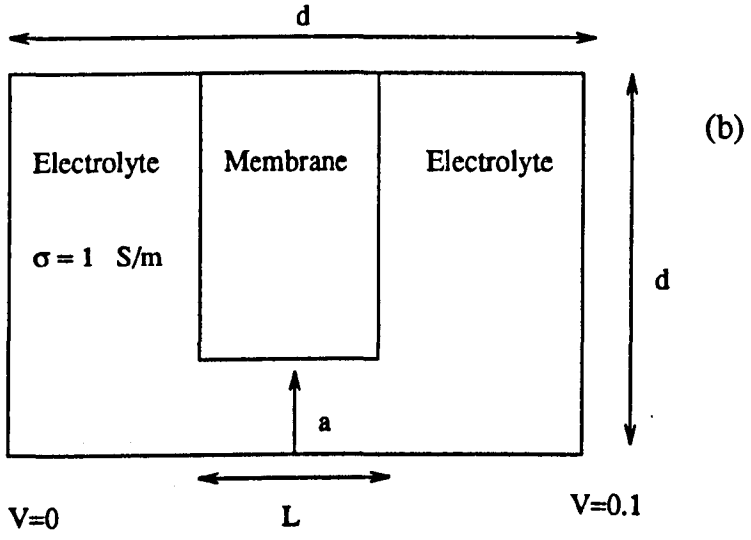

FIGURE 2.4 a) The effect of channel radius on the current density in a 5 nm long channel calculated using equation (2.9) with $R_{acc}=\rho/\pi a$ (—+—), $R_{acc}=\rho/2a$ (...*...) and in the third example calculated using equation (2.10) (--o--). The model used for the finite difference computation of E is shown in b). Variable radius is a and the cell size d=480 nm. Calculations for the current density were made using a 250 x 250 grid for all the data points except for the two smallest radii (4.8 and 3.2 nm) where a 400 x400 grid was used.

2.4 ION FLOW THROUGH OPEN CHANNELS

2.4.1 Free Diffusion Models

When describing the free diffusion of ions through open channels, the ions are considered to be moving through a relatively structureless medium. The time averaged properties and movement of each ion species is described by the Nernst-Planck electrodiffusion equation which, in one dimension, is written as

$$J = -zFD\left[\frac{dC}{dx} + \left(\frac{qzC}{kT}\right)\frac{dV}{dx}\right] \tag{2.11}$$

where J is the current density, z the valence of the ion species, C the concentration, F is Faraday's constant, k is Boltzmann's constant, q the fundamental unit of charge, V the local potential and D the diffusion coefficient.

This equation, integrated subject to particular boundary conditions, is the starting point of many theories of channel conductance. Free diffusion models can be very simple, as in the partitioning-electrodiffusion model described in section 2.4.1.1, or they can be refined to take into account factors such as the shape of the channel, the access resistance to the channel mouth and the potential profile within the channel. A common assumption in all these models, however, is that ion movement across the membrane is independent of all other ions. Practically, this means that ion fluxes should be linearly related to the ion concentration, but this is not the case for many channels e.g. gramicidin, the sodium channel in neurones and the sarcoplasmic reticulum channel. The non-linear relation of single channel conductance to ion concentration for gramicidin A is discussed in section 2.4.3.1. Porin channels have been reported as having ion fluxes which are linearly related to the ion concentration (Stein, 1986) and this has been confirmed in this research.

If there is no coupling between ionic fluxes, the Ussing flux ratio criterion should be obeyed (Ussing, 1949). The Ussing test required measuring with a tracer ion the unidirectional flux across a membrane from the left side to the right $^{1\rightarrow 2}J$ and right side to left $^{1\leftarrow 2}J$. With passive diffusion and no flux coupling, the ratio of these fluxes should equal the ratio of the electrochemical activities of the ions in the two solutions. Thus the flux ratio of an ion of valence z is

$$\frac{^{1\rightarrow 2}J}{^{1\leftarrow 2}J} = \frac{[S_1]}{[S_2]}\exp\left(\frac{zFV}{RT}\right) \tag{2.12}$$

where $[S_1]$, $[S_2]$ are the concentrations of the ion species on either side of the membrane, V is the transmembrane potential, R the gas constant and T the absolute temperature.

There are several common types of flux coupling which lead to flux ratios which do not obey equation (2.12). If transport through the membrane is not through a channel forming protein but is in fact via a carrier type of protein, i.e. the ion transport is mediated, the flux is not directly proportional to concentration. In long pores it is possible for the movement of one ion to sweep other ions with it i.e. the flow is correlated. Another type of flux coupling is co-transport or counter-transport where the flow of one ion is coupled to the flow of another diffusing species.

2.4.1.1 Partitioning Electrodiffusion Model

In the partitioning electrodiffusion model, the channel-containing-membrane is viewed as a homogenous slab of material into which permeant particles partition instantly from the bulk solution (Goldman, 1943 and Hodgkin and Katz, 1949). It is assumed that the field in the membrane is constant and the ions do not interact with each other. Hence, this model is also known as the GHK constant-field theory. Membrane permeability is defined by the empirical equation

$$J_m = -P\Delta C \tag{2.13}$$

where J_m is the molar flux density of the ion species, P is the membrane permeability to the ion species and ΔC is the concentration difference between the two bulk solutions separated by the membrane. The partitioning of the ion species between bulk solution and the membrane is considered to occur rapidly at the two interfaces so that it may be considered to be in equilibrium. The permeant particles are considered to partition into the membrane material from the bulk solution with a partition coefficient β. Thus the concentration gradient within the membrane itself is given by $\beta\Delta C$ (see Figure 2.5). From Fick's first law the flux is

$$J_m = -\frac{\Delta C D \beta}{l} \tag{2.14}$$

where D is the diffusion coefficient and l is the width of the membrane. Combining equations (2.13) and (2.14) yields

$$P = \frac{D\beta}{l}.$$

(2.15)

From this simple approach permeability is seen to be governed by the solubility and diffusion coefficient of the test molecule in the membrane.

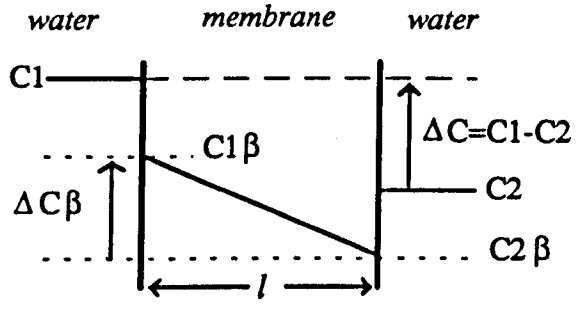

FIGURE 2.5 Model representing ion permeation as a diffusion through a sheet of membrane material. C1 and C2 are concentrations of the ion on each side of the membrane. β is the water-membrane partition coefficient. The permeant particles partition into the membrane material and the flux is determined by the steepness of the intramembrane concentration gradient (Hille, 1984).

These assumptions lead to two expressions, the Goldman-Hodgkin-Katz (GHK) current and the GHK voltage equations (see Appendix A for derivation). Assuming independence of ionic movements enables the current equation

$$J = \frac{Pz^2VF^2}{RT}\left[\frac{[S_2]\exp\left(\frac{-zFV}{RT}\right)-[S_1]}{\exp\left(\frac{-zFV}{RT}\right)-1}\right]$$

(2.16)

to be split into two independent, unidirectional expressions of the influx and efflux of ions:

$$\vec{J} = \frac{Pz^2VF^2}{RT}\left[\frac{[S_1]}{1-\exp\left(\frac{-zFV}{RT}\right)}\right] \tag{2.17}$$

and

$$\overleftarrow{J} = \frac{Pz^2VF^2}{RT}\left[\frac{[S_2]}{1-\exp\left(\frac{zFV}{RT}\right)}\right]. \tag{2.18}$$

The size of each unidirectional flux varies linearly with the driving concentration, as is required by independence. Both equations (2.17) and (2.18) are non-linear functions of membrane potential. For large favourable driving potentials they asymptote to straight lines passing through the origin whose slopes are proportional to the ion concentration since

$$\vec{J} = \frac{Pz^2VF^2}{RT}[S_1] \qquad V\rangle\rangle 0 \tag{2.19}$$

$$\overleftarrow{J} = \frac{Pz^2VF^2}{RT}[S_2] \qquad V\langle\langle 0 \tag{2.20}$$

Hence the GHK current equation predicts rectifying I-V relationships whenever the permeant ion concentrations are unequal. Figure 2.6 shows the theoretical I-V relationship for a single permeant ion. When there are two permeant ion species, for example an anion and a cation of equal valence, the net current (derived in Appendix A) approximates to

$$\vec{J}_T = \frac{z^2VF^2}{RT}\left(P_+[S_1] + P_-[S_2]\right) \qquad \text{for} \quad V\rangle\rangle 0$$

and

$$\overleftarrow{J}_T = \frac{z^2VF^2}{RT}\left(P_+[S_2] + P_-[S_1]\right) \qquad \text{for} \quad V\langle\langle 0$$

where P_+ is the permeability of the cation and P_- is the permeability of the anion (as shown in Figure 2.7).

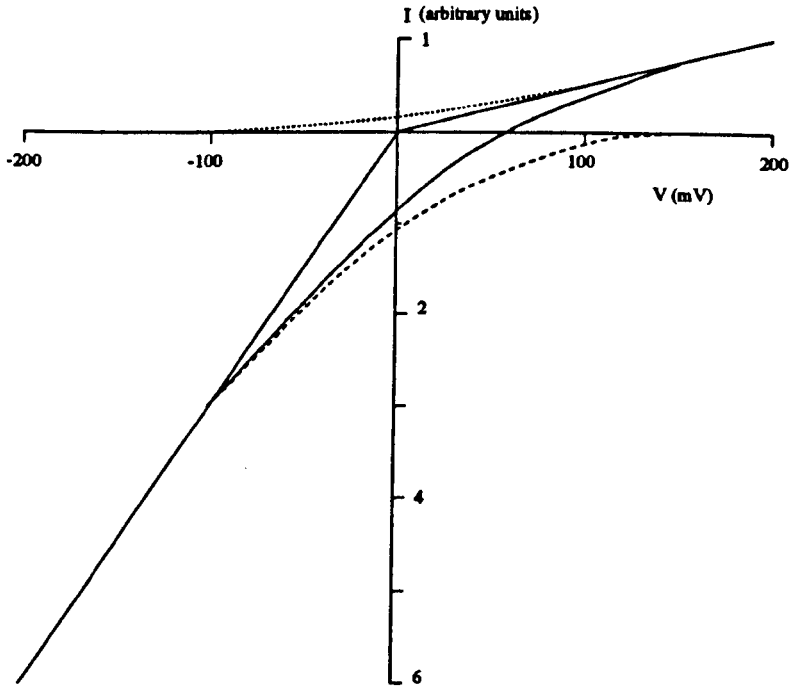

FIGURE 2.6 Current-voltage relationship predicted by the GHK theory for a single permeant ion [So]/[Si] = 8, I_{total} (–), I⇒ (....), I⇐ (--). (Hille, 1984)

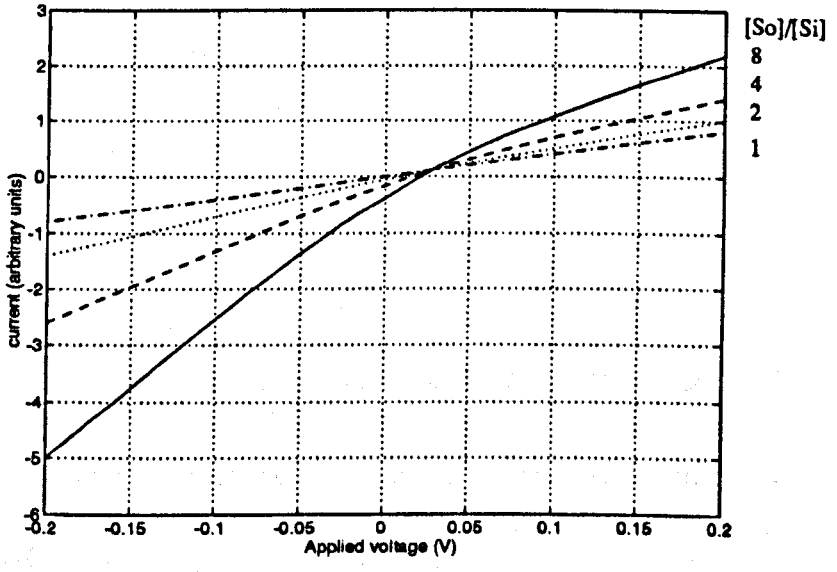

FIGURE 2.7 Current-voltage curves predicted by the GHK theory for two permeant ions, K^+ and Cl^-, for a range of concentration gradients. Cation to anion permeability ratio (Pc/Pa) was taken as 3.

The GHK voltage equation predicts the transmembrane potential at which no current flows, this is called the reverse current voltage or zero current potential. In the case where only one ion species is permeant, it is simply the Nernst potential for that ion, see equation (2.2). With several permeant ions, the reverse current voltage is a weighted mean of all the Nernst potentials. For a membrane permeable to two ionic species, for example K^+ and Cl^- the GHK voltage equation is (see Appendix A)

$$V_{rev} = \frac{RT}{zF} \ln\left[\frac{P_k[K_1] + P_{Cl}[Cl_2]}{P_k[K_2] + P_{Cl}[Cl_1]}\right] \tag{2.21}$$

where V_{rev} is the reverse current voltage, P_k is the permeability for K^+ ions , P_{Cl} the permeability for Cl^- ions, $[K_1]$, $[K_2]$ and $[Cl_1]$ and $[Cl_2]$ the concentrations of potassium and chloride ions on either side of the membrane. Because of the simple assumptions used, equations (2.11)-(2.21) give few clues for explaining ionic selectivity in molecular terms. They are useful, however, because they enable the relative permeabilities of two or more ions species to be determined. The GHK voltage equation is widely used and is sometimes called the generalised null potential equation. This is because, under certain conditions, a number of other models and approaches give rise to an equation of identical form. In many systems, including some which show current saturation, the absolute permeability varies widely with the test conditions but permeability ratios remain relatively constant. Figure 2.8 shows plots of reverse current voltage, V_{rev}, versus concentration gradient for a membrane bathed with an electrolyte containing two ion species. Each curve corresponds to a different value for the ratio of cation to anion permeability.

2.4.2 Electrostatic Modelling of Channels

The partitioning electrodiffusion model described above regarded the channel-containing-membrane as a homogeneous slab of material thus ignoring the microscopic heterogeneity of the system. Clearly, this is unsatisfactory and attempts have been made to better model the microscopic molecular mechanisms that control ion fluxes through channels. The most promising of these are based on the continuum theory (Levitt, 1985) which is founded on the Nernst-Planck equations

$$J_p = -p(r)q\mu_+\nabla\Phi(r) - qD_+\nabla p(r) \tag{2.22}$$

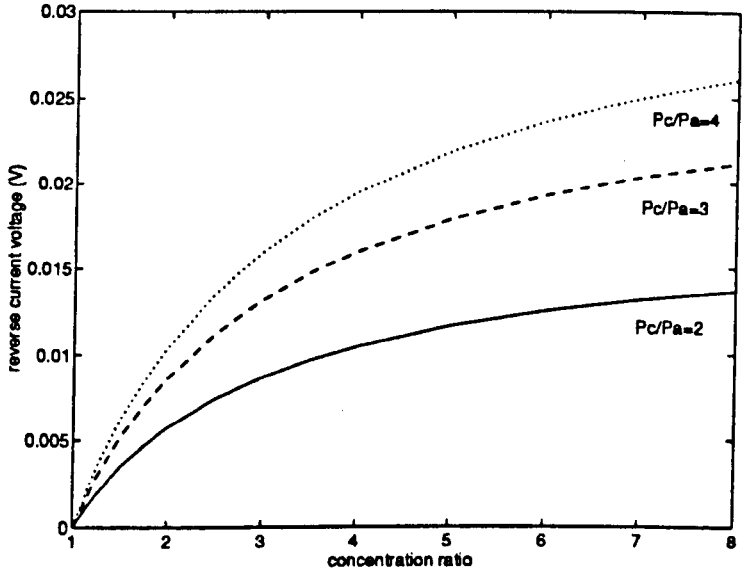

FIGURE 2.8 Reverse current voltage, V_{rev}, versus salt concentration ratio for a series of cation to anion permeability ratios (Pc/Pa)

and

$$J_n = -n(r)q\mu\_\nabla\Phi(r) + qD\_\nabla n(r) \tag{2.23}$$

where J_p and J_n are the densities of positive and negative ion fluxes, $\mu_\pm$ and $D_\pm$ are the mobilities and diffusion coefficients respectively of the ions, p(r) and n(r) the positive and negative ion concentrations and Φ(r) the potential. Since ion fluxes must be continuous throughout the system then

$$\nabla \cdot J_n = \nabla \cdot J_p = 0. \tag{2.24}$$

The presence of charged residues in the channel coupled to the applied voltage results in an imbalance in the ion concentrations. This leads to a local space-charge perturbation of potential, which must satisfy Poisson's equation

$$\nabla \cdot [\varepsilon_r \varepsilon_0 \nabla \Phi(r)] + \rho_T(r) = 0$$

(2.25)

where $\rho_T(r)$ is the local charge density and ε_r is the relative permittivity of the medium in which the charge resides. It is generally assumed that in the membrane $\rho_T = 0$ and $\varepsilon_r \approx 2$, while in the bulk electrolyte $\varepsilon_r \approx 80$ and

$$\rho_T(r) = (p(r) - n(r))q.$$

(2.26)

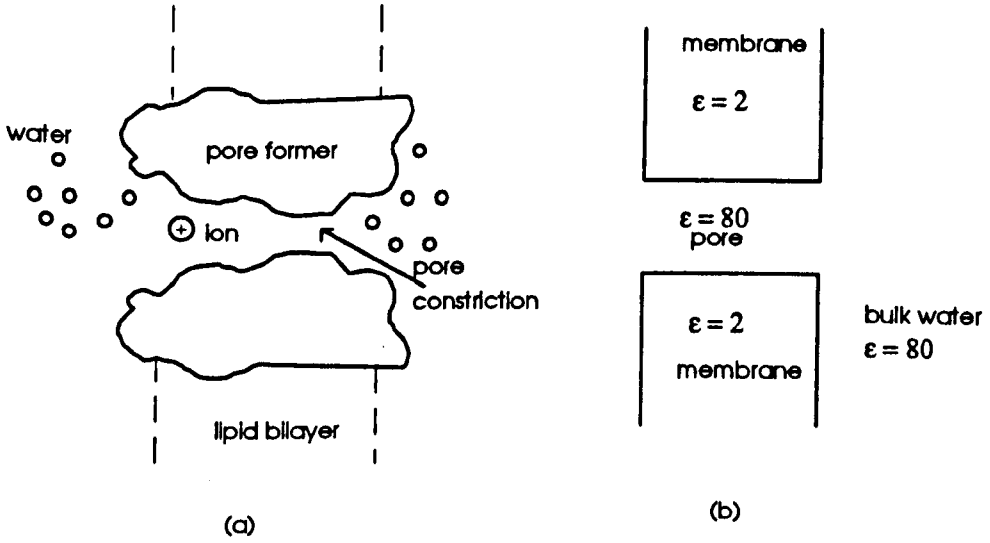

FIGURE 2.9 a) Topology of the ion-water-pore former-lipid ensemble. b) Simplified two dielectric description.

The simplest model (Figure 2.9) has only two dielectric continua, one with $\varepsilon_r \approx 80$ (bulk water and polar surface of the pore former) and one with $\varepsilon_r \approx 2$ (the lipid membrane and hydrophobic part of the pore former). For gramicidin-like channels Levitt (1978) used an effective pore radius greater than the physical radius of the channel to account for the hydrophilic portion of the pore former. Using information from dielectric measurements on polyalanylglycine (Tredgold and Hole, 1976), which has a structure similar to the α-helix backbone of gramicidin A, Levitt (1978) estimated that the inner 0.2 nm of the gramicidin channel wall should have an $\varepsilon_r \approx 10$ and the rest of the wall should be similar to hydrocarbon. Levitt assumed that the 0.2 nm inner wall could be approximated by an 0.1 nm wall with an $\varepsilon_r \approx 80$. Similar measurements for channel proteins such as porin which are comprised largely of β-

pleated sheet (see section 3.4) are not currently available. Sancho and Martinez (1991) used a three dielectric model which assigned a lower value of ε_r inside the pore to account for the lower polarizability of pore water compared to bulk water in narrow pores (Lee and Jordan, 1984 and Hasted, 1973). For relatively open channels such as porins the pore water would be expected to maintain a structure closer to that of bulk water.

The effects of charges in the channel have variously been modelled as charged sheets perpendicular to the channel axis (Levitt, 1985), discrete ions on the channel axis (Jordan *et al.* 1989) and dipole rings at the channel wall (Sancho and Martinez, 1991).

The complexity of the suite of equations (2.22) to (2.26) is such that only approximate solutions, often numerical, have been obtained. Nevertheless, they provide a qualitative insight into the impact of structural and electrical parameters on ion permeation.

2.4.2.1 Examples of Electrostatic Models

In this section three electrostatic models, based on the equations (2.22)-(2.26) in the previous section are described and some of their predictions of the effect of structural and electrical parameters on ion permeation are shown.

(a) Jordan *et al.* (1989)

Jordan *et al.* model the simple case where there is no current flow i.e.

$$J_n = J_p = 0 \tag{2.27}$$

and calculate equilibrium potentials. The concentration of the electrolyte ions can then be determined by the Boltzmann equation

$$n(r) = n_\infty \exp\left[\frac{q\Phi(r)}{kT}\right]$$

$$p(r) = p_\infty \exp\left[-\frac{q\Phi(r)}{kT}\right] \tag{2.28}$$

where $n_- = p_-$ are the concentrations of negative and positive ions in the undisturbed electrolyte well away from the membrane. Jordan *et al.* (1989) then proceeded to solve the Boltzmann equation in combination with the Poisson equation (2.25).

Ionic size was accounted for by assuming that electrolyte was excluded from the regions within one ionic radius of an ionic source, which was taken as 0.1 nm. The potential due to an ion located at arbitrary positions along the channel length was calculated for different ionic strengths of bulk electrolyte. A cylindrically symmetrical geometry for the channel was used (Figure 2.10) and the ion was located axially. In Figure 2.11 the potential calculated for a channel with gramicidin-like dimensions is plotted, from which it is seen that within the channel only relatively small changes in potential occur even when the ionic strength is changed. Exterior to the channel and sufficiently far from the membrane the potential falls exponentially to zero. The model also shows that shielding substantially increases the ability of a channel to solvate a second ion. When an ion is located near one end of the channel (Figure 2.11b) the potential at the corresponding site at the other mouth decreases by 30 mV as ionic strength is increased from 0 to 2.5M and decreases by more than 50 mV at the centre of the channel. Ionic strength also influences the accessibility of the channel to a second ion (Figures 2.11b and 2.11c). When one ion is located at the mouth of the channel (z=0.1 nm) or in the bulk electrolyte (z=0.15 nm) an increase in ionic strength from 0 to 2.5M decreases the electrical potential at the complementary site at the other end of the channel. Jordan reports this to be as much as 70 mV but in fact the decrease at the mouth of the channel in Figure 2.11c is only about 7 mV.

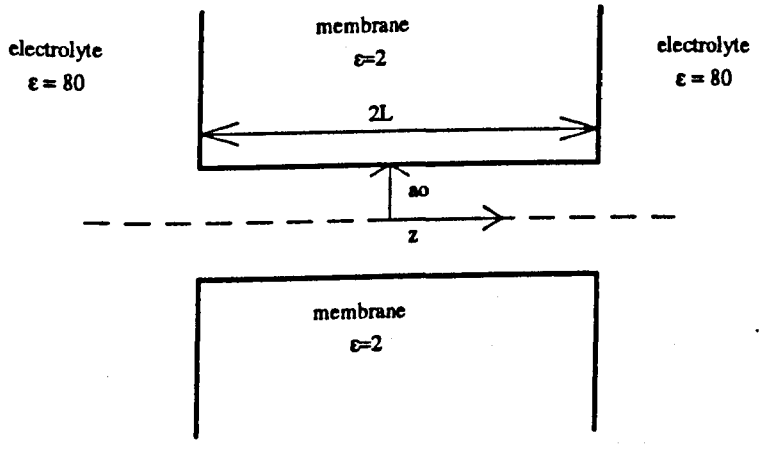

FIGURE 2.10 Geometry of the cylindrically-symmetric membrane-electrolyte system of Jordan *et al.* (1989). Effective radius of the channel= ao, length = 2L.

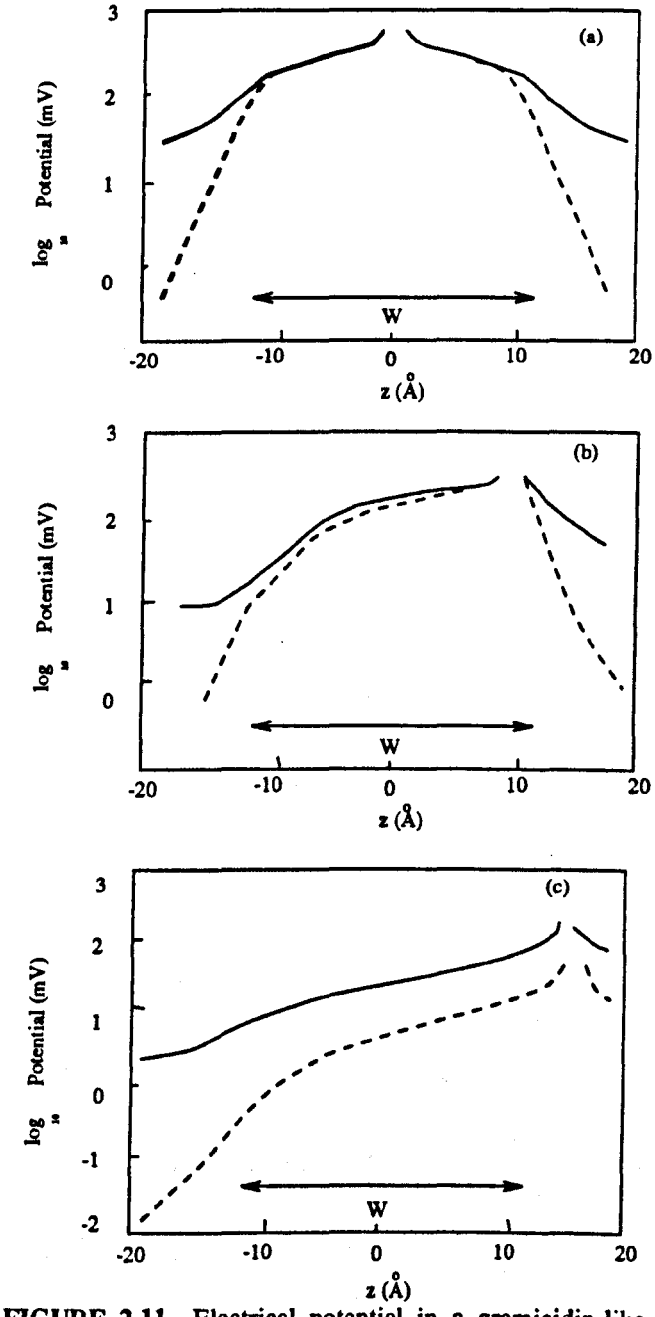

FIGURE 2.11 Electrical potential in a gramicidin-like pore, 2.5 nm long with an electrical radius of 0.25 nm. ε (pore)=80 and electrolyte is excluded from the pore. Three cases are contrasted a) source located at z=0, b) z=0.1 nm and c) z=0.15 nm. Ionic strength is 0.0 M (-) and 2.5 M (---). (Jordan, 1989)

In Table 2.1 the values of total image energy are compared using ε(channel water)=40 and ε(channel water)=80. Well within the channel the image energy is increased by a factor of about 1.5 due to the lowering of the dielectric constant.

In the model, electrolyte concentration had a much greater influence on the electrical potential and the image energy for large diameter channels, such as porin, than for relatively small pores such as gramicidin. This is because electrolyte is able to enter the wide channel and is approximately the same concentration as in the bulk solution. The effect of electrolyte screening on the total image energy at selected points along the axis of a channel with porin-like dimensions are shown in Table 2.2. When the ionic strength is increased to 0.1 M the peak of the image potential is only 13% of its value in electrolyte-free solution. Electrolyte shielding essentially neutralises the influence of the surrounding low dielectric domain and the model shows that most of the increase in energy takes place in the channel entrance. The model suggests that there should be a measurable reduction of conductance for a concentration change from 0.1 to 0.01 M, but experimental results from Benz *et al.* (1980) and from this research do not support this contention. The values in Table 2.2 have been calculated using a radius of 0.6 nm for porin (Garavito *et al.*, 1983). However the geometry of porin is complex (see section 3.4.3) and the radius given represents the narrowest part of the aqueous channel. Over a large portion of channel length the porin channel will have radius substantially greater than 0.6 nm. This would considerably reduce the image energy barriers and would explain perhaps why there is not a measurable change in conductance when the electrolyte concentration is changed.

(b) Levitt (1985)

Levitt provided an analytical solution for the potential equations, assuming that $\varepsilon_{water}/\varepsilon_{lipid} \approx 40$ was sufficiently large so that the perpendicular component of the electric field at the lipid/water interface may be considered zero. This means that the E field lines are confined within the channel and spread into the bulk solution as illustrated in Figure 2.12. Simple Gaussian surfaces drawn at the mouth of the channel enabled the Born (image) potential to be calculated. The accuracy of the approximation was evaluated by comparing the Born potential so calculated with exact numerical solutions (Jordan, 1982). For relatively wide channels and assuming $\varepsilon_{channel\ water} = 40$ the error introduced by the approximation was of the same magnitude as other uncertainties i.e. value of dielectric constant of water within the pore and effective radius of the channel.

TABLE 2.1 Comparison of total image energy of a realistic gramicidin-like channel ($\varepsilon = 40$) with test case ($\varepsilon = 80$) as a function of ionic strength. (Jordan *et al.*, 1989)

Ionic strength (M)	Total image energy (kJ/mol)			
	z =0 nm		z = 0.1 nm	
	$\varepsilon = 80$	$\varepsilon = 40$	$\varepsilon = 80$	$\varepsilon = 40$
0.1	22.8	35.2	9.5	13.2
0.5	23.1	36.2	9.0	13.4
1.0	23.2	36.6	8.8	13.5
2.5	23.3	37.0	8.6	13.6

TABLE 2.2 Effect of electrolyte screening on the total image energy at selected points along the axis of a porin-like channel as a function of ionic strength. Length of channel (2L) = 5.5 nm, radius (a_0) = 0.6 nm. Image energies are in kJ/mol.

z (nm)	Ionic strength (M)			
	0.000	0.005	0.016	0.1
00.0	8.9	3.9	2.8	1.2
2.5	2.8	2.0	1.5	0.7
3.0	1.0	0.7	0.55	0.2
3.50	0.4	0.3	0.2	0.05

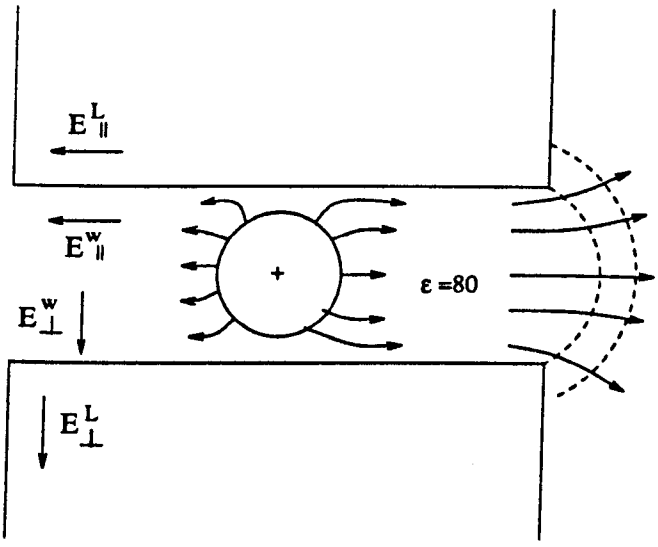

FIGURE 2.12 Schematic diagram of a water-filled channel through a lipid membrane. E^W(perpendicular) is zero at the water-lipid interface so that the field lines are constrained to the aqueous region. (Levitt, 1985).

Levitt (1985) then proceeded to solve the Nernst-Planck equations numerically for the potential at all locations assuming fixed values for the current flux. The influence of charges within the channel were modelled by placing charged sheets in the channel perpendicular to the channel axis.

When a negative charge sheet is placed in the centre of the channel the calculations predict a) a channel conductance which falls with increasing voltage at low ion concentration but is almost constant at high ion concentration and b) an ion flux which tends to saturate as the ionic strength is raised. Both of the previous effects are due to screening of the fixed charge by counter ions when the ion concentration is high. The charged channel shows a strong discrimination between cations and anions; at low ion concentrations the cation conductance is about 10^5 that of the anion for a fixed charge of -1 unit.

When the charged sheet is at one end of the channel the voltage dependence of conductance was asymmetrical (Figure 2.13a) with the corresponding I/V relationship showing superlinear behaviour. The asymmetry was greatly reduced by increasing the ionic strength, owing to the screening of the fixed charge by counter ions. The cation conductance is ≈10 times smaller than when the charge is in the centre of the channel and is reduced to only ≈1.5 times that of the anion.

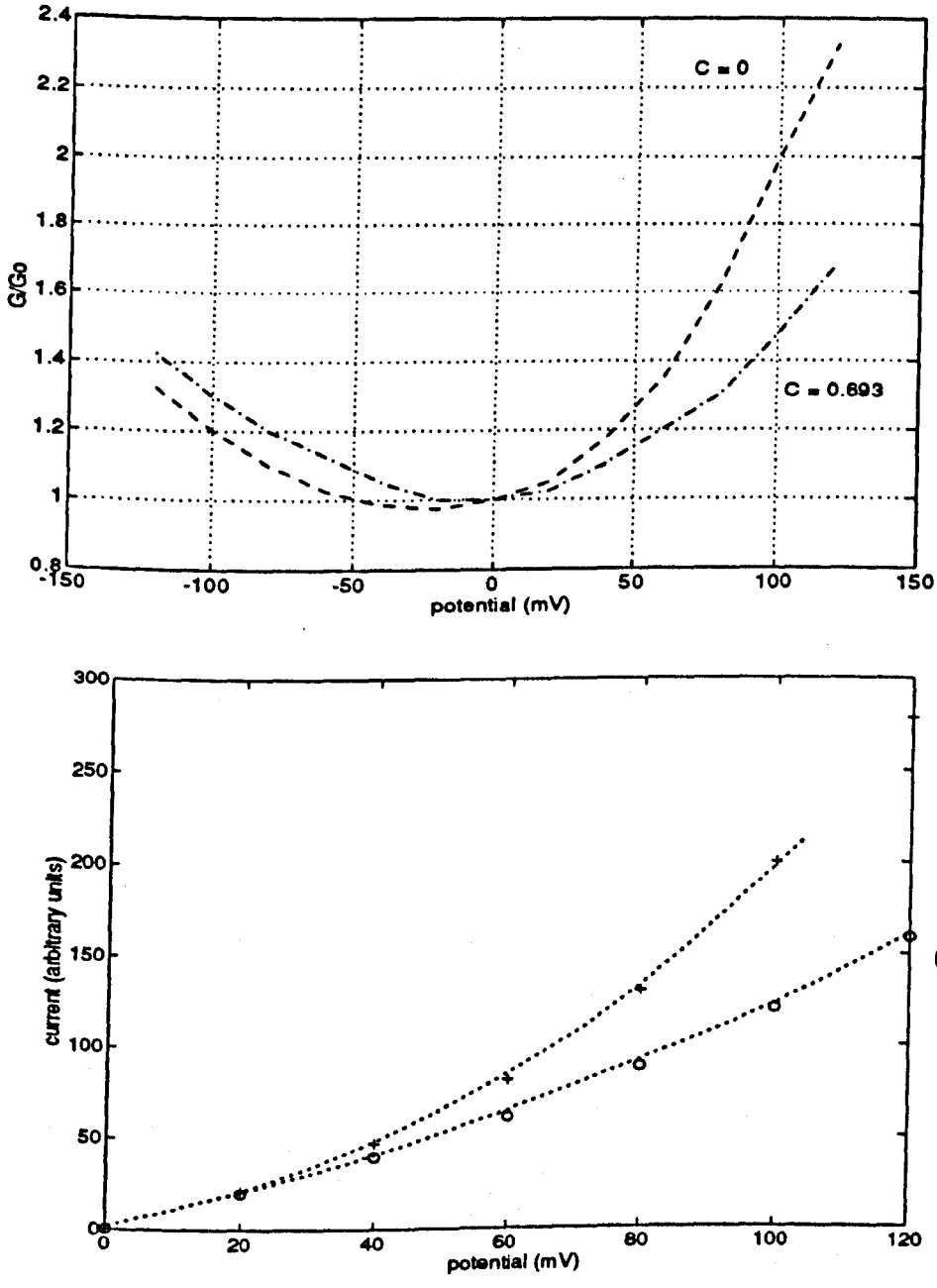

FIGURE 2.13 a) Voltage dependence of conductance of a monovalent cation in a channel with a fixed charge of -1 at the left end for low (c=0) and high (c=0.693 mol) concentrations. b) Corresponding current-voltage relationship deduced from a) for c=0.

(c) Sancho and Martinez (1991)

The approach of Sancho and Martinez (1991) was to solve the equations for potential in the presence of axial or dipole rings, in the equilibrium case ($J_n=J_p=0$), and then use the equilibrium potentials to calculate the current flow using the Nernst-Planck equations. Their model was for a gramicidin-like channel and included a net axial polarization to account for the charge distribution of the α-helical backbone of the protein monomer as well as accounting for polar side chains within the channel.

A study of the potential profiles within the channel as a function of dipole position (Figure 2.14), shows that a radial component of the dipole moment is more effective in changing the potential barrier than the corresponding axial dipole moment. When the dipole is located centrally the potential profile is symmetrical. As the axially directed dipole shifts towards the channel mouth, the symmetry is lost and the negative values of potential increase. For a radial component, of +1D, with positive end of the dipole pointing away from the axis, the shift is in the same direction but the negative potential maximum decreases (Figure 2.14b).

Figure 2.15a shows calculated conductances for different values and orientations of dipole moments. The dipole rings are situated in representative mean positions of $\pm$ 0.8 nm to model a gramicidin dimer made up of monomers of the same type. The similarity between the theoretical plots of conductance (Figure 2.15a) with the experimentally obtained conductances of modified gramicidins is striking (Figure 2.15b). When the dipole moment is small, superlinear I/V behaviour is found and when the dipole moment is large the I/V behaviour is sublinear. Sancho and Martinez (1991) use this same approach to account for asymmetrical I/V behaviour in hybrid channels where the dimer is formed from different monomers.

This model gives the first indication that a dipole rotation in response to applied voltage is sufficient to 'gate' the channel current. This means that geometrical changes in the channel (see section 2.5.2) are not always necessary for changing the channel conductance. See for example the changes in normalised conductance in Figure 2.15c when the magnitude and orientation of the dipole are changed.

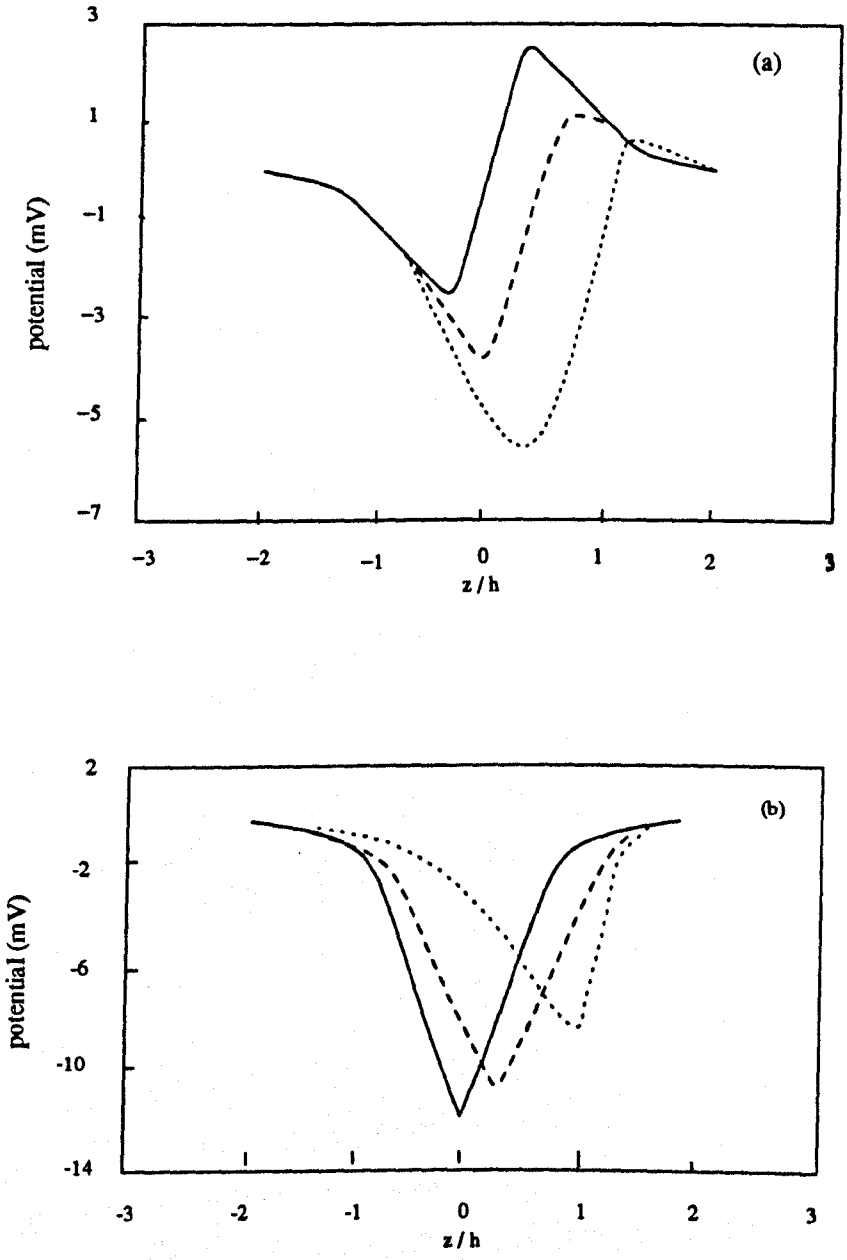

FIGURE 2.14 Potential created by a dipole ring with a radius of 0.5 nm and situated at different positions along the channel normalised to the channel half length, h (1.25 nm). The curves are for dipole positions (–) 0 nm, (---) 0.5 nm, (...) 1 nm. a) P_{axial} = +1D, P_{radial} = 0 (positive moment means that positive end of dipole is pointing toward nearest end of channel). b) P_{axial} = 0, P_{radial} = +1D (positive end of dipole pointing away from axis). (Sancho and Martinez, 1991)

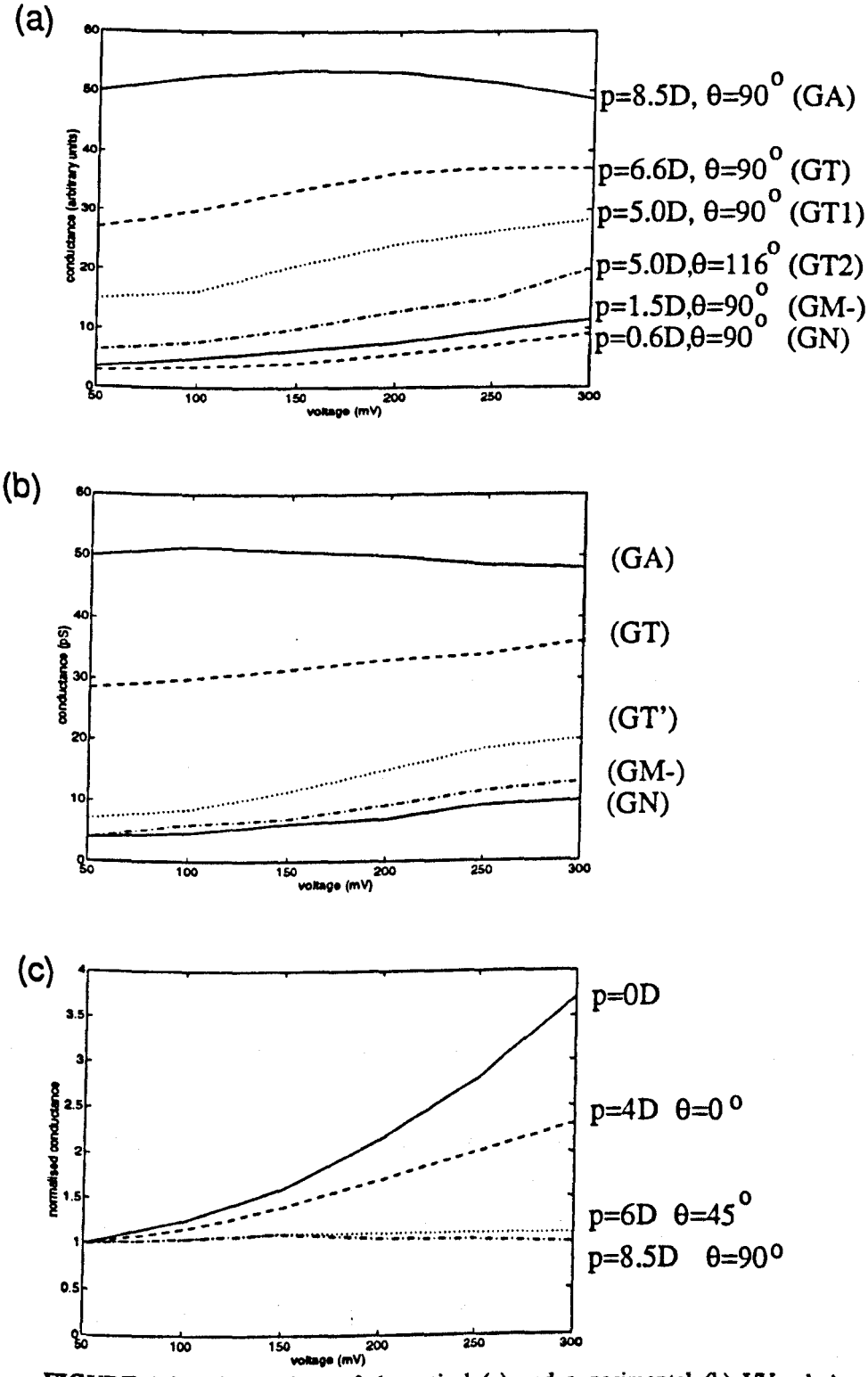

FIGURE 2.15 Comparison of theoretical (a) and experimental (b) I/V relationships for various gramicidins with different amino acid residues in positions 9,11,13 and 15.GA, tryptophan, native gramicidin A; GT, tyrosine; GT', benzyl tyrosine; GM-, phenylalanine; GN, naphthyl. (c) Effect of dipole moment and orientation The dipole rings are situated in representative mean positions of ± 0.85 nm to model a gramicidin dimer. θ is the angle between the dipole moment and the z-axis in the channel. (From Sancho and Martinez, 1991 and Martinez and Sancho, 1992)

2.4.3 Kinetic Models

2.4.3.1 Introduction

In the previous section ion permeation was considered to be a smooth flow of particles through a continuum. Alternatively, ion permeation through channels in membranes can be regarded as a process of moving from bulk water over a sequence of energy barriers and back to bulk water (Figure 2.16). Deviations from independence such as saturation of fluxes can be explained by such models if it is assumed that ions must bind to certain sites within the pore as part of the permeation. An example of non-independence of ion flow is illustrated for gramicidin A in Figure 2.17. The single channel conductance is seen to vary with the concentration and nature of the cation. As the concentration of sodium ions is increased, the single channel conductance reaches a limiting value, i.e. saturates. For some ion species, the single channel conductance passes through a maximum and then decreases; this is known as inhibition.

If ion movement is independent of all other ions the kinetic or rate-theory models are merely alternatives to the continuum approach. In this research the emphasis has been on comparing the predictions of continuum models with the experimental results. Therefore, only a basic overview of kinetic models will be given. Reviews of rate-theory models can be found in Hille (1984), Stein (1986), Cooper *et al.* (1985) and Levitt (1986) whilst a thorough discussion of ion movement through channels is given by Laüger (1980, 1984, 1985).

2.4.3.2 Single Occupancy Channel

The simplest kinetic model assumes that there is only one ion at a time in the channel and therefore assumes no ion-ion interactions. However, there may be several internal sites for interaction with ions and the channel may be permeable to more than one ion. The simplest saturable system has one binding site, X, and a permeating cation, S. The steps of permeation from side 1 to side 2 of the membrane become

$$X + S_1 \underset{k_{-1}}{\overset{k_1}{\rightleftharpoons}} XS \underset{k_{-2}}{\overset{k_2}{\rightleftharpoons}} X + S_2 \qquad (2.29)$$

where the rate constants k_1, k_2, k_{-1}, k_{-2} are, in general, dependent on voltage. X is the empty channel and it can interact with ion S_1 from side 1 of the membrane or with ion S_2 from side 2 of the membrane. The rate of formation of the intermediate XS is

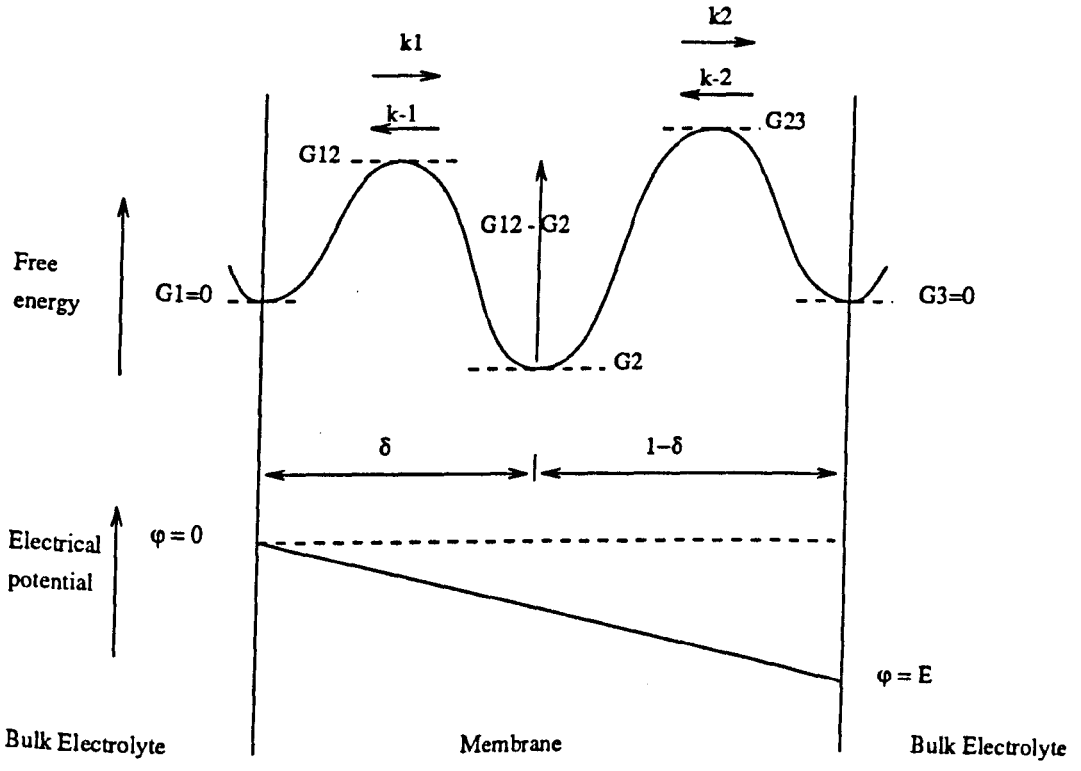

FIGURE 2.16 Barrier model of a channel. (Adapted from Hille, 1984)

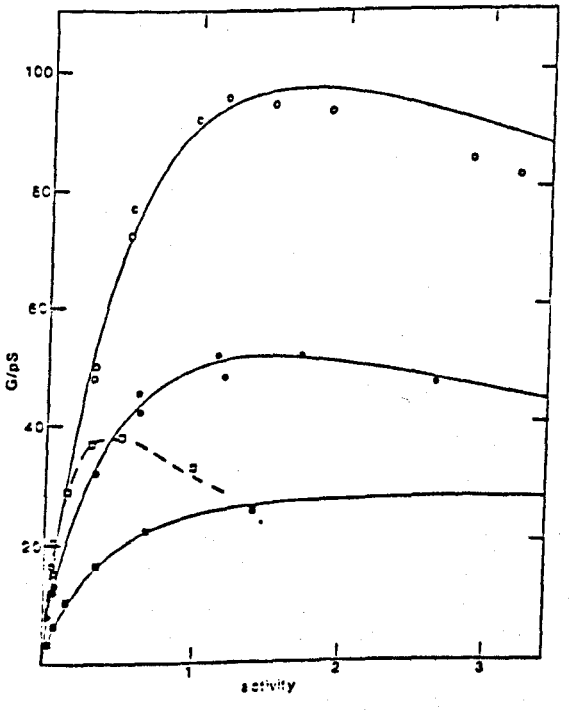

FIGURE 2.17 Variation of the conductance of the gramicidin A channel with the nature and concentration of the cation. (o) CsCl, (•) KCl, (open square) TlCl, (filled square) NaCl. The curves are theoretical fits of a model involving a two-site channel. (From Hladky and Haydon, 1984)

determined by the rate constant k_1 from side 1 and k_{-2} from side 2. The rate constants for the breakdown of the intermediate is given by k_{-1} and k_2. Figure 2.16 shows a two barrier model with one site inside the channel. The energy well in the centre is the free energy state of the intermediate XS. To reach XS from $X + S_1$ or from $X + S_2$ the system has to pass through transition states and the free energies of these activated states are represented by the activation energy barriers in Figure 2.16. The rate constants in this model are the rate at which jumps or hops occur across the energy barriers. The relation between the rate constants and heights of the energy barriers are given by Eyring's transition rate theory (Glasstone *et al.*, 1941). The value of k_{-1} at zero membrane potential is given by

$$k_{-1} = \frac{kT}{h} \exp-\left(\frac{G_{12} - G_2}{RT}\right) \tag{2.30}$$

where R is the gas constant, T is the absolute temperature and kT/h is a universal frequency having dimensions of $(\text{time})^{-1}$. The values of the other rate constants, k_1, k_2 and k_{-2}, can be calculated for zero potential in a similar manner. This relation means that an increase by amount RT in the height of the activation energy barrier corresponds to an e-fold decrease in the rate constant. The height of the activation energy barrier depends on the detailed chemical structure of the transition complex XS. If many bonds have to be broken during formation of the transition state or a significant increase in the order is required, then the activation energy will be high. If the substrate S is electrically charged and there is an additional potential gradient across the channel or local potential gradient within the channel, then electrical forces will contribute to the height of the energy barrier. The energy barrier may be raised or lowered depending on the direction of the electric field and the charge on the substrate. In Figure 2.16 δ represents the fraction of the total electrical potential dropped between the outside of the membrane and the energy well and is often called the electrical distance. If the energy maxima lie at an electrical distance halfway between neighbouring minima the rate constants can be written as

$$X + S_1 \underset{k_{-1}\exp\left(\frac{\delta v}{2}\right)}{\overset{k_1 \exp\left(\frac{-\delta v}{2}\right)}{\rightleftharpoons}} XS \underset{k_{-2}\exp\left(\frac{(1-\delta)v}{2}\right)}{\overset{k_2 \exp\left(\frac{-(1-\delta)v}{2}\right)}{\rightleftharpoons}} X + S_2 \tag{2.31}$$

where k_1, k_{-1}, k_2 and k_{-2} are the rate constants at zero applied potential. 1-δ and δ are electrical distances as shown in Figure 2.16 and ν stands for zEF/RT.

From chemical kinetics (Hille, 1984) the steady state expression for current from side 1 of the membrane to side 2 is

$$I_{1\to 2} = ze\frac{k_{-1}k_{-2}[S_2] - k_1k_2[S_1]}{k_{-1} + k_2 + k_1[S_1] + k_{-2}[S_2]}. \tag{2.32}$$

When ions are present on only one side of the membrane the current simplifies to

$$I_{1\to 2} = -ze\frac{k_2}{(1 + k_{-1} - k_{-2})/k_1[S_1]}. \tag{2.33}$$

Writing equation (2.33) as

$$I(E) = \frac{I_{max}(E)}{1 + K_s(E)/S} \tag{2.34}$$

we have a function identical to the Michaelis-Menten function used in enzyme kinetics, which predicts saturation as the concentration of substrate (or in the case of channels the permeant ion) is increased, as shown in Figure 2.18. It is interesting to compare this with the saturation in ion flux demonstrated by the electrostatic model of Levitt (1985) in Section 2.4.2.1, which was due to screening of fixed charges within the channel by counter ions.

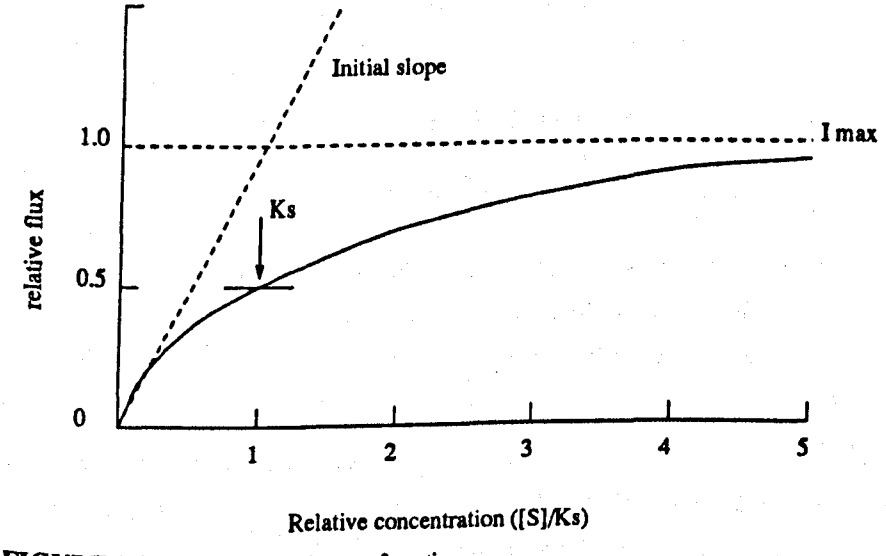

FIGURE 2.18 Michaelis-Menten function.

The kinetic model can be extended to include more than one binding site, as shown below:

$$X + S_1 \underset{k_{-1}}{\overset{k_1}{\rightleftharpoons}} XS_1 \underset{g_2}{\overset{g_1}{\rightleftharpoons}} XS_2 \underset{k_{-2}}{\overset{k_2}{\rightleftharpoons}} X + S_2 \qquad (2.35)$$

where two new rate constants g_1 and g_2 are introduced to describe the transition rates of the ion between two sites within the channel. This model takes into account the finite thickness of the membrane and allows for the likely situation that the ion takes more than one step or jump in its passage across the membrane. Pullman and Etchebest (1983), as reviewed by Stein (1986), computed from first principles an activation energy profile for gramicidin which supports the concept of two binding sites within the channel. Stein (1986), using the methods of Britton (1966, 1975), shows how the unidirectional flux of such a system can be calculated by successive replacement. He shows that a channel which can be occupied by only one ion at a time, no matter how many binding sites it possesses, will have a concentration dependence exactly like a one site channel. Stein (1986) also describes how the measurable transport parameters, such as the maximum conductance and the substrate concentration giving one half of the maximum conductance, depend on the applied voltage. These measurable parameters can be used to determine the voltage dependence of the rate constants by making assumptions about the potential drop across the membrane (e.g. in the absence of an applied potential, the system is assumed to be symmetrical).

2.4.3.3 Multiple Occupancy Channel

The experimental findings with gramicidin, which show curves of conductance against concentration that go through a maximum (Figure 2.17), cannot be accounted for by the single occupancy channel model. The explanation of this deviation has been made for many years in terms of multiple occupancy channels. The favoured model has been the long narrow channel within which ions cannot pass one another. The simplest multiple occupancy model is one in which there are two binding sites within the channel and both can be occupied. Ion-ion interactions are usually limited in this type of model to nearest neighbour interactions. As the concentration of the bathing solution is raised symmetrically, the channel reaches a state where both binding sites are occupied. The conductance decreases because the flux depends on the existence of

vacant sites within the channel to which ions may move. At high concentrations, any vacancy formed by one ion jumping into the solution, is immediately cancelled by another ion coming back in from solution. Nuclear magnetic resonance spectroscopic studies have provided evidence for the existence of a two binding site model in gramicidin (Urry *et al.*, 1980, 1982). Gramicidin is the most widely studied of all ion channels and detailed studies of double occupancy models have been made by many authors including Hladky and Haydon (1984) and Levitt (1982).

2.5 MODELS OF VOLTAGE-GATING

2.5.1 Introduction

Gating is a reversible change of the channel from a high conducting (open) state to a lower or non-conducting (closed) state. There are two main gating mechanisms that occur in channels. The first, ligand-induced gating, occurs when a specific substrate binds to a portion of the channel and consequently alters its conformation. The second, voltage-induced gating, is the mechanism investigated in this study. In this mechanism a component of, or protein companion to, the channel is sensitive to the sign and/or magnitude of the transmembrane potential. The voltage sensitive component of the channel may be a collection of charges or equivalent dipoles that moves under the influence of the membrane electric field. An example of this type of channel is the potassium channel from sarcoplasmic reticulum (Labarca *et al.*, 1980).

In the present work it is established unequivocally that porin undergoes voltage-gating. It should be noted though, that when this work commenced there was some dispute as to whether voltage-gating in porin was real. Benz (1985) suggested that such observations were merely experimental artefacts and that porin in its native state is unlikely to undergo voltage-gating. These arguments will be discussed further in Chapter 3, which reviews the structure and function of porin channels.

2.5.2 Gating Mechanisms

A hypothetical channel is shown in Figure 2.19. When open, the channel forms a water filled pore extending fully across the membrane but may narrow to molecular dimensions over a short distance. Gating in this hypothetical channel requires a conformational change in the protein such that a 'gate' is moved into and out of an occluding position in the channel. The probabilities of opening and closing are controlled by a voltage sensor. It is possible that the sensor is remote from the gate or that one part of the protein consists of both gate and sensor. Experimental work on a number of voltage sensitive cation channels (reviewed by Hille, 1984) indicates that the voltage sensor is an intrinsic component of the protein. The voltage dependent anion

channel (VDAC) of mitochondria may have a voltage sensor which is readily accessible from the aqueous channel (Colombini, 1980). The gate itself could be comprised of a swinging door or a slider as shown diagrammatically in Figure 2.20. Jan and Jan (1989) review voltage sensitive ion channels, with emphasis on the cation selective channels, i.e. sodium, potassium and calcium channels. They discuss the evidence for the position of the gate and the sensor in these channels. The hypothetical channel in Figure 2.19, with the gate located at one end of the channel, could well be a good model for the sodium channel. Specific substrates are still able to enter and interact with the channel from one side when the channel is in its non-conducting state.

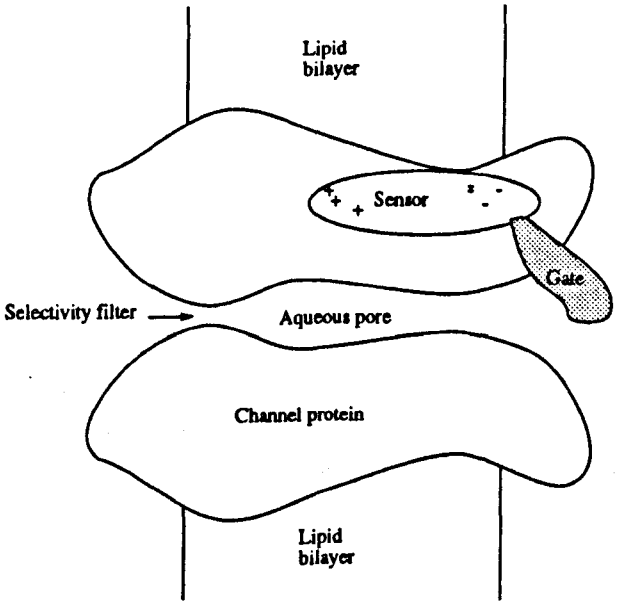

FIGURE 2.19 Working hypothesis for a channel. (Adapted from Hille, 1984)

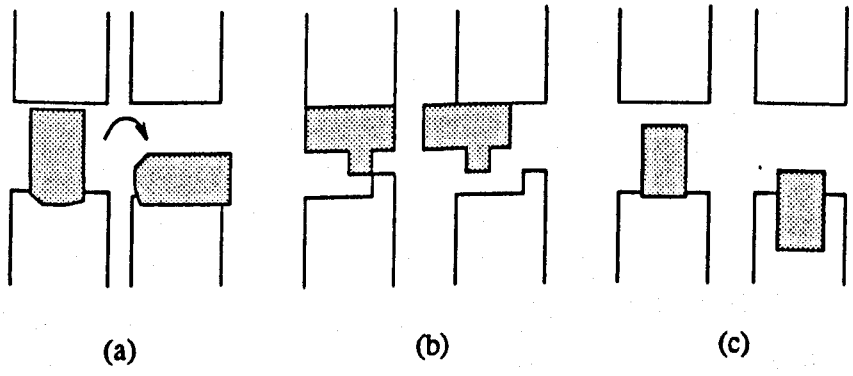

FIGURE 2.20 Gate mechanisms that swing or slide.

It is possible that the presence of a transmembrane voltage in some channels results in a more widespread conformational change which 'pinches' off the entire length of the channel. Unwin (1989) describes small but co-operative tilting movements of α-helical type channels which are translated into large changes of pore diameter. The movement of sub-units is predominantly parallel to the membrane and energetically possible because the partitioning of the polar and non-polar protein surfaces between lipid and water remain unperturbed. Two channels have been shown to display these tilting movements by using cryo-electron microscopy (Unwin, 1989). These are the calcium sensitive gap junction channel whose conformation change is shown in Figure 2.21 and the ligand-gated acetylcholine receptor channel. Local movement of charged groups or dipoles in voltage sensitive channels could also trigger such conformational changes.

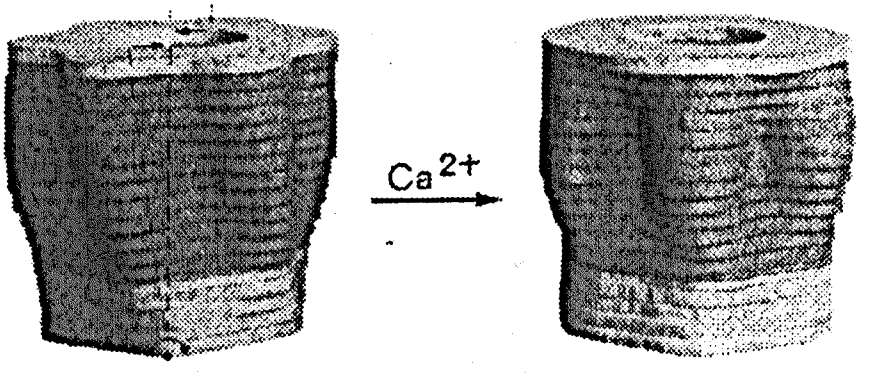

FIGURE 2.21 Two configurations of an ion channel. Cryo-electron microscopy and three dimensional image analysis have revealed two calcium sensitive configurations of the gap junction channel. (From Unwin, 1989).

Some channel forming antibiotics such as gramicidin A, alamethicin and amphotericin B have probabilities of channel formation which depend super-linearly on the antibiotic concentration. This is thought to reflect aggregation of sub-units to form the channel. The conducting gramicidin channel is made up of two monomers (Bamberg and Laüger, 1973) as shown in Figure 2.22. Alamethicin and amphotericin are made up of 6-12 monomers which are believed to form a barrel as shown in Figure 2.22 (Hall *et al.*, 1984). The association and dissociation of the monomers is strongly voltage dependent for alamethicin which has multiple conducting states. Alamethicin has been observed to have a large molecular dipole that could interact with membrane

fields (Archer and Cafiso, 1991). Kinetic models describing conductance changes induced by voltage in gramicidin and alamethicin channels can be found in Lakshminarayanaiah (1984) and Ehrenstein and Lecar (1977).

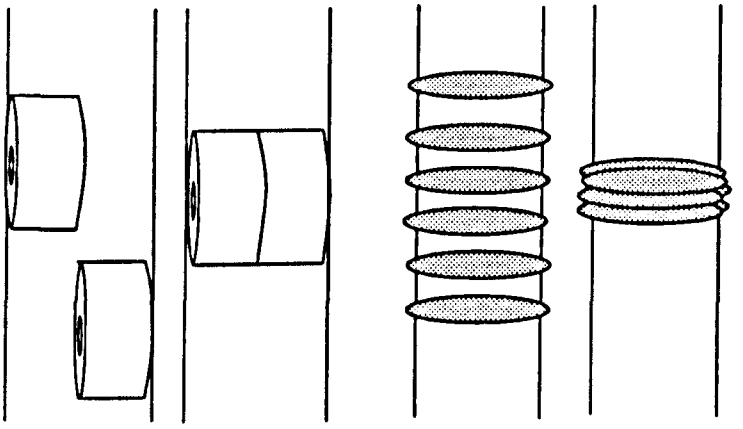

(a) (b)

FIGURE 2.22 Possible gating mechanisms for a) gramicidin and b) alamethicin and amphotericin.

The porin channel is made up of three sub-units (trimeric) and each individual sub-unit (monomer) is able to gate independently (Chapter 3). Current information on the 3-D structure of porin (Cowan *et al.*, 1992) show regions of the protein that extend as long loops into the channel mouth (Figure 3.7). The movement of one or more of these loops to occlude the channel entrance could very well act as a gate. It seems unlikely that the monomers making up the porin trimer could dissociate and re-associate as in gramicidin and alamethicin. The interaction between monomers to form the porin channel, which consists of a triplet of pores (Section 3.4.3), is very strong. There is a large area of interaction between the monomers and consequently the trimer is very robust; it is not easily denatured by detergents or organic solvents. In addition, the probability of channel formation does not depend super-linearly on porin concentration.

2.5.3 Two State Models

The simplest model of voltage-dependent conductance resulting from channel gating events considers that channels have two states, one open and one closed (Ehrenstein and Lecar, 1977). The rate equation for the transitions between the two states is written as

$$closed \underset{\beta}{\overset{\alpha}{\rightleftharpoons}} open \tag{2.36}$$

where α is the rate constant for the channel opening from the closed state and β is the rate constant for channel closing from the open state. If we consider an energy barrier representation of this model (Figure 2.23) then following the method of Section 2.4.3.2 the rate constants become

$$\alpha = \frac{kT}{h}\exp\left[\frac{-w}{kT}\right] \tag{2.37}$$

and

$$\beta = \frac{kT}{h}\exp\left[\frac{-(w-\Delta w)}{kT}\right]. \tag{2.38}$$

At equilibrium

$$n_o\,\beta = n_c\,\alpha \tag{2.39}$$

where n_O is the number of open channels and n_C is the number of closed channels. Substituting for α and β from equations (2.37) and (2.38) gives

$$\frac{n_o}{n_c} = \exp\left(\frac{-\Delta w}{kT}\right). \tag{2.40}$$

The energy difference between the two states is given by the sum of the intrinsic energy difference between the two conformations (open and closed), Δw_{conf}, and the work needed to push charges or twist dipoles from one state to the other, Δw_{elec}; that is :

$$\Delta w = \Delta w_{conf} + \Delta w_{elec}. \tag{2.41}$$

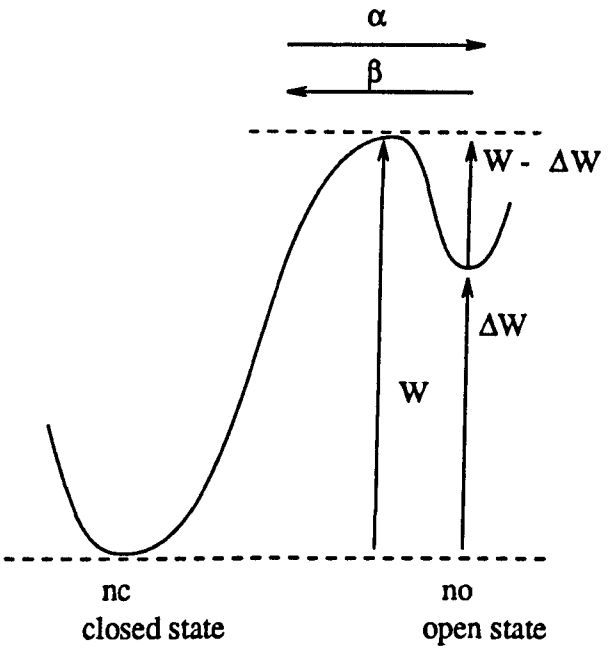

FIGURE 2.23 Energy barrier representation of a two state channel. nc is the population in the closed state, no is the population in the open state. w and (w-Δw) are the energy barrier heights and α, β the rate constants for hopping over the barriers.

If one assumes that the change from one state to the other moves a gating charge of valence z from one side of the membrane to the other across the full membrane potential drop, V, then

$$\Delta w_{elec} = zqV. \tag{2.42}$$

Some authors prefer to use an equivalent dipole moment charge and this is related to the gating charge by

$$\mu = zqd$$

where d is the assumed thickness of the membrane. It is possible to detect the small currents, known as gating currents, associated with the movement of the gating charge. However, it requires the use of patch clamp techniques (see Chapter 3) and the reduction of ionic fluxes by replacing permeant ions with impermeant ones to make the gating current more visible.

The *E. coli* porins OmpC and OmpF have many charged amino acids per monomer and the energy dissipated during gating may in fact be partitioned into the motions of many charged residues, each residue only moving through a small fraction of the transmembrane potential. It has also been shown by Edmonds (1990) that the gating charge transfer measured prior and during channel opening may stem from ionisable sites which remain fixed in position but change their state of charge in response to the transmembrane voltage. These changes involve proton migration across the membrane.

At potential V_0, for which half the channels are open and half are closed $\Delta w = 0$ and, therefore, we can write the energy as

$$\Delta w(V) = zq(V - V_0). \tag{2.43}$$

Equation (2.40) can be rewritten in terms of the applied potential V as

$$\frac{n_o}{n_c} = \exp\left(\frac{-zq(V - V_0)}{kT}\right) \tag{2.44}$$

which, upon rearranging, gives the fraction of open channels

$$\frac{n_0}{n_0 + n_c} = \frac{1}{1 + \exp\left[zq\left(\frac{V - V_0}{kT}\right)\right]}. \tag{2.45}$$

Figure 2.24 is a plot of the predicted fraction of open channels as a function of applied voltage and for different valences z of the gating charge. The voltage dependence is sigmoidal and the higher the charge the steeper the gradient at Vo (= 100 mV in this example). From equation (2.45) we may write the fraction of closed channels at any voltage as

$$\frac{n_c}{n_0 + n_c} = 1 - \frac{1}{1 + \exp\left[zq\left(\frac{V - V_0}{kT}\right)\right]}. \tag{2.46}$$

Equation (2.45) can also be written in terms of the relative conductance

$$\frac{G}{G_{max}} = \frac{1}{1+\exp\left[zq\left(\frac{V-V_0}{kT}\right)\right]}.$$

If g_0 is the open conductance of a single channel then

$$G = n_0\, g_0$$

and

$$G_{max} = (n_0 + n_c)g_0.$$

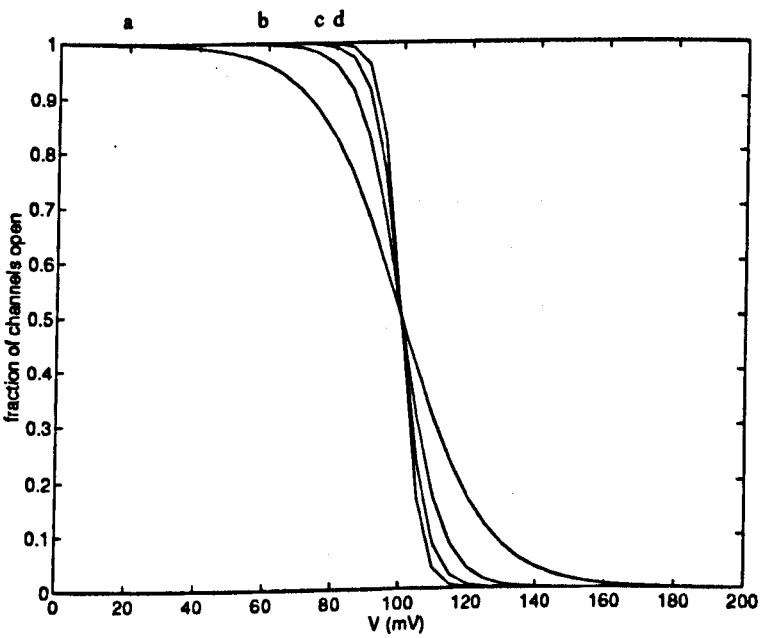

FIGURE 2.24 Fraction of open channels as a function of transmembrane voltage. Each curve represents a different charge valence: a=2, b=4, c=6 and d=8. These curves were calculated for Vo=100 mV.

It has already been stated that at $V=V_0$ the energy levels of the open and closed states are equal and this is shown diagrammatically in Figure 2.25a . If we assume that a change in transmembrane voltage from V_0 perturbs the energy levels of the open and closed states by equal and opposite amounts, i.e. $\pm\Delta w/2$, as illustrated in Figure 2.25b, we can write the rate constants α and β in terms of α_0 or β_0 ($\alpha_0=\beta_0$), the rate constants at $V=V_0$. Thus, assuming that the peak of the energy barrier is independent of voltage, the rate constants become

$$\alpha,\beta = \alpha_0 \exp\left[\mp\frac{zq(V-V_0)}{2kT}\right]. \tag{2.47}$$

If the rates of reaction in both directions follow first order kinetics, the relaxation time, τ, for the system can be described as

$$\tau = \frac{1}{\alpha+\beta} \tag{2.48}$$

Substituting for α and β in equation (2.48) and simplifying gives

$$\tau = \tau_{max}\,\mathrm{sech}\left[\frac{zq(V-V_0)}{2kT}\right] \tag{2.49}$$

where

$$\tau_{max} = \frac{1}{2\alpha_0}. \tag{2.50}$$

The τ versus V relationship is bell shaped (Figure 2.26) with the peak occurring at V_0.

For membranes with few channels the opening and closing rates can be determined directly and independently from the time course of the spontaneous opening and closing of individual channels. For a membrane with many channels the individual rates cannot be determined directly, but it is possible to deduce them from experimentally measured values of relative conductance and the relaxation time for the conductance to reach steady state (see Section 2.5.4).

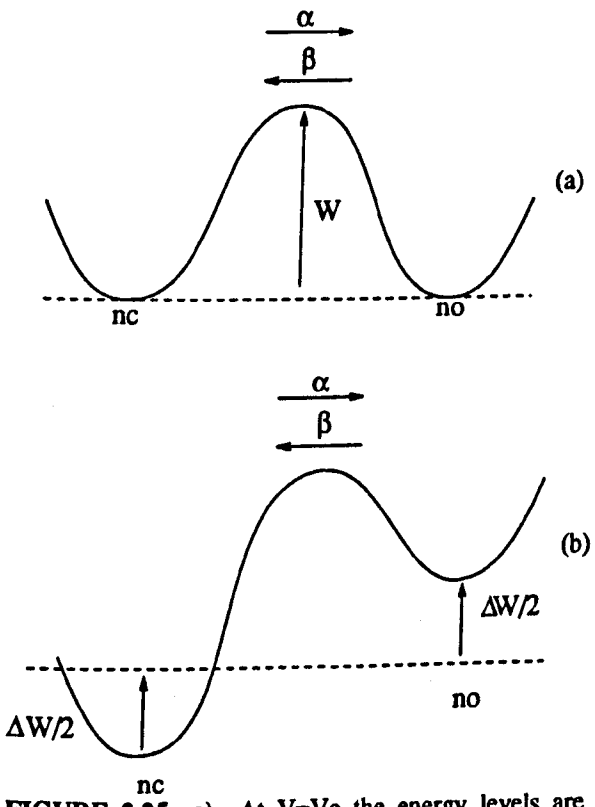

FIGURE 2.25 a) At V=Vo the energy levels are equal and half the channels are in the closed state and half in the open state. b) Changing the voltage lowers the energy of the closed state and raises the energy of the open state by the same amount (Δw/2). The height of the energy barrier is independent of voltage.

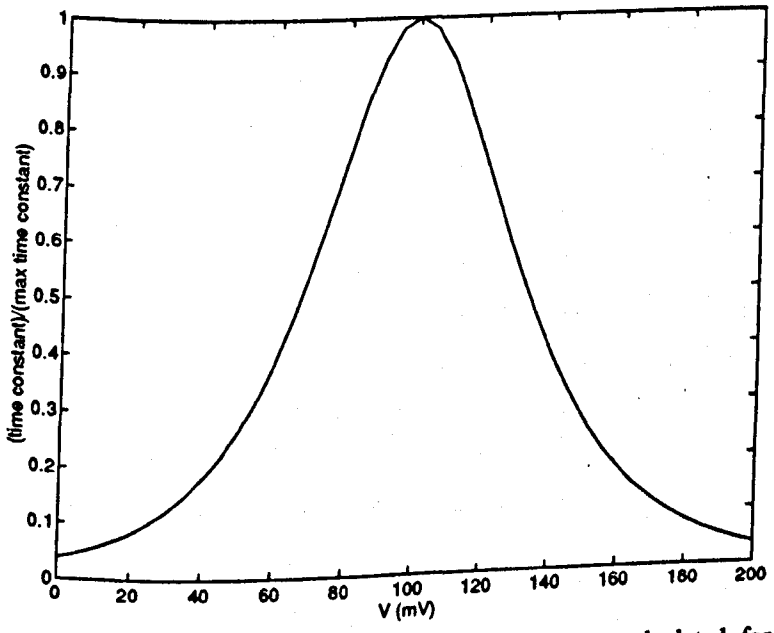

FIGURE 2.26 τ/τ_{max} versus transmembrane voltage calculated for Vo=100 mV.

2.5.4 Applications of the Two-State Model

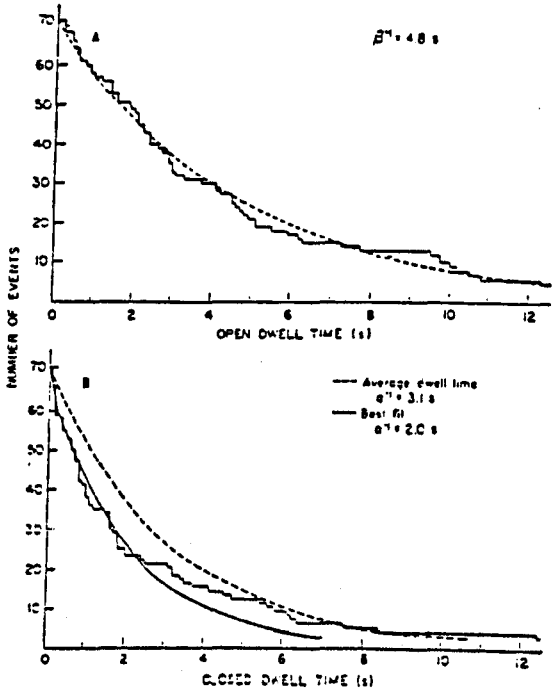

FIGURE 2.27 Distribution of dwell times for a single channel held at a constant potential of 53 mV. The graph shows the number of dwell times longer than the time indicated by the abscissa. (A) Open dwell times, τ=4.8 s. (B) closed dwell times, τ=3.1 s. (From Ehrenstein and Lecar, 1977).

Ehrenstein and Lecar (1977) used a two state model to describe the properties of excitability inducing material (EIM) in oxidised cholesterol membrane. At positive potentials the channels show two states of conductance, 80 and 400 pS in 0.1 M KCL. For membranes with only 1-6 channels which displayed single square current fluctuations, they measured the time duration between successive conductance transitions. They called this the dwell time, t_d, in one of the two conductance states. If the transition between the two conductance states is a Poisson process, then the probability of a transition per unit time is constant, i.e. is independent of the time measured from the previous transition. This should give rise to an exponential distribution of dwell times which is confirmed in Figure 2.27 where the data from a single EIM channel is plotted . The rate constant for such a conductance transition is given by

$$k_j = \frac{1}{\overline{t_d}} = \frac{m}{\sum t_{di}} \qquad (2.51)$$

where t_{di} is an individual dwell time, m is the number of jumps in a record and $\overline{t_d}$ is the average dwell time. The opening rate α is equal to the reciprocal of the average dwell time in the closed state and the closing rate β is equal to the reciprocal of the average dwell time in the open state. For a single channel, the fraction of time the channel was in the open state was found to follow a sigmoidal dependence on membrane potential, as predicted by equation (2.45). They found that log α and log β were linear functions of voltage and they could be written as

$$\alpha = \lambda \exp[-a(V - Vo)]$$
$$\beta = \lambda \exp[b(V - Vo)] \qquad (2.52)$$

where λ is the transition rate measured at the voltage Vo and a and b have dimensions mV^{-1}. A semi-logarithmic plot of the opening and closing rates as a function of voltage enabled λ, Vo and a and b to be found from the experimental data. In their experiments a≠b and this resulted in an aysmmetrical bell shaped curve for τ versus voltage with the peak shifted from Vo (Figure 2.28) as predicted by equation (2.48).

That a≠b implies, of course, that the gating charge is different for opening and closing events. This assumption should be questioned since it suggests that a gating charge does not return immediately to its original energy state when the channel opens. Such a system is not, therefore, a simple two-state system and could have, say, two open states and one closed state.

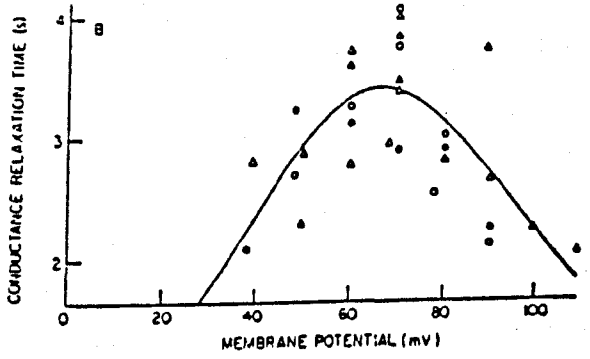

FIGURE 2.28 Conductance relaxation time as a function of potential. Data from three membranes is plotted indicated by triangles, open circles and filled circles. The parameters for the fitted curves were determined from previous experiments with one/few channels. Vo=58 ± 11 mV, λ^{-1} =8±7s, a=0.07 ±0.03 mV^{-1} and b=0.05 ±0.02 mV^{-1}.

To explain the asymmetrical experimental rate distribution in Figure 2.28, we adopt the more realistic assumption below, that entropy changes should be considered and included in the rate equations. The Gibbs free energy G is given by

$$G = H - TS \tag{2.53}$$

where H is the enthalpy and S the entropy. A change, ΔG, in the Gibbs free energy may be written as

$$\Delta G = \Delta H - T\Delta S \tag{2.54}$$

Substituting equation (2.54) into equation (2.30) gives a new expression for the rate constant, k_{-1}, i.e.

$$k_{-1} = \frac{kT}{h}\exp\left(-\frac{\Delta G}{RT}\right) = \frac{kT}{h}\exp\left(\frac{\Delta S}{R}\right)\exp\left(-\frac{\Delta H}{RT}\right). \tag{2.55}$$

The entropy contribution to the free energy is temperature independent and therefore becomes part of the pre-exponential factor, and the empirical activation energy determined by Arrhenius' classical equation is approximately equal to ΔH. Introducing unequal pre-exponential factors in the equations describing the rate constants is equivalent, then, to having different entropy terms in the two equations. This implies that the sign and/or magnitude of the entropy change experienced by a gating charge in going from the open to the closed state differs from that which it experiences in going from the closed to the open state. It would not be unrealistic to assume that the entropy change required for gating is reversed when the channel re-opens so that

$$\Delta S_{close} = -\Delta S_{open}. \tag{2.56}$$

To account for entropy changes, the equations derived by Ehrenstein and Lecar (1977) may be modified to

$$\alpha = A\exp\left[\frac{-aq}{2kT}(V - Vo)\right]$$

$$\beta = B\exp\left[\frac{bq}{2kT}(V - Vo)\right] \tag{2.57}$$

where A and B include the entropy factor. Using the above equations, the expression for τ becomes

$$\tau = \frac{1}{A\exp\left[\frac{-aq}{2kT}(V - Vo)\right] + B\exp\left[\frac{bq}{2kT}(V - Vo)\right]} \tag{2.58}$$

Theoretical plots of τ versus voltage using equation (2.58) and adjusting the parameters A, B, a, b, and Vo are shown in Figure 2.29. These show that the asymmetrical bell shaped curve in Figure 2.28 can be reproduced by adjusting the pre-exponential factors rather than the exponent.

The original definition of Vo in Section 2.4.3 was that at V=Vo the energy levels of the open and closed states are equal and that the population in each state is also equal, i.e. $n_O/n_C=1$. Substituting the expressions for the rate constants in equation (2.57) into the equilibrium equation (2.39) now gives the ratio of open to closed channels at steady-state, n_O/n_C as

$$\frac{n_o}{n_c} = \frac{A\exp\left(\frac{-a}{2kT}(V - V_0)\right)}{B\exp\left(\frac{+b}{2kT}(V - V_0)\right)}. \tag{2.59}$$

Inspection of the above equation shows that if $A \neq B$ then, at $V=V_O$, $n_O/n_C=A/B$ so that the open and closed populations are no longer equal, even though their energy states are equal. Equation (2.59) can also be written as

$$\log_e \frac{n_0}{n_c} = -\left(\frac{a+b}{2kT}\right)qV + \left(\frac{a+b}{2kT}\right)qV_0 + \log_e \frac{A}{B}. \tag{2.60}$$

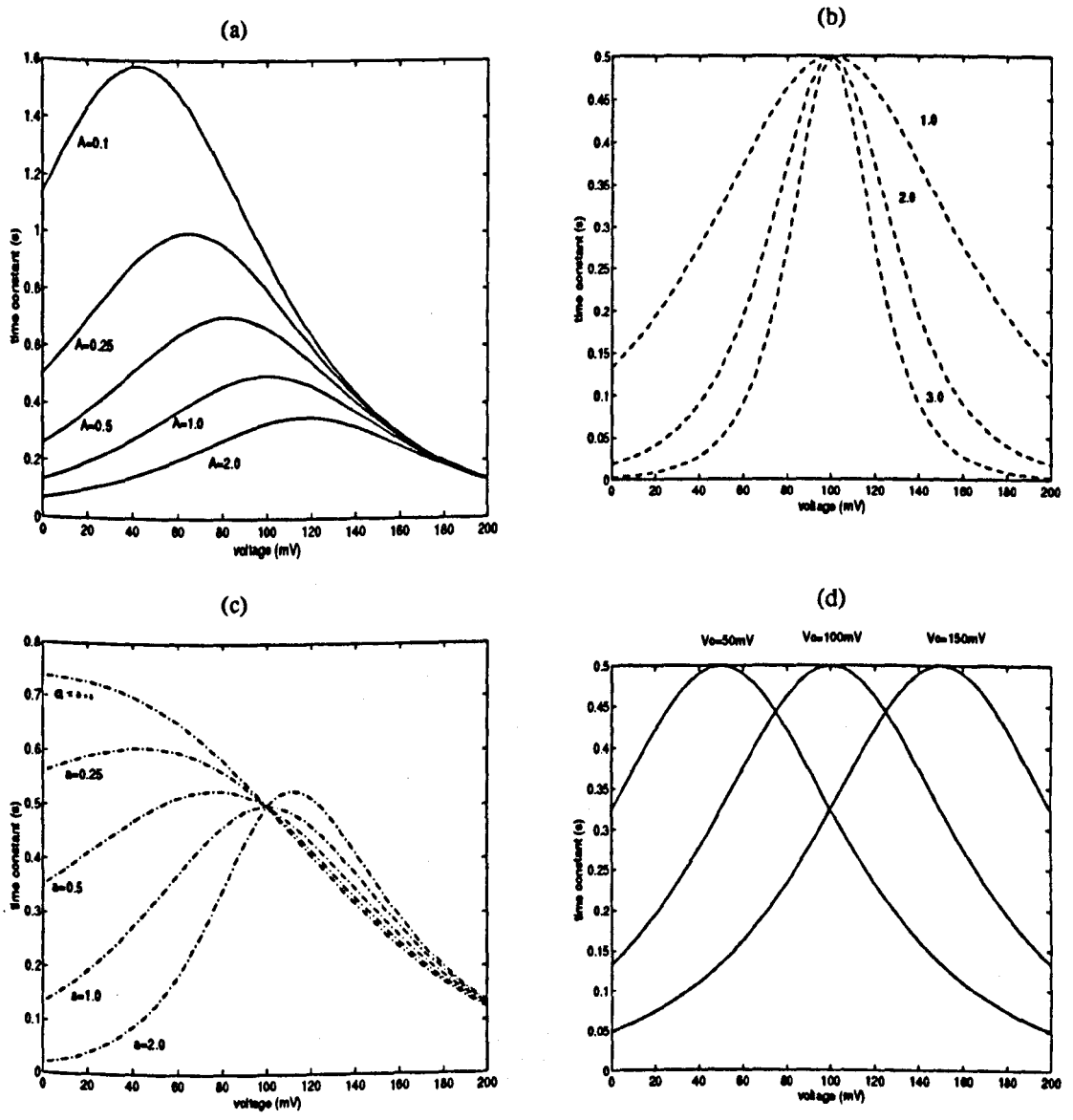

FIGURE 2.29 Theoretical plots of τ versus applied voltage using equation 2.57 to calculate the rate constants α and β. (a) Vo=100 mV, A is adjusted as shown whilst B, a and b are set to 1.0. (b) Vo= 100 mV, A=B=1.0, a and b are equal but are increased as indicated. (c) Vo=100 mV, A=B=1.0, b=1.0 and a is adjusted. (c) A=B=1.0, a=b=1.0, Vo is adjusted.

If this model applies, then a plot of $\log_e(n_o/n_c)$ versus applied voltage, V, should give a linear relationship with a slope identical to the Ehrenstein and Lecar model, but with an intercept differing by the term $\log_e A/B$.

The two state model as applied by Ehrenstein and Lecar (1977) only considered positive applied potentials. In fact, EIM channels also show gating with negative applied potentials and two separate closed states have been identified, one for positive bias and one for negative (Ehrenstein *et al.*, 1977). When the voltage was changed from extreme positive to extreme negative values, transitions between the two closed states always proceeded via the open state. Thus it would be more appropriate to consider the EIM channels as three-state systems for which the rate equation is written as

$$closed \underset{\alpha 2}{\overset{\beta 2}{\rightleftharpoons}} open \underset{\alpha 1}{\overset{\beta 1}{\rightleftharpoons}} closed.$$

The kinetics of such three-state systems are discussed by Arndt and Roper (1975).

The two-state model also assumed that the rate constants depend only on the actual membrane potential and are independent of the past history of the membrane. As will be seen, this assumption was not always found to be true in the present experiments with lipid bilayers and porin channels.

2.6 CONCLUDING REMARKS

Models describing ion flow through channels range from the very simple ohmic equivalent models, which make no attempt to describe how ions are actually moving within a channel, to the more complex, which may include the voltage profile within the channel and ion-ion interaction. The electrostatic models have been shown to predict reasonably well some of the properties of real channels such as gramicidin. The main features of channel behaviour predicted by these models will, therefore, be used in the interpretation of the experimental results from bilayer membranes containing porins (Chapter 6).

The two-state model which Ehrenstein and Lecar (1977) applied to membranes containing EIM has been developed to include entropy changes during gating. This resulted in asymmetrical, bell-shaped distributions of relaxation times without the need to invoke different magnitudes of gating charge for opening and closing events. In Chapter 7 the results of voltage-gating experiments will be compared to the predictions of the original two-state model (Ehrenstein and Lecar, 1977) and also the modified two-state model.

CHAPTER 3

PORIN STRUCTURE AND FUNCTION

3.1 INTRODUCTION

The cell envelope of Gram-negative bacteria such as *Escherichia coli, Salmonella typhimurium* and *Pseudomonas aeruginosa* consists of three different layers: the outer membrane, the peptidoglycan layer and the inner, cytoplasmic, membrane (Figure 3.1). The inner membrane acts as a diffusion barrier and contains a large number of different transport systems as well as containing the components of the respiratory chain. The peptidoglycan (or murein) layer protects the cell from osmotic lysis and gives the cell mechanical rigidity. The outer membrane is a molecular sieve with well defined exclusion limits for hydrophilic substrates. The active components of the molecular sieving properties of the outer membrane are a major class of proteins called matrix proteins (Rosenbusch, 1974) or porins (Nakae, 1976). Gram-negative bacteria may be the ancestors of mitochondria and chloroplasts according to the endosymbiotic theory (i.e. the symbiosis of two or three prokaryotic cells resulting in the first eukaryotic cell). In agreement with this theory, mitochondria have outer membranes with pores having similar properties to the bacterial porins, in particular, their large size. Mitochondrial porin is discussed by Benz *et al.* (1985). This chapter however will concentrate on the structure and function of porins from Gram-negative bacteria, beginning with a description of the outer membrane of Gram-negative bacteria where porins are to be found.

3.2. OUTER MEMBRANE OF GRAM-NEGATIVE BACTERIA

3.2.1 Outer Membrane Permeability

The structure and composition of the outer membrane of Gram-negative bacteria have been discussed in a number of reviews (Nikaido and Nakae, 1979., Lugtenberg and van Alphen, 1983). Here are discussed only the basic features of the outer membrane required to understand the function of the porins and to appreciate those features of the outer membrane, and of the porins, which can be exploited in the isolation of the proteins. Of the three layers of the cell envelope the outer membrane is specific to Gram-negative bacteria. It is extremely important in the physiology of Gram-negative bacteria making them resistant to host defence factors such as lysozyme, β-lysin and various leukocyte proteins, which are very toxic to Gram-positive bacteria. In enteric Gram-negative bacteria, which line the intestinal tract of animals, the outer membrane

has developed into a very effective barrier giving protection to the cells from the detergent action of bile salts and degradation by digestive enzymes (Nikaido and Nakae, 1979). At the same time the outer membrane of enteric and some other Gram-negative bacteria acts as a strong permeability barrier to some antibiotics (e.g. macrolides, novobiocin, rifamycins, lincomycin, clindamycin and fusidic acid) that are effective against other bacteria . Even if the barrier is not perfect and some antibiotic diffuses through the outer membrane, the bacterium needs only to inactivate the relatively small amounts of penetrating antibiotic. High levels of resistance are easily established and this is borne out by the prevalence of Gram-negative infections in modern hospitals. The outer membrane is therefore an extremely effective permeability barrier and the description of the major components of the outer membrane in the following sections will indicate how this is achieved.

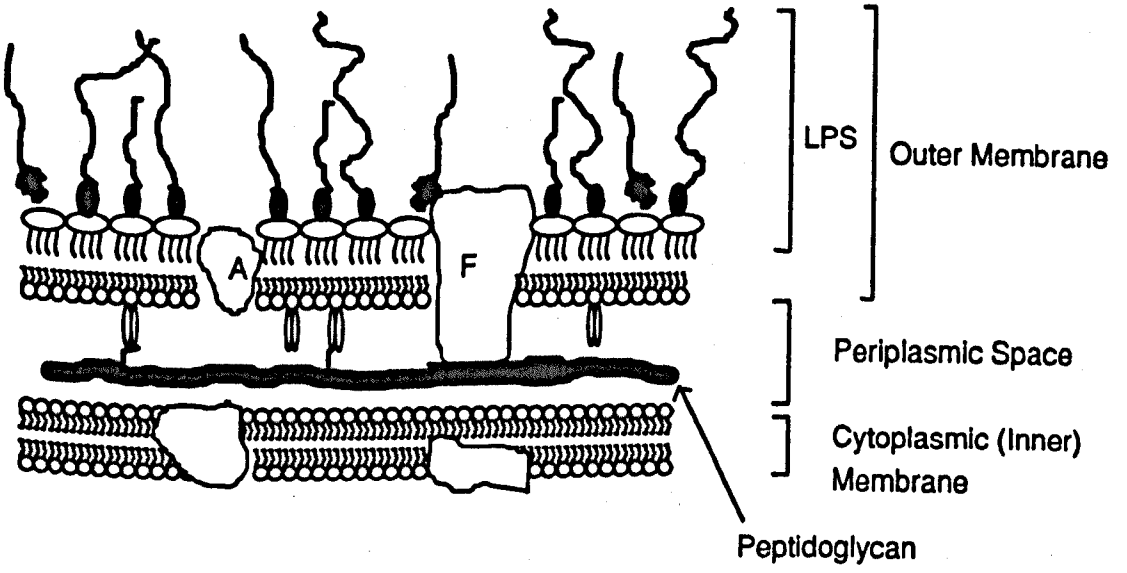

FIGURE 3.1 Structure of the cell envelope of enteric bacteria. (A) OmpA; (F) OmpF trimer; (LPS) lipopolysaccharide. Adapted from Benz (1985).

3.2.2 Phospholipids

The outer membrane of Gram-negative bacteria contains lipids, lipopolysaccharides (LPS) and proteins as major components. The major lipid of the enteric bacteria *E. coli* and *S. typhimurium* is the zwitterionic phospholipid phosphatidylethanolamine. Besides this neutral lipid the outer membrane contains small amounts of the negatively charged phospholipids phosphatidylglycerol and diphosphatidylglycerol; the latter is also known as cardiolipin (Benz, 1985). The fatty acid residues of the phospholipids

contain mostly C18 chains. In enteric bacteria the phospholipids are located exclusively in the inner monolayer of the outer membrane (see Figure 3.1) where they cover about 50% of the surface; the rest is covered by proteins. Non enteric bacteria like *Neisseria gonorrhoeae* and some of the cyanobacteria also contain phospholipids in the outer monolayer of the membrane.

3.2.3 Lipopolysaccharides

The extracted porin used in the present work always had LPS associated with it. Since this may have some bearing on the experimental results a short discussion of the main properties of LPS follows.

The outer surface of enteric bacteria is covered by about 40% LPS and 60% protein. LPS are a family of structurally related amphipathic molecules showing the same general architecture. A review of bacterial lipopolysaccharides is given by Mayer *et al.* (1989). The molecule consists of three distinct regions, as shown in Figure 3.2. These are lipid A, a core region of polysaccharide and a chain of polysaccharide called the O-specific chain or O-antigen region. Lipid A is the hydrophobic anchoring region of LPS and it is highly conserved in all Gram-negative bacteria. Unlike phospholipids which have only two fatty acids connected to the backbone structure, the LPS molecule has six or seven fatty acids linked to a glucosamine disaccharide backbone as shown in Figure 3.3. Unlike phospholipids all of the fatty acid chains in LPS are saturated and some are 3-hydroxy fatty acids. Some of the fatty acid residues are linked to the 3-hydroxy group of another fatty acid, producing a 3-acyl-oxy-acyl structure which is characteristic of lipid A. The presence of these hydroxy fatty acids and absence of unsaturated fatty acids are important in maintaining the organised state and permeation barrier of the outer membrane (Nikaido and Vaara , 1985). The structural diversity of the core region (see Figure 3.2) is rather limited in enterobacterial LPS. The core region contains the unique sugars 3-deoxy-D-manno-2-octulosonic acid (KDO) and L-glycero-D-manno-heptose in addition to more common sugars as described by Lambert (1988). Linkage of the core region to lipid A is via the KDO group. The core region has negatively charged residues, such as KDO, and the lipid A backbone also has negatively charged groups. These groups are responsible for the binding of divalent cations. This binding of cations to LPS neutralises the repulsion between the anionic groups and permits a tightly folded conformation of lipid A and the core oligosaccharides. The importance of metal ion cross bridges between LPS is mentioned by Brass (1986) who quotes that treatment with ethylenediamine tetra-acetic acid (EDTA) results in the loss of LPS and a decrease in permeability function of the outer membrane.

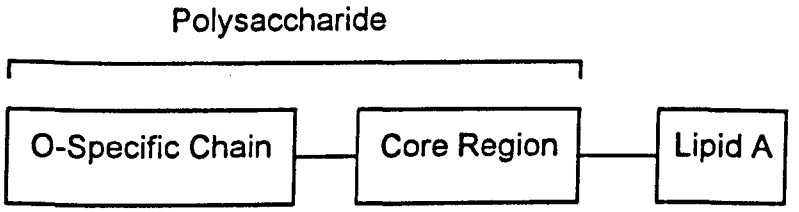

FIGURE 3.2 General architecture of lipopolysaccharide (LPS) from enteric bacteria

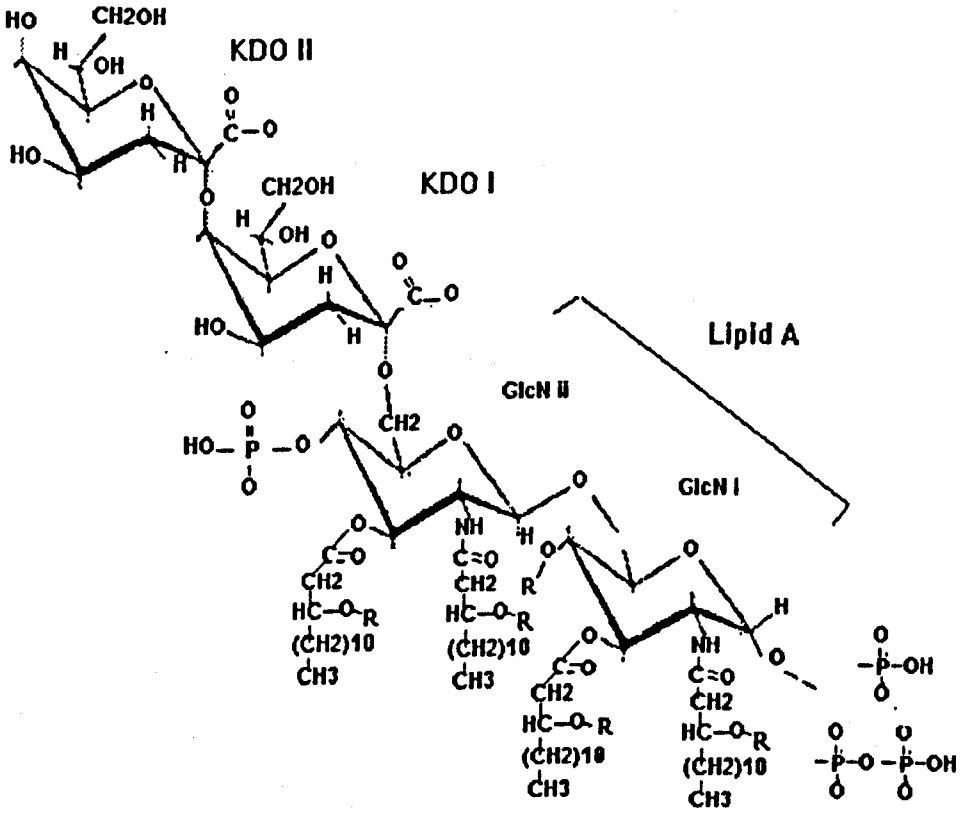

FIGURE 3.3 Structure of Lipid A and the inner core region of *E. coli*. GlcNi and ii are glucosamine. R= Lauroyl, myristoyl or D-3-hydroxymyristoyl. KDOi and ii are 2-keto-3-deoxyoctulosomic acid. (from Brass, 1986)

The O-specific chain of the polysaccharide region shown in Figure 3.2 shows high structural variability even within a single genus. Bacteria invading a higher organism can be recognised by the body's defence system due to these distinct surface groups known as antigens. The diversity in the O-specific chain has been widely exploited in the classification (serotyping) of many Gram-negative species. The O-specific chain is composed of 1-40 repeating oligosaccharides. In contrast to lipid A the O-specific chains adopt a low ordered conformation on the cell surface. Although the chains are usually depicted as protruding from the cell surface, Labischinski *et al.* (1985), as quoted by Lambert (1988), provide evidence that they are densely packed on the surface.

Colonies of strains with or without the O-specific chain often have a smooth or rough appearance respectively, as viewed by electron microscopy. The K12 strain used in this work is a rough mutant which has no O-specific chain, as illustrated in Figure 3.4. In contrast the 0111:B4 strain has smooth LPS and the repeating sugar units which make up the polysaccharide chain are shown in Figure 3.5. Rough mutants show an increased permeability of the outer membrane to hydrophobic compounds. The LPS, as well as being important in the permeability of the outer membrane, endows it with strong hydrophilicity which is important in evading phagocytosis. It also gives the bacterial cell the capacity to avoid specific immune attack by altering the surface antigen constitution.

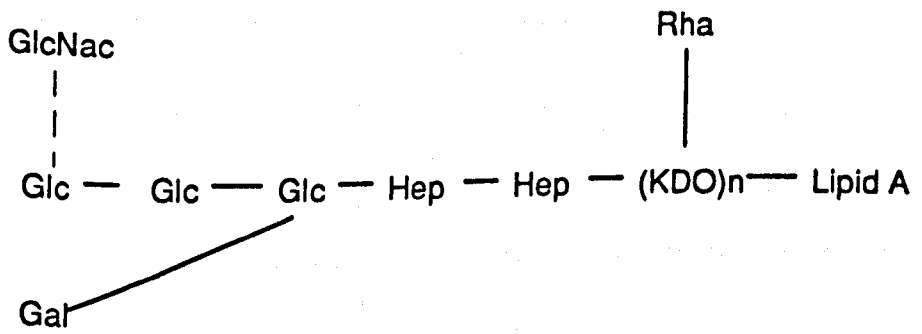

FIGURE 3.4 Oligosaccharide chains of Escherichia coli K12 LPS. GlcNac, N-acetyl-D-glucosamine: Glc, D-glucose: Gal, D-galactose; Hep, L-glycero-D-manno-heptose. KDO, 2-keto-3-deoxyoctulosomic acid; Rha, L-rhamnose. Adapted from Nikaido and Vaara (1985).

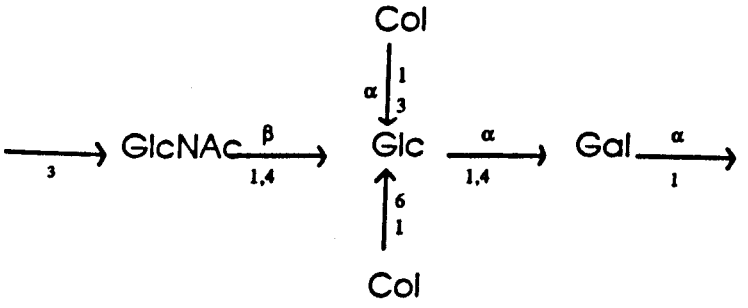

FIGURE 3.5 Example of repeating unit from LPS of *E. coli* 0111. GlcNAc, N-acetyl-D-glucosamine. Gal, D-galactose. Glc, D-glucose. Col, Colitose (3-6-dideoxy-L-xylo-hexose). From Mayer *et al.* (1989).

3.2.4 Outer Membrane Proteins (Omp)

The protein composition of the outer membrane, as revealed by electrophoresis is dominated by 4-6 proteins which occur in high numbers (about 1-2 x 10^5 per cell). In *E. coli* K12 and 0111:B4 these are lipoprotein, OmpA, OmpF and OmpC. Other proteins such as PhoE may be expressed under certain conditions which are discussed later. In the past it was thought that the outer membrane contained just a few species of protein, but more sensitive methods of detection have revealed many protein species which occur in much smaller numbers per cell.

The most abundant protein of the outer membrane is lipoprotein with a molecular weight of 7200. About one third of the total population of this protein is covalently bound to the peptidoglycan layer; the remainder is believed to be in free form. This protein differs from the other prominent outer membrane proteins in that it is not exposed to the outer surface of the cell and is to a large degree α-helical in structure (Braun *et al.*, 1976). It is thought to play an important role in the structure and stability of the outer membrane.

The OmpA protein is known to play a role in the structural stability of the outer membrane. It is also known as heat modifiable protein II*. If the sample is boiled in the presence of SDS before being examined by electrophoresis the apparent molecular weight of the protein is 35,000. If the sample added to the electrophoresis gel is not boiled the molecular weight appears to be only 25,000. Chen *et al.* (1980) deduced the molecular weight of the protein from the amino acid sequence as 35,159. Jap & Walian (1990) quote from Palva (1979) who reports that OmpA is often a complex with lipoprotein. The protein is believed to exist in its monomeric form in its natural state, unlike the OmpC and OmpF proteins which we shall see later exist as trimers in

their natural state. Until recently there was no evidence that OmpA behaved as a pore forming protein. However, Sugawara & Nikaido (1992) have reported pore forming activity of OmpA monomers extracted from an *E. coli* K12 strain deficient in OmpF and OmpC. In their work, proteoliposomes reconstituted from the OmpA were tested for permeability to small molecules by osmotic swelling, with positive results. Following the work with proteoliposomes, Saint *et al.* (1993) have reported channel forming behaviour of OmpA reconstituted into lipid bilayer membranes.

Whilst acting as a permeability barrier the outer membrane must also allow solutes such as nutrients to diffuse into the cell and waste products to diffuse out. This is achieved via some of the outer membrane proteins which behave as channels or pores. Such proteins provide both specific and non-specific diffusion pathways across the outer membrane and are generally known as porins. OmpF and OmpC, previously mentioned above, are examples of porins. Unlike lipoprotein, which is covalently attached to the peptidoglycan layer, the porins are tightly associated with the peptidoglycan through ion bridges. This feature is exploited in the isolation of porins as discussed in Chapter 4. The other main difference between the porins and lipoprotein is that they are composed largely of β-pleated sheet. The primary and secondary structures of some of the porins are described in detail in later sections.

3.3 PORINS

3.3.1 Introduction

It is well recognised that the outer membrane serves as a molecular sieve and permits the passage of small hydrophilic molecules with a well defined exclusion limit of around 600 Daltons (Nakae, 1986). This is thought to be determined by the dimensions of the porins which form water filled channels spanning the outer membrane. Porins usually form trimeric aggregates in their native state (Nakae *et al.*, 1979) and the molecular weights of the monomers from all sources are in the 30,000 - 50,000 range. The widely accepted nomenclature system for the porins from *E. coli* and *S. typhimurium* was first proposed by Reeves (1979). This system names the protein after its structural gene i.e. OmpF is the product of the ompF gene. Table 3.1 gives a comparison of the nomenclatures used by different laboratories before this system was widely adopted.

In the natural environment, *E. coli* K12 and 0111:B4 produce two porins, OmpC and OmpF, to varying degrees depending on the growth conditions, whilst *S. typhimurium* produces the three porins OmpF, OmpC and OmpD. The relative amounts of OmpF and OmpC porins in *E. coli* are determined by the temperature and osmolarity of the growth medium (van Alphen and Lugtenberg, 1977). It is therefore possible to adjust the growing conditions to selectively express one of these proteins in

preference to the other. The growth medium used for the *E. coli* 0111:B4 strain in this work was chosen specifically to express OmpF in excess. It was also hoped to produce OmpF in excess in the K12 strain, but as shown by the electrophoresis gels at the end of the protein isolation, OmpC was in fact produced in excess rather than OmpF (see Chapter 4 for further details). These two proteins are relatively non-specific channels, both OmpC and OmpF showing only slight cation selectivity. A further porin PhoE, produced under conditions of phosphate starvation, was in the past thought to be selective for the transport of phosphate containing compounds. It is now believed that no specific binding site for phosphate occurs within the protein (Bauer *et al.*, 1988) and it is regarded as a general diffusion pore with slight anionic selectivity. The growth of *E. coli* on maltose or maltodextrin containing media leads to the induction of another porin, LamB or maltoporin which has specific binding sites for maltodextrins. In the present work only OmpF and OmpC porins from *E. coli* K12 and 0111:B4 were used. Therefore the following sections will concentrate on the structure and function of OmpF and OmpC porins and where possible will refer to *E. coli* porin in particular. In view of its similarity to OmpF, PhoE porin will also be discussed.

TABLE 3.1 Nomenclature of the major outer membrane proteins of Escherichia coli K12

Uniform Nomenclature Reeves (1979)	Lugtenberg et al. (1975)	Henning et al. (1977)	Schnaitman (1974)
OmpA	d	II*	3a
OmpF	b	Ia	1a
OmpC	c	Ib	1b
PhoE	e	Ic	Nmp AB

3.3.2 Electrophoresis

In his review of bacterial and mitochondrial porin Benz (1985) indicated that there was some confusion in the past concerning the electrophoretograms of the outer membrane proteins of *E. coli*. The number of bands obtained and the molecular weights of the corresponding proteins varied from laboratory to laboratory. These differences were accounted for by the different solubilisation temperatures used during preparation of the sample for electrophoresis and because different gel systems were applied. Since

some interactions between outer membrane constituents are very strong, temperatures above 70°C are required for complete solubilisation of the outer membrane proteins. It is now generally accepted that *E. coli* outer membrane proteins need to be boiled in 2% SDS for at least 5 minutes in order to obtain reliable results. Incomplete unfolding of a polypeptide chain can result in insufficient binding of SDS and the electrophoretic mobility will be altered, as illustrated by the OmpA protein (Section 3.2.4).

The impression in the literature is that the previous confusion regarding number of protein bands and their corresponding molecular weights has now been completely resolved. While there does seem to be general agreement on the number of protein bands seen by electrophoresis, there still seems to be some confusion concerning the molecular weights of the corresponding proteins and their relative positions on the electrophoresis gels. This is compounded by some obvious errors in the literature. For instance, the review by Lugtenberg and van Alphen (1983), which is cited by many authors, gives the molecular weight of OmpF as 37,205 and of OmpC as 36,000. The latter was taken from Lugtenberg *et al.* (1975) which actually gives the molecular weight of OmpC monomers as 38,000 and not 36,000 as quoted in the review. The molecular weight of OmpF is quoted correctly but, whereas the molecular weight of OmpC was estimated from an electrophoresis gel, the molecular weight of OmpF was taken from the amino acid sequence by Chen *et al.* (1979). Chen *et al.* updated the amino acid sequence in 1982 and proposed a molecular weight of 37,083. Nikaido and Vaara (1985) in their review of porin give the molecular weights of *E. coli* K12 OmpF and OmpC as 37,083 and 38,306 respectively. These were deduced from the nucleotide sequence of the genes and were taken from Mizuno *et al.* (1983). In the same review Nikaido and Vaara have a diagram of an electrophoresis gel showing the bands corresponding to the *E. coli* K12 outer membrane proteins. However, the relative positions of the porin bands on the gel are not in the order expected from the quoted molecular weights of 38,306 and 37,083 for OmpC and OmpF respectively. The OmpF protein band travelled less distance on the gel than the OmpC protein band despite its lower molecular weight. No comment was made concerning this apparent conflict and so it is not clear whether this is a real finding or whether the diagram is incorrectly labelled! Brass (1986) also has conflicting evidence between his pictured electrophoresis gels and his quoted molecular weights for the OmpF and OmpC porins. He identified the outer membrane proteins on the gels by using mutants lacking in one or more of the outer membrane proteins. His gels show OmpC, OmpF and OmpA proteins in that order from the top of the gel (i.e. OmpC appears to be the heaviest). He then gives a table of the estimated molecular weights which was adapted from Lugtenberg (1981) and quotes the molecular weight of OmpC as 36,000 and OmpF as 37,205. He does not discuss this apparent discrepancy.

In the present work strains of *E. coli* lacking in one or more of the outer membrane proteins were used to identify the relative locations of OmpF, OmpC and OmpA on the gels. Proteins were isolated from the mutant strains and also from the K12 and 0111:B4 strains used in this work. The samples were all prepared identically and run on the same gel systems for comparison (Figure 4.3). Starting from the top, the order of the bands was OmpF, OmpC and then OmpA. This is in contradiction with the molecular weights as deduced from the nucleotide sequences of the genes. The identification of the proteins in this study is corroborated by the evidence provided by the comparisons with mutant strains. It seems therefore that in the gel sample preparation and the gel system used during this study the proteins OmpF and OmpC, which are of very similar molecular weight, uncoil to a different degree, thus affecting the binding of SDS and giving the observed altered electrophoretic mobility.

3.4 STRUCTURE OF PORINS

3.4.1 Primary Structure

The amino acid sequences of OmpC, OmpF, PhoE and LamB porins of *E. coli* have been deduced from their nucleic acid sequences (Mizuno *et al.*, 1983.; Chen *et al.*, 1979 and Inokuchi *et al.*, 1982). The amino acid sequence of OmpF from *E. coli* K12 has also been obtained from the purified protein by Chen *et al.* (1982) and is in agreement with the deduced sequence from the nucleic acids. Figure 3.6 shows the primary sequences of OmpF, OmpC and PhoE porins from which it can be seen that the sequences are highly homologous. According to Mizuno *et al.* (1983) this indicates that the structural genes for the three porins evolved from a common ancestral gene. The LamB porin shares no obvious sequence homology with the other porins. In *E. coli* comparison of OmpC with OmpF shows 73% identity and comparison of OmpC with PhoE shows 76% identity (Mizuno *et al.*, 1983 and Inokuchi *et al.*, 1982). Van der Ley *et al.* (1987) have shown that comparison of the sequence of PhoE porin from three different enterobacterial species shows a high degree of sequence homology with 81% identity.

Porins have primary amino acid sequences which contain charged residues distributed uniformly along their sequences. They are unusual for membrane proteins in that they do not have stretches of hydrophobic residues long enough to span the membrane in an α-helix conformation. Hydropathy profiles of OmpF, OmpC and PhoE porins show that there are two hydrophobic segments in all three porins, which are distinctly similar. These are located approximately between residues Asn135 and Ser190 of the PhoE sequence shown in Figure 3.6. Nikaido and Wu (1984) have identified a segment in this hydrophobic region common to all the porins, including LamB and OmpA. It is possible that these two hydrophobic segments of the amino

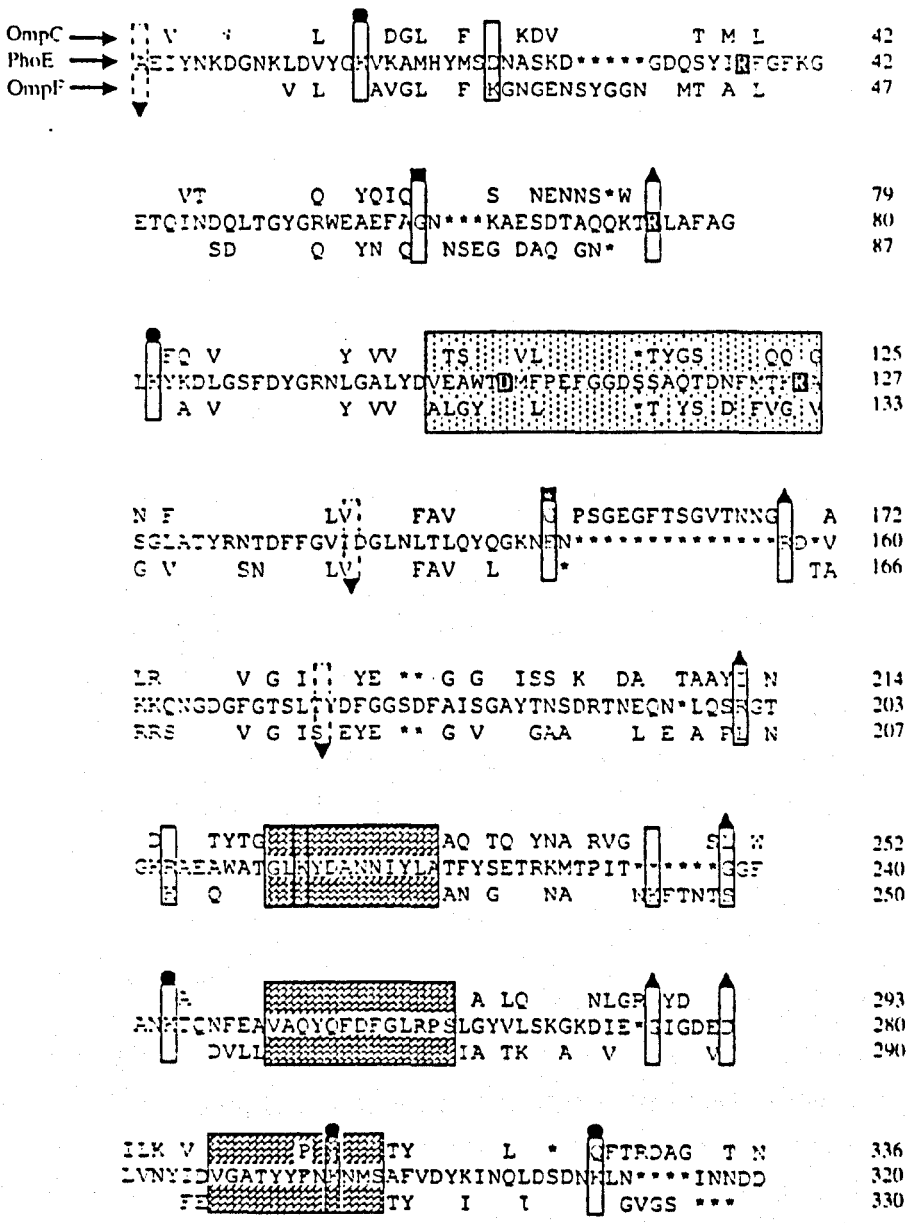

FIGURE 3.6 Primary sequences of OmpC, OmpF and PhoE, which are aligned according to Mizuno *et al.* (1983). Only residues that differ from the sequence of PhoE are shown. (*) Indicates deletions of amino acids, (box and crown) indicates residues exposed to the external surface, (dashed-line box and crown) indicates residues proposed by Tommassen (1988) to be exposed to the periplasm, (box without crown) residues believed to be inside channel or on the rim of the opening. Residues printed in white on top of a dark background depict point mutations that result in an increase in channel permeability (Misra and Benson, 1988). Three dark shaded boxed regions are long highly conserved segments proposed to be located at the contact of the monomer. The light shaded box region of PhoE is the region in which deletions greatly increase the permeability of the channel. (From Jap and Walian, 1990). See Appendix B for the single letter code of amino acids.

acid sequences may play an important role in the incorporation of the proteins into the outer membrane. Bosch and Tommassen (1987) inserted a four amino acid sequence into one of the two hydrophobic segments of the PhoE porin. They found that the normal incorporation of protein into the outer membrane was affected in a manner depending upon the nature of the inserted residues. The biosynthesis and assembly of outer membrane proteins is not fully understood and is the subject of a great deal of research. For a discussion of the expression and biosynthesis of porins the reader is referred to Benz and Bauer (1988).

In earlier works, it was suggested that the ion selectivity of porins was related to the net number of charged residues. It is now clear that the topological positions of the charged residues play the major role in selectivity. The relationship between particular charged residues and the selectivity of porins will be discussed further in Section 3.4.3.

The amino acid sequences of OmpF, OmpC and PhoE porins show at least three extremely conserved segments of their respective sequences. It is thought that these regions could form part of the monomer-monomer contact region in trimeric porin. According to Gehring and Nikaido (1989), the existence of stable heterotrimers among OmpF, OmpC and PhoE porins from *E. coli* suggests a highly conserved region between monomers in the areas where they contact to form the trimeric porin . Based on the temperature at which trimers reverted to monomers in the presence of SDS, it was concluded that the stability of these heterotrimers is not significantly different from homotrimers .

3.4.2 Secondary Structure

Various spectroscopic techniques have been used to study the secondary structure of porins. Rosenbusch (1974), using circular dichroism, and Nakamura *et al.* (1974), using infra-red spectroscopy, concluded that porins are predominantly in a β-pleated sheet conformation with only a small fraction of the structure in an α-helical conformation. Kleffel *et al.* (1985) studied OmpF porin from *E. coli* using x-ray diffraction and infra-red spectroscopy. They showed that the β-sheet strands are anti parallel, consisting of 10-12 residues in length, and are orientated perpendicularly to the membrane. More recently Nabedryk *et al.* (1988) using Fourier transform infra-red linear dichroism suggested that the anti parallel β-sheets are in fact tilted with an average angle of 45°.

In addition to the spectroscopic evidence, other techniques have also suggested a β-pleated sheet structure for porin. The Chou-Fasman structure-prediction algorithm, when used by Vogel and Jähnig (1986) on OmpF, predicts a predominantly

β-pleated sheet conformation with a minor fraction of α-helix. The β-strand segments are predicted to be almost uniformly distributed along the entire sequence. Charged residues are separated by an odd number of residues in several of the β-strand segments. This suggests that these segments are orientated in β-sheet with their charged residues clustered along one side of the β-sheet. Such β-sheet could form part of the β-sheet wall, facing the hydrophobic lipid environment on one side and the water filled porin channel on the other.

3.4.3 Tertiary and Quaternary Structure

Structural information about porins has been obtained using electron crystallography, electron microscopy and x-ray crystallography. Electron crystallography and microscopy are carried out by reconstituting the porin with lipid to obtain patches of 2-dimensional crystalline membrane with associated porins, whilst x-ray crystallography requires 3-dimensional crystals of porin usually associated with detergent. The earliest structural information obtained on porin was from electron microscope measurements which were combined with electron intensity data to obtain 3-D images. The studies performed by Dorset *et al.* (1984) and Steven *et al.* (1977) showed that porin molecules from *E. coli* were arranged according to a three fold symmetry and their conclusion, supported by functional evidence (discussed in later sections), was that the basic unit of porin was a trimer. Dorset *et al.* (1984) also mentioned that the openings of the triplet of pores at the outer surface appeared to coalesce into a single channel before reaching the inner membrane surface. This finding was supported by Engel *et al.* (1985) using similar electron microscopy and image reconstruction techniques, but as we shall see later, this merging of the triplet of pores is now in dispute.

In 1980 OmpF porin from *E. coli* was crystallised to form 3-D crystals by Garavito and Rosenbusch. The quality of porin crystals has greatly improved in recent years and other porins including OmpA and LamB have also been crystallised (Garavito *et al.*, 1984). This has led the way for improved x-ray crystallographic images of porin molecules. Porin from *Rhodobacter capsulatus* has been studied by x-ray diffraction using isomorphous replacement. In 1989 Weiss *et al.* looked at the structure of porin from *R. capsulatus* at 0.6 nm resolution and by 1991 had published the structure of porin at 0.18 nm. The monomer was observed to be a 16 stranded β barrel, the strands are all anti parallel and the barrel is twisted in a right handed manner. Unfortunately the porins from *E. coli* do not show very good sequence homology with the *R. capsulatus* porin. Molecular replacement methods were used by Pauptit *et al.* (1991) to confirm the barrel motif for three *E. coli* porins but the structures were too different to be determined by this method. Recently the crystal

structure of OmpF and PhoE porins from *E. coli* have been determined by Cowan *et al.* (1992). They solve the structure of OmpF by single isomorphous replacement at 0.24 nm resolution and solve the PhoE structure by molecular replacement at 0.3 nm resolution. At present this is the only high resolution description of the structure of the porins from *E. coli* The following details of 3-D structure are largely taken from this one paper, but are compared with other findings where possible.

In agreement with the known secondary structure, as determined by spectroscopy, and in common with the structure of *R. capsulatus* porin, the channel forming motif for both OmpF and PhoE is a 16 stranded anti-parallel β barrel. The strands tilt relative to the barrel axis with an angle of between 35° and 50°. The amino and carboxy termini are linked by a salt bridge within the 16^{th} β-strand, as shown in Figure 3.7, to form a pseudo-cyclic structure which makes up the porin monomer. Short β-hairpin turns define one end of the barrel, whereas long irregular loops are found at the other end. One of the long loops, (L3) as depicted in Figure 3.7, folds into the barrel and constricts the size of the pore at about half the height of the barrel. The unrolled picture of the β barrel viewed from the outside is shown in Figure 3.8. The regions involved in sub-unit interactions to form the trimer are shaded in Figure 3.8. 35% of the surface of each monomer is involved in a combination of hydrophobic and hydrophilic interaction with the other monomers. Kleffel *et al.* (1985) concluded from hydrogen-deuterium exchange experiments that most of the amide protons of porin were shielded, i.e. inaccessible to bulk water, and that porin was a uniquely tightly packed molecule. Schindler and Rosenbusch (1984) established that porin was resistant to proteases, extremes of pH (1.6-12.4), detergents and non-polar solvents, such as benzene. Structural findings, therefore, may well explain why these porins are so robust and not easily dissociated.

In contrast to the evidence provided by Dorset *et al.* (1984) and Engel *et al.* (1985), discussed earlier in this section, Cowan *et al.* (1992) show that the triplet of pores do not actually merge as they traverse the membrane. In fact as early as 1989 Jap suggested that the merging of the triplet of pores in OmpF porin was due to a false interpretation of the structure as a result of poor quality crystals. Jap's 3-D structure of PhoE porin in 1989 showed that the triplet of pores only converged as they traversed the membrane and did not merge. As OmpF and PhoE have high sequence homology he thought it unlikely that the channel design would be very different in the two porins. Cowan *et al.* (1992) suggest that the loops L4-L8 shown in Figure 3.7 could accumulate stain resulting in the previous interpretation that the channels merge.

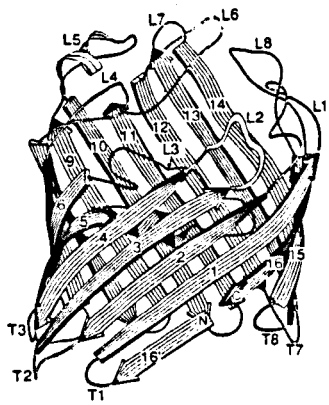

FIGURE 3.7 Ribbon diagram of OmpF monomer. Arrows represent β-strands and are labelled 1-16. The long loops are labelled L1-L8, the short turns at the other end T1-T8. Loop L2 protrudes towards the viewer. (From Cowan *et al*, 1992)

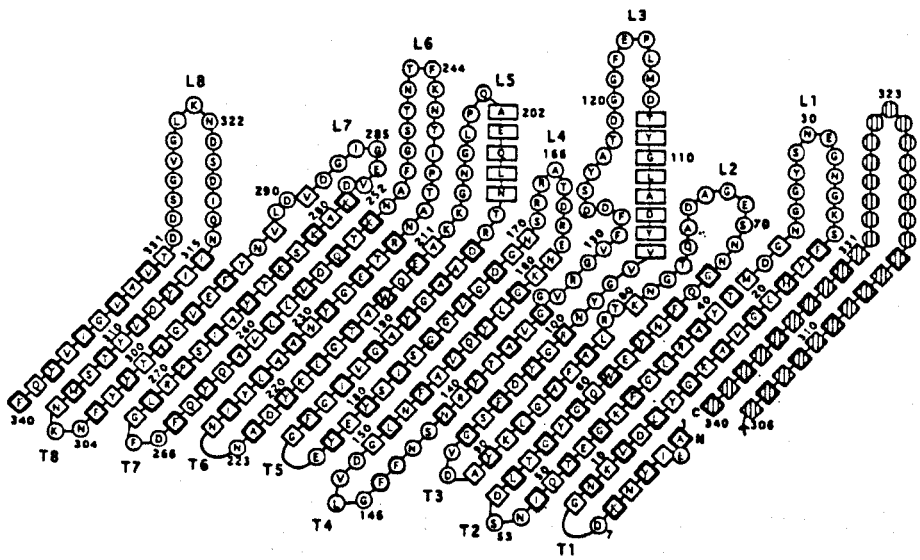

FIGURE 3.8 Structure of OmpF monomers. Topology of OmpF with amino acid sequence in one letter code (see Appendix B). The view is from the outside with the 16-stranded anti-parallel β-barrel unrolled. Residues with side chains that are external are shown in bold, those which are part of β-barrel strands are shown as diamonds, whilst rectangles indicate they are part of α-helices and circles indicate they form turns or loops. (From Cowan *et al.*, 1992).

The outer surface structure of porin, as determined by Cowan *et al.* (1992) shows a pronounced partitioning with respect to hydrophilicity. A hydrophobic band of 2.5 nm in width encircles the trimer, consistent with the thickness of the non-polar outer membrane core based on the lengths of its fatty acyl chains and x-ray studies of model membranes. A similar distribution was observed in the structure of *R. capsulatus* porin by Weiss *et al.* (1991). The end of the barrel with the short β-hairpin turns, illustrated in Figure 3.7, has residues which are mainly negatively charged and Cowan *et al.* propose that these would contact with the polar head groups of the membrane phospholipids. The end of the barrel with the long loops has a less uniform distribution of charge. Here there are well conserved residues, which include anionic side chains, hydrogen bonded to tyrosines, and clusters of carboxyl groups that could interact with LPS through divalent cations. Therefore, this end of the barrel is facing the outside of the cell in the native state and the other end of the barrel, with the β-hairpin bends, faces the inside of the outer membrane. This interpretation is confirmed by work involving point mutations on PhoE by Bosch *et al.* (1989). Mutations located in the loops L2 and L4-L8 resulted in impaired bacteriophage and antibody binding, showing that this end of the PhoE porin is exposed at the cell surface (see Table 3.2). (A bacteriophage is a virus that requires a bacterium to replicate).

TABLE 3.2 Effect of point mutations and deletions on porins from Cowan et al. (1992).
(a) Numbering scheme based on the OmpF sequence in Figure 3.8. Residues that have been mutated and analysed are underlined. Deletion mutants are indicated by Δ. (b) Effects of mutations on solute flux, phage and monoclonal antibody binding. Altered selectivity : minus, no effect; ±, minor effect; +, significant effect, ++, large effect. Location: Pore (d), below constriction zone; pore (c), in constriction zone. (See Appendix B for the three letter codes of the amino acids).

Number	Residue(s) [a] Type			Location	Effect [b]		
	OmpF	PhoE	OmpC		Increased pore size	Altered selectivity	Impaired phage/ antibody binding
18	Val	Lys	Asp	Pore (d)		±	
34	Gly	Lys	Val	L1		±	
42	Arg	Arg	Arg	Pore (c)	+		-
69	Asn	Lys	Ser	L2		+	
82	Arg	Arg	Arg	Pore (c)	+		-
108-133	Δ			L3	+		-
111-118			Δ	L3	+		
113	Asp	Asp	Asp	Pore (c)	+		-
131	Gly	Lys	Gln	Pore (c)		++	
132	Arg	Arg	Arg	Pore (c)	+		-
164	Asp	Arg	Arg	L4		-	+
205	Leu	Arg	Ile	L5		-	+
248	Ser	Gly	Leu	L6			+
285	Gly	Gly	Arg	L7		-	+

The aqueous pore has a lining similar to the outer surface of water soluble proteins. The entrance (or mouth) of each pore in the triplet is narrowed by the long loops shown in Figure 3.7. The internal loop L3 constricts each pore to an elliptical cross section of 0.7 x 1.1 nm at half the height of the barrel. At the other end of the barrel the pore is delineated by side chains from the β barrel itself. The area increases just beyond the constriction zone to 1.5 x 2.2 nm. The loop L3 has interactions with the barrel wall which may involve buried charges and polar residues. The constriction zone has an unusual cluster of charged groups and owing to these clusters, the residues would have unusual pKa values. A detailed description of the residues involved and their relative positions is given by Cowan *et al.* (1992). Experiments with mutants of OmpC and OmpF porins with substituted or deleted residues indicate that the loop L3 contributes significantly to the determination of the exclusion size for permeating molecules (Benson *et al.*, 1988 and Misra and Benson, 1988). Table 3.2 shows the actual residues which have been substituted or deleted in each porin, giving the location and indicating whether the pore size has been altered. Also included in this table are mutations resulting in altered selectivity for ions. OmpF and OmpC are slightly cation selective whilst PhoE is slightly anion selective. In PhoE there is a lysine at position 131 instead of glycine as in OmpF. This lysine residue in the constriction zone critically influences the selectivity of PhoE. Other residues at the mouth of the pore also have some influence on selectivity, whilst residues below the constriction zone only have minor effects. Selectivity of the porin channels will be discussed in more detail in the description of porin function. The charge distribution at the end of the barrel with the β-hairpin turns is similar for OmpF, OmpC and PhoE, whilst at the mouth of the pore a substantial number of differences occur.

3.4.4 Summary of Porin Structure

The porin molecule is a trimer spanning the outer membrane. Three separate channels traverse the membrane converging at the inner leaflet of the outer membrane. The monomer is a 16 stranded anti parallel β barrel. The end of the barrel which is on the outside of the outer membrane has long loops which do the initial screening with respect to charge and size of permeating molecules. Approximately 0.9 nm into the channel there is a constriction zone of 0.7 x 1.1 nm. Here amino acid side chains determine the size limitation and ion selectivity. The channel then opens abruptly to approximately 1.5 x 2.2 nm and permeating molecules are effectively released into bulk solvent at this point. Porin is a tightly packed molecule, 35% of the surface of each monomer being involved in hydrophobic and hydrophilic interactions to form the trimer. This endows the molecule with unusual robustness; it is resistant to proteases, detergents and non-polar organic solvents.

3.5 INVESTIGATION OF PORIN FUNCTION

3.5.1 *In vivo* methods

The permeability of porins to hydrophilic solutes can be studied *in vivo* or *in vitro*. *In vivo* experiments study the pores in their natural environment which means that the substrates can interact with the whole uptake system including periplasmic binding proteins and periplasmic enzymes. Two different methods are used. In the first, radioactively labelled substrates are added to the external media and the uptake of the radioactivity into the cell is measured. In the second, the β-lactamase activity in the periplasmic space is used to study the uptake of β-lactam antibiotics through the outer membrane. β-lactamase is an enzyme present in some resistant bacteria which hydrolyses and thereby renders β-lactam antibiotics, such as penicillin, inactive. The type of information gained by these experiments and also their limitations are discussed by Benz (1988) and Benz and Bauer (1988). The first indications that porins form hydrophilic channels came from a study in which the flux of a series of β-lactams was measured. In this study, increasing the hydrophobicity of the antibiotic reduced significantly the β-lactam flux.

OmpF, OmpC and PhoE porins were studied by Nikaido and Rosenberg (1983) and it was shown that PhoE was selective for negatively charged solutes whilst OmpC was selective for positively charged solutes. For OmpC, the rate of hydrolysis of positively charged β-lactam was larger than that of a negatively charged analogue. Precise information can only be obtained if the flow of β-lactam antibiotics across the outer membrane is rate limiting i.e. the β-lactamase activity is so high that the enzyme is not saturated and the gradient of the β-lactam antibiotic is established across the outer membrane.

In vitro experiments allow much better control of the experimental conditions and the bulk of data for porins comes from model membrane studies which will be described in the following sections. For *in vitro* experiments, the porin first must be isolated. The unusually high stability of porin in detergents and its ionic association with the peptidoglycan layer (described in earlier sections of this chapter) are the two features usually exploited for the isolation. The method of porin isolation for the experiments performed in this work is described in detail in chapter 4. The isolated porin must then be incorporated into liposomes, vesicles or lipid bilayers for subsequent experiments. The main disadvantages of *in vitro* systems is that artefacts are possible and that components are missing that may be necessary for the full activity of the porin channels. In the following sections several types of *in vitro* experiments are described and their possible artefacts discussed.

3.5.2 *In Vitro* Methods

3.5.2.1 Liposome Permeability

Reconstitution of proteins into lipid vesicles or liposomes enables experiments to be carried out to identify the pore forming proteins of the outer membrane of bacteria. The size of the pores has been estimated by measuring the penetration of radio-labelled solutes. Liposomes are formed in a buffer solution containing two radio-labelled solutes from lipids and LPS in the presence of pure protein or protein fractions. The liposomes are obtained by shaking the suspension followed by mild sonication. Both radio-labelled solutes are entrapped within the liposomes during the liposome formation. One of them is usually a ^{3}H dextran with a large molecular weight such that it does not penetrate the pores. The other solute is of lower molecular weight and is labelled with ^{14}C. Subsequently the liposomes are passed through a Sepharose 4B column. The impermeable ^{3}H dextran is retained in the liposomes whereas the low molecular weight ^{14}C solute may leave the liposomes through the porin during the elution process and be retained in the column. The original ^{3}H to ^{14}C ratio is drastically reduced and may be used to calculate the exclusion molecular weight of the porin, as a function of the molecular weight of the ^{14}C solute . For the *E. coli* OmpF porin the upper molecular weight of solutes to pass through the pore is approximately 600 (Nakae, 1976). The diameter of the pore may be estimated from the Stokes' radius of the largest solute to diffuse through the porin channel. Hancock (1987) predicts an average pore diameter of 1.13 nm for OmpF and OmpC using the Stokes' radius of the largest diffusible solute, raffinose. Jap and Walian (1990), among others, indicate that there is a problem with using the Stokes' radius for this calculation. The exclusion limit of a pore is possibly more closely related to the diameter of the dehydrated form of the largest molecule able to diffuse through it. Diffusion of a hydrophilic molecule close in size to the pore's exclusion limit would require the solute to exchange it's hydration shell H-bonds with H-bonds made to the chemical groups lining the pore wall.

Jap and Walian (1990) also point out that the use of raffinose to estimate pore size may not be sufficiently accurate. Raffinose is a linear trimer, containing three hexose units, essentially cylindrical in shape and with a diameter similar to glucose. OmpF and OmpC porins from *E. coli* show a dramatic difference in permeability to raffinose compared to glucose even though the narrowest dimensions of the two sugars are comparable. Thermal motions along the length of raffinose would cause it to sweep out a larger volume of space, presenting a wider diameter to the pore and the raffinose molecule would have to 'worm' its way through the channel.

Hydrophobic molecules in water are believed to be surrounded by a 'cage' of ordered water molecules. In a porin pore the removal of this water for H-bond exchange with atoms in the pore wall would be energetically unfavourable, according

to Jap and Walian (1990). Experimental evidence for this comes from work with hydrophobic cephalosporins. These have an approximate minimum diameter of 0.7 nm but, unlike hydrated glucose which has an approximate diameter of 0.85 nm and zwitterionic cephalosporins also with a minimum diameter of 0.7 nm, they do not measurably diffuse through porin channels. It appears that the 'water-caged' version of the hydrophobic cephalosporins exceeds the dimensions of the pore's constriction region.

3.5.2.2 Liposome Swelling

The method described in the previous section cannot allow measurement of the penetration kinetics of hydrophilic solutes through the pores or measure their specificity. This is because the elution of the Sepharose 4B column needs such a long time that only "all or nothing" processes can be measured. For the liposome swelling method, the liposomes are formed from phospholipids and porin in a buffer which contains a certain concentration of dextran impermeable through the porin. The liposomes are added under rapid mixing to an isotonic solution of test solute. If this solute can penetrate the porin, the total concentration of solutes inside the liposomes increases. The liposomes swell because of the influx of water driven by the osmotic gradient across the liposome membrane. The swelling process is detected by a decrease of the average refractive index of the liposomes i.e. the optical density. The initial swelling rate can be used as a measure of the penetration rate of the test solute through the porin if the movement of the test solute and not the water permeability of the liposome membrane is rate limiting.

This technique has been widely used to study the properties of porins and particularly *E. coli* porins. It does however have a number of possible complications which are discussed by Hancock (1987). One example is that the change in optical density may be influenced by light scattering or refractivity of the solutes. Despite the problems with the technique, it allows an estimate of relative diffusion rates of a variety of solutes. By studying the behaviour of solutes with differing molecular weights an estimate of pore diameter can be made by applying a modified version of the Renkin equation (Nikaido and Rosenberg, 1983). This equation is based on Fick's Law but is modified to correct for steric hindrance and friction within the pore. It assumes that the pores are uniform cylinders and that the pore interior interacts minimally with the diffusing molecule. It also relies on estimates of the molecular radii of hydrated sugars which are somewhat disputed. Table 3.3 shows the estimated pore diameters obtained using this technique compared to those obtained with the liposome permeability studies. Also in the table are estimates of pore diameter from single

channel conductance measurements, obtained from lipid bilayer experiments which are described in the following section. Using the liposome swelling technique, Nikaido and Rosenberg (1983) noted that different disaccharides with similar molecular weight gave substantial variability in the rate of swelling. Jap and Walian (1990) believe that the slower penetrating molecules, despite being of similar molecular weight to the other molecules, must be geometrically closer to the pores exclusion limit. It is clear from the discussion in Section 3.5.2 that when interpreting the results of exclusion limit investigations, the stereo-chemistry involved in solute diffusion through the pores must be taken into account.

TABLE 3.3 Comparison of estimated pore diameters. (a) Hancock (1987), based on estimates that raffinose (d=1.128 nm) is the largest molecule penetrating the outer membrane. (b) Nikaido and Rosenberg (1983) (c) Benz *et al.* (1985) (d) data from Benz *et al.* (1985) divided by three to obtain conductance of one pore within the triplet (e) Morgan et al. (1990) data from insertion events and (f) data from closing events. For lipid bilayer estimates the channel length is taken as 6 nm.

	Estimated Pore Diameter (nm)					
Porin	Liposome permeability (a)	Liposome swelling (b)	Lipid bilayer (c)	(d)	(e)	(f)
OmpF	1.13	1.16	1.15	0.66	1.54	0.83
OmpC	1.13	1.08	1.02	0.59	-	-
PhoE	1.13	1.06	1.11	0.65	-	-

3.5.2.3 Lipid Bilayer Membranes

Experiments with liposomes provide good information about the presence and size of the pores formed by porin. More detailed information about the pore interior and pore selectivity can be obtained from experiments with lipid bilayers incorporating porin molecules. In addition, this approach allows resolution of single channels and is the method used for investigating the functional properties of porin in this research. Therefore the description of the different lipid bilayer techniques and the information obtained about porin using these various techniques are given below.

3.6 RECONSTITUTION OF CHANNELS INTO LIPID BILAYERS

3.6.1 Methods of Bilayer Formation

Isolated channels can be reconstituted into planar lipid bilayers separating two aqueous compartments. This allows the lipid and aqueous environment of the protein to be manipulated so as to elucidate their roles in channel assembly and function. Electrodes dip into the aqueous solutions on both sides of the bilayer, enabling the ionic current through the membrane to be measured with suitable electronic equipment. The lipid bilayer membrane is almost impermeable to ions and application of a trans-membrane voltage does not result in substantial current. The formation of pores by porin molecules increases the membrane conductance in discrete steps corresponding to the incorporation of single pore forming porin oligomers into the membrane. The conductance of one porin trimer (triplet of pores) in 250 mM KCl is at least 50 x the conductance of the bilayer, therefore single channels are easily resolved. Porins have been successfully reconstituted into planar lipid bilayers prepared by the classic black-film method of Mueller *et al.* (1962) or by the more recent methods of Montal and Mueller (1972) and Schindler (1980). These methods are often referred to as the Mueller-Rudin, Montal-Mueller and Schindler methods respectively.

Black lipid bilayers or painted bilayers (sometimes called films) are formed by spreading lipid "dissolved" in a non-polar liquid across a small (1-2 mm) aperture in a hydrophobic partition separating two aqueous phases. The resulting structure consists of a bilayer film surrounded by an annulus of the lipid/solvent solution. When viewed under reflected light, the very thin (2.5 -5 nm) bilayer reflects very little light relative to its surroundings and thus appears black.

Bilayers formed by the Montal-Mueller method are often referred to as solvent-free bilayers. They are formed by spreading lipid at the air-water interface so that after solvent evaporation a monolayer remains. The aqueous phase is separated into compartments by a septum with a small aperture, typically 100-500 μm in diameter pre-treated with a non-polar solvent. The levels of the aqueous phases in the two compartments on either side of the aperture are raised so that the floating monolayers are apposed over the aperture to form a bilayer. A big advantage of the Montal-Mueller method is that it is possible to form asymmetric bilayers. This is the technique used in this work and it is described in detail in chapter 5. The Schindler technique also uses monolayer apposition as in the Montal-Mueller technique, but in this case the monolayer is formed by adding a suspension of vesicles to the aqueous phase.

3.6.2 Reconstitution of Porin

The simplest method of incorporating porin into the bilayers formed by the methods described above is to add detergent-solubilised porin to the aqueous bathing medium.

3.6 RECONSTITUTION OF CHANNELS INTO LIPID BILAYERS

3.6.1 Methods of Bilayer Formation

Isolated channels can be reconstituted into planar lipid bilayers separating two aqueous compartments. This allows the lipid and aqueous environment of the protein to be manipulated so as to elucidate their roles in channel assembly and function. Electrodes dip into the aqueous solutions on both sides of the bilayer, enabling the ionic current through the membrane to be measured with suitable electronic equipment. The lipid bilayer membrane is almost impermeable to ions and application of a trans-membrane voltage does not result in substantial current. The formation of pores by porin molecules increases the membrane conductance in discrete steps corresponding to the incorporation of single pore forming porin oligomers into the membrane. The conductance of one porin trimer (triplet of pores) in 250 mM KCl is at least 50 x the conductance of the bilayer, therefore single channels are easily resolved. Porins have been successfully reconstituted into planar lipid bilayers prepared by the classic black-film method of Mueller *et al.* (1962) or by the more recent methods of Montal and Mueller (1972) and Schindler (1980). These methods are often referred to as the Mueller-Rudin, Montal-Mueller and Schindler methods respectively.

Black lipid bilayers or painted bilayers (sometimes called films) are formed by spreading lipid "dissolved" in a non-polar liquid across a small (1-2 mm) aperture in a hydrophobic partition separating two aqueous phases. The resulting structure consists of a bilayer film surrounded by an annulus of the lipid/solvent solution. When viewed under reflected light, the very thin (2.5 -5 nm) bilayer reflects very little light relative to its surroundings and thus appears black.

Bilayers formed by the Montal-Mueller method are often referred to as solvent-free bilayers. They are formed by spreading lipid at the air-water interface so that after solvent evaporation a monolayer remains. The aqueous phase is separated into compartments by a septum with a small aperture, typically 100-500 μm in diameter pre-treated with a non-polar solvent. The levels of the aqueous phases in the two compartments on either side of the aperture are raised so that the floating monolayers are apposed over the aperture to form a bilayer. A big advantage of the Montal-Mueller method is that it is possible to form asymmetric bilayers. This is the technique used in this work and it is described in detail in chapter 5. The Schindler technique also uses monolayer apposition as in the Montal-Mueller technique, but in this case the monolayer is formed by adding a suspension of vesicles to the aqueous phase.

3.6.2 Reconstitution of Porin

The simplest method of incorporating porin into the bilayers formed by the methods described above is to add detergent-solubilised porin to the aqueous bathing medium.

This was the technique used in the present work and is described in detail in chapter 5. Generally with this method a small voltage, typically 50 mV, is applied across the bilayer. After an initial lag of 1-5 minutes, presumably due to diffusion of porin through unstirred layers, the conductance of the bilayer increases. An alternative method is used by Schindler and Rosenbusch (1978). Vesicles formed from a lipid/protein mixture are spread on the aqueous phase so that porin is incorporated directly into the bilayer as it forms. Interestingly, no pores are observed in the membrane immediately after formation with only low voltages applied. Membrane potentials of around 100 mV are needed to induce or activate the pores though why this is necessary is not clear. A third, less often used method, incorporates porin molecules by fusion of reconstituted vesicles with planar bilayers. A brief description of this method can be found in the review by Benz (1984).

The successful reconstitution of channels is dependent ultimately on the physico-chemical behaviour of the bilayer system. The physical nature of planar bilayers in the context of ion channel reconstitution is discussed by White (1986).

3.7 SINGLE CHANNEL CONDUCTANCE

3.7.1 Single Pore or Three Independent Pores?

The single channel conductance of porin channels has been measured by many researchers but in the past there has been some dispute as to whether the porin trimer behaved as a single pore or as a triplet of three independent pores. This led to vastly different values for the single channel conductance and subsequent estimates of pore diameter. Schindler and Rosenbusch (1978) using their technique of proteolipid vesicles, described in the last section, found that activation of a single porin channel resulted in a single conductance increment. Application of higher trans-membrane potentials inactivated the porin in three well-defined decrements. Similar observations have been made for the *E. coli* porins OmpF and OmpC (Schindler and Rosenbusch, 1981, Xu *et al.*, 1986 and Morgan *et al.*, 1990) and for PhoE porin (Dargent *et al.*, 1986). It was concluded, therefore, that the OmpF, OmpC and PhoE porins were composed of three independent channels. Each protein has three conductance states. The largest conductance, corresponding to the porin oligomer, was usually measured during porin incorporation into the membrane. The smaller conductance units corresponding to 1/3 and 2/3 the conductance of the porin oligomer measured at higher trans-membrane voltages were attributed to the individual channels making up the triplet of pores. Many authors do not make it clear which conductance values they are measuring when quoting single channel conductance measurements. Morgan *et al.* (1990) used a similar experimental technique to investigate OmpF porin as the one used in this study. For clarity they described the conductance events occurring during

porin incorporation ('opening events') separately from the conductance events produced by high applied voltage ('closing events'). The majority of opening events in the presence of 250 mM KCl, pH 7.0 occurred with a conductance in the 0.8-0.9 nS range and the closing events occurred at 0.5 nS and 0.25 nS. In contrast, Benz (1985), Benz (1984) and Bauer (1988), who have provided much information on the functional properties of porin, including single channel conductance, did not find any evidence to suggest that the porin molecule behaved as three independent channels. The conductance increments obtained during porin insertion and assumed to be the single channel conductance were found to be 1.9 nS, 1.5 nS and 1.8 nS from K12 OmpF, OmpC and PhoE porins respectively when measured in 1M KCl, pH 6.0.

The early structural evidence on porin, discussed in Section 3.4.3, which indicated that the triplet of channels merged about half way across the membrane was used by Benz (1985) to argue against the existence of the 1/3 and 2/3 conductance steps found by Schindler and Rosenbusch (1981). Using the channel dimensions provided by Dorset *et al.* (1984) he argued that the central position where the channels merged would be rate limiting for the movement of ions. Closing one of the openings would reduce the current by only 5% (not 33%); closing of a second opening would only reduce the current by a further 10 to 20% (not 33%). More recent structural evidence for OmpF porin by Cowan *et al.* (1992) and for PhoE porin by Jap (1989) shows the triplet of channels as three separate entities supporting the electrical data of Schindler and Rosenbusch (1981), Xu *et al.* (1986) and Morgan *et al.* (1990) that the porin could have conductance states corresponding to 1/3 and 2/3 that of the oligomer. This would require the individual channels of each triplet to be able to 'open' and 'close' independently. The finding by Schindler and Rosenbusch (1981) that these small decrements in conductance could be produced by applying high trans-membrane voltages provided the first evidence that porin channels may be 'voltage-gated'. The existence of the 1/3 and 2/3 conductance steps is now generally accepted but the conclusion that porins are 'voltage-gated' is still under debate and will be discussed further in Section 3.9.

3.7.2 Measurements of Single Channel Conductance

The conductance steps observed during porin incorporation, which are generally increases in conductance, are not uniform in size but are distributed over a range of conductance values. This distribution has been noted for porins from different bacterial species and with different detergents (Benz, 1985). The smaller conductance steps produced by high trans-membrane voltages, mainly closing events, show a similar distribution. The conductance steps are usually plotted in the form of a histogram. If

the data is normalised, then the conductance with the peak probability of occurrence is quoted as the single channel conductance of the porin.

Single channel measurements have been performed with a variety of salts and salt concentrations (Benz *et al.*, 1979,1980, Benz and Hancock, 1981 and Benz and Bohme, 1985). For the non-specific porins OmpF, OmpC and PhoE of *E. coli* and *S. typhimurium* the single channel conductance, Λ, was a linear function of the specific conductance, σ, of the aqueous phase.

3.7.3 Pore Size Estimates

Estimates of the diameter of the porin channels have been made using an expression relating single channel and specific (bulk) conductance to a cylindrical pore geometry. The pore diameter is then calculated according to

$$\Lambda = \frac{\sigma \pi r^2}{L}$$

where Λ and σ represent the single channel and specific conductance respectively. L is the channel length and r is the channel radius. In common with the Renkin equation this model assumes that the pores are uniform cylinders and that interaction with the pore interior is minimal. The most commonly used estimate for pore length, L, has been taken from structural information provided by Engel *et al.* (1985) and is 6 nm. Jap and Walian (1990) use a smaller channel length of 4.5 nm which more closely fits the results from their 3-D electron diffraction studies on PhoE porin. Nikaido (1992) is of the opinion that the length should correspond to the limiting portion of the channel and not the entire length. For OmpF and PhoE porins this would be 0.9 nm according to the structural information obtained by Cowan *et al.* (1992). The single channel conductance should be the conductance of one of the triplets of the pore if the diameter is to have any physical meaning. Many reviews on porin still use the data provided by Benz (1985) even though he did not demonstrate the three conductance units per porin oligomer. Jap and Walian (1990) for instance have taken Benz's data and divided the quoted conductances by three in order to calculate pore diameters. Table 3.4 shows estimates of pore diameter using different channel lengths and taking data from Benz (1985) and Morgan *et al.* (1990). The diameters calculated using a channel length of 0.9 nm are clearly unrealistic if we consider that disaccharides can freely diffuse through the channels with significant rates.

The linear relationship of single channel conductance to the specific conductance of the aqueous phase led to the conclusion that ions move inside the pore

as they do in the bulk aqueous environment. However, the slight cation selectivity of OmpF and OmpC channels and slight anion selectivity of the PhoE channel indicate that the ions do interact with the pore interior. Charged amino acid side chains within the channel are known to influence selectivity, which is pH dependent (see Section 3.8). This model also assumes that the single channel conductance is independent of applied voltage over a wide range of voltages. In this research the current/voltage behaviour of the OmpF and OmpC channels have been shown to be asymmetric and non-linear and dependent on pH.

TABLE 3.4 Comparison of pore diameters using different channel lengths. (a) Data from Benz *et al.* (1985), electrolyte=1 M KCl, pH 6. (b) Data from Benz *et al.* divided by three to obtain conductance of one pore in the triplet. (c) Data from Morgan et al. (1990), electrolyte =250 mM KCl, pH 7. (1) opening event and (2) closing event.

Porin	Λ (nS)	Diameter (nm)		
		L=6 nm	L=4.5 nm	L=0.9 nm
(a) OmpF	1.9	1.15	1.00	0.44
OmpC	1.5	1.02	0.88	0.40
PhoE	1.8	1.12	0.97	0.43
(b) OmpF	0.63	0.66	0.57	0.26
OmpC	0.5	0.59	0.51	0.23
PhoE	0.6	0.65	0.56	0.25
(c) OmpF	0.85 (1)	1.54	1.33	0.60
OmpF	0.25 (2)	0.83	0.72	0.32

3.8 PORE SELECTIVITY

3.8.1 Zero-Current Potential Measurements

The study of porin trimers in lipid vesicles by Nikaido and Rosenberg (1983) presented some evidence that the pores were not simply water filled channels but exhibited a certain selectivity, albeit, small for cations or anions. The lipid bilayer technique allows access to both sides of the membrane so that the properties of porin channels can be studied as a function of changes in pH and salt concentration. This enables the ionic selectivity of pores to be studied using zero-current potential measurements. The measurements are made by creating a salt concentration gradient across the membrane to provide a driving force for the movement of ions through the porin to the more

dilute side of the membrane. The ions move according to the selectivity of the porins (e.g. cation selective channels preferentially allow passage of cations). For KCl, where the mobility of the K^+ ion and the Cl^- ions are very similar in aqueous solution, ionic diffusion should result in no net current. If one ion moves preferentially a current will be observed. The direction of the current and the polarity of the voltage required to reduce the current to zero depend upon the polarity of the ion. The voltage required to reduce the diffusion current to zero is known as the zero-current potential (see equation 2.21).

Benz(1984) studied the selectivity of matrix porin (OmpF/OmpC) and PhoE porin from *E. coli*. At physiological pH the OmpF/OmpC porins are cation selective and PhoE porin is anion selective as shown in Table 3.5. The permeability ratio P_C/P_a for OmpF/OmpC in KCl is approximately 3.7 whilst in NaCl it is 2.5. Na^+ has a lower mobility in bulk solution than K^+ and this is reflected in the lower permeability ratio. The decrease in selectivity of the OmpF/OmpC porins as the pH was decreased (Table 3.5) was the first indication that charged amino acid side groups could be responsible for the selectivity of the pores. Experiments with chemically modified porin helped to support this conclusion. OmpF porin from *E. coli* completely loses its cation selectivity after amidation, a process which neutralises negative charges (Benz *et al.*, 1984). PhoE becomes cation selective after positive charges are neutralised by acetylation (Darveau *et al.*, 1984). Before detailed information about the secondary and tertiary structure was available the precise location of the charged groups was unknown, although they obviously had to lie within the channel itself or near the channel entrance. The study of porins with single/multiple amino acid deletions or substitutions, used in conjunction with the recent 3-D information on porin structure, has enabled the location of the groups responsible for ion selectivity to be determined. The substitution in PhoE of lysine 131, which from Table 3.2 is seen to be in the constriction zone, has the most pronounced effect on anion selectivity. Substitutions of other lysine groups in the region of the constriction zone and in the mouth of the pore have minor effects.

TABLE 3.5 Permeability ratios for the different porins in the presence of a 10-fold KCl gradient. Vm is the zero current potential of the dilute side minus the potential of the concentrated side. P_c/P_a is the cation to anion permeability ratio calculated from the GHK current equation. (From Benz, 1984).

Porin	pH	Vm (mV)	P_c/P_a
OmpF/OmpC	6	27	3.8
OmpF/OmpC	3	-5	0.8
OmpF/OmpC	9	30	4.6
PhoE	6	-25	0.29

3.9 VOLTAGE-DEPENDENT GATING

Voltage-dependent gating is a phenomenon in which application of a critical voltage causes opening or closing of the porin channel. Whether a porin channel can exhibit voltage-gating is still not fully resolved. Where voltage-gating of porin channels in lipid bilayers has been demonstrated, there still exists the problem of whether the phenomenon is an artefact of the *in vitro* measurement or whether it is genuinely a property of porin in intact cells.

3.9.1 Effect of Different Planar Bilayer Reconstitutions

Schindler and Rosenbusch (1978) demonstrated that the application of high trans-membrane voltages resulted in discrete decrements in channel conductance. The conductance of each porin oligomer was seen to decrease in three discrete steps which were thought to correspond to closure of individual channels within the triplet. This behaviour was seen in OmpF (Schindler and Rosenbusch, 1978,1981, Xu *et al.*, 1986 and Morgan *et al.*, 1990) and in PhoE (Dargent *et al.*, 1986). For bilayer membranes with many channels the discrete changes in conductance cannot be resolved but the closure of the channels produces an overall reduction in the conductance of the bilayer system. A plot of current versus voltage for these systems shows a negative resistance region, where further increases in applied voltage cause the current to decrease rather than increase. Some investigators have been unable to find evidence of porin channel closure on a regular and reliable basis (Benz, 1985, Vachon *et al.*, 1986 and Hancock, 1987). Decreases in conductance were cited by Benz (1985) as a rare occurrence and as such they were dismissed as the result of porin inactivation in response to applied potentials approaching the breakdown voltage of the membrane. The reversibility of the channel closing process (Lakey and Pattus, 1989 and Morgan *et al.*, 1990) and the

existence of the consistent discrete steps of 1/3 and 2/3 the total trimer conductance make protein inactivation due to denaturation an unlikely explanation. It is possible that the observational differences are due to the different experimental techniques employed. The groups which consistently report voltage-gating in porin channels use the Schindler or Montal-Mueller method for making bilayers (see Section 3.6.1). Some groups using the Mueller-Rudin (Black Film) method have reported voltage-gating in porin channels but many others including Benz (1985) and Hancock (1987) have not.

Lakey and Pattus (1989) attempted to resolve these discrepancies by purifying porin in three different ways and reconstituting the isolated porin into lipid bilayers formed by different methods. The porin from each purification had similar closing activity in Schindler type bilayers despite the different procedures used for the purification. Lakey and Pattus (1989) had tried the purification methods used by most of the major research groups and therefore they excluded denaturation during the porin preparation as being responsible for the reported differences between different laboratories. They found that porins reconstituted into Mueller-Rudin films on thick polyethylene septa had reduced voltage sensitivity and they attributed this to the impeded thinning of these particular decane films. Mere presence of solvent in the membrane did not impede voltage closing and a secondary effect such as increased membrane thickness was thought to be responsible for stabilising porins in the open state. In bilayers formed by the Montal-Mueller method a time dependent increase in voltage sensitivity was noted. Niles *et al.* (1988) have shown that Montal-Mueller lipid bilayers form by a thinning process in the manner of Mueller-Rudin films and consequently solvent redistribution may be occurring and thus affecting the properties of the porins.

3.9.2 Other Explanations for Failure to Demonstrate Voltage-gating

Another possible explanation of why some researchers fail to demonstrate voltage-gating could be that the voltages they have applied may not have been large enough or applied for long enough (Lakey *et al.*, 1985). Morgan *et al.* (1990), using OmpF porin in Montal-Mueller type bilayers, demonstrated voltage-gating with applied voltages as low as 50 mV. However, in most studies on porin, including the present work, voltage-gating has not been seen until voltages in excess of 100 mV have been applied. Lakey and Pattus (1989) demonstrated closure of OmpF porin channels in Schindler type bilayers with applied voltages > 150 mV and in Montal-Mueller bilayers with voltages > 140 mV. They also pointed out that Schindler bilayers withstood higher potential differences better than Mueller-Rudin type bilayers. This may explain the

reluctance of some researchers using the Mueller-Rudin technique to use voltages in excess of 150 mV.

Benz (1985) mentions that porin incorporation continued during the course of his experiments and the membranes did not reach a steady conductance level. It is possible that high concentrations of solubilised porin producing rapid increases in conductance will mask the effect of channel closing. Typical times reported for the conductance of the membrane to reach a new steady state on application of high voltage is of the order of minutes (Lakey and Pattus, 1989 and Morgan *et al.*, 1990). It was certainly the experience in the present work that a high rate of channel incorporation made it difficult to resolve any voltage-gating effects.

3.9.3 Voltage-gating in Intact Cells

Controversy exists as to whether the property of voltage-dependent conductance is solely an *in vitro* phenomenon. Sen *et al.* (1988) have provided strong evidence that voltage does not control porins in intact cells. They investigated whether Donnan potential, which is the only type of electrical potential known to exist across the outer membrane, could modulate permeability in intact cells. The Donnan potential arises from asymmetric distribution of diffusible ions about a semi-permeable membrane enclosing charged molecules unable to diffuse across the membrane. The bacterial outer membrane confines a large amount of negatively charged membrane-derived oligosaccharides (MDO) to the periplasmic space. The Donnan potential of Gram-negative bacteria has been shown to vary from 5-80 mV with the inside of the cell negative. Sen *et al.* (1988) measured membrane permeability over a range of Donnan potentials from 5-100 mV with no measurable change. In the lipid bilayer experiments, channel closure was noted for OmpF with voltages as low as 50 mV (Morgan *et al.*, 1990) and for PhoE at about 80 mV (Dargent *et al.*, 1986). It is always possible that the effective potential drop across the porins is not the same in the two different environments of intact cells and lipid bilayers. Effects such as membrane surface potentials could be important and therefore the direct comparison of voltage applied via an electrode and the same size voltage drop in the form of a Donnan potential may not be appropriate.

Bilayers used in the lipid bilayer experiments differ significantly from the composition of the bacterial outer membrane described in Section 3.2. This is used as an argument for *in vitro* voltage-gating being merely an experimental artefact. It is argued, for instance, that in intact cells the porin is strongly attached to the peptidoglycan layer and that removal of the peptidoglycan/porin link could alter the behaviour of the porin. Until recently, patch clamp techniques were of no use in the

study of porins because of the minute size of bacterial cells. This method originally developed by Neher and Sakman (1976) uses a pipette pressed against the cell or membrane to form a gigaohm seal. It has the advantage over the lipid bilayer system of being able to detect faster channel events because the small size of the patch reduces any capacitive effects. The experimental developments by Delcour *et al.* (1991,1992) and Berrier *et al.* (1989) have enabled porins to be studied by the patch clamp technique. Evidence for voltage-gating of OmpC porin in cell membrane extracts, studied by patch clamp (Delcour *et al.*, 1991), support the argument that voltage-gating is a natural phenomenon.

It is also possible that other physico-chemical changes in the bilayer, initiated by the high trans-membrane voltage, are responsible for channel closure. The identification by Berrier *et al.* (1992) of a mechanosensitive channel in *E. coli* proves that other physical factors besides voltage can induce channel closure. Mechanical vibration of the lipid bilayer was observed to induce channel closures in the present work. It is however not possible to distinguish between channels closing or channels being physically expelled from the bilayer with this method.

3.10 SUMMARY

Porin is found in the bacterial outer membrane where it forms large water filled pores with slight ion selectivity, allowing the passage of hydrophilic solutes up to about 600 Daltons in molecular weight. Porin is unusual for membrane proteins in that it consists largely of β-pleated sheet. Three tightly packed monomers make up the functional channel which is therefore trimeric in form. Each monomer is a β barrel and together form three separate channels which converge at the inner leaflet of the outer membrane. Inside each separate channel is a constriction zone containing charged side chains which determine the size limitation and selectivity of the pore.

In vivo measurements of the rate of hydrolysis of β-lactams have suggested that OmpF and OmpC are selective for positively charged solutes whilst PhoE is selective for negatively charged solutes. The bulk of measurements on porins, however, has been obtained using model membrane studies such as liposome permeability, liposome swelling and lipid bilayer techniques. Estimated pore diameters using liposomes range from 1.06 - 1.16 nm. Using the lipid bilayer technique many laboratories have demonstrated three conductance states per porin oligomer, in agreement with the structural evidence that porin is composed of three separate channels. A number of laboratories, however, have failed to demonstrate these smaller conductance states. This had led to some confusion, with widely different values of single channel

conductance being quoted. In general, pore size estimates using single channel conductance measurements are less than the other *in vitro* methods.

The three conductance states per channel are most readily demonstrated by application of high trans-membrane potentials which results in reversible channel closure. This phenomenon, known as voltage-gating, is the subject of much debate. The precise method of porin purification, bilayer formation and porin incorporation may be responsible for the reported differences in porin behaviour. Where voltage-gating has been reported it is still unclear whether the phenomenon is an artefact of the *in vitro* experiment or whether it is a property of porin in intact cells.

CHAPTER 4

PORIN EXTRACTION AND PURIFICATION

4.1 INTRODUCTION

This chapter describes the isolation and purification of porins from *E. coli* 0111:B4 and K12. Most of the procedures used for porin isolation were originally developed during a co-operative research programme between the University College of North Wales, Bangor and SmithKline Beecham Pharmaceuticals (Morgan *et al.*, 1990). The purification procedure exploits both the high level of detergent resistance of native porin trimers and their tight non-covalent association with peptidoglycan.

4.2 BIOMASS PREPARATION

The growth medium used for biomass preparation was Tryptone soya broth (TSB; Oxoid CM129, 30 g/l). 10 ml of TSB was inoculated with the test strain and incubated at 37°C overnight. A shake flask containing 100 ml TSB was inoculated with 1 ml of the overnight culture and incubated for 8 hours at 37°C. 1 ml aliquots were then used as inocula for 10 flasks each containing 100 ml of TSB. The latter were incubated at 37°C overnight with shaking, the cultures aseptically combined and used as the inoculum for a 100 litre fermentation carried out in a microbiological pilot plant.

Culture absorbance at 550 nm was monitored and biomass harvested by centrifugation after 4.5 hours at which time exponential growth was ending. Cells were washed in 2 litres of 10 mM phosphate buffer (pH 7.0) and centrifuged at 30,000g for 30 minutes. The biomass was frozen at -20°C.

4.3 PORIN ISOLATION

4.3.1 Introduction

Three extractions of porin were made, each from a separate biomass preparation, one in March 1991 (0111:B4) and two in July 1992 (0111:B4 and K12). Figure 4.1 outlines the method used for porin isolation and Figure 4.2 gives the yields of protein at each stage and the starting weights/volumes at the beginning of each procedure. The detailed description of the procedures is given below.

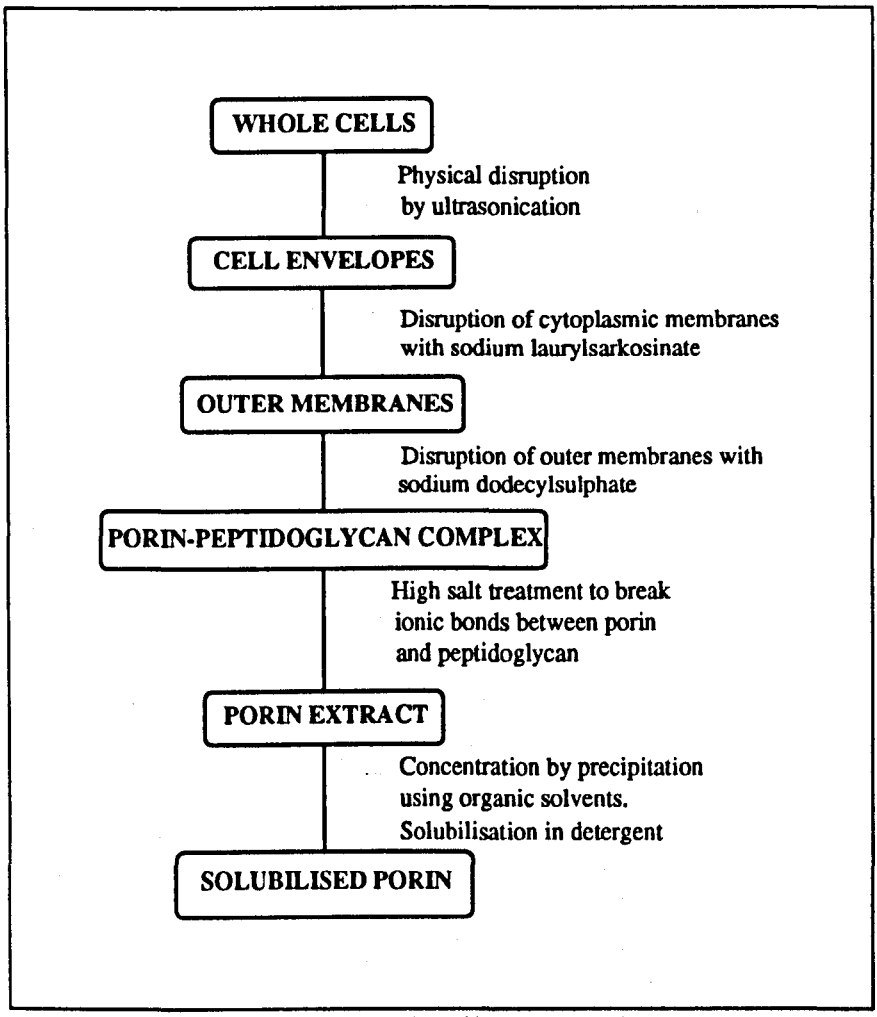

FIGURE 4.1 Outline of isolation technique

4.3.2 Cell Disruption and Cell Envelope Preparation

To extract membrane bound proteins the cells must first be disrupted. The previous collaborative work used a Manton-Gaulin homogeniser, but for the present extractions ultrasonication was used. When frequencies of 20 kHz and above are applied to solutions they cause 'gaseous cavitation' i.e. areas of rarefaction and compression which rapidly interchange. As the gas bubbles collapse, shock waves are formed which disrupt the cells. The thawed cells were suspended in phosphate buffer (pH 7.2); 40g of cells were made up to 100 ml in buffer (this was scaled up as necessary). This dilution is necessary because at very high cell concentrations there is insufficient mixing of the cells and their disruption is decreased. Cell breakage occurs at an exponential rate dependent on exposure time to the ultrasound, but as the contact time increases heat is produced as well as free radicals and ions which may cause protein denaturation. The sample is therefore kept on ice and the ultrasonication carried out in

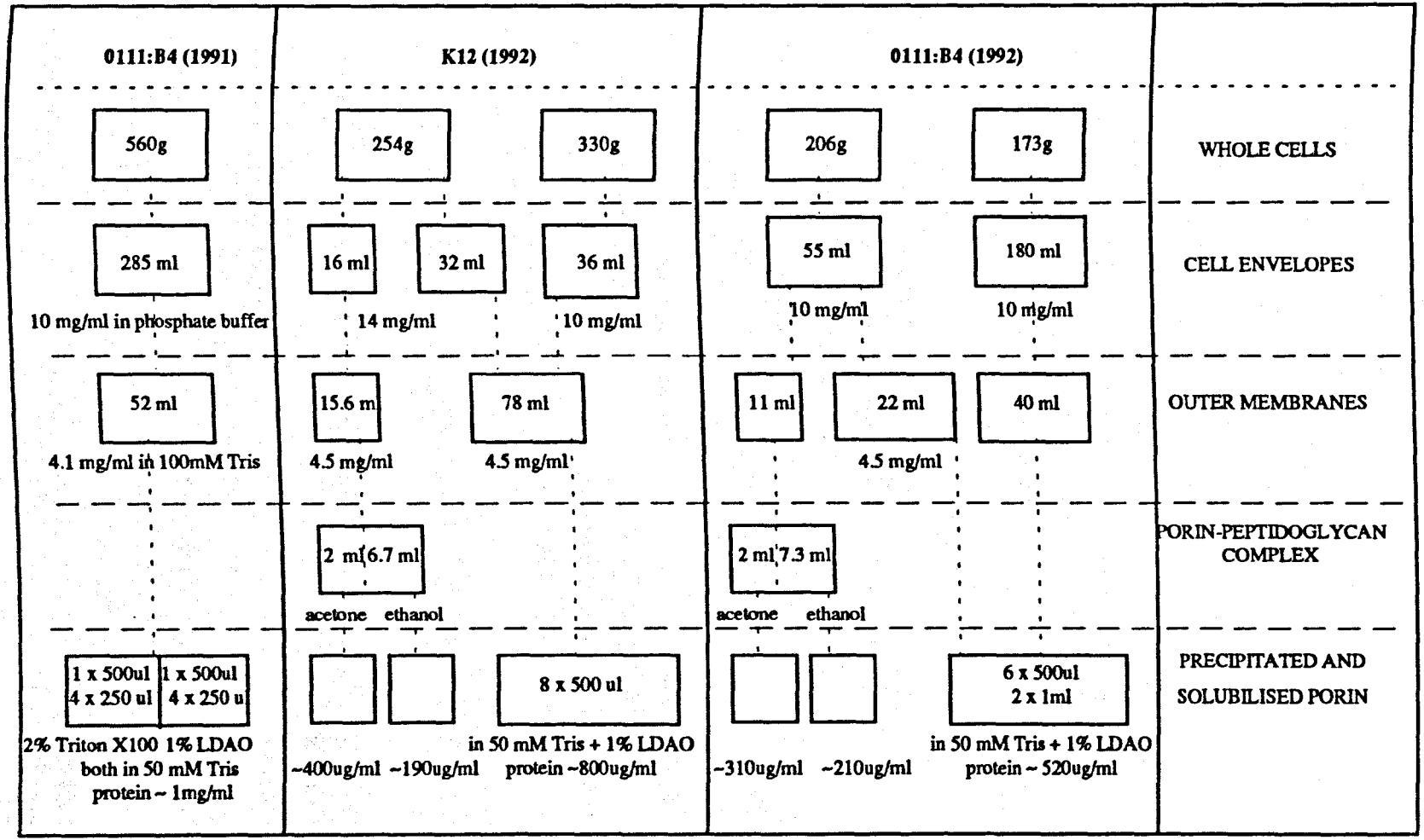

FIGURE 4.2 Stages of the isolation procedure for each individual porin extraction giving weights/volumes and protein content per ml at each stage.

bursts. The cells were sonicated in 40 ml batches for 12 cycles of 45 seconds on and 45 seconds off at an amplitude of 14 μm.

Undamaged cells were removed from the suspension by centrifugation at 5000g for 30 minutes. To increase the final protein yield the pellets were collected and resonicated. Cell envelopes were collected by centrifuging the supernatant at 100,000g for 30 minutes. Envelopes were washed by re-suspension in a small volume of phosphate buffer and recentrifuged. Pelleted material was re-suspended in phosphate buffer and collected together. Its protein content was estimated using the Bicinchoninic acid (BCA) protein assay (Pierce product no. 23225) following the microtiter plate protocol. The preparation was diluted with phosphate buffer to give a final concentration of 10 mg/ml. Cell envelopes were stored frozen at -20°C.

4.3.3 Outer Membrane Preparation

When required, the cell envelopes were thawed and treated with detergent which dissolves the cytoplasmic membrane but leaves the outer membrane intact. A sufficient volume of 20% sodium lauryl sarkosinate (sarkosyl) in 100 mM Tris-HCl (pH 8.0) was added to the diluted envelopes to give a final sarkosyl concentration of 2% w/v. The mixture was incubated at room temperature for 30 minutes with occasional vigorous mixing but trying to minimise the amount of foaming. Sarkosyl insoluble outer membranes were collected by centrifugation at 200,000g for 30 minutes and gently rinsed with 100 mM Tris-HCl (pH 8.0). The protein concentration of the resuspended pellets was estimated using BCA assay and the final concentration of protein adjusted to 4.5 mg/ml.

4.3.4 Selective Release of Porin

The outer membranes were treated with a second detergent to dissolve all material not associated with the peptidoglycan. 300 ml of 10 mM Tris-HCl (pH 8.0), containing 2% sodium dodecyl sulphate (SDS) was added to a 15 ml solution of outer membranes. This was mixed and incubated at 60°C for 30 minutes. The insoluble peptidoglycan-porin complex was collected by centrifugation at 200,000g for 30 minutes, re-suspended in distilled water and re-centrifuged. The complex was then treated with a high salt solution to break the ionic bonds between porin and peptidoglycan; the pellets were suspended in 10 ml of 50 mM Tris-HCl (pH 8.0) containing 0.4M NaCl. In addition the buffer contained 1% w/v SDS, 5 mM ethylenediamine tetra-acetic acid (EDTA), 3 mM NaN_3 and 0.05% v/v mercaptoethanol. This mixture was heated at 37°C for 2 hours with occasional stirring. The mercaptoethanol was used as a protective agent to prevent oxidation of

thiol groups and the EDTA also minimised oxidation by chelating metal ions. NaN_3, which inhibits mitochondrial and chloroplast function., was used to preserve the porin from attack by micro-organisms. The insoluble peptidoglycan was removed by centrifugation at 200,000g for 30 minutes. Porin-containing supernatant was frozen at -20°C. The pellet was suspended in 2 ml of distilled water and also frozen; if necessary the pellet could be re-processed to yield more porin.

4.3.5 Precipitation of Porins Using Organic Solvents

In order to concentrate the porin, and to dissolve it in a solution suitable for use with lipid bilayer membranes, precipitation using organic solvents was carried out. Many proteins can be precipitated by addition of water-miscible organic solvents, such as acetone and ethanol (Harris and Angal, 1989). Addition of the organic solvent lowers the dielectric constant of the solution and hence its solvating power. Thus, the solubility of the protein is decreased and aggregation through electrostatic attraction can occur. The size of the protein influences its precipitation behaviour; a larger protein will precipitate in lower concentrations of organic solvent than a smaller protein with similar properties. To minimise denaturation and to promote the necessary degree of precipitation this procedure is carried out at low temperatures.

To perform acetone precipitation, 2 ml each of porin containing solution and acetone were mixed together and incubated at 4°C for 2 hours. The precipitate was collected by centrifugation at 10,000g for 15 minutes and re-suspended in acetone followed by distilled water. At each stage the pellet was collected by centrifugation. Finally the pellet was dissolved in 50 mM Tris-HCl (pH7.2) containing 1% lauryl dimethylamine oxide (LDAO) or 2% Triton X-100. Ethanol precipitation was carried out using the method described by Garavito and Rosenbusch (1986). 94% ethanol, pre-cooled to -70°C, was added to the porin-containing supernatant at room temperature, to a final concentration of 50% v/v. The precipitate was collected by centrifugation at 5000g for 30 minutes. The pellet was re-suspended in 5 mM sodium phosphate buffer (pH7.6) containing 3 mM NaN_3 and 1% LDAO followed by the addition of two volumes of ethanol to a concentration of 66% v/v. The final pellet was re-suspended in 50 mM Tris-HCl (pH7.2) containing 1% LDAO.

The acetone precipitation produced greater protein yields than the corresponding ethanol precipitation (see Figure 4.2). The bulk of the samples were therefore acetone precipitated. The final detergent solubilised solutions were dialysed for 2 x 12 hour periods against 2 changes of 50 mM Tris-HCl (pH8.0) containing 5 mM EDTA. The dialysate was stored in 1 ml aliquots at -20°C for subsequent use with lipid bilayer membranes.

4.4 QUALITATIVE EVALUATION

4.4.1 SDS - PAGE

Porin suitably diluted with 50 mM Tris-HCl (pH7.2) was examined by SDS-polyacrylamide gel electrophoresis (SDS-PAGE). Proteins bind SDS, which effectively masks their net charge, and subsequent electrophoresis separation is dependent only on their effective molecular mass. Most proteins are denatured by SDS and therefore SDS-PAGE is generally regarded as a denaturing technique. Porin is very robust and remains in its native trimeric state unless the sample is pre-heated to 85°C for about 5 minutes. Proteins substituted with lipid or oligosaccharide moieties (e.g. glycoproteins, lipoproteins) can bind varying amounts of SDS, resulting in anomalous mobility on analysis by SDS-PAGE. Similarly, proteins formed from multiple sub-units do not necessarily bind stoichiometric amounts of SDS (Rosenbusch, 1974) and this must be taken into account when comparing the apparent molecular weights of the trimer (unheated sample) to the monomer (heated sample).

A 4% stacking gel and 12% separating gel, both containing 0.1% w/v SDS, was used. Running buffer contained glycine (28.8 g/L), Tris (6.0 g/L) and SDS (1.0 g/L) in distilled water. Each protein preparation was examined in duplicate, one of the pair being heated in gel sample buffer (Tris 0.125M, SDS 3.6% w/v, mercaptoethanol 10% v/v, glycerol 20% v/v, bromophenol blue 0.0001% w/v in distilled water) at 100°C for 5 minutes, the other at 20°C. 100 µL porin was mixed with 50 µL gel sample buffer and aliquots of each sample (40 µL) were loaded onto the gel, which was stacked at 20 mA per gel and then run at 40 mA per gel until the dye front reached the bottom of the gel. Separated components were visualised either by silver staining (Bio-Rad) for lipopolysaccharide (LPS) or by staining with PAGE blue 83 for proteins only. Stained gels were dried between cellophane for quantitative evaluation of bands and permanent storage.

4.4.2 Porin from 0111:B4 (March 1991)

Figure 4.3 shows the PAGE blue 83 stained gel of the first extraction of porin from 0111:B4 in March 1991. The protein content of the final porin solution was estimated as 1 mg/ml using BCA protein assay. The unheated tracks show an LPS like ladder profile instead of one or two bands representing native porins. Lonsdale (personal communication) established that these multiple bands do not solely represent proteins. They are in fact complexes of trimeric porins with varying amounts of LPS. The heated tracks show the denatured proteins; these are OmpF, OmpC and OmpA monomers with estimated molecular weights of 41k, 40k and 37k respectively. The preparation of the sample for the gel and the particular gel system used greatly affects the position of the porins on the gel. It is not possible to directly compare the porins

from gels performed in other laboratories. Therefore previous gels performed by Lonsdale (personal communication) running outer membrane proteins from strains of *E. coli* lacking in one or more of the major proteins were used in the identification of the bands.

4.4.3 Porin from 0111:B4 and K12 (July 1992)

Figures 4.4 and 4.5 show the PAGE blue 83 stained gels for 0111:B4 and K12 porins respectively. The final protein yield from 0111:B4 is less than for K12. This is reflected in the protein assay which gives concentrations of 520 μg/ml for 0111:B4 and 800 μg/ml for K12. The OmpA band seen in the previous extraction is not seen, indicating that the final preparation of porin from 0111:B4 is purer than in March 1991. The gels also show that the two strains produce different ratios of OmpF:OmpC. O111:B4 has an OmpF:OmpC ratio of approximately 50:1 whilst K12 has an OmpC:OmpF ratio of approximately 50:1, as estimated by the relative thicknesses of the relevant protein bands.

4.5 REMOVAL OF LPS

Parr *et al.* (1986) reported functionally active OmpF porin devoid of LPS. Their method of removing LPS using SDS-PAGE followed by electroelution was investigated. It was hoped to compare the function of this LPS devoid porin, particularly with respect to gating behaviour, with the porin containing LPS. SDS-PAGE was performed with the previously extracted porin as described in Section 4.4.1. A portion of the gel was stained with PAGE blue 83 to locate the appropriate trimeric bands. A corresponding region was cut from the unstained, unfixed portion of the gel. The porin-containing gel was cut into small pieces (approximately 5 mm^2) to increase its surface area and loaded into the electroelution cells (Bio-Rad). The protein elution buffer was 3g Tris, 14.4 g glycine and 1 g SDS made up to 1 litre in distilled water. The eluted sample was examined by SDS-PAGE.

Initial experiments resulted in very little protein in the eluted sample; no bands or very faint native porin bands were visible on the final gels. It was established that porin should be loaded 'neat' onto the initial gels and loaded into the electroelution cells to a height of only 1-2 cm. Long electroelution times were needed in order to elute the protein from the gel. The final samples were electroeluted for 6 hours 45 minutes at a constant current of 10 mA per cell. Examination by SDS-PAGE showed increased yields of protein but unfortunately very little of it was in the native trimer form: most was in the denatured monomeric form. It is possible that a set of conditions between those used in the initial experiments and this final experiment

would prove successful in providing LPS devoid porin in the eluted sample. However, a large proportion of the extracted porin had already been used in these experiments leaving less available for lipid bilayer experiments. It was considered undesirable, therefore, to spend further time on another porin extraction followed by electroelution experiments as the emphasis of this research was on the functional behaviour of porin in lipid bilayer membranes and not on the purification techniques.

4.6 CONCLUSION

Porin was extracted from whole cells of *E. coli* K12 and 0111:B4. The high level of detergent resistance of porin trimers enabled all material not associated with the peptidoglycan to be dissolved by detergent and removed. The ionic association of peptidoglycan and porin was then broken by high salt treatment to release the porin. The porin was concentrated by acetone precipitation and then dissolved in a detergent suitable for use with lipid bilayer membranes.

An initial extraction of porin from 0111:B4 was made in March 1991 yielding approximately 3 ml of detergent solubilised porin at a concentration of 1 mg/ml. In July 1992 porin was extracted from 0111:B4 and K12 (which has rough LPS). The extraction from K12 yielded approximately 4 ml of solution at 800 μg/ml and that from 0111:B4 yielded approximately 5 ml of solution at 520 μg/ml. The porin from 0111:B4 had a ratio of OmpF:OmpC of approximately 50:1 whilst the porin from K12 had a ratio of OmpC:OmpF of approximately 50:1.

The role of LPS, which is associated with the porin, has not been studied with respect to the voltage-gating behaviour of the porin. It was hoped to remove varying degrees of LPS and compare the behaviour of these porins. Unfortunately in the time available successful removal of LPS was not attained.

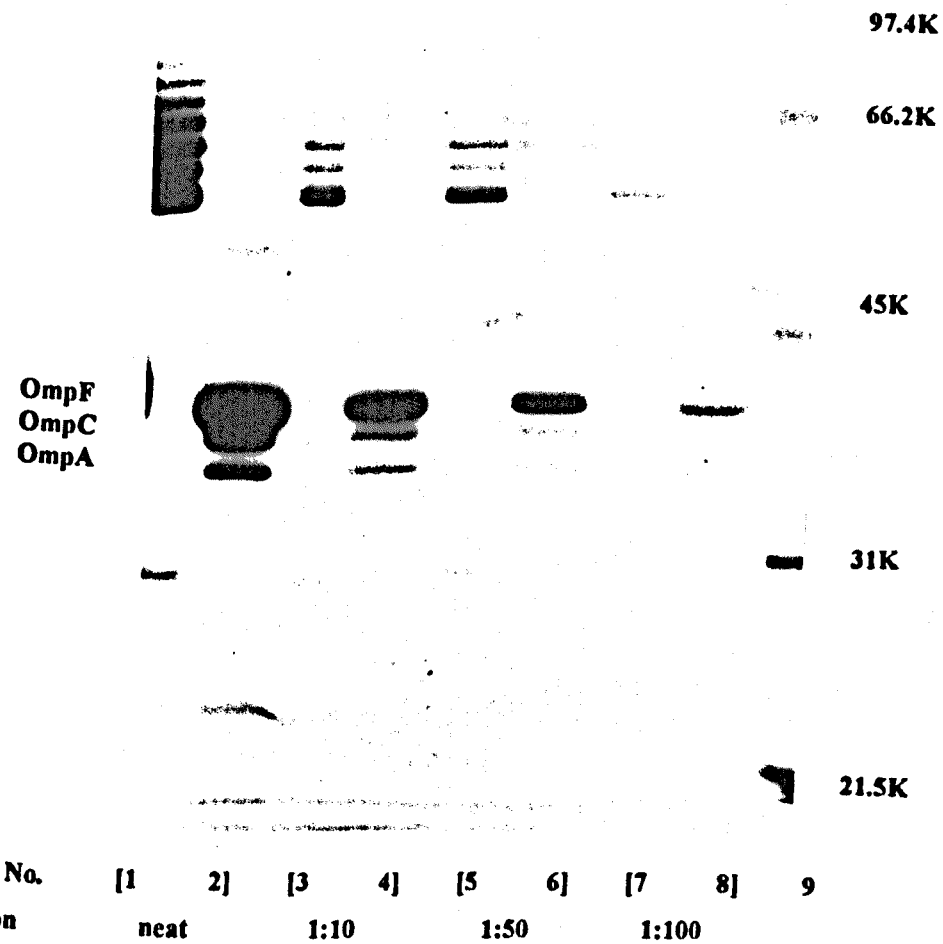

FIGURE 4.3 SDS-PAGE gel of porin from 0111:B4 (1991 extraction) stained with PAGE blue 83. Tracks 1-8 are in pairs, odd numbers corresponding to unheated samples and even numbers to heated samples. The protein content of the undiluted sample was approximately 1 mg/mL. Track 9 shows molecular weight markers.

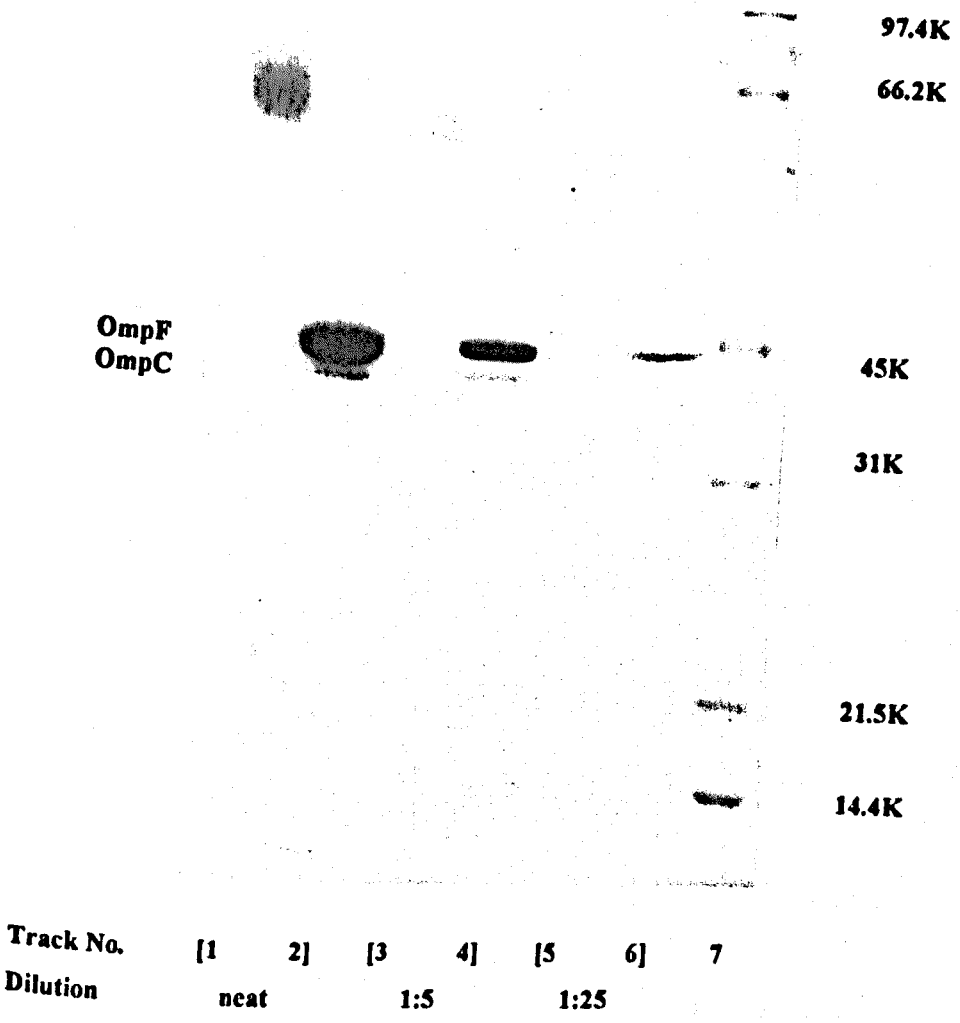

FIGURE 4.4 SDS-PAGE gel of porin from 0111:B4 (1992 extraction). Tracks 1-6 are in pairs, odd numbers corresponding to unheated samples and even numbers to heated samples. The protein content of the undiluted sample was approximately 520 μg/mL. Track 7 shows molecular weight markers.

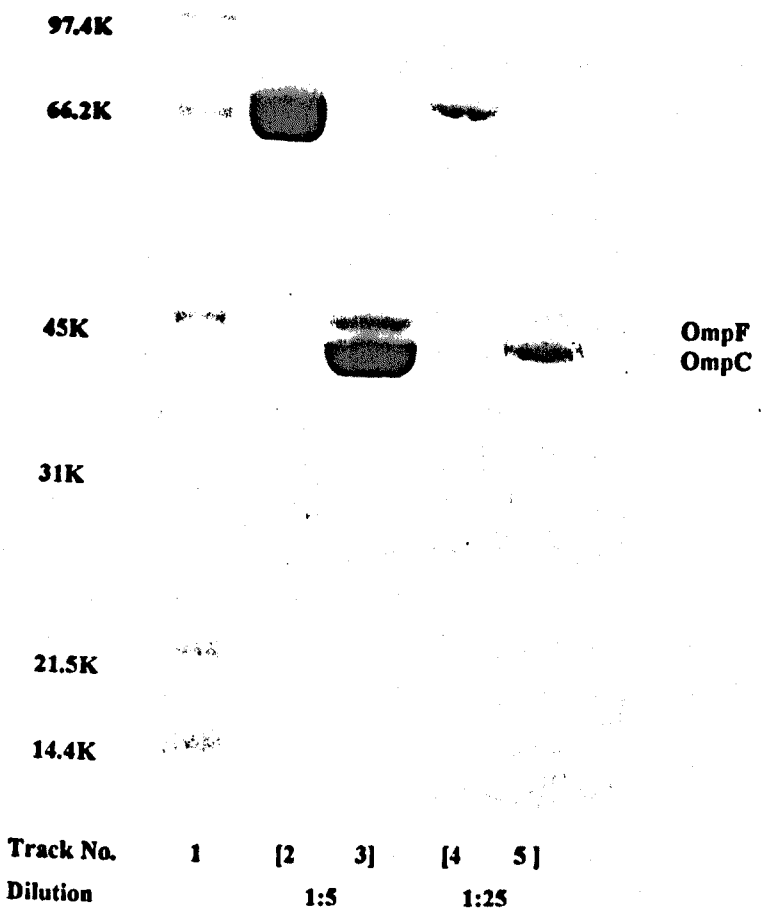

FIGURE 4.5 SDS-PAGE gel of porin from K12 (1992 extraction). **Track 1 shows molecular weight markers.** Tracks 2-5 are in pairs, even numbers corresponding to unheated samples and odd numbers to heated samples. The protein content of the undiluted sample was approximately 800 μg/mL.

CHAPTER 5

EXPERIMENTAL TECHNIQUES

5.1 INTRODUCTION

The preparation of phospholipid bilayers and the subsequent incorporation of porins requires specialised apparatus and careful attention to detail. In this chapter the method of producing bilayers, incorporation of porin channels and measurement of current flow through the channels is described. An account is also given of preparation, storage of materials and cleaning procedures, all of which were found to be important for the successful formation of lipid bilayers and subsequent incorporation of porin. Using the techniques described in this section it was possible to form stable bilayers and, within certain limits, incorporate an appropriate number of channels as required. Sections 5.5 - 5.11 give the techniques used for specific experiments, the results of which can be found in Chapters 6 and 7.

5.2 LIPID PREPARATION

The lipid used for all experiments was L-α-phosphatidylcholine (PC) from fresh egg yolk (Sigma Chemical Co. product no. P2772). This lipid consists of various chain lengths, the major components being dipalmitoyl phosphatidylcholine (32%), distearoyl phosphatidylcholine (13%), dioleoylphosphatidylcholine (31%), dilinoleoyl phosphatidylcholine (15%) and diarachidoyl phosphatidylcholine (3%) (information obtained from Sigma Chemical Company's database in the USA). The lipid was purchased dissolved in chloroform at a concentration of 100 mg/ml and stored at -20°C. The lipid was further diluted by a factor of 10 in hexane before use with bilayer membranes. This diluted lipid was made up freshly every day and stored in glass containers at -20°C between experiments. Glass containers were found to be preferable over polypropylene Eppendorf containers for storage of hexane diluted lipid. Hexane diluted lipid stored in polypropylene containers consistently resulted in experiments with no incorporation of porin into the lipid bilayer, despite the resulting bilayer appearing of reasonable surface area and quality as judged from capacitance and current measurements. An explanation could be that the hexane was causing impurities to leech from the polypropylene (Partridge, 1967 and Rogers, 1965) and that the impurities were either acting on the bilayer or on the protein itself, preventing normal incorporation of protein or even denaturing the protein. Another explanation is

that the unsaturated lipids were adhering to the walls of the polypropylene tube, in preference to the saturated lipids, resulting in bilayers of mainly saturated lipids with a high transition temperature.

5.3 PORIN PREPARATION

5.3.1 Introduction

Porin was isolated and purified as described in Chapter 4. Stock solutions of porin were stored at -20°C in 50 mM Tris-HCl (pH 7.2) containing 1% LDAO. The estimated protein concentrations in the stock solutions were as follows: 0111:B4(1991) 1 mg/ml, 0111:B4(1992) 520 µg/ml and K12(1992) 800 µg/ml. Initially these stock solutions were diluted to 100 µg/ml, 250 µg/ml and 500 µg/ml with distilled water before adding to the aqueous solutions bathing the bilayer, as in the work by Morgan *et al.* (1990). However, when the stock solutions were diluted with distilled water protein incorporation (that is the number of channels in the membrane after a given time interval, as measured by the conductance of the bilayer) was found to be very variable despite adding the same volume of diluted stock to the bilayer. This behaviour was seen for all three preparations of porin. The 0111:B4(1991) porin also produced occasional large increases in bilayer conductance (up to times 5 the expected conductance change for a single channel). A series of experiments, in which conductance changes in the bilayer were recorded following addition of porin to the aqueous phase bathing the bilayer, indicated that the stock solutions did not appear to be homogeneous even if vortex-mixed after thawing. This could be accounted for by 'clumping' of the protein within the solution. The large conductance increases described above for 0111:B4(1991) would support this idea. There was also evidence that protein could be 'sticking' to the sides of the storage tube. This was indicated by an increase in the number of incorporated channels when the Eppendorf tubes were nearly empty when, as a consequence, the syringe taking up the porin scraped against the sides of the Eppendorf. It was necessary therefore to further process the stock solutions to try and achieve more homogenous solutions of dissolved porin. The precise method used to achieve this for each porin extraction is described in the following paragraphs.

5.3.2 0111:B4 (1991)

The detergent concentration of the stock solution of 0111:B4 (1991) was increased from 1% to 2% LDAO by adding a small volume of concentrated detergent, thus diluting the protein concentration as little as possible. This new stock solution of porin

in 50 mM Tris-HCl (pH 7.2) with 2% LDAO was then sonicated. The solution was kept on ice and sonication was carried out in 5 bursts each lasting 10s, with 10s in-between, at an amplitude of 6 μm. Prior to use with bilayer membranes a further dilution was made so that the final protein concentration was 1/10, 1/100 or 1/1000 the original stock concentration. The final concentration of detergent was kept at 1% LDAO for all of the three protein dilutions. The diluted samples were also sonicated using the same procedure as for the stock solution. Using this technique it was possible within certain limits to incorporate an appropriate number of channels as required.

The conductance and capacitance of several bilayer membranes were monitored over a 3-4 hour period. The behaviour of these bilayers was compared to bilayer membranes where detergent, dissolved in the same buffer as the protein, was added to the bathing medium. It was found that volumes of 1% LDAO, similar to those used when porin/detergent was added, did not affect the bilayer. Concentrations greater than 2.5% LDAO produced 'noisy' bilayers with shorter than average lifetimes, whilst concentrations greater than 5% LDAO always caused the bilayer to break.

5.3.3 0111:B4 (1992) & K12 (1992)

The stock solutions of protein from the 1992 extractions (50 mM Tris-HCl (pH 7.2) with 1% LDAO) were thawed and mixed using a vortex mixer. The detergent concentration was increased to 2% LDAO and the solution thoroughly re-mixed. Before use with bilayer membranes a suitable dilution was made (the final protein concentration was 1/10, 1/100 or 1/100 the original stock concentration) so that the final detergent concentration was 1% LDAO. The sonicator used for the 0111:B4 (1991) porin was not available; nevertheless, thorough mixing appeared to be achieved with vortex mixing alone.

5.4 BILAYER MEMBRANE SYSTEM

5.4.1 General Overview

The experimental apparatus used for forming bilayers and measuring their conductance was similar to that used by Morgan *et al.* (1990) and is manufactured by Industrial Development Bangor (UCNW) Ltd. Figure 5.1 gives a diagrammatic representation of the apparatus. Bilayers were formed across a hole in a thin PTFE sheet according to the technique of Montal and Mueller (1972). Section 5.4.3 describes the formation of lipid bilayers in more detail. The cell for supporting the bilayer (Figure 5.2) is housed in a cabinet which acts as a Faraday cage to reduce electrical interference (Figure 5.3).

The cabinet itself is located on an anti-vibration mount to reduce mechanical disturbance. The cabinet area under the cell also functions as a magnetic stirrer, the speed of which can be controlled from the electronics unit. Silver/silver chloride electrodes connect the aqueous medium bathing the membrane to a head amplifier within the cabinet, which in turn is connected to the main electronics signal processing unit.

The electronics unit is used either to measure membrane capacitance or to supply bias voltage across the membrane for measurement of current across the membrane. Outputs are provided for connection to a chart recorder and/or an oscilloscope. In capacitance mode the unit measures capacitances in the ranges 0-100 pF and 0-1000 pF. The bias voltage can be varied from 0-1 V positive or negative with respect to earth. Currents can be measured in the range 10^{-12} to 10^{-6} A with x10 or x3 range switching.

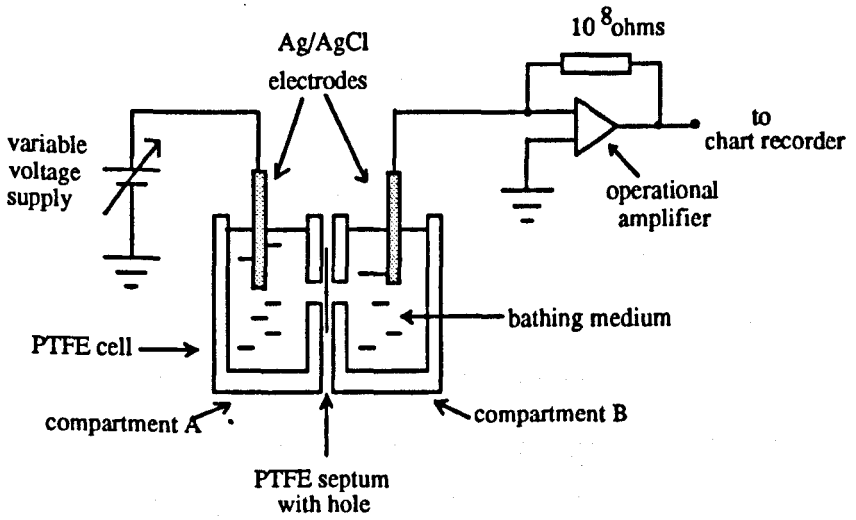

FIGURE 5.1 Diagrammatic representation of the experimental apparatus.

5.4.2 Ag/AgCl Electrodes

Silver wire of 1mm diameter (99.99% purity) from Goodfellow Cambridge Ltd. was electrolytically chlorided to make suitable electrodes for use with the lipid bilayer system. To ensure even chloriding and to avoid bare spots the silver wire was gently abraded with emery paper and then polished with finer emery paper to expose the virgin metal (Geddes *et al.*, 1969). Old electrodes were also electrolytically cleaned by making them negative with respect to an indifferent silver electrode in 0.1 M HCl and passing about 10 mA of current for a few minutes.

Silver wires were chlorided in pairs connected together as the positive electrode with respect to a platinum electrode. Chloriding was carried out in room

light with 0.1 M HCl as the electrolyte. The current density for chloriding was approximately 7 mA/cm^2 and the final chloride deposit was approximately 28500 $(mA.s)/cm^2$. The final Ag/AgCl deposit appeared rose-plum coloured.

Pairs of electrodes were stored connected together in electrolyte which was of the same composition and concentration as the electrolyte to be used in subsequent experiments, e.g. 250 mM KCl. The potential difference between the electrodes of a given pair when immersed in 250 mM KCl was generally < 1mV as measured by an electrometer (Keithley 602).

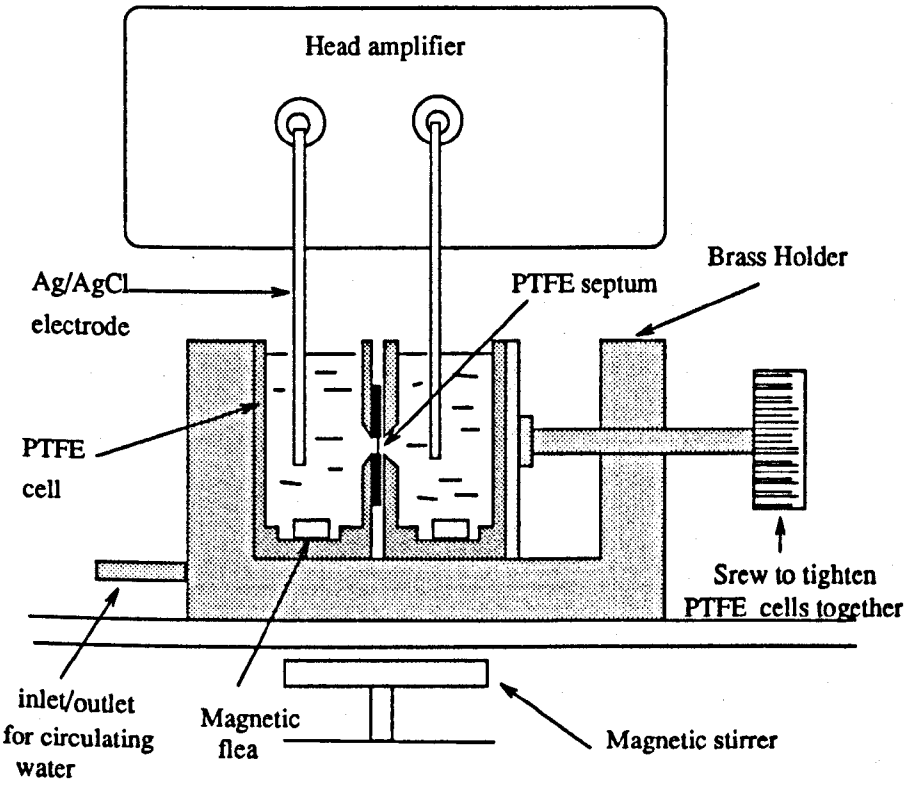

FIGURE 5.2 Cross-section of Montal-Mueller cell. (scale: actual size).

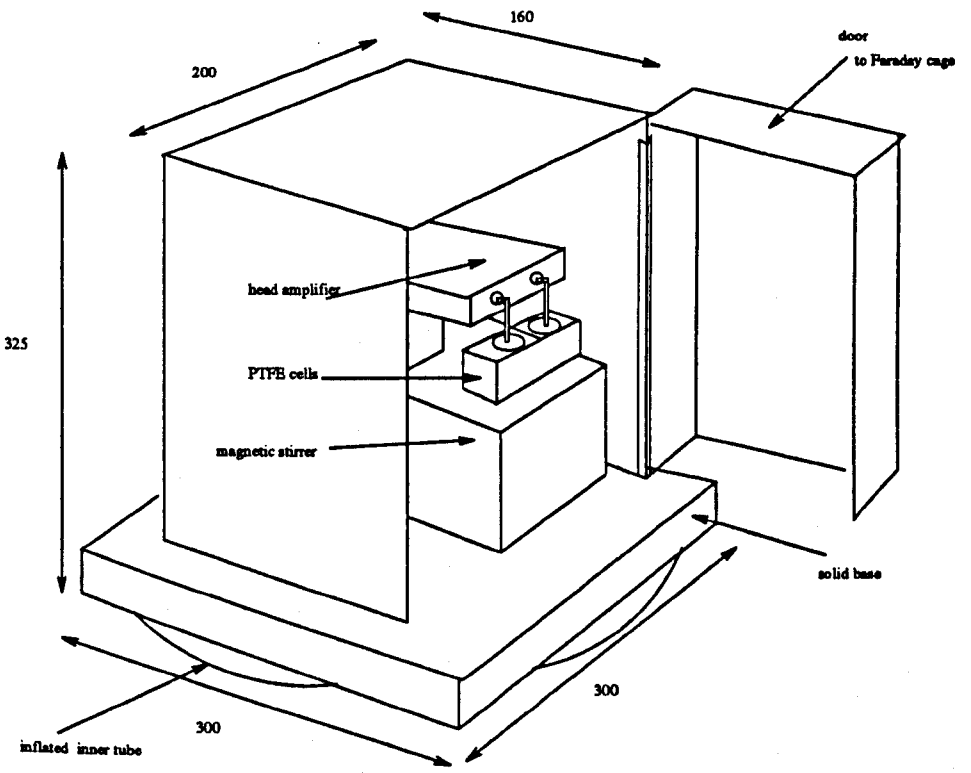

FIGURE 5.3 Measurement cell enclosure. Dimensions given are in mm.

5.4.3 PTFE Cells and Septum

To make the PTFE septum 10 μm thick PTFE sheeting (Goodfellow Cambridge Ltd.) was placed between two PTFE coated glass fibre washers with outer diameter 15 mm and inner diameter 3mm. The washers and enclosed PTFE sheeting were then heated at 600°C for 10 minutes until fused. A loop of tungsten wire (0.01 inch in diameter) was spot welded to the nickel arms of a suitable holder (Figure 5.4) and a further length of tungsten wire, approximately 10 mm in length, was welded onto the original loop. This final length of tungsten was etched electrolytically until it formed a sharp point. This was achieved by using a copper electrode (negative) in 0.1 M NaOH and making the tungsten wire the positive electrode. The wire was gently lowered and then raised a few times, using a micro-manipulator, in the NaOH. The quality of the point was judged by viewing the wire with a low power microscope (x10). The exact radius of the point was not measured.

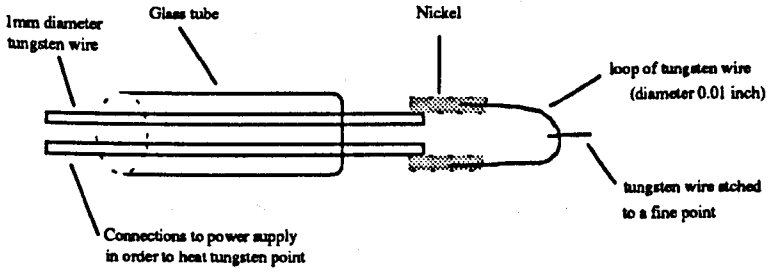

FIGURE 5.4 Diagram of glass holder with etched tungsten wire used to make holes in PTFE septum by local heating.

Using a micro-manipulator, and observing with the aid of a light microscope, the etched wire was lowered toward the PTFE sheet until it just touched the surface. The wire was then heated by connecting the arms of the holder in Figure 5.4 to a voltage supply. In general, as soon as the wire began to glow the voltage was turned off and local melting resulted in the formation of a hole in the PTFE sheet. Bilayers were most easily formed with holes in the range 75 μm to 150 μm in diameter. However, the most important feature of the hole in terms of easily producing bilayers, which were stable and non-leaky (i.e. of high resistance), was the 'smoothness' of the edge; holes with ragged edges were rejected. The holes were pre-treated with 10% hexadecane in hexane immediately prior to use. This non-polar solvent assisted in bilayer formation and also further ensured the 'smoothness' of the hole.

The two PTFE half cells were brought together with the PTFE septum between them as shown in Figure 5.2. Vacuum grease was used to provide a 'watertight' seal between the two cells. The cell was then placed in a brass holder which clamped the

two halves tightly together. The temperature of the cell was controlled by circulating liquid through channels in the brass holder (Figure 5.2) by means of a peristaltic pump and a water bath. Temperature was recorded using a platinum resistance thermometer (DRT2 Farnell Instruments Ltd., accuracy ± 0.5°C) which was placed into the aqueous solution bathing the membrane. A two channel chart recorder enabled both the conductance and temperature of the bilayer to be monitored simultaneously.

5.4.4 Formation of Lipid Bilayers

To form bilayers each half of the cell was filled with suitable subphase (e.g. 250 mM KCl) to just below the level of the hole using a glass pipette (Figure 5.5a). 10 μL of lipid diluted in hexane (see Section 5.2) was deposited onto the subphase surface using a 50 μL glass Hamilton syringe (Figure 5.5b). This was left for approximately 5 minutes to allow the lipid to spread and for some of the solvent to evaporate. Subsequently, the subphase level on one side of the cell was raised above the hole (Figure 5.5c). This caused a monolayer of lipid to form over the hole as shown in Figure 5.5c. Immediately afterwards the subphase level on the other side of the cell was raised, thus forming the bilayer (Figure 5.5d). Care had to be taken at this stage not to introduce air bubbles in the region of the hole. The geometry of the cell in the region of the PTFE septum was found to be important in reducing the likelihood of air bubbles forming near the hole and the most successful bilayers were formed when the PTFE cell was counter-bored in this region (Figure 5.2).

The capacitance of the bilayer was continually monitored during the above process. Capacitance (C) is related to bilayer area (A) and thickness (d) according to the equation:

$$C = \frac{\varepsilon_r \varepsilon_o A}{d} \qquad (5.1)$$

where ε_o (8.85×10^{-12} F/m) is the permittivity of free space and ε_r is the relative permittivity of the lipid used to form the membrane (normally taken as 2.8, Tien, 1987). The length of a C18 lipid molecule is typically 2.5 nm, giving a bilayer thickness of 5 nm. Thus, for a given diameter of hole, the area of the bilayer can be estimated and hence the characteristic capacitance, which in the present work was 0.7 $\mu F/cm^2$. In some experiments the bilayer was formed immediately the level in the second half cell was raised. Generally, however, it was necessary to raise and lower the levels in both cells several times before the bilayer formed. The resistance of the bilayer was also measured. Typically, a bias voltage of 50 mV resulted in 1-2 pA of

current. 'Leaky' membranes passing more than 10 pA were always rejected, as experience showed that they had short lifetimes and became increasingly more 'leaky' during the course of experiments.

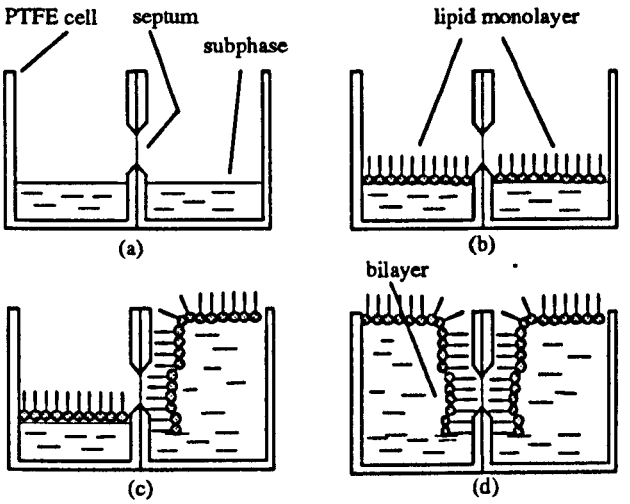

FIGURE 5.5 Steps involved in the making of a lipid bilayer using the Montal-Mueller technique.

5.4.5 Incorporation of Porin

Detergent-solubilised porin prepared as described in Section 5.3, was added to the aqueous phase surrounding the bilayer. Generally, no more than 10 μL of porin containing solution was added at a time with a 50 μL glass Hamilton syringe. For experiments requiring only 1-10 channels the 1/1000 dilution was used, whilst for experiments requiring 100+ channels the 1/10 dilution was used. This small volume, which was added as near to the bilayer as possible and as slowly as possible, was less likely to cause mechanical disturbance of the bilayer. For the majority of experiments porin was added to compartment A (see Figure 5.1) but occasionally porin was added to compartment B (see Chapter 6). To aid insertion the solutions bathing the membrane were gently stirred with electromagnetic stirrers and a bias voltage, usually 50 mV, was applied. Experimental evidence in the present work had shown that if porin was added to compartment A positive applied potentials were favourable for insertion (bias potentials are measured with respect to the virtual earth of the amplifier as shown in Figure 5.1).

5.5 CLEANING & STORAGE PROCEDURES

It was important to keep the PTFE cells and PTFE septum scrupulously clean, otherwise complete failure to make bilayers or the production of unstable, 'leaky' bilayers resulted. After use, the cell components were rinsed twice in each of the following solutions in the order given:

1. Distilled water
2. methanol
3. toluene
4. chloroform.

Between use, the cell components were stored in a stoppered bottle containing chloroform. Immediately before use they were rinsed in methanol and dried with nitrogen from a compressed cylinder. An occasional build up of hexadecane on the PTFE septum was detected by routine examination of the hole under a light microscope. To clear this deposit, the PTFE septum was soaked in hexane overnight. Forceps and gloves were used to handle the cells and septum to avoid contamination. Separate glass Hamilton syringes were used for each porin to avoid cross-contamination during experimentation. This procedure was adopted after it was discovered that some porin remained in the syringe and appeared to form functional channels even after the syringe was washed in organic solvents. This finding confirms that of Schindler and Rosenbusch (1984), who report that porin is extremely robust, remaining in its native state even in the presence of organic solvents. Glassware was washed in Decon-90 and thoroughly rinsed in de-ionised water and finally in ultra-pure water before being dried.

5.6 DIGITAL ACQUISITION OF DATA

In the later stages of the project, data were digitally stored using a Walter's IBM compatible personal computer with a 32 bit analogue-digital (A-D) card. The 0-1 V output of the electronics unit was amplified by 10 before connecting to the A-D card and the data were sampled at 10 Hz. The resulting data files (of variable length) were stored as ASCII files for later use with signal processing or graph plotting packages.

5.7 CONDUCTANCE MEASUREMENTS

Single channel conductances were measured from the discrete increases in membrane conductance occurring in the first few minutes after porin was added to the aqueous

subphase. These conductance steps were generally in the increasing conductance direction and unless otherwise stated were measured with a bias of +50 mV. The electrolyte used and its concentration and pH are shown with the relevant experimental results. For single channel and macroscopic conductance measurements the pH of the aqueous salt solution was adjusted to the values given in the results section by either adding the corresponding hydroxide or acid or, if indicated, they were buffered with 1 mM citrate or 1 mM Tris.

5.8 SELECTIVITY MEASUREMENTS

To measure selectivity, unequal salt concentrations were introduced across the bilayer and it was therefore necessary to use 3M KCl salt bridges in order to eliminate concentration cell potentials. The bilayer was made and porin inserted with equal salt concentrations on either side of the membrane. Small volumes (μL) of 5M salt were then added to compartment A, whilst stirring, to create a salt concentration gradient. The starting concentration was kept low (typically 50 mM) in order to produce a reasonable range of concentration gradients. Voltage was applied to the more concentrated side (compartment A) and when the diffusion current was reduced to zero this was taken as the zero-current potential.

5.9 INSTANTANEOUS I/V MEASUREMENTS

Instantaneous current/voltage (I/V) measurements were not made until the membrane had stabilised with respect to porin insertion with the applied voltage at +50 mV. Instantaneous I/V measurements were then made by brief application, typically 1-2 seconds, of an applied voltage. Initially a small positive potential (e.g. 10 mV) was applied and the resulting current was recorded. Following a rest at zero volts for about 5 seconds, the corresponding negative voltage was then applied. This pattern was repeated in steps of 5, 10 or 25 mV, depending on the particular experiment up to a maximum of about 200 mV. The pattern was repeated with descending values to confirm reproducibility. With some experiments the ascending pattern was also repeated, but beginning with negative applied potentials as opposed to positive ones.

5.10 STEADY-STATE MEASUREMENTS

Steady-state measurements of the I/V relationship were also made on membranes that had stabilised with respect to porin insertion. Before applying voltages > 50 mV for sustained intervals it was sometimes necessary to re-stabilise the membranes, in terms

of porin incorporation, at higher voltages such as +125 mV. The voltage was applied either until the current decay due to voltage-gating had reached steady-state or, in the few cases where steady-state was not reached, for a fixed period of time (e.g. 10-20 minutes). Where possible each voltage was applied 2-3 times to check for reproducibility.

For each individual membrane an initial shorter application of several voltages in the 75 - 150 mV range was used to establish the approximate threshold of gating. The sustained voltage applications were then made, starting just below this threshold and then at approximately 25 or 50 mV intervals up to a maximum of 250 mV. This maximum depended upon the breakdown voltage of the bilayer in question; variation between bilayers was large, the range being about 175 mV - 275 mV. Tien (1974) quotes the breakdown voltage of lecithin black lipid membranes as being 200 mV in 0.1 N NaCl. He further notes that the breakdown voltage generally depends on the past history of the membrane, the duration of the applied potential, the lipid composition and the nature of the electrolyte in the aqueous phase. He also mentions that the breakdown voltage is influenced by the concentration of impurities and changes in local conditions in the bilayer (e.g. thickness fluctuations due to mechanical vibration). Certainly the wide range of breakdown voltages of lipid bilayers in the present work suggests that many factors influence the actual breakdown voltage. These could include the number of porin channels in the membrane, electrolyte composition, time since the bilayer was first made and the size and duration of previously applied voltages. Control experiments with bilayers devoid of porin showed that applied voltages up to about 50 mV, sustained for up to 4 hours, resulted in a gradual increase in random noise in the measured current through the membrane, but that the d.c. current level remained negligible. Sustained application of voltages greater than 100 mV on newly formed bilayers produced irreversible changes in the bilayer after about 45 minutes to 1 hour. These changes were in the form of a substantial increase in d.c. current level, which fluctuated markedly. Bilayers which had been formed 1-2 hours previously and which had low d.c. current levels with 25 mV or 50 mV showed almost immediate irreversible changes when voltages greater than 100 mV were applied. Given these irreversible changes, which were related to the time elapsed since bilayer formation and the size of the applied potential, only 3-4 voltages were applied between the established threshold and say 200 mV.

5.11 TEMPERATURE CONDUCTANCE/GATING

As described in Section 5.4.3 the temperature of the test cells was controlled using a water bath, with heater and thermostat, and peristaltic pump. To achieve temperatures lower than room temperature iced water was used. After the subphase had reached the desired temperature, a further 5-10 minutes elapsed before measurements were taken to ensure that the temperature was stable and to give the membrane time to equilibrate at the subphase temperature.

The conductance of the bilayer at +/- 25 mV was monitored continuously during the heating/cooling process, in order to confirm that changes in bilayer conductance were due entirely to temperature related changes of the electrolyte rather than channel insertion or closure.

Measurements of conductivity change with temperature for various electrolyte solutions were made using an impedance bridge (Hewlett Packard Impedance Analyser, 4192A). The electrolyte to be tested was placed in the PTFE cell used for bilayer membrane experiments so that changes of temperature were made using the same method as for bilayer membrane experiments.

5.12 SUMMARY

Preparation of bilayers with incorporated porin is time consuming and requires careful attention to detail. Firstly, the factors important for the successful formation of lipid bilayers, which were also required to be stable, long lasting and of high resistance, were identified. Secondly, a method of incorporating the required number of porin channels was developed which involved further processing of the original stock solutions of detergent-solubilised porin. Having established the basic details of successful bilayer formation and porin incorporation details were also given of the methods used to determine the conductance, I/V characteristic and voltage-behaviour of porin channels.

CHAPTER 6
CURRENT FLOW THROUGH OPEN CHANNELS

6.1 INTRODUCTION

In Chapter 2 it was shown that the current flow through a channel depended on the applied voltage in two ways. With brief application of voltage the current increased with increasing voltage because of the higher transport velocity of ions in the channel. When the applied voltage exceeded some critical voltage and was sustained, gating occurred i.e. the channel closed. In this chapter the results relating to current flow through 'open' channels are presented. The bulk of the results of voltage-gating experiments are presented in the next chapter. Some of the results are mentioned in the following sections where they are relevant to the discussion of the 'open' channel data.

The methods used in the formation of lipid bilayer membranes, preparation of porin and incorporation of porin into bilayers were described in Sections 5.3 and 5.4. Departures from these procedures were occasionally necessary and are described with the relevant experimental results in this chapter. Porin used in the following experiments was extracted from two strains of *E. coli*: K12 (July 1992) and 0111:B4 (March 1991 & July 1992). The K12 strain lacks the O-specific chain on the lipopolysaccharide (Section 3.2.3). In addition the final extractions of porin from 0111:B4 were found to be OmpF rich whilst the porin from K12 was OmpC rich (Section 4.4). The results obtained for the two separate extractions from 0111:B4 will be lumped together except where any difference in the behaviour was noted.

6.2 MACROSCOPIC CONDUCTANCE

6.2.1 Conductance of Multi-Channel Membranes

In common with other researchers (Morgan *et al.*, 1990 and Benz, 1985) it was found that addition of relatively large amounts of porin to the aqueous solution bathing the membrane (10-100 ng/ml) produced a rapid increase in membrane conductance. Typical results for 0111:B4 and K12 porins are shown in Figure 6.1 Following an initial delay the membrane conductance increased rapidly by several orders of magnitude. Within a minute or two, however, this rapid rise gave way to a more gradual increase in conductance. With final concentrations of porin of the order of 10 ng/ml or less and with the applied potential kept constant the conductance reached a steady state value. Addition of porin to final concentrations > 50 ng/ml produced

membranes which continued to show an increase in conductance over 40-60 minutes. Eventually when the conductance reached about 10^{-5}-10^{-4}S the membrane ruptured, as found by Morgan *et al.* (1990).

The effect of detergent was assessed by addition of 1% LDAO (in 50 mM Tris, pH 7.2) to the membrane to final concentrations of up to x3 that normally used when porin was added. A gradual increase in conductance was seen during the course of the experiment but this was typically only x2 or x3 the initial membrane conductance in contrast to the x40 to x60 change in conductance seen with a single porin channel entering the membrane.

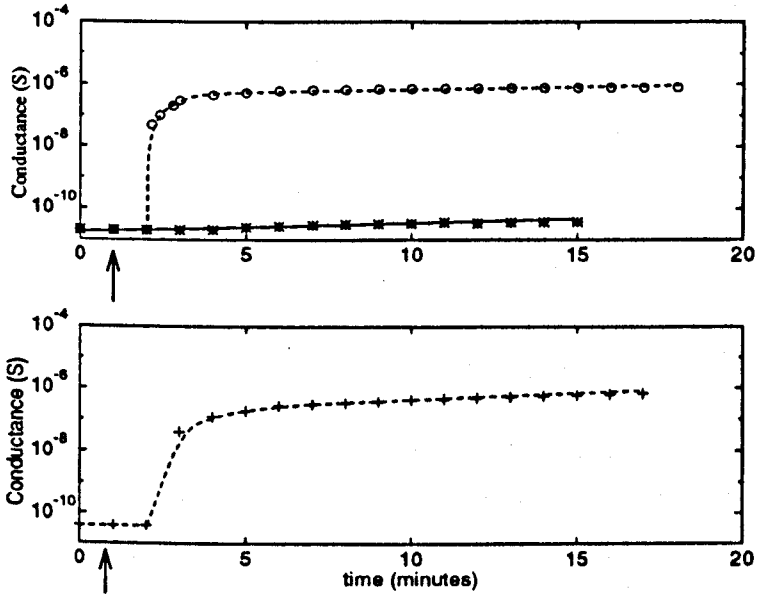

FIGURE 6.1 Increase in membrane conductance following the addition of porin. Electrolyte = 250 mM KCl, pH 7.2, applied potential = + 50 mV, T=26°C. Porin was dissolved in 1% LDAO in 50 mM Tris, pH 7.2 and was added at the time indicated by the arrows to compartment A only. (o) 0111:B4 porin, final concentration 14 ng/ml. (*) control of 1% LDAO in 50 mM Tris, pH 7.2. (+) K12 porin, final concentration 10 ng/ml.

In general, the initial rate of increase in conductance and the magnitude of the steady state level obtained (if obtained) were dependent upon the final concentration of porin in the aqueous medium bathing the membrane. However, the variability amongst experiments was large because porin incorporation into bilayers was dependent on a number of other factors. These include the physico-chemical state of the bilayer e.g.

fluidity, the presence of impurities, e.g. dust, and the composition of the dissolved porin i.e. whether it was homogeneous or in clumps. The importance of these other factors has already been alluded to in Chapter 5 where it was reported that seemingly well formed bilayers made from lipid/hexane mixtures stored in polypropylene Eppendorfs did not allow the incorporation of porin. This problem was attributed to i) impurities leaching out of the polypropylene which either denatured the protein or created unusually 'rigid' bilayers or ii) the unsaturated lipids adhering to the walls of the Eppendorf in preference to the saturated lipids resulting in bilayers of mainly saturated lipids with a high transition temperature. Some credence is given to the latter view by the work of Benz (1985) who established that the lipid composition of the bilayer influenced the incorporation of porins from *E. coli*. Our results suggest that even when using the same lipid composition subtle differences between individual bilayers dramatically influence porin incorporation.

6.2.2 Polarity Dependent Insertion

The insertion of porin from both 0111:B4 and K12 showed a marked polarity dependence. Addition of porin to compartment A (connected to the voltage source, Figure 5.1) when a positive potential is applied, results in a greater rate of porin incorporation compared to that when negative potential is applied (Figure 6.2). In some experiments with negative potential even the final, steady level of conductance attained was appreciably lower than would be expected for the corresponding positive potential. Figures 6.3 and 6.4 show the effects of changing the polarity of the applied voltage after adding porin to the bathing medium. With +100 mV applied the conductance increased steadily at a rate of 31 pS/s over a period of 25 minutes. On reversing the polarity of the voltage the rate of increase immediately halved. The 'jump' in conductance in Figure 6.3 at the point where the negative potential is applied is a result of rectification and will be discussed in Section 6.6. With 50 mV applied, the conductance increased with positive bias but remained constant for negative bias (Figure 6.4). The evidence in Figure 6.5 shows that the rate of porin incorporation is dependent upon the magnitude of the applied voltage. When the applied voltage is increased from +100 mV to +125 mV there is a four fold increase in the rate of conductance change. Increasing the applied voltage a further 25 mV to +150 mV increases the rate of conductance change a further 2.5 fold. Despite this clear evidence of voltage dependence, some membranes showed significant rates of porin incorporation with voltages as low as +2 mV. Thus the magnitude of the applied voltage is only one of many factors which influence porin incorporation. When porin was added to compartment B the polarity dependence was consistently reversed.

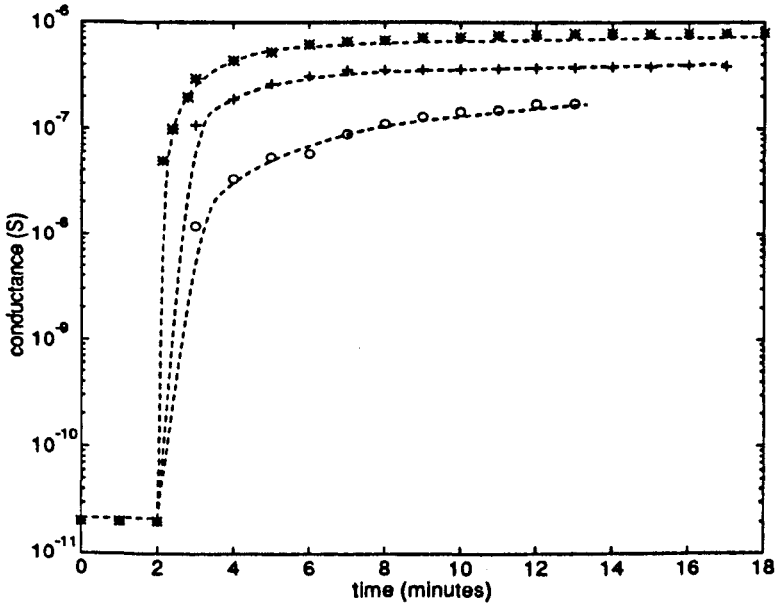

FIGURE 6.2 Conductance time plots for porin from 0111:B4. (*) 14 ng/ml, V= +50 mV. (+) 4 ng/ml, V= +50 mV. (o) 4 ng/ml, V= -50 mV. Electrolyte = 250 mM KCl, pH 7.2, T= 26°C.

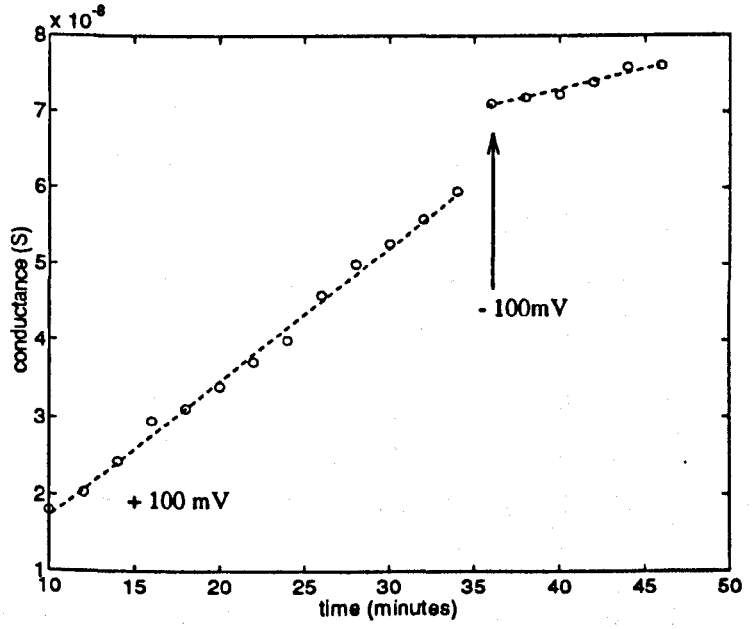

FIGURE 6.3 Polarity dependent insertion of porin from 0111:B4. The x-axis is the time elapsed since addition of porin to compartment A. Applied voltage was changed from +100 mV to - 100 mV at the arrow. Electrolyte = 250 mM KCl, pH 7.2, T= 26°C.

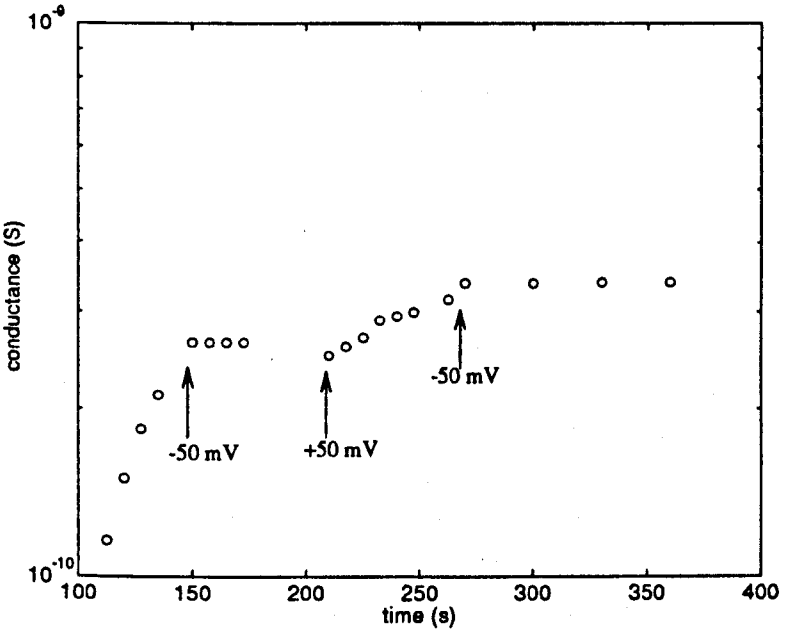

FIGURE 6.4 The effect of alternating the applied voltage during incorporation of 0111:B4 porin which was added to compartment A. Electrolyte = 250 mM KCl, pH 7.2, T=26°C.

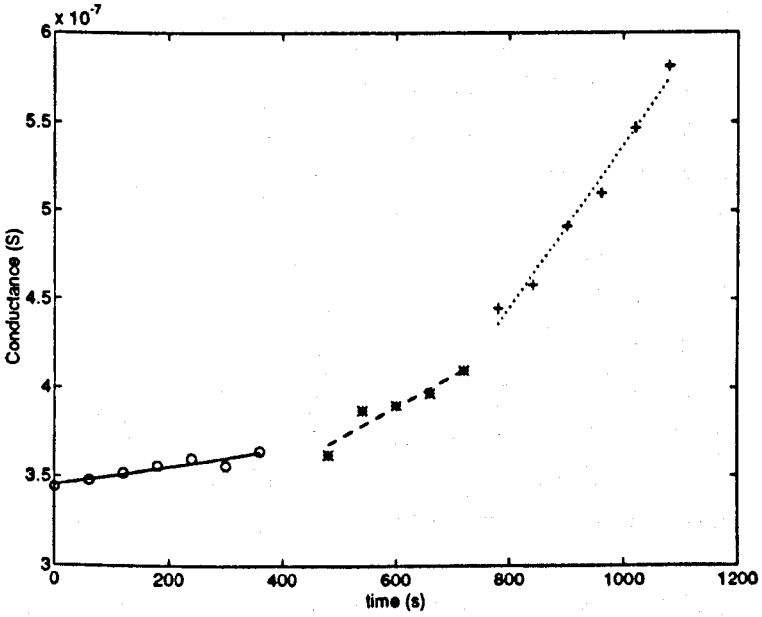

FIGURE 6.5 Dependence of porin incorporation (0111:B4) on the magnitude of the applied voltage. +100 mV (-o-), +125 mV (--*--) and +150 mV (..+..). Electrolyte = 250 mM KCl, pH 7.2, T = 26°C.

To date, no systematic study has been carried out on the polarity dependence of porin insertion. Jap and Walian (1990), in trying to resolve some of the differences in porin behaviour between various laboratories, proposed that directional insertion of solubilised porin into bilayers under the influence of an applied potential could be responsible. Morgan *et al.* (1990) report polarity dependent gating and mention that negative potentials assist porin insertion. The porins in the present study were extracted using the same method as Morgan *et al.* (1990) and were dissolved in the same buffer/detergent mixture. Morgan (private communication) confirms that their electrode conventions are the same as in this research. It appears therefore that the polarity dependent insertion demonstrated consistently in this research is in the opposite sense to that found by Morgan *et al.* (1990). Benz *et al.* (1984), on the other hand, did not detect a polarity-dependent insertion and found no difference when exposed charged groups known to be present on the protein (Cowan *et al.*, 1992) were chemically modified. These differences are difficult to explain, so the following discussion will concentrate on the results obtained here.

Polarity-dependent insertion could result from the influence of the applied field on the porin/LPS/detergent complex, on the lipid bilayer or indeed on both. The LDAO detergent is non-ionic and so does not possess any charged groups that could interact with the electric field. The latest structural information by Cowan *et al.* (1992) indicates that porin has exposed charged residues (at pH 7.2) at each end of the aqueous pore and within the pore itself. At the end of the porin trimer remote from the LPS there is a slight excess of negative charge (Section 3.4.3). Garavito and Rosenbusch (1986), in their work on the purification and crystallisation of porin from 0111:B4 B, give the pI of porin as 4.65. Thus at the pH of the present experiments (7.2) the porin will have a net negative charge. From Chapter 3 we see that the LPS associated with the porin has negatively charged groups on the lipid A and the core region. The porin/LPS complex will have, therefore, a net negative charge. Consequently, if porin is added to compartment A and positive voltages are subsequently applied, the drift of porin is expected to be away from the membrane, making this an unlikely explanation for the greater insertion rates for this polarity. In addition, experiments with the pH of the bathing medium as low as 3.5 still resulted in good rates of porin incorporation, even though this is below the isoelectric point of the porin. However, an orientation of the porin/LPS complex such that the 'bulky' hydrophilic polysaccharides are facing away from the membrane would favour the incorporation of any porin molecule diffusing to the bilayer surface. In Section 6.6.1 evidence is provided which suggests that the LPS end of the porin is more negative consistent with the above argument. There is no demonstrable difference in the polarity dependence of the porins from 0111:B4 and the short LPS mutant K12. This

indicates that porins from both strains of *E. coli* possibly orientate themselves in the electric field, despite the difference in the O-specific chain of the LPS.

The applied electric field will also affect the bilayer, increasing the number, size and mean lifetimes of local defects such as holes or pores (Berg *et al.*, 1987). As such defects would occur in both leaflets of a symmetrical bilayer this does not explain the polarity dependence of insertion. Bowen and Lewis (1983) report that application of an electric field normal to the plane of the bilayer will exert a torque on the P-N dipoles of the phosphatidylcholine head groups. With no voltage applied the dipoles lie approximately in the plane of the bilayer. It is reasonable to suppose then that the head groups move out of the plane of the bilayer rather than into the bilayer in the presence of an applied voltage. The torque will decrease the dipole-dipole attraction 'opening up' the bilayer and will eventually lead to total repulsion and bilayer rupture.

The polarity of the phosphatidylcholine dipole is such that under an applied positive bias the positive ends of the dipole would project into the aqueous solution in compartment B, but little change would occur in compartment A into which the porin is added. At first sight this is unpromising for insertion. However, if the hydrophilic portion of the porin can penetrate the leaflet on side A, then a field-induced 'opening' of the leaflet on side B could enable the protein more readily to pass through the hydrophobic portion of the membrane. If this were indeed the mechanism then the rate of insertion would be expected to depend on the magnitude of the applied voltage (a more open membrane) and on pH (changes in the magnitude of the zwitterionic dipoles of the lipid). We have already seen that the magnitude of the applied voltage influences the incorporation rate. Decreasing pH to 3.5, however, had little effect on incorporation rates, although there is some evidence that the simultaneous insertion of two or more porins is decreased.

Clearly, from the above discussion and on the basis of the available structural evidence for the porin, no plausible explanation for the polarity dependence of insertion is forthcoming. Further work will be required to understand the incorporation mechanism. As the emphasis of this research was to characterise the incorporated porin, little more was done to elucidate this interesting phenomenon.

6.3 SINGLE CHANNEL CONDUCTANCE

6.3.1 Discrete Conductance Steps

When small amounts of porin (0.5-10 ng/ml) were added to the aqueous bathing medium the membrane conductance increased in a series of discrete steps. Figure 6.6 shows a typical example of the conductance changes when 1 ng/ml porin was added to compartment A. With application of voltages in the 25 - 150 mV range and until porin incorporation had stabilised, these steps were usually in the increasing current direction, i.e. opening steps or events. When the membrane conductance had stabilised i.e. porin incorporation has ceased, the current fluctuated in a discrete manner in both the increasing and decreasing current directions (Figure 6.7).

After porin incorporation had stabilised, application of voltages greater than some threshold value resulted in steps which were predominantly in the decreasing current direction i.e. closing steps or events (Figure 6.8). This is evidence for voltage-gating and will be discussed in detail in the next chapter. At present we are interested only in the size and distribution of the opening and closing events and the information that we can obtain from them about porin structure.

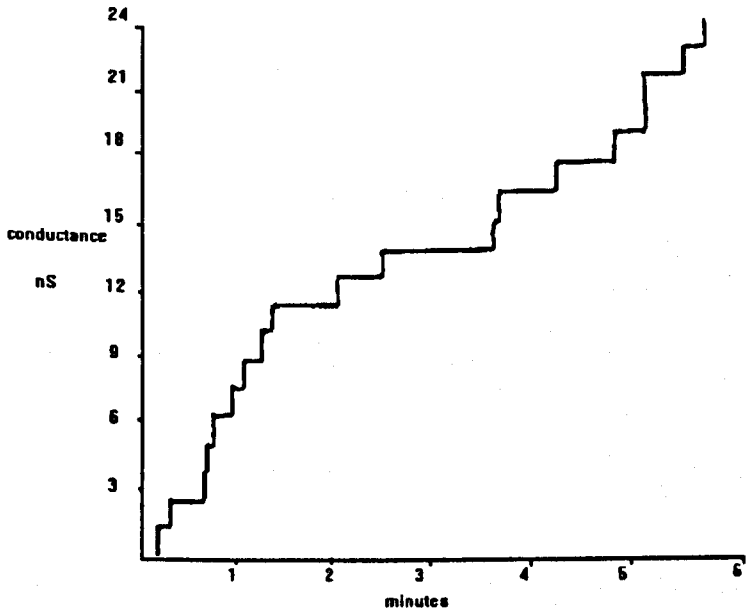

FIGURE 6.6 Discrete increments in conductance produced when 1 ng/ml of 0111:B4 porin is added to the aqueous phase bathing the membrane. Electrolyte is 250 mM KCl, pH 7.2., T= 26^{0}C., applied potential = +50 mV.

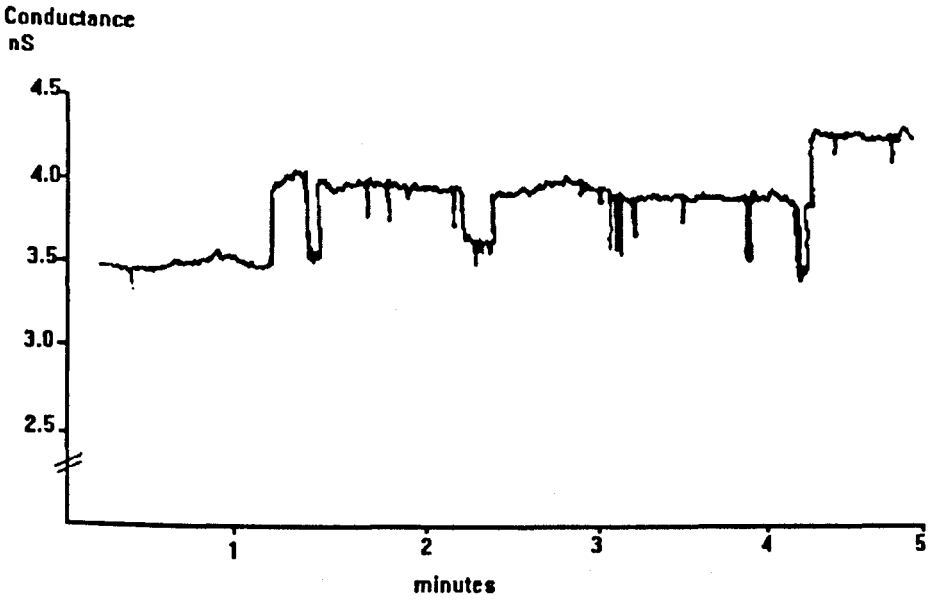

FIGURE 6.7 Discrete fluctuations in conductance seen when porin incorporation has stabilised. Applied voltage = +50 mV.

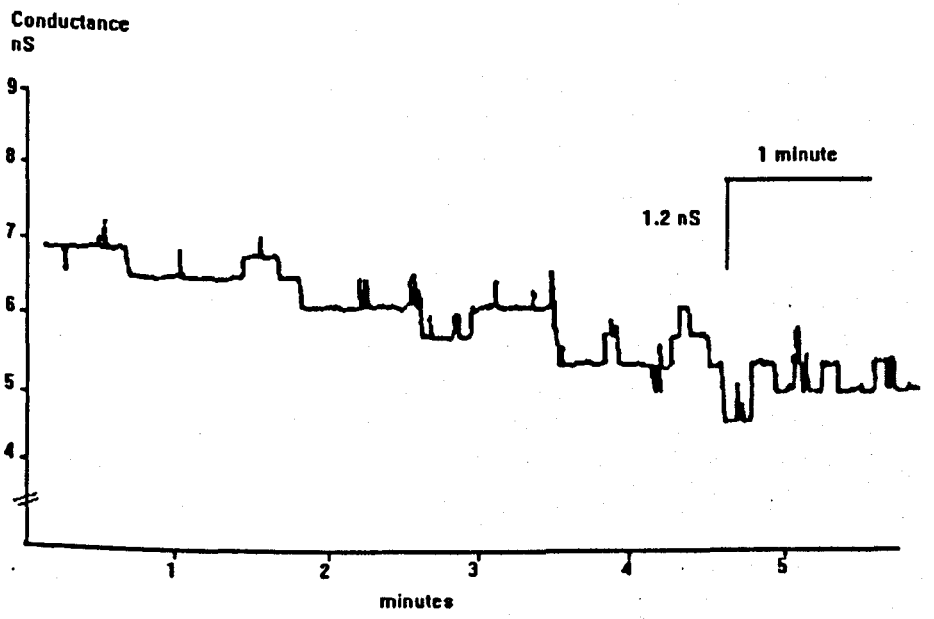

FIGURE 6.8 After porin incorporation has stabilised, application of +150 mV results in discrete closing steps, which are a fraction of the size of the opening steps obtained during porin incorporation.

6.3.2 Analysis of Conductance Steps

The conductance increments obtained during porin incorporation into the membrane are not all of the same size but are distributed over a range of values as found by Benz and Bauer (1988) and Morgan *et al.* (1990). Histograms of the probability of a porin channel having a particular conductance, Λ, as a function of channel conductance at an applied potential of + 50mV,are shown for 0111:B4 in Figure 6.9 and for K12 in Figure 6.10. From the histograms it can be seen that the majority of the opening events for the 0111:B4 porin have a magnitude between 1.15-1.45 nS whilst for the K12 porin the majority of opening events occurred in the 0.75-0.95 nS conductance interval. The data for the two extractions of porin from 0111:B4 were initially analysed separately but no significant statistical difference was observed so they were combined.

The distribution in conductance of the closing events for 0111:B4 porin are shown in Figure 6.11. The majority of events lie between 0.15-0.35 nS but there is a smaller peak in the conductance interval 0.55-0.65 nS. This confirms the findings of Schindler and Rosenbusch (1981), Xu *et al.* (1986) and Morgan *et al.* (1990) that porin does display lower conductance states, approximately 1/3 and 2/3 of the conductance seen during incorporation. In the present work, experiments with single channels from 0111:B4 and K12 have also confirmed that an open porin channel subjected to high transmembrane voltages will close in three well defined steps. These findings agree with the structural evidence provided by Cowan *et al.* (1992) that porin is a triplet of pores which traverse the membrane as separate entities.

Given that the 0111:B4 is OmpF rich and the K12 is OmpC rich the data from the histograms in Figures 6.9 and 6.10 show that the OmpC porin has a smaller single channel conductance than the OmpF porin,which is in agreement with Benz (1985). The most probable single channel conductance for the 0111:B4 porin in 250 mM KCL (pH 7.2) at 1.15-1.25 nS is somewhat larger than the value obtained by Morgan *et al.* (1990) of 0.8-0.9 nS. The distribution in the conductance steps is also much broader than that observed by Morgan *et al.* (1990),with 73% of the opening events appearing in the range 0.95-1.45 nS here compared with 75% in the range 0.8-0.9 in the work of Morgan *et al.*

The larger conductance values in both distributions (Figures 6.9 and 6.10) probably arise from the simultaneous insertion of more than one porin. It could be argued that the broad distribution of 0111:B4 in Figure 6.9 comes from the presence of both OmpF and OmpC in the sample. However, since the ratio of the major to minor

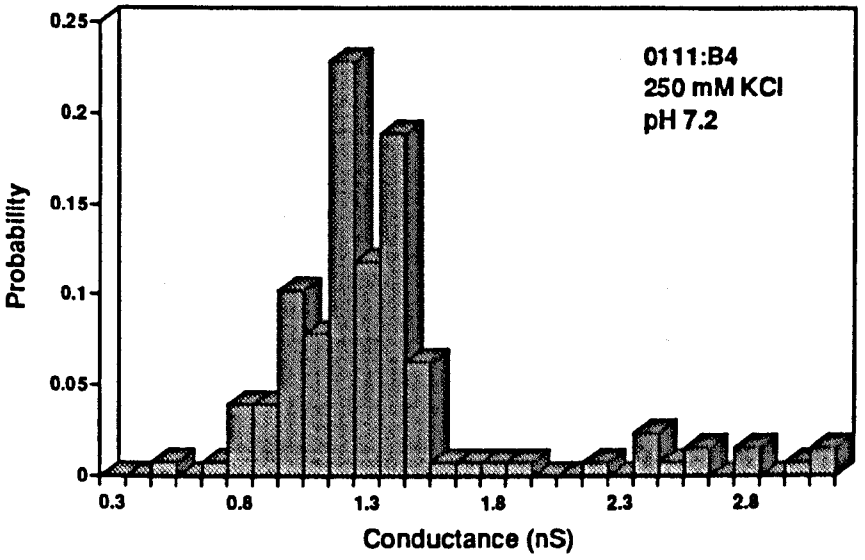

FIGURE 6.9 Histogram of opening steps obtained during porin incorporation for porin from 0111:B4. The probability of a porin channel having a particular conductance is plotted as a function of channel conductance. The labelled conductance values are the values on which each bar is centred. The applied potential was + 50 mV, T= 26°C.

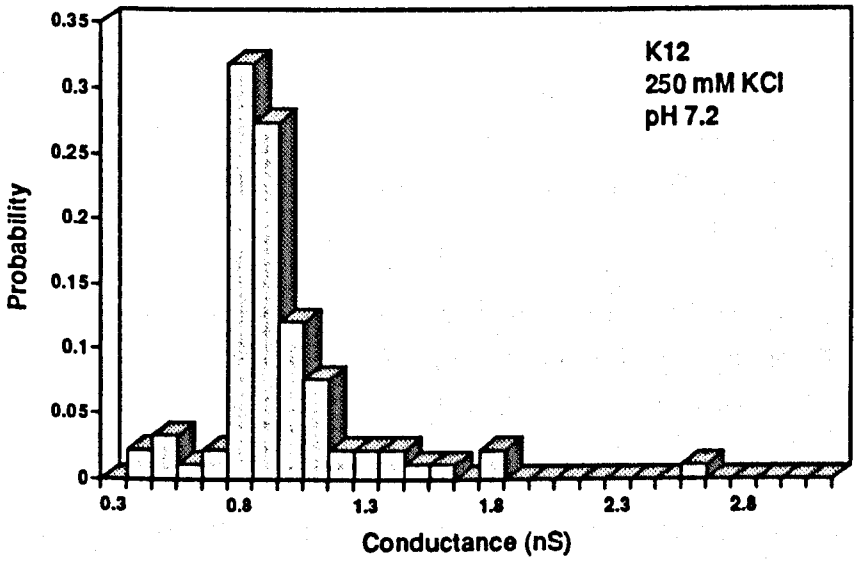

FIGURE 6.10 Histogram of opening steps obtained during porin incorporation for porin from K12. The probability of a porin channel having a particular conductance is plotted as a function of channel conductance. The labelled conductance values are the values on which each bar is centred. The applied potential was + 50 mV, T= 26°C

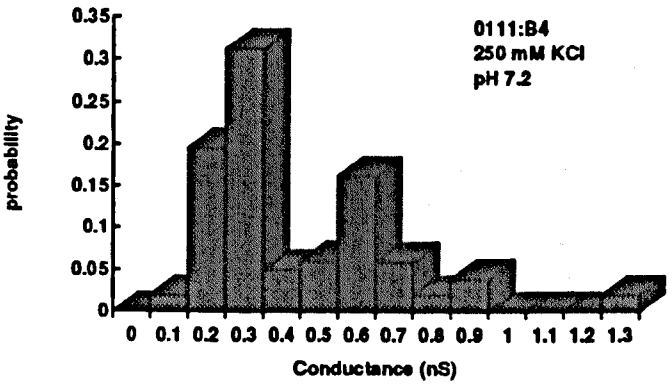

FIGURE 6.11 Histogram of closing steps for porin from 0111:B4. The probability of a porin channel having a particular conductance is plotted as a function of channel conductance. The labelled conductance values are the values on which each bar is centred. The applied potential was +150 mV, T= 26°C

constituent is about 50:1 this is unlikely to be the case, so that the broad distribution is considered to genuinely reflect real differences in the OmpF porins.

Interestingly, both the magnitude of the most probable conductance step and the narrower distribution in values obtained here for the K12 porin are closer to the data obtained by Morgan *et al.* (1990) for their OmpF from 0111:B4. Evidence is provided later (Section 6.3.5) which complements recent findings that a variety of experimental conditions can produce changes in the single channel conductances of porins. Buehler *et al.* (1991) report that reconstitution of "LPS free" OmpC porin from K12 into bilayers of asolectin and extraneous LPS resulted in a mixed population of channels. These were called F and C type channels and were distinguished by (i) the frequency, size and width of single channel conductance distribution and (ii) their threshold for voltage-gating. The F channel is so-called because its single channel conductance behaviour is similar to that of OmpF porin. Substitution of mitochondrial lipids for asolectin showed only native C type channels. It is not surprising, then, that the agreement between laboratories and even between batches of porin grown under nominally the same conditions is poor.

In Chapter 2 it was shown that conductance is a sensitive indicator of the magnitude and location of charges and dipoles within the channel. It is possible, therefore, that statistical fluctuations in the degree of ionisation of the residues could lead to differences in channel conductances between individual porins of the same type, resulting in a broad range of single channel conductances as demonstrated in Figures 6.9 and 6.10.

6.3.3 Effect of Salt Concentration

Measurements of the opening events seen during porin incorporation were performed with a variety of salts and salt concentrations. For porins from both 0111:B4 and K12, the single channel conductance is linearly related to KCl and NaCl concentration, up to 1 Molar, as shown in Figure 6.12. The single channel conductance obtained using different salts is shown in Table 6.1 and is seen to be related to the specific conductance of the aqueous phase. This is in agreement with Benz *et al.* (1979, 1985) and Benz and Hancock (1981). This means that for ion permeation for porin channels is not limited by the transport rate through the channel. In gramicidin channels, current saturation at high ion concentrations would be expected due to 'queuing' of the electrolyte ions in the channel.

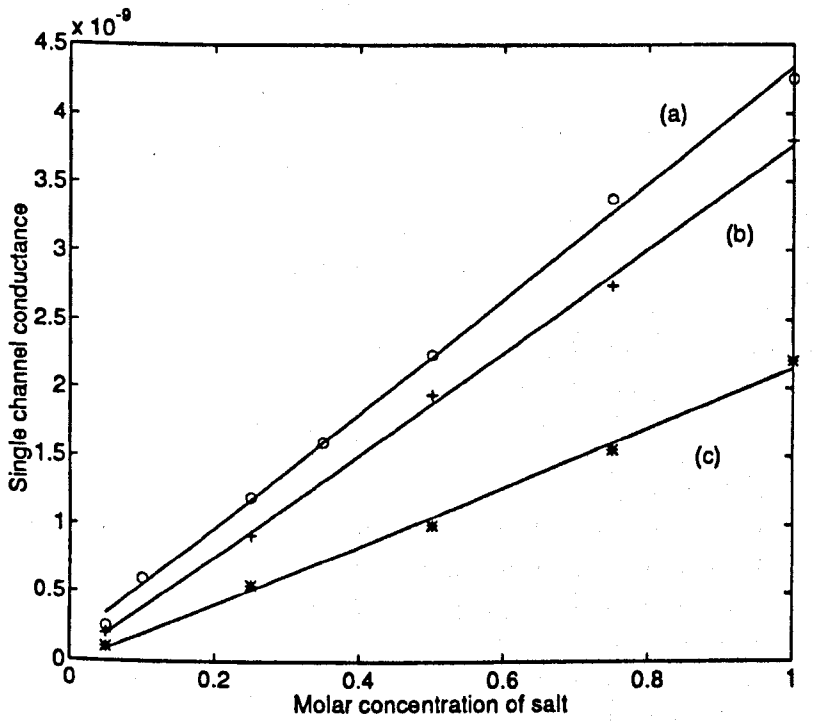

FIGURE 6.12 Effect of salt concentration on the size of channel conductance increments obtained during porin incorporation into the membrane. The curves are for 0111:B4 porin in (a) KCl (b) NaCl and (c) K12 porin in NaCl. The pH of the electrolyte was 6.0, applied potential was + 50 mV.

TABLE 6.1 Comparison of the channel conductance increments obtained during porin incorporation with different salts. Single channel conductances are the average values taken from at least 15 events. The porin was from 0111:B4, pH of the electrolyte was 6.0, applied voltage = +50 mV, T = 26°C.

salt	specific conductance, σ, (mS/cm) 25°C	single channel conductance, Λ, (nS)	Λ/σ (10^{-8} cm)
183 mM $CaCl_2$	29.4	1.3	4.42
213 mM $MgCl_2$	31.2	1.45	4.64
250 mM KCl	27.5	1.36	4.9
250 mM NaCl	21.0	0.92	4.4

6.3.4 Estimates of Pore Diameter

Based on the assumption of a cylindrical channel and taking the most probable conductance of a closing step, the channel diameter of one of the triplets of the porin trimer may be estimated. The values so obtained are given in Table 6.2 for two different channel lengths (see Section 3.7.3), namely 6 nm (Engel *et al.*, 1985) and 4.5 nm (Jap and Walian, 1990). The effective pore diameter for OmpF (L=6 nm) is approximately 8% larger than OmpC, in agreement with Benz *et al.* (1979) who estimated that OmpF was 9% larger than OmpC.

However, these estimates for pore diameter are significantly larger than those based on the conductance data reported by Benz (1985) and given in Table 3.4. The present estimate for the pore diameter of OmpF is also about 8% larger than determined by Morgan *et al.* (1990), also seen in Table 3.4. The values reported here, though, are much closer to estimates of 1-1.16 nm based on liposome permeability rates and liposome swelling assays given in Table 3.3. Exclusion limit experiments using cephalosporin antibiotics as probe solutes give a lower limit of 0.7 nm (diameter of dehydrated cephalosporin) for the pore diameter. A pore diameter of less than 0.7 nm deduced from Benz's (1985) data is clearly unrealistic, therefore, given that zwitterionic cephalosporins freely diffuse through porin channels.

Although the single channel conductance is a linear function of the specific conductance of the aqueous phase we cannot assume that ions move inside the pore as they do in bulk solution as concluded by Benz (1985). In later sections evidence is presented that the single channel conductance is a non-linear function of voltage and is also pH dependent. This non-linearity and pH dependence may well reflect genuine changes in channel dimensions (see Section 6.3.5) but changes in the potential profile within the channel must also be determined before this method of estimating pore

diameter can be considered valid. The OmpF and OmpC channels are slightly cation selective and this selectivity can be changed by pH or point mutations of amino acid groups within the constriction zone of the channel (see Section 3.8). This clearly demonstrates interaction of ions with the pore interior as they pass through the channel. Other problems in the estimate of pore diameter were mentioned in Section 3.7.3 and include the choice of channel length and the assumption of cylindrical geometry.

TABLE 6.2 Estimates of pore diameter from single channel conductance. The smallest conductance unit, 1/3 the opening event seen during porin incorporation, is used. Electrolyte = 250 mM KCl, pH 7.2. Applied potential = + 50 mV.

	Pore diameter (nm)	
	L = 6 nm	L = 4.5 nm
$OmpF^+/OmpC$ (0111:B4) Λ=0.3 nS	0.90	0.78
$OmpC^+/OmpF$ (K12) Λ=0.25 nS	0.83	0.72

6.3.5 Effect of pH on Single Channel Conductance

The pH of the bathing solution had a marked effect on the most probable single channel conductance and the distribution of conductances for porins from both 0111:B4 and K12. Figures 6.13 and 6.14 show the effects on the 0111:B4 porin of changing the pH from 3.5 to 8.5. Acidic pH not only shifts the peak probability to lower conductance but also reduces the spread in conductance values observed. When the pH is much lower than the pI of pure porin, aggregation of the protein is more likely to occur leading to higher incidences of large conductance steps. This is not observed, confirming that the appearance of large conductance events at the higher pH is the result of simultaneous incorporation of individual proteins as opposed to the incorporation of protein aggregates. At a pH of 3.5 the most probable single channel conductance is in the interval 0.95-1.15 nS and accounts for 45% of events. Alkaline pH produces a much broader range of single channel conductances, with many more events occurring in the 2.1 - 3.0 nS interval. The most probable single channel conductance is in the 1.35 - 1.45 nS interval, which accounts for approximately 32% of

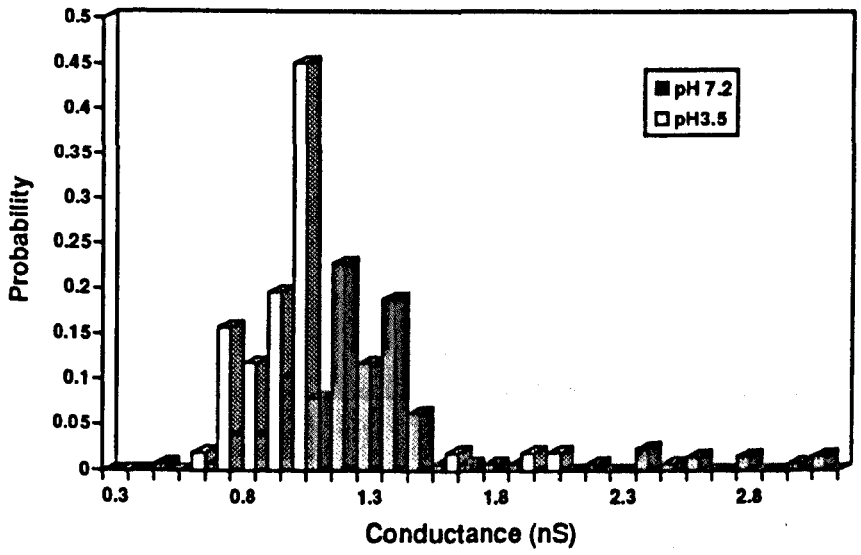

FIGURE 6.13 Histograms showing the effect of pH on opening events obtained during porin incorporation for 0111:B4. The electrolyte was 250 mM KCl, applied potential was + 50 mV, T = 26°C.

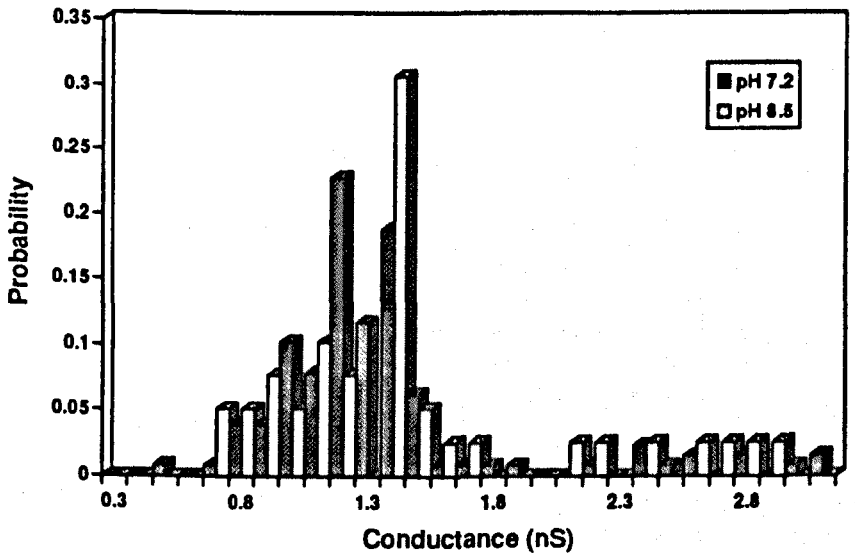

FIGURE 6.14 Histograms showing the effect of pH on the opening events obtained during porin incorporation for 0111:B4. The electrolyte was 250 mM KCl, applied potential was + 50 mV, T = 26°C.

the events. Most experiments were performed with solutions buffered with 5 mM citrate (acidic) or 5 mM Tris (basic) as these were more stable during the course of the experiment. It should be noted, though, that no significant differences were observed when the pH was controlled by addition of acid or base.

Todt *et al.* (1992) report pH-induced changes in the single channel conductance of OmpF, OmpC and PhoE porins from *E. coli*. Instead of using single channel conductance in their histograms of opening and closing events, they use the ratio Λ/σ (channel conductance increment/specific conductance of the aqueous phase). This ratio is essentially a size parameter which allows comparison between experiments without making any assumptions about pore geometry.

In their work Todt *et al.* (1992) found that the size parameter, Λ/σ, more than doubled in value over a narrow range close to neutral pH (see Table 6.3). In the present work the increase was smaller (~ 40%) and occurred over a larger pH range (3.5 - 8.5). Interestingly, at low pH the size parameter in the present work is approximately double that reported by Todt *et al.* (1992). While the variability in single channel conductance reported by various laboratories could be due to differences in the pH of the bathing solutions, as suggested by Todt *et al.* (1992), clearly other factors must be involved. These could include the amount of endogenous LPS on the purified porin and the lipid used to form the bilayer, both of which have been implicated in possible single channel conductance differences by Buehler *et al.* (1991).

TABLE 6.3 Comparison of the ratio Λ/σ obtained from conductance increments during porin incorporation into the membrane at different values of pH.

From Todt *et al.* (1992)			Results from this research		
pH	Λ/σ (10^{-10} m)	% events	pH	Λ/σ (10^{-10} m)	% events
5.4	1.6	25	3.5	3.57	45
7.5	3.5	20	7.2	4.3	22.5
8.15	3.5	35	8.5	5	32

At values of pH away from neutral, Buehler *et al.* (1991) observed a multiplicity of larger channel substates in OmpF and OmpC porins from *E. coli*. These larger conductances at low pH contradict the findings here and those of Todt *et al.* (1992). Todt *et al.* suggest that the increased channel conductance at pH 4.5 in Buehler's research may be a precursor to protein denaturation (Todt *et al.* only went as low as pH 5.4). However, in the present research the pH was reduced to 3.5 with no evidence of increased channel conductance. Furthermore, Schindler and Rosenbusch (1984) had already established that porin was resistant to extremes of pH in the range 1.4 - 12.4, making denaturation an unlikely explanation. At low ionic strength Buehler *et al.* (1991) also showed that OmpC had two sub-populations with conductance steps larger than the previously identified unit step. This phenomenon was attributed to "considerable plasticity" of the channels!

The conductance increments measured in the present experiments were those obtained during porin insertion and correspond to the three pores in the triplet all being open. It could be argued that smaller conductances reflect a lack of co-operativity between the monomers such that only 2 out of the three pores in each porin are open at the time of insertion. In the present work, data from channels which have been induced to close by application of high transmembrane potentials indicate that the conductance units corresponding to each triplet also decrease in size as the pH of the bathing medium is decreased. Thus the decrease in conductance during insertion is due to a general change in the porin affecting all three monomers.

Todt *et al.* (1992), using the liposome swelling assay, confirmed that the change in single channel conductance with pH reflected changes in channel dimensions, since porins showed a greater rate of influx of glucose and maltose at pH 9.4 than at pH 5.4. *In vivo* studies of the permeability of uncharged cephalosporin antibiotics into whole cells have also indicated that at higher pH's the size of the porin channel increases (Todt and McGroarty., 1992). The reduction in channel size at acidic pH, which has been demonstrated *in vitro* and *in vivo*, could explain why Gram-negative bacteria are resistant to some hydrophilic antibiotics at acid pH. This is of medical significance because the fluid from sites of bacterial infection in humans is acidic (Gudmundsson *et al.*, 1991). The pH-induced changes in channel diameter seen by Todt *et al.* (1992) and Todt and McGroarty (1992) are complementary to the preferential expression of OmpC porin by *E.coli* grown in acidic growth conditions. However, changes in the charge state of acidic/basic moieties in the channel or at its entrance will also influence the single channel conductance, so that the observed changes in single channel conductance cannot all be attributed to changes in channel dimensions.

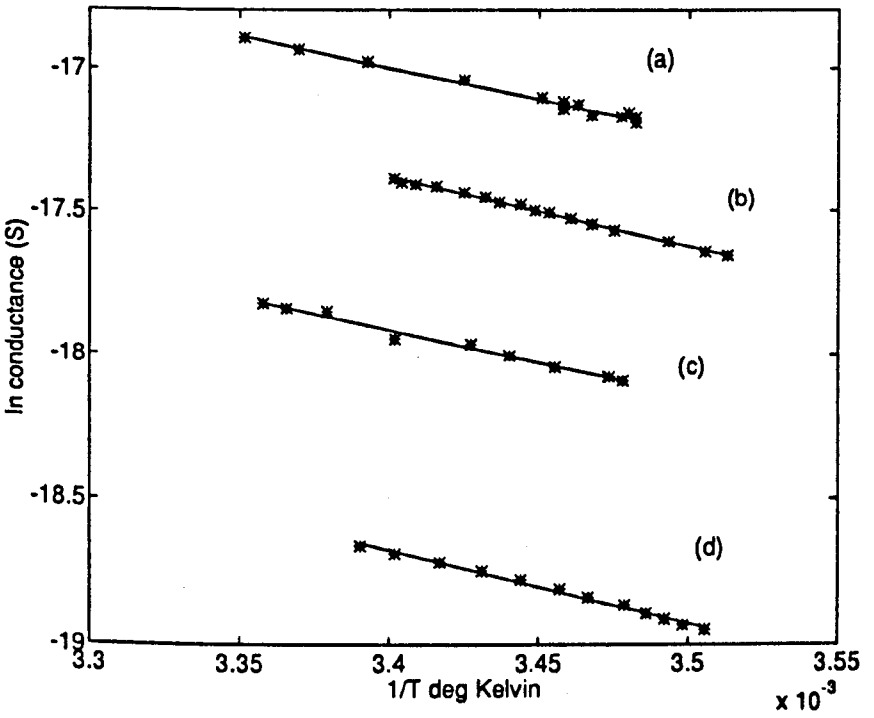

FIGURE 6.15 Plots of ln conductance versus 1/T to obtain the activation energy (Ea) for conduction through channel containing membranes. All electrolytes were buffered to pH 7.2. (a) membrane with 38 channels in 250 mM KCl, Ea=18 kJ/mole (b) membrane with 26 channels in 183 mM $CaCl_2$, Ea=21 kJ/mole (c) membrane with 22 channels in 250 mM NaCl, Ea=18.7 kJ/mole (d) membrane with 5 channels in 213 mM $MgCl_2$, Ea=21 kJ/mole.

6.4 EFFECT OF TEMPERATURE ON MEMBRANE CONDUCTANCE

The effect of temperature on the conductance of membranes containing from 5-38 channels of 0111:B4 porin was measured in different salt solutions (Figure 6.15). The temperature range was limited to approximately 0°C to 35°C as control experiments showed that bilayers became 'noisy' and unstable at higher temperatures, presumably due to increased fluidity of the bilayer. The transition temperature for the phosphatidylcholine used in these experiments was not known and would need to be found experimentally due to the mixture of chain lengths (Section 5.2). Activation energies, deduced from the slopes of the linear plots in Figure 6.15, for the univalent salts NaCl and KCl are in the range 18-19 kJ/mole (4.45 kCal/mole). The divalent salts $CaCl_2$ and $MgCl_2$ gave slightly larger activation energies of around 21 kJ/mole (5 kCal/mole). In Table 6.4 the activation energies for the channel conductance are compared with the activation energies of bulk electrolyte solutions. The latter were

calculated from conductance measurements made, with an a.c. admittance bridge at 750 kHz, at different temperatures. Also for comparison are activation energies from literature data.

TABLE 6.4 Comparison of activation energies (Ea) obtained for (a) channel containing membranes with (transmembrane potential +/- 25 mV) (b) values of Ea obtained using impedance bridge to measure conductivity of bulk electrolyte at different temperatures and with (c) Ea calculated from limiting equivalent conductances of the separate ions at different temperatures. Data from CRC Handbook of Chemistry and Physics, 68 th edition.

Electrolyte	Ea (kJ/mole) experimental (a)	Ea (kJ/mole) control (b)	Ea (kJ/mole) calculated (c)
250 mM KCl pH7.2	18.0	14.8	15.8
250 mM NaCl pH 7.2	18.7	15.2	15.2
213 mM $MgCl_2$ pH7.2	21.0	15.13	-
183 mM $CaCl_2$ pH7.2	21.5	15.2	15.8
1M KCl pH 7.2	19.1	15.35	-
250 mM KCl pH3.5	20.8	-	-

In all cases, the activation energy for channel conductance is 25-30% larger than for bulk electrolyte. Conduction in the channel is controlled, therefore, by another temperature dependent process. It is of note, that the barrier heights calculated by Sancho and Martinez (1991) and Levitt (1985) (see Section 2.4.2.1), in their electrostatic models, are approximately 30 mV which is consistent with the additional activation energy required for transport through the channel.

The activation energies obtained did not depend on whether the membrane was being cooled or heated or indeed re-cooled after initial heating or re-heated after initial cooling as shown in Figure 6.16a. At relatively low applied potentials there was no difference in the activation energy obtained at positive and negative voltages (Figure 6.16b). Unfortunately, the high failure rate of membranes at the higher temperatures and voltages coupled with voltage-gating meant that corresponding plots could not be obtained for the more interesting asymmetrical region in the I-V plots (see Section 6.6).

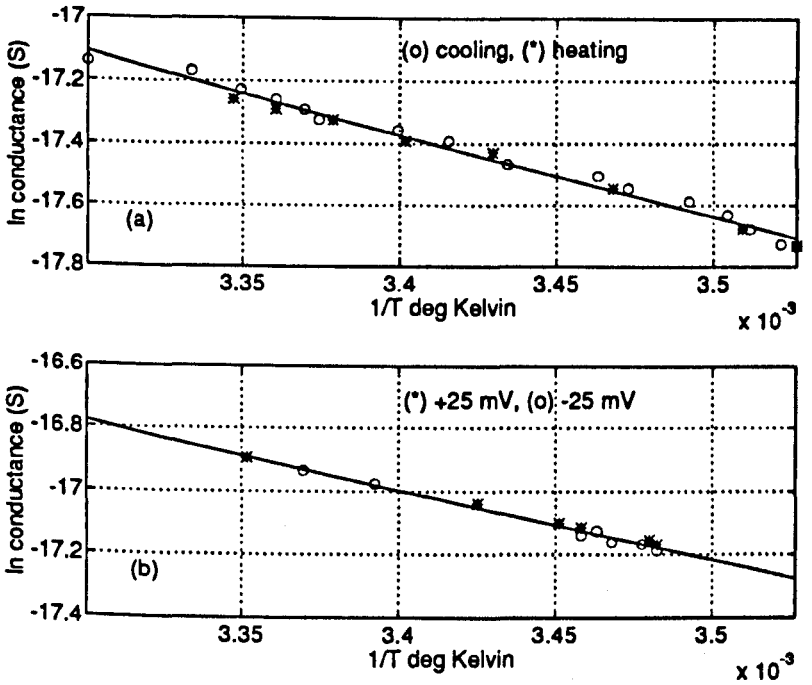

FIGURE 6.16 Arrhenius plots of conductance versus reciprocal temperature for (a) a membrane containing 27 channels in 250 mM KCl, pH 7.2, data when heating (*) and cooling (o) the membrane. Ea= 21 kJ/mole, applied voltage = +50mV (b) a membrane containing 38 channels in 250 mM KCl, pH 7.2. Data was collected for two transmembrane voltages (*) +25 mV and (o) -25 mV. Ea = 18 kJ/mole.

6.5 SELECTIVITY MEASUREMENTS

The selectivity of the porin channels was assessed by measuring reverse current voltage potentials, V_{rev}, in the presence of different concentrations of the same electrolyte on both sides of the membrane (see Section 5.8 for method). As described in Section 3.8.1, unequal concentrations of KCl on either side of the membrane should result in a diffusive flux of both anions and cations from the high to the low concentration side of the membrane. Given that the diffusion coefficients of the two ions are similar, the net current flow should be zero. In the present work, unequal salt concentrations produced a net current whose polarity indicated the preferential diffusion of cations through the porin. The voltage needed to offset this diffusion current was the zero-current or reverse current membrane potential. Values of V_{rev} were plotted against the salt concentration ratio across the membrane (Figure 6.17) and were compared with the theoretical curves produced using the Goldman-Hodgkin-Katz (GHK) voltage equation (equation 2.21). The theoretical curve obtained using a cation to anion

permeability ratio (Pc/Pa) of 3.0 best fits the data obtained from membranes bathed in KCl. In NaCl the Pc/Pa ratio which best fits the data is lower at 2.1, which can be explained by the slightly lower ionic mobility of Na^+ compared to K^+.

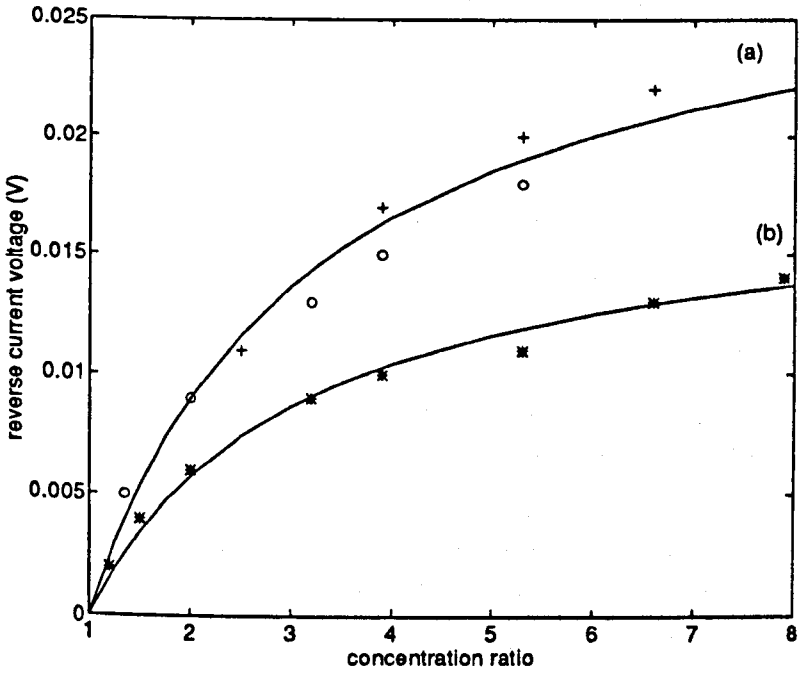

FIGURE 6.17 Reverse current voltage versus the salt concentration gradient across the membrane for (a) K12 (o) and 0111:B4 (+) in 250 mM KCl, pH 7.2. The solid line is calculated from the GHK voltage equation assuming the cation to anion permeability ratio (Pc/Pa) is 3.0. (b) 0111:B4 porin in 250 mM NaCl, pH 7.2. The solid line is calculated from the GHK voltage equation using Pc/Pa = 2.1.

These findings are in excellent agreement with those of Benz *et al.* (1979) as shown in Table 6.5. Lowering the pH of the bathing medium reduced the ratio of Pc/Pa in KCl from 3.0 to 1.1, again in excellent agreement with Benz *et al.* (1979). These experimental findings support the view that at physiological pH (7.2) porin is weakly cation selective. In Section 3.8 evidence was presented that charged amino acid side groups were responsible for the selectivity of porin channels. The lowering of the Pc/Pa ratio with decreasing pH also supports this hypothesis.

TABLE 6.5 Cation to anion permeability ratios Pc/Pa for porin channels obtained from zero-current membrane potentials in the presence of unequal salt concentrations of the same electrolyte across the membrane.

From Benz *et al.* (1979) OmpF/OmpC porin in oxidised cholesterol membranes		(0111:B4) and (K12) porins in egg PC bilayers	
Electrolyte	Pc/Pa	Electrolyte	Pc/Pa
NaCl pH 6.0	2.5	NaCl pH 7.2	2.1
KCl pH 6.0	3.7	KCl pH 7.2	3.0
KCl pH 3.0	1.2	KCl pH 3.5	1.1

The I/V relationship for a membrane with both equal and unequal KCl concentrations on either side is shown in Figure 6.18 and compared with theoretical curves. The latter were calculated using the GHK current equation (equation 2.14), for each ion species, and setting Pc/Pa = 3.0. With equal salt concentrations across the membrane the GHK current equation predicts a linear I/V relationship. As can be seen from Figure 6.18 the relationship for a channel containing membrane is not linear and this is studied in more detail in Section 6.6. With a salt concentration ratio of 1:2, 1:4 and 1:6 the experimental data did not show the degree of rectification predicted by the GHK current equation, as can be seen for the 1:4 data in Figure 6.18. The departure from the GHK current theory is not due to concentration saturation (see Figure 6.12), as this was not seen in porin channels at these salt concentrations. The lack of agreement with the GHK theory is not surprising because the GHK current equation is derived from a rather simple partitioning electro-diffusion model which assumes that the field in the channel is uniform (amongst other assumptions). As discussed earlier (Section 2.4.2.1) the presence of fixed charges and/or dipoles in the constriction zone of the channel (Section 3.8) will influence the potential profile within the channel and also the voltage dependence of conduction through the channel.

6.6 INSTANTANEOUS I/V MEASUREMENTS

6.6.1 Asymmetrical, Non-Linear I/V Relationship

The voltage-dependence of channel conductance was determined by measuring the instantaneous current/voltage (I/V) characteristics of the channel-containing membrane, as described in Section 5.9. Where obvious evidence of voltage-gating was present or if the I/V plots were not reproducible, the data were disregarded. Figure 6.19, which shows the I/V behaviour containing 1, 2 and then 3 0111:B4 channels,

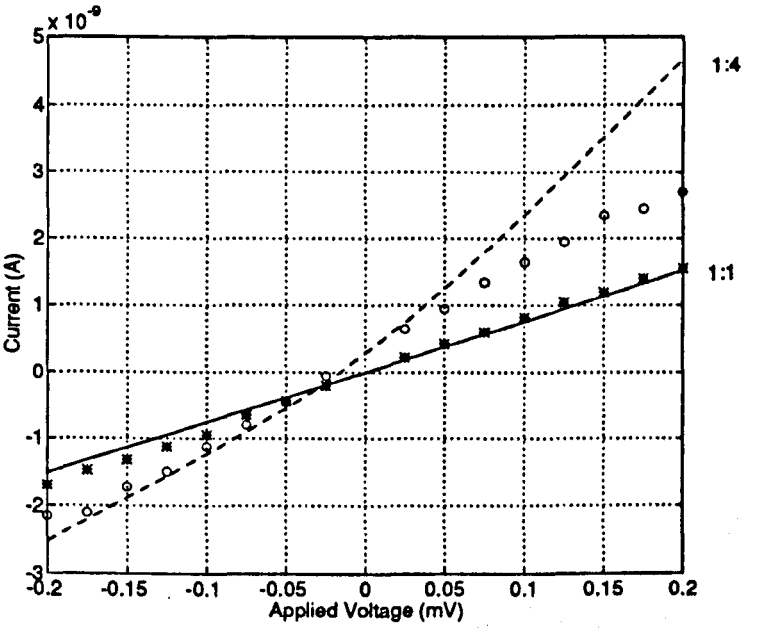

FIGURE 6.18 I/V relationship for a membrane with approximately 67 channels and with equal and unequal concentrations of KCl on each side. pH = 7.2. Experimental data is for a concentration gradient of (*) 1:1 (50mM:50mM) and for (o) 1:4 (50mM:200mM). The transmembrane voltage is applied to the more concentrated side (compartment A). The lines are calculated using the GHK current equation using Pc/Pa = 3.0 and for concentration gradients of 1:1 (solid line) and 1:4 (dashed line).

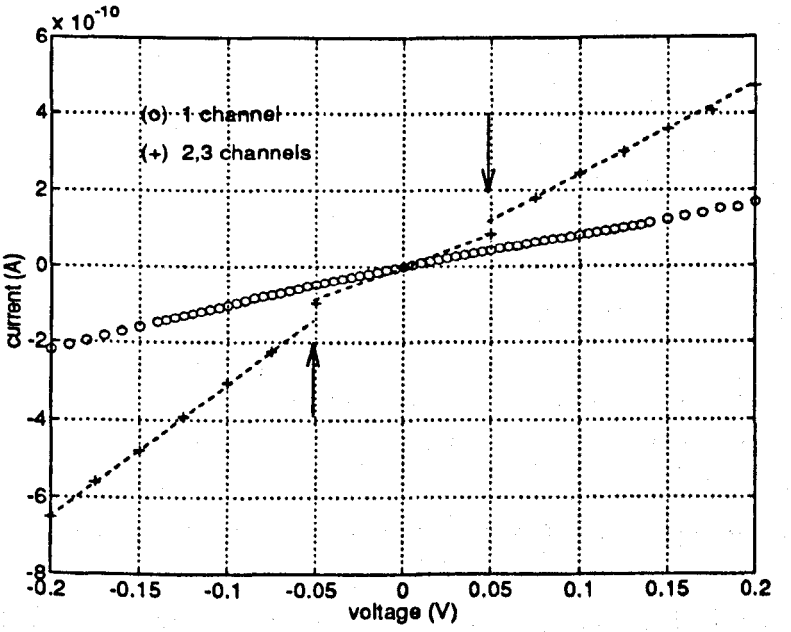

FIGURE 6.19 I/V characteristic for K12 porin. Electrolyte = 250 mM KCl, pH 7.2. T = 26°C. (o) 1 channel (+) 2 channels until the points marked by the arrows where a third channel has entered the membrane. Porin was added to compartment A.

represents the true behaviour of such channels (data presented in Figure 6.18 were also collected in this way). As can be seen, the slopes of the I/V plots increase in proportion to the number of channels in the membrane, although a slight asymmetry exists between positive and negative bias above about 40 mV (in 250 mM KCl, pH 7.2). Closer inspection of the plot reveals also a slight non-linearity. Figure 6.20 shows the effect of bias polarity on the magnitude of the currents flowing through a channel.

The only reports of asymmetries or non-linearities in channel conductance have come from patch clamp studies of spheroplasts or bacterial membranes fused with liposomes. To date authors using the lipid bilayer method have all reported symmetrical, linear instantaneous I/V relationships with equal salt concentrations across the membrane (Benz, 1985; Morgan *et al.*, 1990; Lakey and Pattus, 1989; Xu *et al.*, 1986; Schindler and Rosenbusch, 1978). Martinac *et al.* (1987) and Buechner *et al.* (1990) found a pressure sensitive cell, thought to be a porin, in giant spheroplasts of *E. coli* which had a larger conductance with depolarizing voltages (negative outside) than polarizing voltages (positive outside). Delcour *et al.* (1989) found a channel in the outer bacterial membrane which rectified slightly. Again the channel was thought to be a porin. It was thought by some authors that association of the porin with outer membrane components, e.g. peptidoglycan, was responsible for the different results obtained from patch clamp and lipid bilayer studies. Clearly this cannot be the case here since the purified porin is associated with LPS only, but still shows asymmetrical, non-linear behaviour.

With porin added to compartment A the asymmetry was consistently in the same direction, whether there were only a few channels or many channels in the membrane (the number of channels in a membrane was estimated by measuring the conductance at +50 mV and dividing by the most probable single channel conductance obtained at the same potential (see Section 6.3.2)). Upon addition of porin to compartment B the asymmetry changed polarity (Figure 6.21). Addition of porin to both compartments resulted in a symmetrical and near-linear I/V relationship (Figure 6.22), which is presumably a composite of Figures 6.20 and 6.21. In Section 6.2.2 the polarity dependent insertion was attributed to field induced orientation of the porin. The orientation most preferable for insertion into the membrane was thought to be one in which the 'bulky' hydrophilic LPS was facing away from the membrane. The change in the sense of the asymmetry when porin is added to different compartments and the disappearance of the asymmetry when porin is added to both compartments provide further evidence that the porin inserts into the membrane in a specific orientation.

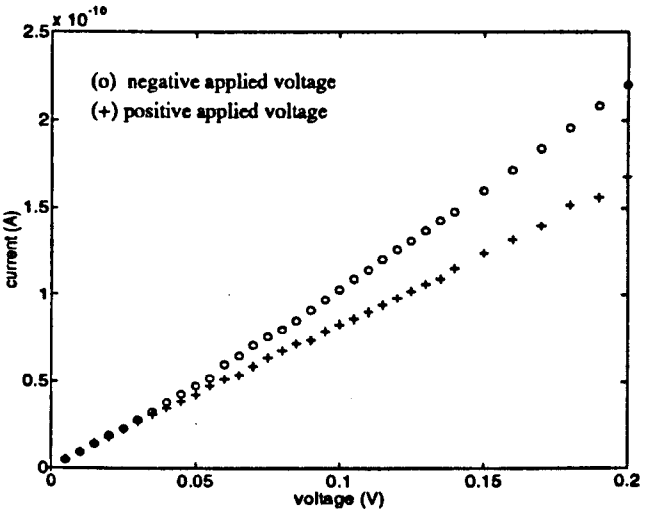

FIGURE 6.20 I/V characteristic for 1 channel of K12 porin. Currents obtained for positive and negative applied potentials are plotted in the same quadrant. Electrolyte = 250 mM KCl, pH 7.2. T = 26°C. Porin was added to compartment A.

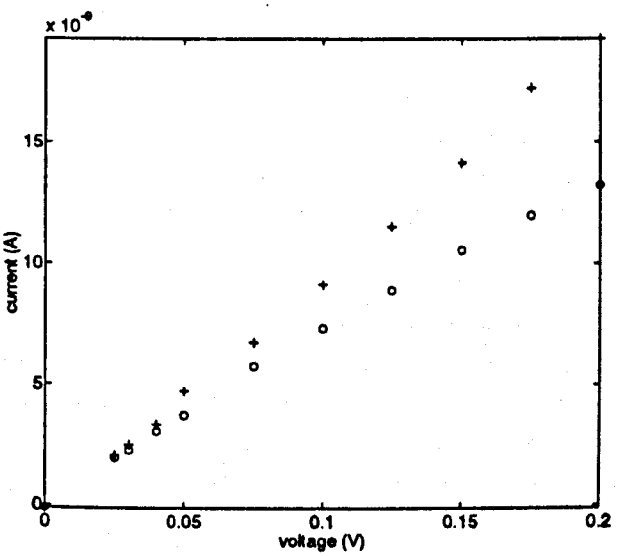

FIGURE 6.21 I/V characteristic for a membrane containing approximately 60 channels of 0111:B4 porin which was added to compartment B. (+) positive applied potentials (o) negative applied potentials. Electrolyte = 250 mM KCl, pH 7.2. T = 26°C

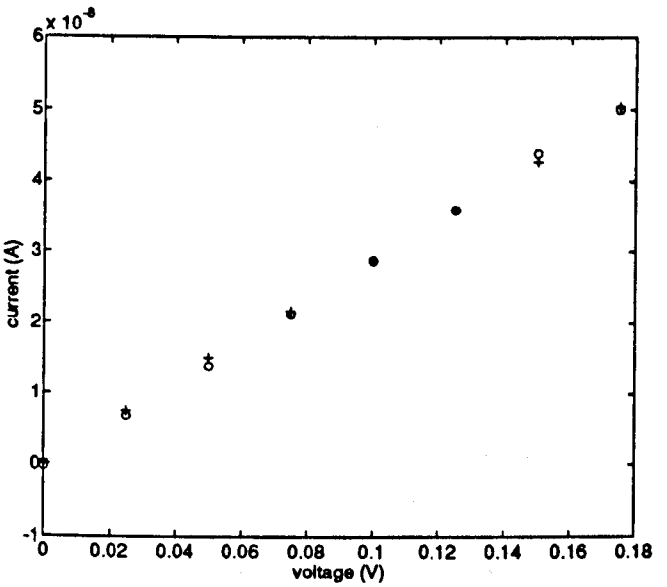

FIGURE 6.22 Symmetrical I/V characteristic when porin is added to both compartments. The membrane contains approximately 200 channels of 0111:B4 porin. positive applied potentials (+), negative applied potentials (o). Electrolyte = 250 mM KCl, T= 26°C.

The asymmetrical, super-linear I/V behaviour in Figure 6.20 is similar to the behaviour predicted by Levitt (1985) for channels with fixed charges at one end (Figure 2.13). Since the porin in this work has been shown to be cation selective (Figure 6.17) it must have an overall negative charge within or near the mouth of the channel. In Levitt's model, positive potentials applied to the right hand side of the channel gave higher currents than negative potentials when the charge was located at the left end of the channel. Assuming that the porin inserts into the bilayer in a specific orientation, i.e. with the LPS facing into the compartment in which porin was added, the experimental results (Figure 6.20) suggest that the charge is located at the LPS end of the channel. This is consistent with the notion that a voltage induced orientation of the porin may aid insertion into the bilayer (Section 6.2.2). Positive potentials applied to the compartment in which porin has been added would orientate the 'bulky' hydrophilic polysaccharides away from the bilayer. The position, magnitude and orientation of dipoles within the channel could also be responsible for asymmetrical, super-linear I/V behaviour, as shown by Sancho and Martinez (1991) (see Section 2.4.2.1). The amino acid sequence of OmpF porin (Figure 3.8) shows polar amino acids distributed along the β-barrel strands and on the loops folding into the barrel, which could lead to similar effects.

Figure 6.23 shows that the I/V characteristic for a single 0111:B4 porin is identical to that presented for the K12. These two particular channels had near identical values for single channel conductance of 1 nS, giving rise to the possibility that they are in fact the same species of porin. This single channel conductance is lower than the most probable conductance for 0111:B4 and slightly higher than for K12, so the channel could in fact be OmpF or OmpC. However, we can conclusively say that the difference in the LPS on the two porins does not appear to affect the I/V characteristic.

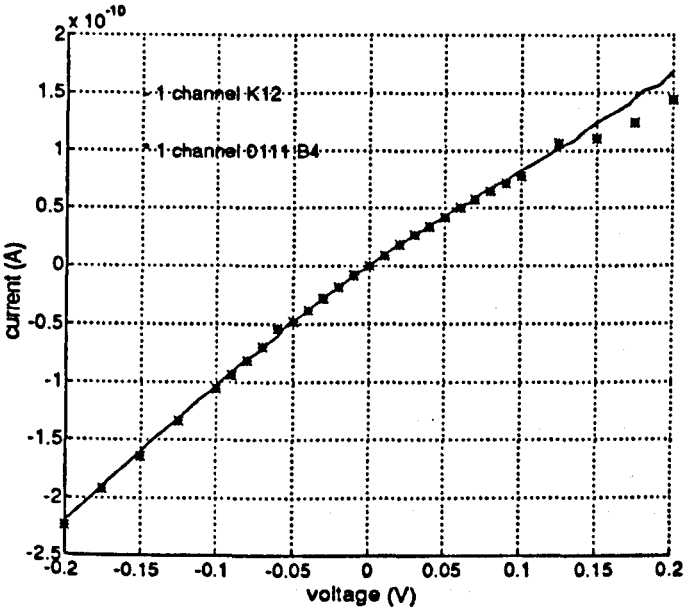

FIGURE 6.23 I/V characteristic for 1 channel of 0111:B4 (*) superimposed upon the characteristic for 1 channel of K12 (solid line). Electrolyte = 250 mM KCl, pH 7.2, T = 26 °C. Porin was added to compartment A.

6.6.2 Effect of the Number of Channels in the Membrane

For membranes containing only a few channels the conductance normalised to 1 channel was superimposable upon the I/V characteristic obtained for a single channel. This is illustrated in Figure 6.24 for K12 porin. When more than a few tens of channels were incorporated into the membrane, the normalised I/V curves departed from that of a single channel. Interestingly, the voltage at which the I/V relationship becomes non-linear (30-40 mV) was not influenced by the number of channels in the membrane. Figure 6.25 shows that even adjusting the estimated number of channels from 126 to 110 cannot improve the correlation with the single channel behaviour.

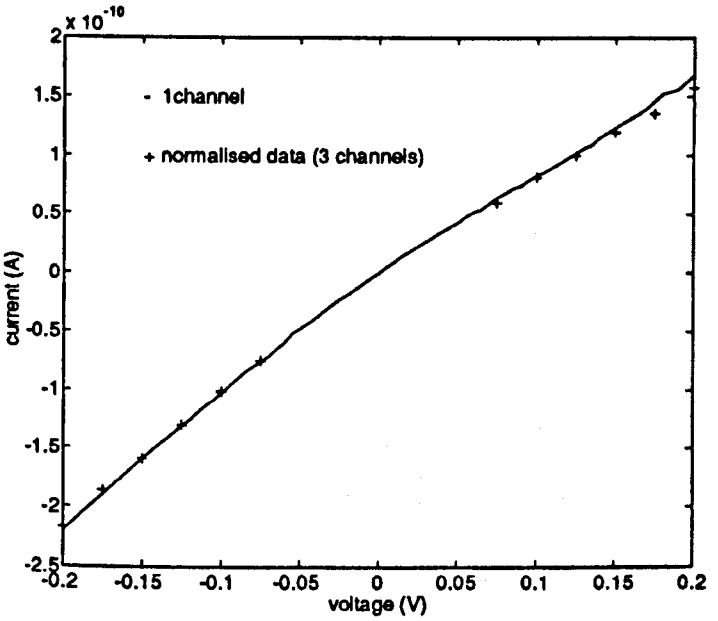

FIGURE 6.24 Data from a membrane containing 3 K12 channels normalised to 1 channel (+) and superimposed upon the single channel I/V relationship (solid line). The porin was added to compartment A. Electrolyte = 250 mM KCl, pH 7.2, T = 26°C.

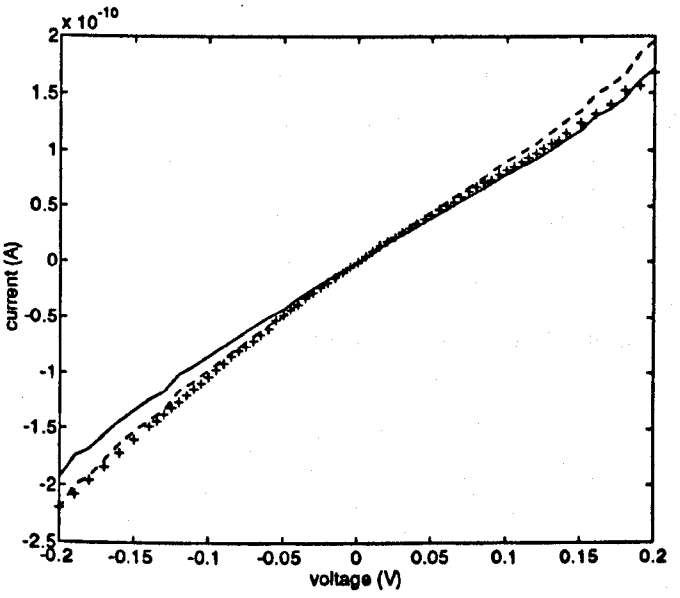

FIGURE 6.25 Data from multi-channel membrane normalised to 1 channel, estimating that the number of incorporated channels is 110 (dashed line) or 126 (solid line), superimposed upon the single channel I/V relationship (x). Porin from K12 was added to compartment A. Electrolyte = 250 mM KCl, pH 7.2, T = 26°C.

With multi-channel membranes, it is much more difficult to determine whether the results are being affected by voltage-gating events. At these high current levels the ability of the measuring equipment to discriminate single channel events is clearly very poor. However, the experimental procedure adopted in these measurements i.e. alternate application of steadily increasing and then decreasing positive and negative voltages, often provided an indication of gating. Such behaviour led the descending voltage curve to depart from the ascending curve. In the plots given in this chapter the descending curves superimpose exactly on the ascending curves. Gating effects will be discussed in the next chapter

The change in the I/V characteristics with increasing numbers of incorporated channels may be expressed in terms of the asymmetry ratio R=In/Ip where In and Ip correspond to the currents flowing at -150 mV and +150 mV respectively. Values of R for 12 membranes with increasing numbers of 0111:B4 channels are shown in Figure 6.26a and a clear decrease in R is seen as the number of channels in the membrane increases. Interestingly, the porin from K12 does not show any correlation between R and the number of channels incorporated (Figure 6.26b).

Based on the maximum number of porins that can be incorporated into the membrane before it breaks (125×10^3 porins/mm^2) the average distance between neighbouring porins is estimated to be approximately 3×10^{-6}m. At such large separation, each porin would be expected to act independently of all others. Clearly, this is not so for the 0111:B4 porin. The decreasing asymmetry for increasing numbers of incorporated porins points towards aggregation or cluster formation leading to interactions between neighbouring channels. There is evidence from voltage-gating experiments (Section 7.3.3) to support this argument.

Chapman *et al.* (1977) demonstrated that mixtures of dipalmitoyl lecithin, dilauroyl lecithin and polypeptide (in small amounts), when cooled, resulted in a collection of the polypeptide in the more fluid dilauroyl lecithin rich region. Scotto and Zakim (1988) found that incorporation of membrane proteins into lipid vesicles was dependent on the extent of the packing defects in the bilayer, which could be induced by impurities such as protein. It is clear then that clustering of porin could occur because of distinct crystalline and fluid regions in the bilayer or because of packing defects around a previously incorporated porin. A third reason for clustering could be the influence of the electric field, which will be concentrated in the region of a channel which has already entered the membrane. These arguments would apply equally to both K12 and 0111:B4 porins and so do not explain why one should form 'clusters' and the other not. The obvious difference between the two strains is in the length of associated LPS and it is possible that neighbouring 0111:B4 channels have their long oligosaccharide chains intertwined thus forcing them into tighter groups. Another

explanation is that both porins do in fact form clusters, but the 0111:B4 influences the single channel conductance of neighbouring channels to a greater extent, again the long chain LPS being implicated.

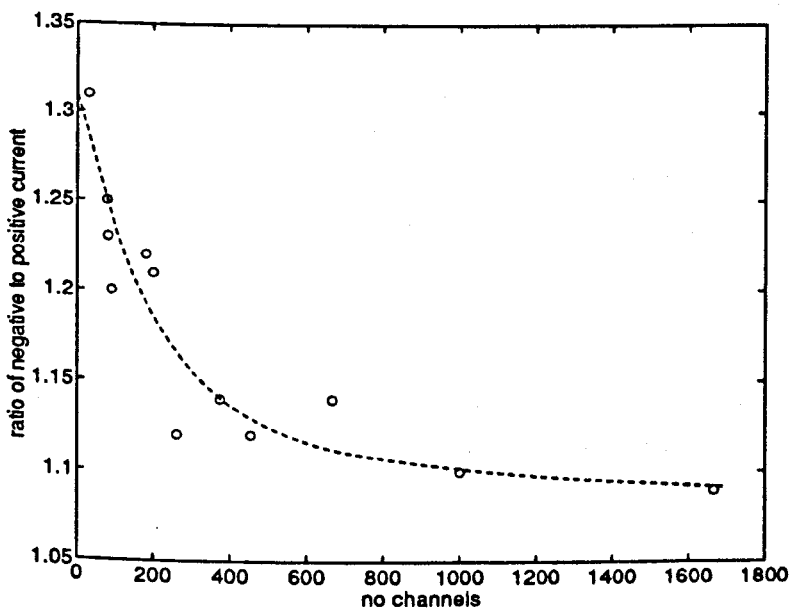

(a)

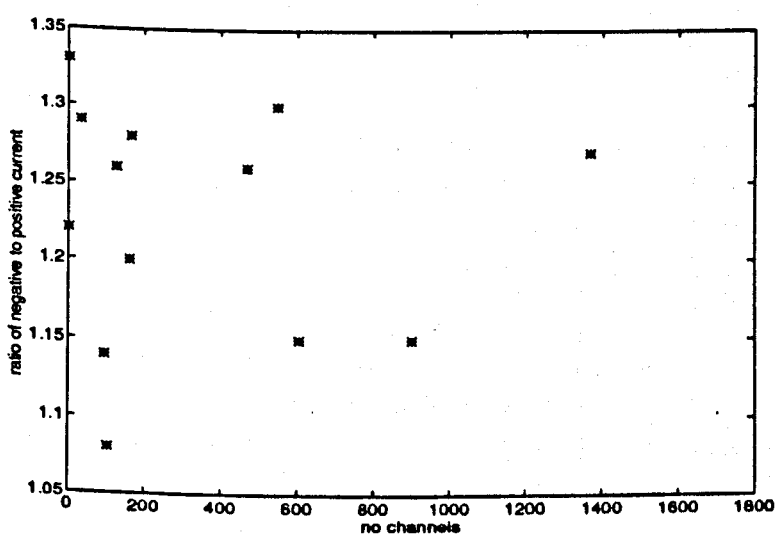

(b)

FIGURE 6.26 Ratio of current obtained at -150 mV to that obtained at +150 mV (In/Ip) versus the number of channels in the membrane for **a)** 0111:B4 and **b)** K12 porins which were added to compartment A. Electrolyte = 250 mM KCl, pH 7.2, T = 26^{0}C.

The question arises then as to how channels in close proximity may influence each other. Possibilities are i) charges and/or dipoles at the mouth of the channel influencing ion flow in neighbouring channels, ii) changes in the electric field pattern and iii) changes in channel geometry and/or size. In low salt concentrations, e.g. 100 mM KCl, the Debye length is approximately 0.9 nm and is small compared to the width of the channel walls, so that ions entering the aqueous channel are far removed from the electrostatic effects of neighbouring channels. We are thus left with only possibilities (ii) and (iii). The size of the channels can only be determined by , say, measuring the permeability rates of uncharged solutes to probe for channel size changes.

As for possibility (ii), the channel conductance calculations in Chapter 2 may have some bearing on this problem, especially the plot in Figure 2.4. Here it is shown that as the channel radius increases the apparent current density in the channel decreases, owing to the increasing influence of the access resistance. To a first approximation, a cluster of porins will behave as a large pore so that individual channel properties will be masked to some extent by the access resistance. Clustering could also contribute to the spread in channel conductances observed in Figures 6.9 and 6.10, since it would now depend on whether the incorporated porin entered a section of membrane remote from all others or joined a cluster. It would even matter whether the porin joined the periphery or the middle of a cluster.

6.6.3 Effect of Salt Concentration and pH

When the concentration of the bathing medium (KCl or NaCl) was increased to 1M, the asymmetry virtually disappeared (Figure 6.27). The results of a large number of experiments with membranes containing different numbers of channels are summarised in Figure 6.28. In order to disentangle the effects of molarity from the number of channels, the data have been given in three batches, corresponding to low, moderate and high numbers of porins. The effect of pH on the current ratio, R, is shown in Figure 6.29. At low pH an almost linear, symmetrical I/V characteristic is obtained (occasionally, the asymmetry being actually reversed). The reduction of the asymmetry in the I/V characteristic with low pH and high salt concentrations is consistent with the idea that charged groups or dipoles within the channel are responsible for the asymmetry (Section 6.6.1).

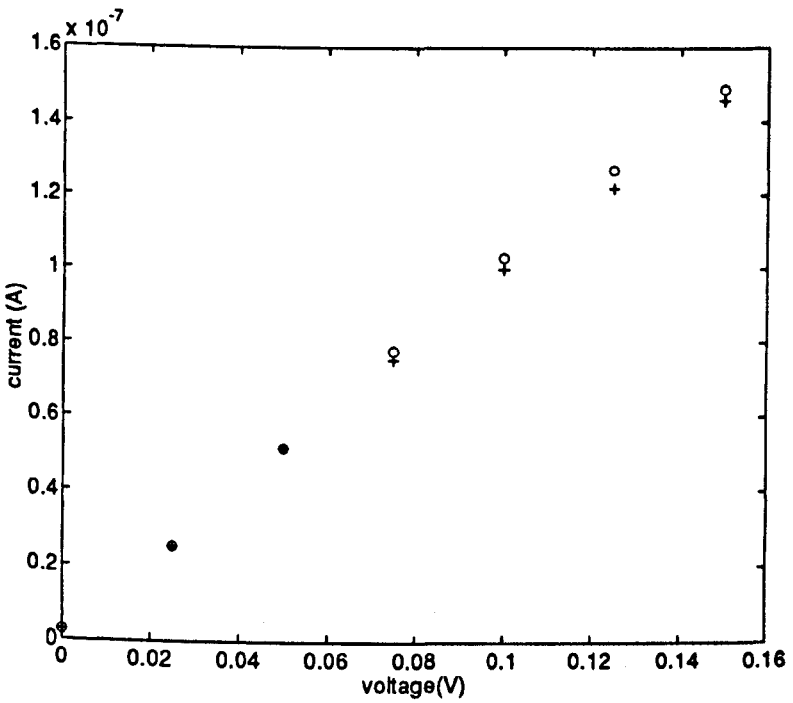

FIGURE 6.27 I/V characteristic for a membrane containing approximately 100 channels of 0111:B4 porin which was added to compartment A. (+) positive applied potentials (o) negative applied potentials. Electrolyte = 1M KCl, pH 7.2. T = 26°C.

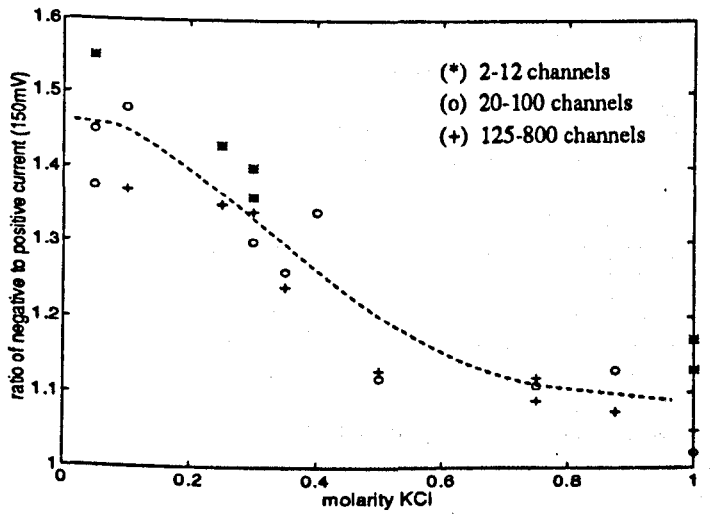

FIGURE 6.28 Ratio of current obtained at -150 mV to that obtained at +150 mV (R) versus the concentration of KCl in the bathing medium. pH of the electrolyte = 7.2. T = 26°C.

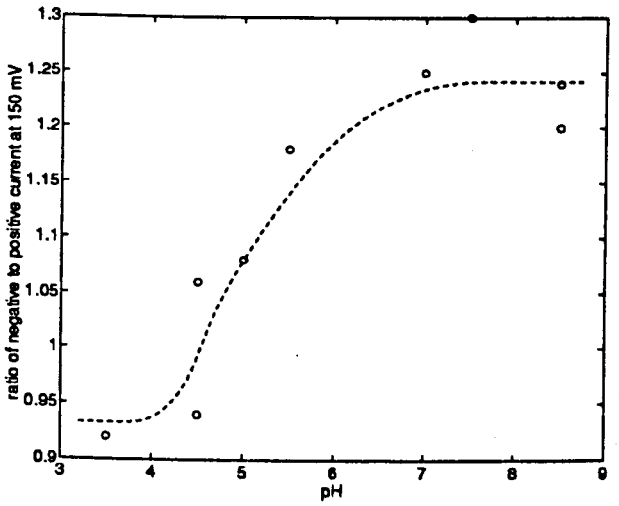

FIGURE 6.29 Effect of pH on the ratio R. Each data point has been collected from a membrane containing approximately 20 channels. $OmpF^{+}$/OmpC (0111:B4) porin was added to compartment A. Electrolyte = 200 mM KCl, T = 26°C.

6.7 CONCLUSION

Porins from 0111:B4 (OmpF rich) and K12 (OmpC rich) have been shown to form slightly cation selective channels, with single channel conductances related to the specific conductance of the aqueous phase in common with Benz (1985) and Benz and Bauer (1988). After porin incorporation had stabilised application of transmembrane voltages > 100 mV resulted in the decrease of the single channel conductance in three well defined steps, as previously demonstrated by Schindler and Rosenbusch (1981), Xu *et al.* (1986) and Morgan *et al.* (1990). This is in agreement with Cowan *et al.* (1992) that porin is a triplet of pores which traverse the membrane as three separate entities.

Previous research on porin has largely been concerned with comparisons between porin obtained from different strains and species of bacteria (and mitochondria). Consequently, research has only been concerned with such things as the approximate magnitude of the single channel conductance, the presence and degree of selectivity and whether voltage-gating is present or not. In this research approximately 200 experiments were performed on the same two types of porins over a two-year period so that a thorough and systematic study of the behaviour of porin channels could be made. This research has demonstrated non-linear, asymmetrical current-voltage characteristics for both porins, a behaviour not previously described

for porins in lipid bilayer membranes. Single channels from both *E. coli* strains, 0111:B4 and K12, had superimposable current voltage characteristics. This suggests that the LPS composition of the porin channel does not affect its I/V characteristic.

Electrostatic models by Levitt (1985) and Sancho and Martinez (1991) predict asymmetries and non-linearities in channel conductance when fixed charges or dipoles are located at one end of the channel. When using Levitt's model, the direction of asymmetry, coupled with the evidence that both porins are cation selective, suggest that the LPS end of the porin/LPS complex has a net negative charge. This is consistent with the notion that porins insert into the bilayer with the LPS end facing the aqueous solution and that such an orientation is aided by the application of positive potentials to the compartment into which porin is added. In addition, the models by Levitt (1985) and Sancho and Martinez (1991) predict super-linear I/V behaviour which is similar to that obtained experimentally for a single porin channel. The experimental results here, then, indicate that the electrostatic models of Levitt (1985) and Sancho and Martinez (1991) reasonably predict the current/voltage behaviour of a porin channel. High salt concentrations were shown to reduce the asymmetry, as would be expected due to 'screening' of fixed charges. Low pH reduced the cation selectivity of the channel and also reduced the asymmetry of the I/V characteristic, presumably due to changes in the ionisation of charged residues.

From the above it is evident that conductance is a sensitive indicator of the magnitude and location of charges and dipoles within the channel and also of the direction of the dipole. Statistical fluctuations in the degree of ionisation of charged residues and slight differences in the relative positions of charged groups and dipoles could be partly responsible for the broad distribution of conductances typical for porin channels. Although there is some evidence from *in vivo* studies that the physical radius of porin increases with decreases in pH (Todt *et al.* 1992, and Todt and McGroarty, 1992), the observed differences in single channel conductance when the pH is changed cannot all be attributed to size changes of the aqueous channel, given the above information.

There is great variability between the single channel conductances of OmpF and OmpC porins measured in different laboratories and Todt *et al.* (1992) concluded that differences in the pH of the bathing medium were responsible. Although pH is clearly important, the single channel conductance in this research did not overlap with the values of Todt *et al.*, despite performing experiments over a larger pH range. The lipid used to form the bilayer and the amount of endogenous LPS on the purified porin have also been suggested by Buehler *et al.* (1991) to affect single channel conductance. It is not unreasonable to suppose that the lipid environment and the amount of endogenous LPS could affect the conformation of the protein, which would in turn change the

relative positions of charged groups and dipoles. The differences in single channel conductance between the OmpF porin in this work and that studied by Morgan *et al.* (1990), whose experimental technique including protein extraction were essentially similar to this work, points to differences in the porin itself being responsible.

Estimates of pore diameter have in the past been made from single channel conductance measurements based on the assumption that the pore is a cylinder filled with bulk electrolyte. The complex geometry of porin (Cowan *et al.*, 1992) is an obvious limitation of this model, but the non-linearity and asymmetry of the single channel conductance with voltage, demonstrated in this research, is a further indication of the inappropriateness of this model. In addition the asymmetry is dependent upon pH and the salt concentration.

The degree of asymmetry of the I/V relationship for the 0111:B4 porin was reduced as the number of channels in the membrane increased. Such behaviour indicates that there is some interaction between channels, which can only be explained if the channels form aggregates or 'clusters'. Evidence for 'clustering' is also seen with voltage-gating experiments (Chapter 7). It is not clear why the 0111:B4 porin should form clusters while the K12 apparently does not; perhaps the length of LPS is important. To a first approximation a 'cluster' of channels can be modelled as a large channel. In Chapter 2 it was shown that as the channel radius increases the apparent current density in the channel is decreased owing to the increasing influence of the access resistance. Individual properties of porins will therefore be masked to some extent by the access resistance when porins cluster together. Clustering may also contribute to the spread of conductances observed for OmpF porins. The observed conductance during porin incorporation will depend upon whether a porin enters a remote portion of the bilayer, a 'cluster' or indeed the centre or periphery of a 'cluster'.

CHAPTER 7

VOLTAGE-GATING

7.1 INTRODUCTION

In this chapter the results obtained using sustained application of voltage are presented. Details of the experimental method have been given in Section 5.10. Here the evidence for voltage-gating in porins from 0111:B4 and K12 is presented and discussed. Several types of gating behaviour were noted and these are described and, where appropriate, two-state models are applied to the time dependent changes in conductance produced by the sustained voltage application.

7.2 EVIDENCE FOR VOLTAGE-GATING

7.2.1 Membranes with Few Channels

In Section 6.3.2 it was shown that after porin incorporation had stabilised, application of high transmembrane voltages (typically > 100 mV) resulted in closing steps. These steps were approximately 1/3 and 2/3 the size of the opening events seen during porin incorporation (Figure 6.11). In addition, single channels from both 0111:B4 and K12 were shown to close in three well defined steps and would re-open when the voltage was returned to zero for a few seconds. It has been argued that channel closure occurs simply due to electrical breakdown of the protein, given that 100mV dropped across a 5 nm membrane corresponds to an electric field of 2×10^7 V/m . The consistent and orderly nature of the closing steps, coupled with the observed reversibility, make such an explanation implausible. Results from this work, then, support the findings of Schindler and Rosenbusch (1978, 1981), Dargent *et al.* (1986), Xu *et al.* (1986) and Morgan *et al.* (1990) that porin does indeed undergo voltage-gating. The conductance decreases or closing events are quantised in fractions of the porin open state conductance and given the structural evidence of Cowan *et al.* (1992) suggest that each monomer of the trimeric porin may open and close independently.

7.2.2 Multi-Channel Membranes

With multi-channels membranes it is not possible to resolve the discrete closing events. Sustained application of voltage, however, results in a relaxation of the membrane current which settles at a new steady-state level. In Figure 7.1a typical examples of the

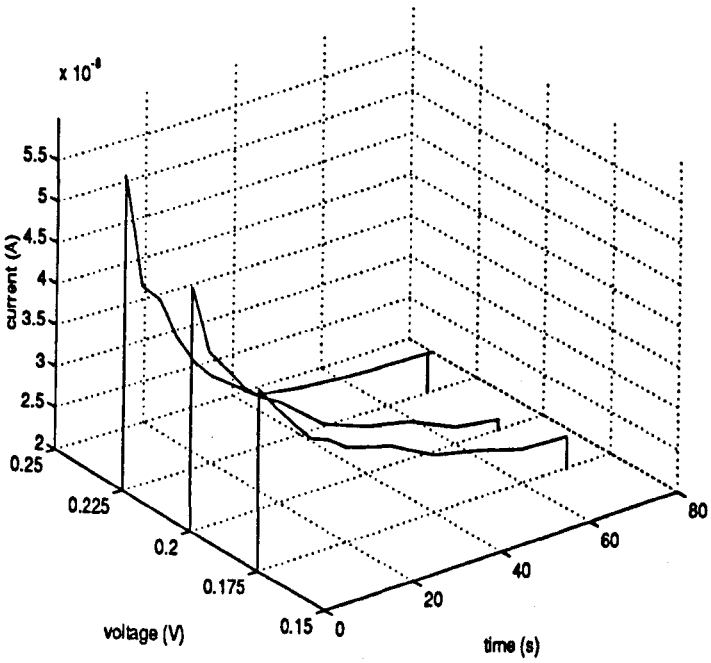

(a)

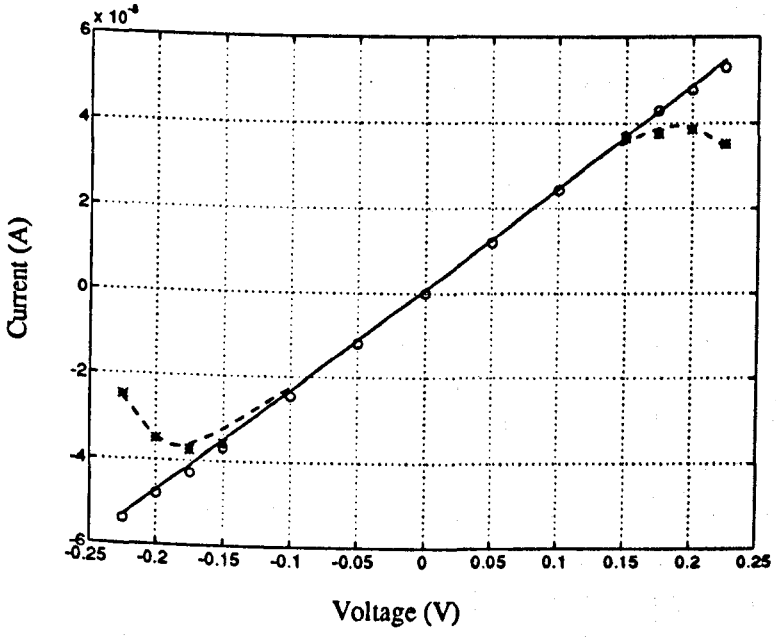

(b)

FIGURE 7.1 (a) Typical current relaxation behaviour for a multi-channel membrane at three different voltages. (b) Current/voltage plots of initial current (solid line) and steady-state current (dashed line) taken from the data in (a).

current relaxation are shown, illustrating the effect of increasing the applied voltage on the same channel containing membrane. In between each voltage application the sample was rested for at least 30s at zero volts. The relaxation in the current was reversible in a large number of membranes, but not in all, and this will be discussed further in Section 7.3.2. In contrast to the near ohmic relationship of the initial current values, a current/voltage plot using the steady-state current values, from plots such as those in Figure 7.1a, is typically sigmoidal in appearance (Figure 7.1b) in agreement with Lakey and Pattus (1989) and Morgan *et al.* (1990). The regions of negative resistance seen in Figure 7.1b are similar to those observed by Ehrenstein *et al.* (1970) in membranes doped with excitability-inducing material (EIM). EIM was demonstrated to have a two-state behaviour, open and closed, in membranes of oxidised cholesterol.

Only a small number of experiments failed to show some degree of current relaxation and these all had high porin concentrations in the aqueous phase. They showed continuing porin incorporation under positive bias and steady current levels or slight increases in current with negative bias. In these experiments it is likely that channel incorporation is masking the effect of channel closure. The addition of too much porin was proposed by Jap and Walian (1990) to be one of the possible causes of the failure to demonstrate voltage-gating. The findings in this research support this argument.

7.3 VARIABILITY OF CURRENT RELAXATION

In the previous section, the general features of porin behaviour in support of voltage-gating were presented. In practice the nature of the current relaxation was found to fall into several distinct groups. This variability in behaviour has not previously been described in the literature. It is possible, though unlikely, that it is due to the experimental technique employed, or it may simply be that the large number of experiments performed in this research has enabled the different patterns of behaviour to be identified. Some membranes exhibited only one type of behaviour, but in a small proportion of membranes more than one type of behaviour was seen during the course of a single experiment.

7.3.1 Most Common Type of Current Relaxation

The majority of experiments with porin from both 0111:B4 and K12 showed a current relaxation which reached steady-state after several minutes with, in most cases, a large fraction of the channels remaining open. Buehler *et al.* (1991) have also noted that for OmpF and OmpC porins even after several minutes of voltage application a large

fraction of the channels remain open. On careful examination of most of the experimental data, the current relaxation following the application of a gating voltage was seen, in Figure 7.2, to be composed of two exponential decay functions and a d.c. level, I_{∞}, i.e.

$$I = I_1 \exp\left(-\frac{t}{\tau_1}\right) + I_2 \exp\left(-\frac{t}{\tau_2}\right) + I_{\infty} \tag{7.1}$$

where τ_1 and τ_2 are the time constants of the two decay functions. This suggests the presence of two closing populations. In this instance the larger population closes with the longer time constant (45s) and the smaller population has a time constant of 9s.

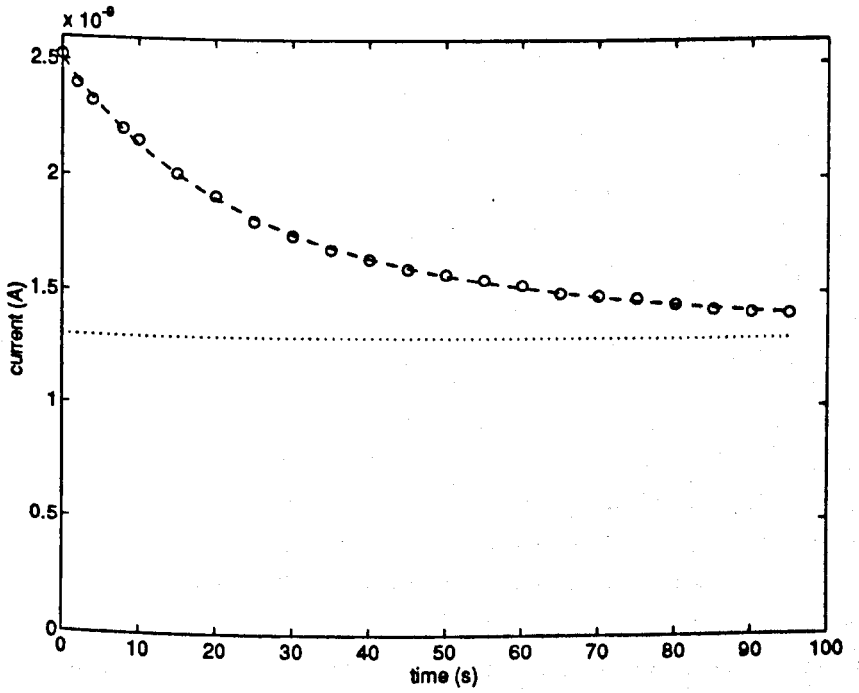

FIGURE 7.2 Current relaxation for a multi-channel membrane with -125 mV applied voltage. The current decay is described by the equation $I = 4.1 \times 10^{-10} \exp(-t/9) + 8.5 \times 10^{-10} \exp(-t/45)$, which was found by a least squares fit method. The steady state level is 1.3×10^{-9} A.

Previous studies of multi-channel membranes have largely been concerned with whether or not current relaxation is present (Lakey and Pattus, 1989 and Schindler and Rosenbusch, 1978) with little attention being paid to the exact nature of the relaxation. Some authors have stated that the current relaxation is characterised by a single time constant (Morgan *et al.*, 1990, Young *et al.*, 1983 and Todt *et al.*, 1992), although they do not provide definitive evidence for this.

The time constants measured here showed great variability, the shorter one ranging from 3-25s, the larger one from 40-900s. Some of this variability was sample related, although it should be noted that for a particular membrane/porin system results at a given applied voltage were generally reproducible. This enabled the identification of a systematic variation in both the short and long time constants with applied bias which will be discussed in Section 7.4.3.

7.3.2 Reversibility of Current Relaxation

7.3.2.1 Partial Irreversibility

The current relaxation was totally reversible in approximately 2/3 of experiments. In the remainder, the relaxation was only partly reversible with about 5-10% of the closed channels not re-opening. In the latter experiments, the failure of the channels to re-open was seen only on the first application of each voltage. Second and subsequent applications of the same voltage produced totally reversible current relaxations. This behaviour could indicate that a small fraction of porin had been partially denatured during the extraction procedure and the application of the high transmembrane voltage was sufficient to completely denature the protein. Another explanation is that the current relaxation is not entirely due to closure of channels but also reflects expulsion of some channels from the bilayer. Unfortunately the Montal-Mueller technique does not allow channel closing to be differentiated from porin expulsion. It should be noted, though, that because porin spans the bilayer, it has a central hydrophobic portion (Section 3.4.3) which makes it energetically unfavourable for it to leave the bilayer and enter the aqueous solution. The porin would be expected to re-enter the aqueous solution only if there was considerable disruption to the bilayer. Indications of bilayer disruption, such as increased conductance, a change in capacitance or subsequent membrane breakage were not, however, obviously associated with the partial irreversibility in the current relaxation.

7.3.2.2 Dependence on the Previously Applied Voltage

If the rate of opening and closing of the channels is dependent only on the applied voltage, the steady-state current level when a particular voltage is applied should be

independent of the previous history of the membrane. In Figure 7.3a an example of current relaxation induced by the application of +200 mV is shown. Reduction of the applied voltage results in the re-opening of some of the closed channels and a new steady-state level is attained. This current should lie on the previously established steady-state I/V plot for the membrane in question. In Figure 7.3b it is shown that for some membranes the above does not hold. The membrane in Figure 7.3b has reversible current relaxation, if allowed to rest at zero bias between voltage applications. (This was verified by applying the higher transmembrane voltages at least twice). When the initial voltage application was approximately +175 mV or less, subsequent reductions to +100 mV and +128 mV resulted in steady-state currents which lie on the previously established I/V plot. When the initial voltage application was greater than +175 mV, reducing the voltage to +100 mV or +108 mV then resulted in steady-state currents well below those expected. This indicates that a fraction of the channels are not re-opening and that the membrane conductance depends on the previous value of applied voltage. However, all the channels could be induced to re-open if the bias was set to zero for a few seconds. Such behaviour again indicates the presence of two populations, one of which can only re-open via some intermediate state which is only reached at zero volts (or voltages below the onset of gating).

7.3.3 Successive Current Decays

If the bias voltage was sustained for 10 minutes or more, about 25% of experiments showed a stepwise relaxation in the current as shown in Figure 7.4, with some experiments showing up to 5 steps over a 1 hour period. With some membranes the decay steps appeared almost linear, the channels closing with very long time constants of the order of tens of minutes. In this type of current decay gating was totally reversible. It is interesting to note that this behaviour, although occurring for both porins, was most marked and occurred more frequently for the porin from 0111:B4. It will be recalled that this porin showed evidence of 'clustering' (Section 6.6.2). The distinct current decay steps in Figure 7.4 could correspond, therefore, to the relaxation of individual porin 'clusters'. As one 'cluster' of channels reaches steady-state another, perhaps a neighbouring 'cluster', begins to show voltage-dependent changes suggesting some interaction between the separate populations. It could be argued that the different populations are due to the relaxations of non-independent porin monomers, which is discussed in Section 7.4.2, but the presence of more than three decay steps, however, makes this idea unlikely.

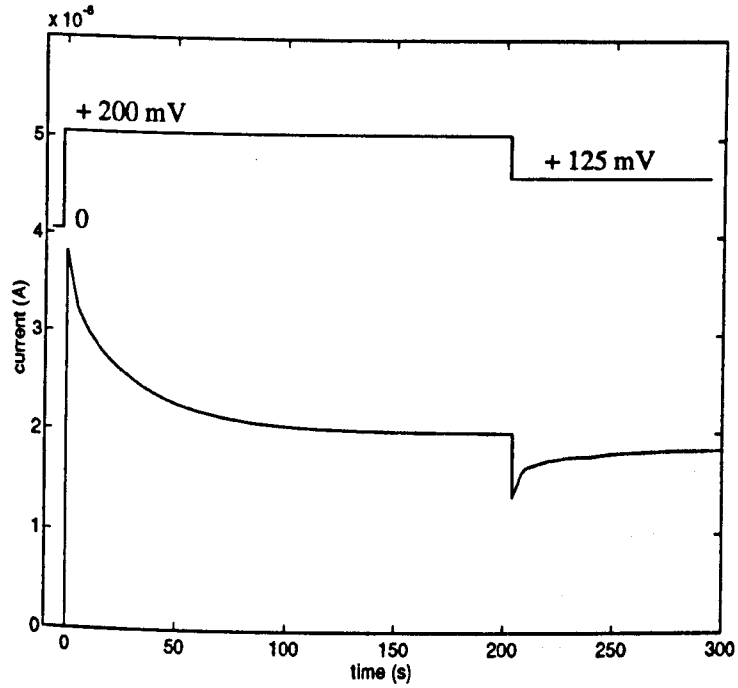

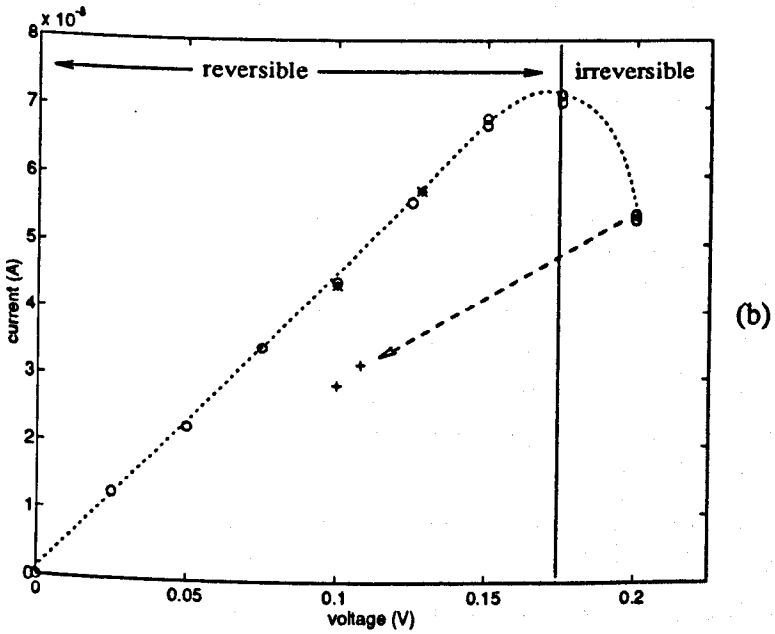

FIGURE 7.3 (a) Multi-channel membrane containing porin from 0111:B4. A voltage of +200 mV is applied at t=0s and then reduced to +125 mV as shown in the top trace. The corresponding current time trace is shown below. (b) Steady-state current voltage plot (o), data points collected after reducing the voltage from +175 mV (*) and from +200 mV (+).

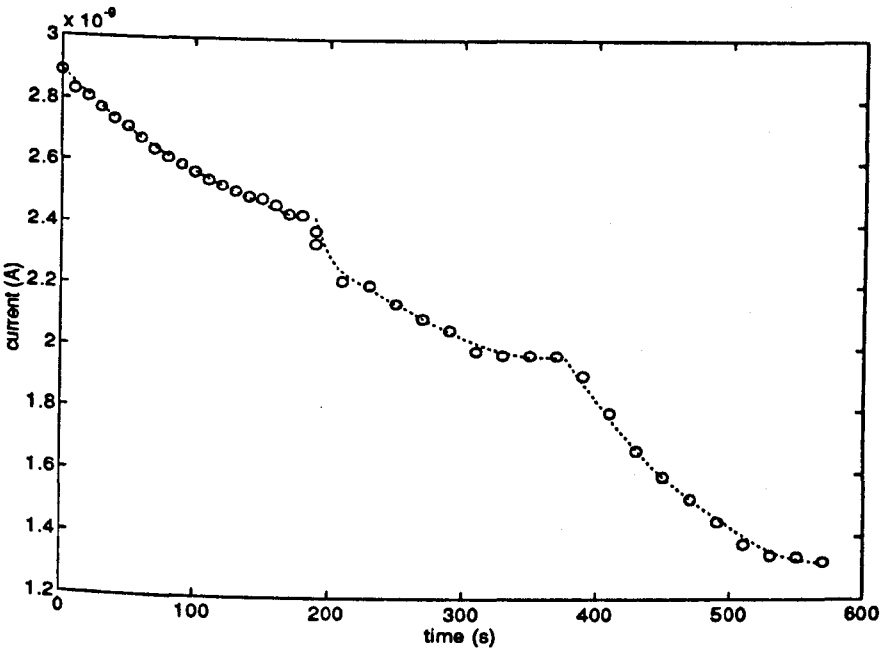

FIGURE 7.4 Multi-channel membrane containing porin form 0111:B4 showing successive current decays.

7.3.4 Completely Irreversible Behaviour

The final type of current relaxation differs from the previous types of behaviour in two main ways: 1) 80-100% of the open channels close and 2) the closure of the channels is completely irreversible. With the bias voltage set to zero for up to one hour the channels showed no sign of re-opening. Subsequent applications of voltage of either polarity, including that expected to aid porin incorporation produced no opening events. The current relaxation (Figure 7.5) can be fitted by a single exponential unlike the reversible behaviour described in Section 7.3.1. This type of current decay, which occurred with voltages as low as 25 mV, bore no obvious relationship to the sign and size of the applied voltage. In one experiment, illustrated in Figure 7.5, an initial application of +150mV (curve (a)) resulted in the typical current decay described in Section 7.3.1. After resting at zero bias for a few minutes re-application of 150 mV resulted in the irreversible behaviour (curve (b)).

This type of channel closure appears to be a completely different process to that described in Section 7.3.1. The lack of new opening events following channel closure, despite applying a favourable bias voltage for porin incorporation, indicates a change in the bilayer itself or in the porin in the bilayer or in the porin in the aqueous solution. Impurities affecting the bilayer and/or porin seem an unlikely explanation, as the behaviour occurred in what appeared to be a random manner over a period of

about 18 months. During this time several batches of lipid, and porin from two separate extractions in the case of 0111:B4, were used. The bilayer capacitance did not change from the beginning of the experiment, ruling out the possibility that a multi-layer had formed over the hole in the PTFE. Therefore, any change in the bilayer must be of a subtle nature, as it was not accompanied by any measurable capacitance changes. The change must also occur over a reasonably short time span as the two curves in Figure 7.5 were obtained within a few minutes of each other. Evidence that the bilayer may not be implicated comes from Delcour *et al.* (1989, 1991), who demonstrated irreversible porin closure, in their case induced by voltage, using the patch clamp technique on outer membrane fractions in liposomes. They concluded that the channels were locked into a long lived stable closed state different from the closed state from which they re-open. This also provides evidence that the irreversible closure in the lipid bilayer experiments may not simply be due to the fact that the channels have left the bilayer. It does not explain, however, why large favourable bias potentials failed to result in further porin incorporation in our experiments.

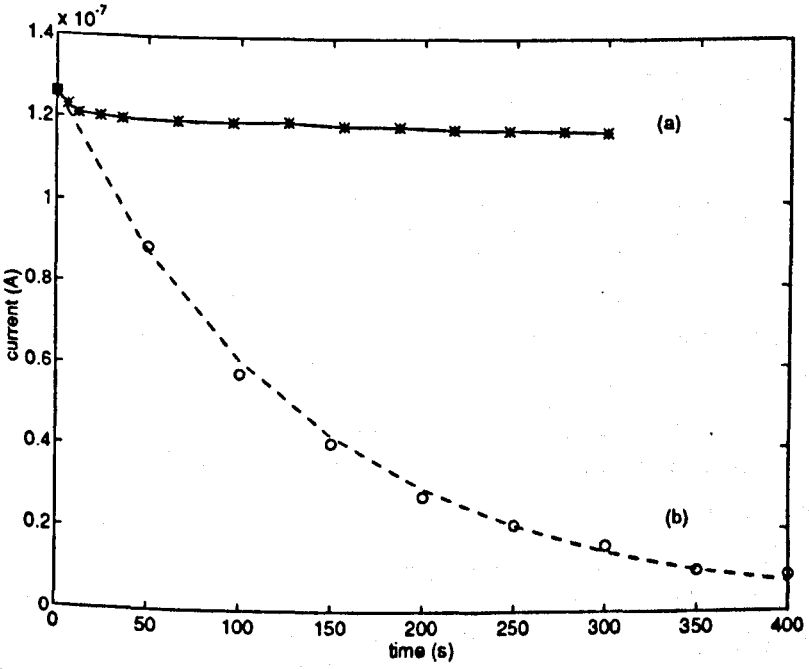

FIGURE 7.5 Application of +150 mV produces the typical current decay in (a). A second application of +150 mV a few minutes later produces the irreversible decay shown in curve (b). The current in (b) is described by the equation $I = 1.2 \times 10^{-7} \exp(-t/139)$, the steady state level is taken as zero.

7.3.5 Time Dependency

In the majority of experiments, porin gated more readily with negative rather than positive applied potentials. In some cases this asymmetry was clearly due to the effects of continuing porin incorporation, which was more marked for positive potentials (Section 6.2.2). Measurement of the magnitude of the initial current at each voltage application was used to assess the effects of porin incorporation; near ohmic I/V plots were expected if the number of channels in the membrane remained relatively constant. Some attempts were made to exchange the aqueous solution bathing the membrane (after a suitable number of porin channels had entered the membrane) in order to reduce the concentration of porin in solution, thereby lowering the probability of further porin incorporation. Unfortunately this approach produced a large number of failed experiments due to membrane breakage, presumably brought about by mechanical disturbance of the bilayer, and was eventually abandoned.

With the remainder of the experiments, the voltage-gating was asymmetrical despite indications that porin incorporation had largely ceased. This contrasts with the work of Lakey and Pattus (1989) who reported that symmetrical gating occurred as a result of sustained voltage application to OmpF porin, solubilised in Triton and incorporated into Montal-Mueller bilayers. In the occasional experiment, their porin was found to be more sensitive to negative potentials. In the present work, only the occasional experiment showed symmetrical gating and then only when the porin had been in the membrane for at least 2 hours.

Interestingly, a voltage-gated channel that closes when the periplasmic side is made positive has been described in native outer membranes (Buechner *et al.*, 1990 and Delcour *et al.*, 1989). These channels, thought to be porins, appear sensitive to the same polarity of applied bias as the porin in this research (assuming that the porin inserts into the membrane with the LPS end facing into the electrolyte).

Lakey and Pattus (1989) mention a time dependent change in the form of a progressive increase in voltage sensitivity, which was also demonstrated in a few experiments in this research. The underlying process responsible for these time dependent changes may be the same as those giving rise to changes in both the asymmetry and the voltage sensitivity. One possible cause could be a progressive change in bilayer properties. Niles *et al.* (1988) have shown that Montal-Mueller bilayers made with phospholipid become thinner over time in a manner similar to Black Lipid Membranes. Measurement of the bilayer capacitance at intervals throughout the experiment did show some evidence of a gradually increasing capacitance over several hours, which would be consistent with a gradual thinning of the bilayer. Thus, there is some degree of solvent redistribution in Montal-Mueller bilayers despite the fact that they have been termed 'solvent free' bilayers in the past.

7.4 TWO-STATE MODEL

7.4.1 Steady-state Measurements

7.4.1.1 Introduction

The simplest model of voltage-gating considers a channel structure to have two states, one open and one closed as described in Section 2.4.3. To apply this model to porin it must be assumed that the monomers making up the trimer open and close independently. This assumption may not be valid as discussed in Section 7.4.2. It is also assumed that the rate constants for channel opening and closing depend only on the membrane potential and are independent of the past history of the membrane. The change in voltage sensitivity of the porin over time in some experiments and the dependence on the magnitude of the previously applied voltage (Section 7.3.2) indicate that this assumption may not always be valid. Data from experiments where there were obvious changes in voltage sensitivity over time were not used in this analysis. Experiments which did not show complete reversibility in the voltage-gating and which had evidence of continuing porin incorporation were also discarded. The third problem in applying the two-state model to the experimental data from this research is that the reversible current decay is not a single exponential. A few authors have used the analysis in Section 2.4.3 to estimate the number of gating charges involved in the gating process (Morgan *et al.*, 1990 and Todt *et al.*, 1992). It is not clear from their work whether the current decay was investigated in detail or just assumed to follow a single exponential.

In Figure 7.2 it was shown that the current relaxation obtained at a given voltage was composed of two exponential decay functions and a d.c. level, as described by equation (7.1). The current decay can also be written in terms of the numbers of channels closing rapidly and those closing more slowly, i.e.

$$I = V\left[g_f\left(n_c \exp-\left(\frac{t}{\tau_1}\right)+n_o\right)+g_s\left(N_c \exp-\left(\frac{t}{\tau_2}\right)+N_o\right)\right]$$

where nc and Nc are the total numbers of channels closing with time constant τ_1 and τ_2 respectively, n_o and N_o are the numbers of 'fast' and 'slow' channels which remain open at steady-state and g_f and g_s are the single channel conductances associated with the fast and slow processes respectively. There is no evidence in Figures 6.9 or 6.10 for the presence of separate populations. Therefore, we may assume that the single channel conductance associated with the fast and slow processes are identical, i.e. $g_f=g_s=g_o$, whence

$$I = g_o V\left[n_c \exp-\left(\frac{t}{\tau_1}\right) + N_c \exp-\left(\frac{t}{\tau_2}\right) + (n_o + N_o)\right].$$

(7.2)

Thus, at a particular value of applied voltage and comparing equations (7.1) and (7.2) we may define a ratio

$$\frac{N_c}{n_c} = \frac{I_2}{I_1}$$

(7.3)

Systematic variation of applied voltage results in a series of current decays as shown in Figure 7.6a, each of which can be fitted with an equation of the form in (7.2). Equation (2.44) gives the expected relationship for the ratio N_O/N_C or n_O/n_C versus voltage for a two-state channel with voltage-dependent transition rates between the two states (see Section 2.5.3). Although the total number of channels open at steady-state ($n_O + N_O$), given by

$$I_\infty = g_o V(n_o + N_o),$$

(7.4)

is known, what fraction of the d.c. level to apportion to each population is unknown. Therefore, in order to apply equation (2.44) to the data, calculations were made for three cases, namely

(i) I_∞ arising entirely from population N,
(ii) I_∞ arising entirely from population n and
(iii) (n+N) forming one population so as to compare data with other workers.

Figure 7.6b shows that plots of log I_∞/I_j versus applied voltage corresponding to these three cases are all linear, enabling the number of charges involved in the gating process, z, and the voltage at which half the channels are open, V_O, to be determined. Knowing z and V_O it then becomes possible to calculate the energy difference, $\Delta\omega$, between the open and closed states (Section 2.5.3). Tables 7.1-7.3 give the values of z and V_O determined for the 0111:B4 porin at neutral pH and acidic pH, and for the K12 porin. Although values of z, V_O and Δw were reasonably consistent for repeat experiments on the same channel-containing membrane, there was some variability between different membranes. To illustrate this variability the results from three

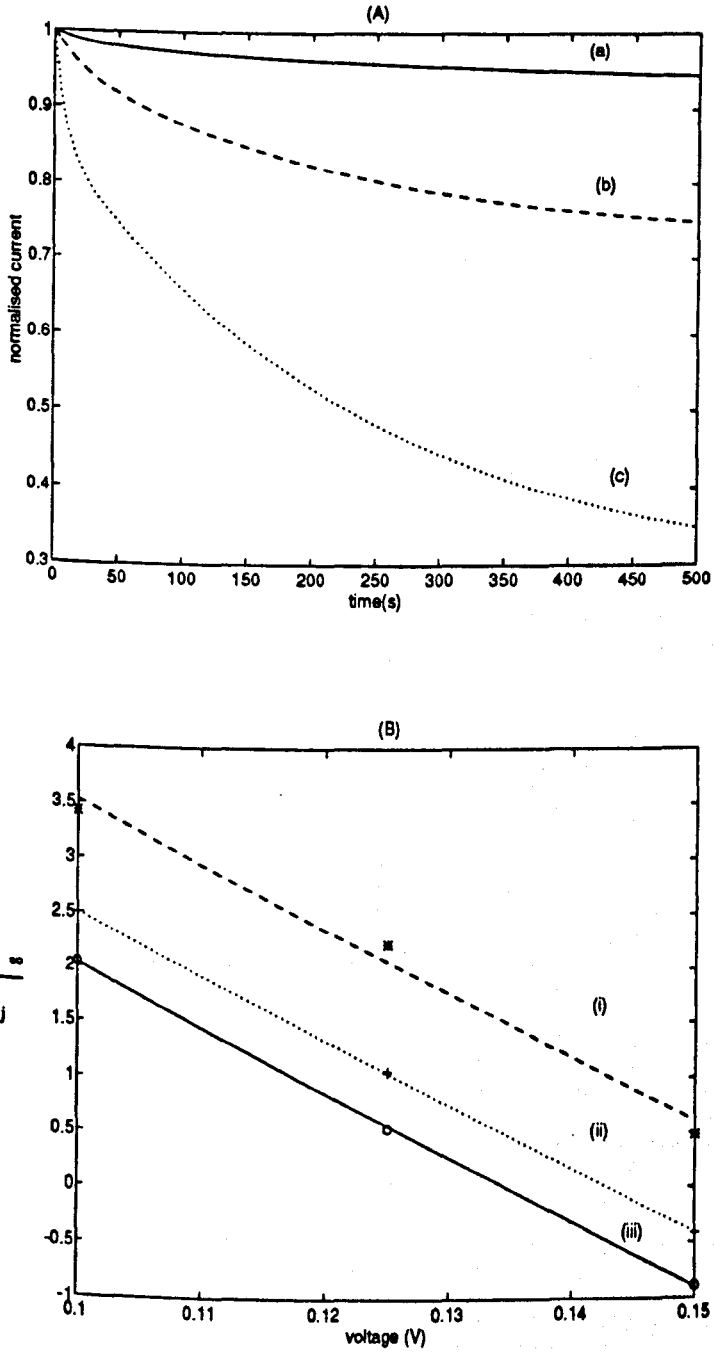

FIGURE 7.6 (a) Normalised current-time plots for the same membrane with the applied voltage at a) -125 mV, b) -150 mV and c) -175 mV. (b) Plots of log I_∞/Ij obtained from the data in (a) where Ij = (i) I_2, (ii) $I_1 + I_2$ and (iii) I_1.

different membranes have been given in each table along with the corresponding average values. As can be seen, the values deduced for z, V_0 and Δw are relatively insensitive to the assumed origin of the d.c. current. This is partly due to the logarithmic dependences of N_o/N_c and n_o/n_c which reduces the sensitivity of equation (2.44) to changes in N_o/N_c and n_o/n_c. The values of V_0 for each case represent maximum possible values, given that the entire d.c. level was assigned to each population in turn in this analysis.

TABLE 7.1 The number of gating charges, z, the voltage at which half the channels are open and half are closed, V_0, and the energy difference between the open and closed states, Δw, for the 0111:B4 porin at pH 7.2. Estimated from plots of log I_∞/I_j versus applied potential, where $I_j=I_1,I_2$ or (I_1+I_2) corresponding to n_c, N_c and n_c+N_c respectively.

Population	sample	z	Vo (mV)	Δw (eV)
N	1	0.93	141	0.13
	2	0.89	131	0.12
	3	1.47	146	0.21
	average	1.10	139	0.15
n	1	1.47	171	0.25
	2	0.85	171	0.14
	3	1.50	163	0.24
	average	1.27	168	0.21
N + n	1	1.47	141	0.21
	2	0.93	126	0.12
	3	1.04	135	0.14
	average	1.15	134	0.16

TABLE 7.2 Estimates of z, V_0 and Δw for K12 porin at pH 7.2. Estimated from plots of log I_∞/I_j versus applied potential, where $I_j=I_1,I_2$ or (I_1+I_2) corresponding to n_c, N_c and n_c+N_c respectively.

Population	sample	z	Vo (mV)	Δw (eV)
N	4	1.92	163	0.31
	5	0.86	141	0.12
	6	0.67	148	0.10
	average	1.15	151	0.18
n	4	0.96	193	0.19
	5	0.66	267	0.18
	6	0.93	234	0.22
	average	0.85	231	0.2
N + n	4	1.56	158	0.25
	5	0.75	232	0.12
	6	0.86	141	0.12
	average	1.1	177	0.16

TABLE 7.3 Estimates of z, V_0 and Δw for 0111:B4 porin at pH 5.5. Estimated from plots of log I_∞/I_j versus applied potential, where $I_j=I_1,I_2$ or (I_1+I_2) corresponding to n_c, N_c and n_c+N_c respectively.

Population	sample	z	Vo (mV)	Δw (eV)
N	7	0.74	121	0.10
	8	0.86	126	0.11
	9	0.96	131	0.13
	average	0.85	126	0.11
n	7	1.23	136	0.17
	8	1.14	149	0.17
	9	1.60	153	0.20
	average	1.32	146	0.18
N + n	7	0.93	110	0.10
	8	0.45	89	0.04
	9	1.23	127	0.16
	average	0.87	108	0.10

7.4.1.2 Estimation of the Number of Gating Charges

The present investigation suggests that within the accuracy imposed by scatter in the experimental data, porins from 0111:B4 and K12 both have charges of about 1 unit involved in gating. A significant reduction in experimental scatter would be necessary to observe any subtle differences between the porin sources. Even if this could be achieved, the general insensitivity of the approach may make it unsuitable. To compare present findings with those published earlier it must be assumed that the current decays are characterised by a single exponential and that the total population is n + N.

Todt *et al.* (1992) reported that for OmpF porin at pH 5.6, z = 0.75 which lies within our range of 0.45-1.23 for 0111:B4 porin at pH 5.5 (Table 7.3). It is interesting that Todt *et al.* (1992) quote a precise value for z and give no indication of the extent of the scatter in their data. It is possible, though unlikely, that using a different lipid for bilayer formation (diphytanoylphosphatidylcholine) and/or their purer preparations of OmpF or OmpC may have given them less variability from membrane to membrane. There is some discrepancy, however, between the present work and the results of Morgan *et al.* (1990) for the 0111:B4 (pH 7.2) porin, despite identical experimental conditions and both the source and purification method of the porin being essentially the same. At neutral pH the range of values obtained by Morgan *et al.* (1990) for z at 1.85-2.4 is significantly larger than the range 0.93-1.47 (Table 7.1) found in this research.

7.4.1.3 Estimation of V_0

The value of 65 mV for V_0 reported by Morgan *et al.* (1990) was substantially lower than that reported for any other voltage-dependent bacterial porin. Their finding has not been confirmed in this research either, with V_0 for the combined population N + n being in the range 126-141 mV (Table 7.1). Morgan *et al.* (1990) found that the voltage required to initiate channel closure was as low as 50 mV. On one occasion, in this research the threshold voltage was as low as 75 mV but in general the channels did not show any evidence of closure until the voltage was at least 100 mV. There was great variability between experiments, with the threshold voltage being as high as 150 mV in some cases. In Section 6.3.2 it was demonstrated that the single channel conductance of the 0111:B4 porin from Morgan *et al.* (1990) was significantly smaller than the value obtained for 0111:B4 porin in this research. This raised the question of whether the 0111:B4 porins were identical, despite the fact that the bacteria from which they were extracted were grown under nominally the same conditions. These additional differences of behaviour in the 0111:B4 porins, under what are apparently identical experimental conditions further raises the above question.

Buehler *et al.* (1991) found that the most significant difference between F and C type channels (Section 6.3.2) was their respective threshold voltages (V_c) above which the channels began to close. C type channels had a V_c of 134-182 mV whilst F type channels had a V_c of 74-104 mV. The higher threshold of gating demonstrated for OmpC is consistent with findings by Lakey *et al.* (1991), who found OmpC largely insensitive to voltages below 200 mV at near neutral pH. From Tables 7.1 and 7.2 it is seen that the 0111:B4 porin (OmpF rich) has slightly lower values for V_o than K12 (OmpC rich), particularly for the n population. This is therefore consistent with the findings of other authors.

7.4.1.4 Effect of Acidic pH

Acidic conditions have been shown by some authors to affect the voltage-gating of porins. Xu *et al.* (1986) found that the probability of a porin channel closing increased at low pH. Todt *et al.* (1992) found that for OmpF the number of charges, z, involved in the gating process increased at low pH. OmpF porin was quoted as having a value for z of 0.75 at pH 5.6 and 0.61 at pH 9.2, a small difference compared with experimental data in the present work. As can be seen from Tables 7.1 and 7.3 the values of z obtained here at acidic pH show considerable overlap with the range of values obtained at neutral pH for both populations (experiments with acidic pH were performed with the porin from 0111:B4 only). There is no conclusive evidence to suggest a shift in z to higher values at low pH as suggested by Todt *et al.* (1992).

The range of values for V_o at acidic pH, however, appears consistently lower than those for neutral pH. The decrease in V_o in the absence of a change in z suggests a shift in the voltage dependence of gating to lower voltages rather than to an increase in the steepness of the voltage dependence as suggested by Todt *et al.* (1992). The change in behaviour could be similar to that described by Xu *et al.* (1986), who found that processes similar to those at high voltage were also detected at low voltage when the pH of the bathing solution was decreased. Further evidence of a pH effect on voltage-gating is discussed in Section 7.4.3.

A simple mechanism giving rise to such behaviour can be explained with the aid of Figure 7.7. It is known that there is an excess of negatively charged residues in the aqueous channel of the porin. Assume that gating requires the movement of a positively (negatively) charged residue away from (towards) some fixed negatively charged residues. This requires a change of energy equal to V_{o1}. At low pH a number of these fixed negative charges will become neutralised so that smaller energies are involved in the gating process. Thus smaller applied voltages will affect the transfer of the positive gating charge from A to B or the negative gating charge from C

to D. Such a mechanism would have an unchanged value for z but a lower Vo in acidic conditions.

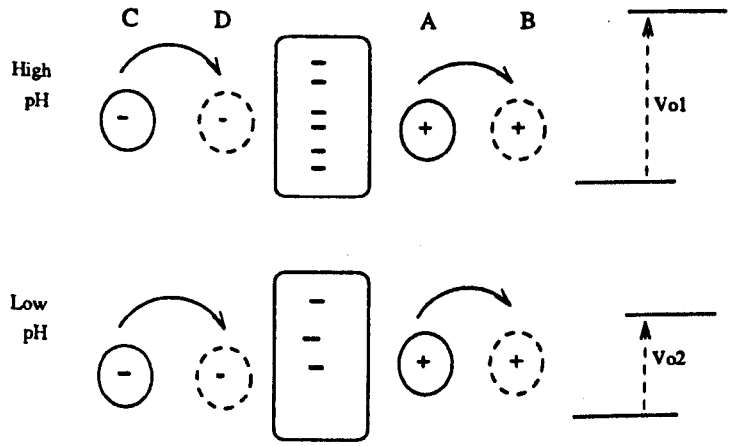

FIGURE 7.7 Schematic diagram showing possible mechanism of pH induced changes in Vo. $V_{o1}>V_{o2}$.

7.4.2 Change in N_c/n_c with Voltage

A plot of either N_c or n_c versus voltage should follow a sigmoidal dependence on bias as predicted by equation (2.46). The data in Figure 7.8 indicate that both N_c and n_c may lie on the almost linear, central portions of sigmoidal curves consistent with equation (2.46). In Figure 7.9 it is shown that N_c/n_c may vary systematically with applied voltage. Such behaviour is to be expected and is caused by differences in V_o and z in the two populations N and n as shown below. According to equation (2.46), if z and V_o are identical for both populations, then the ratio

$$\frac{N_c}{n_c} = \frac{N_0 + N_c}{n_0 + n_c} = \frac{N}{n} = K \tag{7.5}$$

where K is a constant. When the magnitude of the gating charge, z, and V_o are different in the two populations then

$$\frac{N_c}{n_c} = K\left(\frac{\exp\left(\frac{z^{\bullet}q}{kT}(V - V_0^{\bullet})\right)}{1+\exp\left(\frac{z^{\bullet}q}{kT}(V - V_0^{\bullet})\right)}\right)\left(\frac{1+\exp\left(\frac{zq}{kT}(V - V_0)\right)}{\exp\left(\frac{zq}{kT}(V - V_0)\right)}\right) \tag{7.6}$$

where z, V_0 and z^*, V_0^* refer to the n and N populations respectively. If the applied voltage, V, is significantly smaller than both V_0 and V_0^* then equation (7.6) reduces to

$$\frac{N_c}{n_c} = K\left(\frac{\exp\left(\frac{z^* q}{kT}\left(V - V_0^*\right)\right)}{\exp\left(\frac{z\,q}{kT}\left(V - V_0\right)\right)}\right) \tag{7.7}$$

i.e.

$$\frac{N_c}{n_c} = K' \exp\left(\frac{q}{kT}\left(z^* - z\right)V\right)$$

$$\text{where } K' = K\exp\left(\frac{q}{kT}\left(zV_0 - z^*V_0^*\right)\right). \tag{7.8}$$

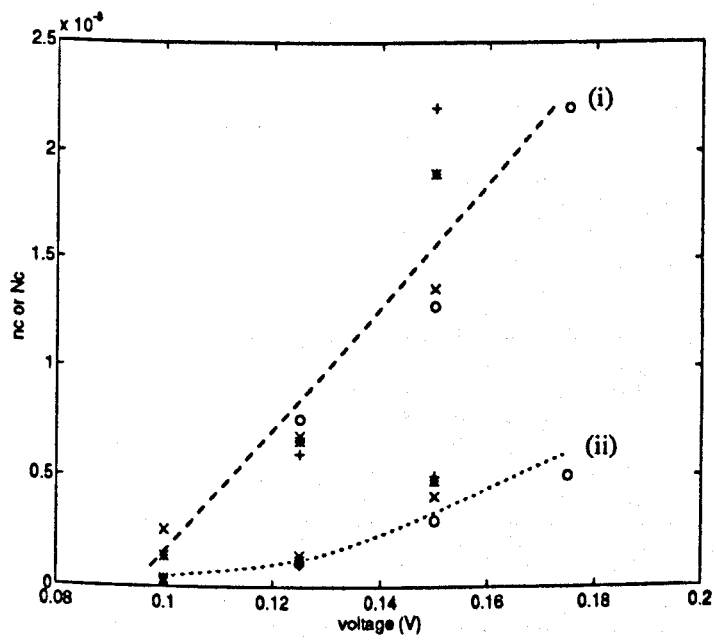

FIGURE 7.8 Variation of (i) N_c and (ii) n_c with applied voltage. Each symbol type represents a different membrane. Dashed and dotted lines have been drawn 'by eye'.

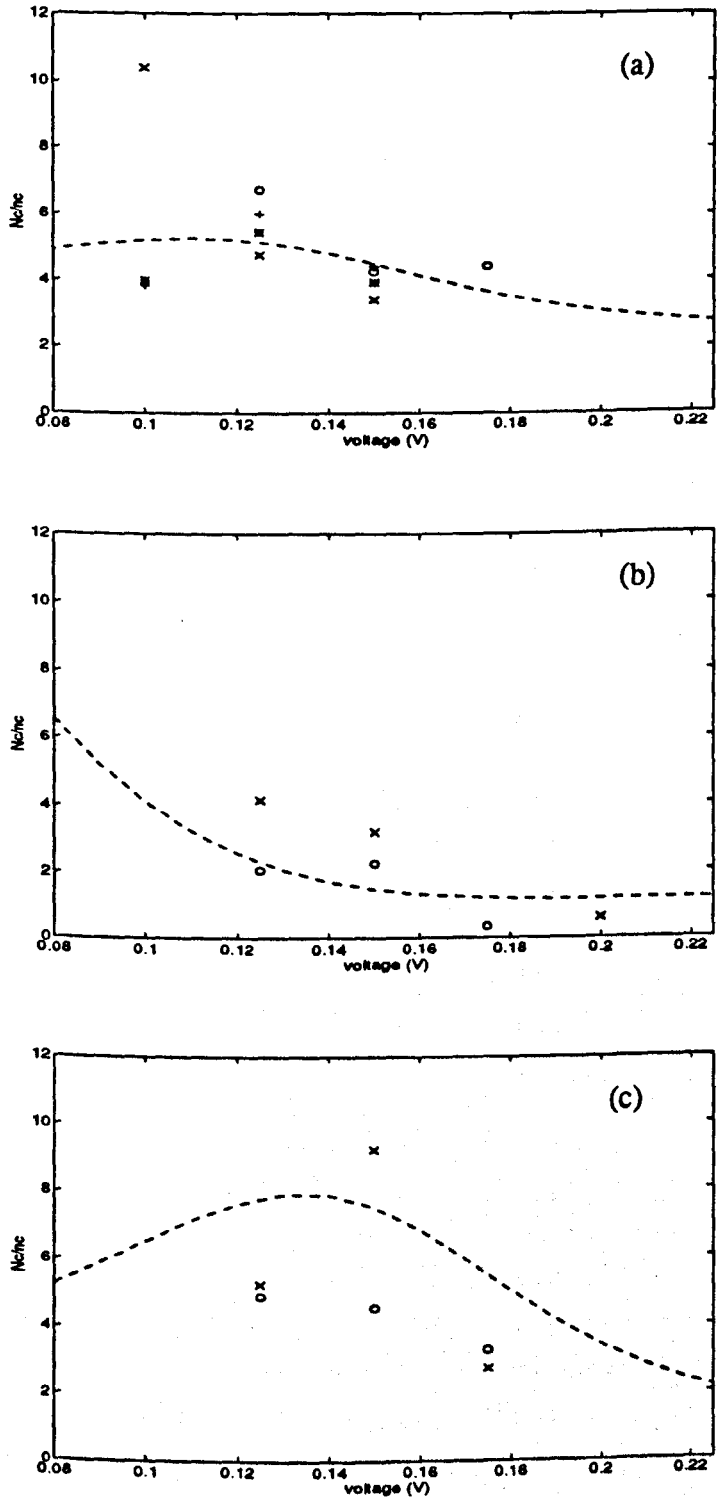

FIGURE 7.9 Variation of N_c/n_c with voltage. Each symbol represents a different membrane. a) 0111:B4, pH 7.2 b) 0111:B4, pH 5.5 and c) K12, pH 7.2. Theoretical lines were calculated using average values of z and Vo from Tables 7.1-7.3 with a) K=2.5 b) K=1.0 and c) K=1.0.

Thus if z is larger (smaller) than z^*, N_C/n_C increases (decreases) exponentially from K' at V=0. For the special case where $z = z^*$ then

$$\frac{N_c}{n_c} = K \exp\left(\frac{qz}{kT}\left(V_0 - V_0^*\right)\right).$$

At the other extreme of applied voltage when V is significantly larger than both V_0 and V_0^* then

$$\frac{N_c}{n_c} = K. \tag{7.9}$$

Taking the average values for the parameters given in Tables 7.1-7.3, i.e. z=1.27, V_0=0.168V, z^*=1.1 and V_0^*=0.139 for 0111:B4 (pH 7.2), the function in equation (7.6) has been evaluated. Estimates of K have been made for each porin by noting that N_C/n_C approaches K at large applied voltages (equation 7.9). From Figure 7.9 the estimates for K are 2.5, 1.0 and 1.0 for 0111:B4 (pH 7.2), 0111:B4 (pH 5.5) and K12 (pH 7.2) respectively. Theoretical plots based on theses values are superimposed on the experimental N_C/n_C data in Figure 7.9, from which it is seen that a reasonable agreement is obtained.

The presence of more than one closing population in the present work could reflect the presence of both OmpF and OmpC porins in the preparations. If this was indeed the case, values for K (=N_C/n_C) at large voltages would be expected to be closer to 1:50 or 50:1 i.e. reflecting the concentrations of OmpF:OmpC in the 0111:B4 and K12 preparations. Clearly this explanation may be ruled out.

It may be that each monomer within the trimeric porin cannot be treated independently. A porin trimer with one or two of the monomers already in the closed state may not behave the same as a porin with all three monomers in the open state. Buehler and Rosenbusch (1991), in their study of single channels of porin in lipid bilayers, found that if two of the monomers within a trimer closed (irreversibly in their case) the residual monomer had different gating properties to the original two open monomers. Results from patch clamp studies by Delcour *et al.* (1991) also suggest that the monomers cannot be regarded as independent: they demonstrated co-operativity between the monomers of OmpC. The previous estimates for N_C/n_C of 2.5 (0111:B4, pH 7.2), 1.0 (0111:B4, pH 5.5) and 1.0 (K12, pH 7.2) from Figure 7.9 could then reflect the non-independence of porin monomers.

Finally, it is also possible that channels experience different local environments, e.g. different lipid regions in the supporting membrane (Section 6.6.2). If the conformational change required during gating is affected by the structure of the supporting membrane, then more than one population would be identified.

7.4.3 Time constant of the Current Relaxation

At low voltages (< 100 mV) the current relaxation is difficult to measure, as the change in current is small compared to the d.c. level, i.e. only a very small proportion of the channels are closing in response to voltage. Consequently data have only been collected for voltages > 100 mV. For each voltage tested the bias was applied for 10 minutes - 1 hour; this was then repeated to check for reversibility in the gating and that further porin incorporation had not occurred. In order to reduce the time between the initial and the final voltage application, and thus reduce the likelihood of time-dependent changes (other than voltage-gating), only 3-4 voltages between 100 and 200 mV were applied to each membrane. In consequence the data points are relatively sparse.

The time constant, τ, for each population was obtained directly from fitting equation (7.1) to the current relaxation at each voltage. For the rapidly closing population, denoted n, plots of τ versus voltage fall into three distinct groups (Figure 7.10) corresponding to (a) the 0111:B4 porin (pH 7.2) (b) the 0111:B4 porin (pH 5.5) and (c) the K12 porin. All three sets of data could lie on bell shaped curves as predicted by equation (2.58). For the slower gating population, N, the data (Figure 7.11) can also be seen to fall into three distinct groups but the possible bell shaped τ versus voltage relationship is not so obvious, particularly for the 0111:B4 porin at pH 7.2. In general the data for the N population are more error prone than for the n population. This is because the current decay associated with the N population is relatively small and its relaxation time relatively long, making it difficult to judge accurately the magnitude of the d.c. current. This contrasts with the rapidly decaying current associated with the n population, which is easily distinguished from the more slowly changing background. The following analysis will therefore concentrate on the more accurate values for τ obtained from the population n.

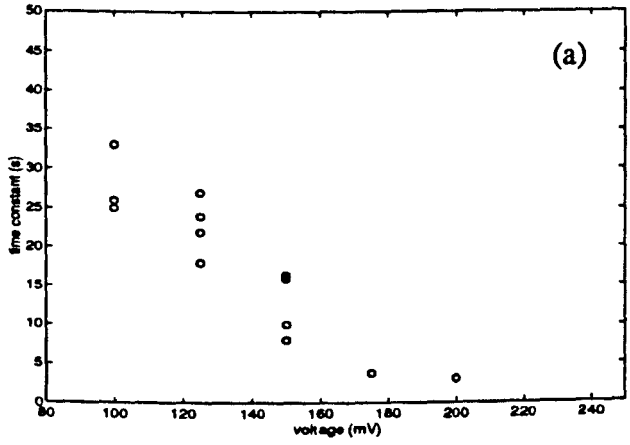

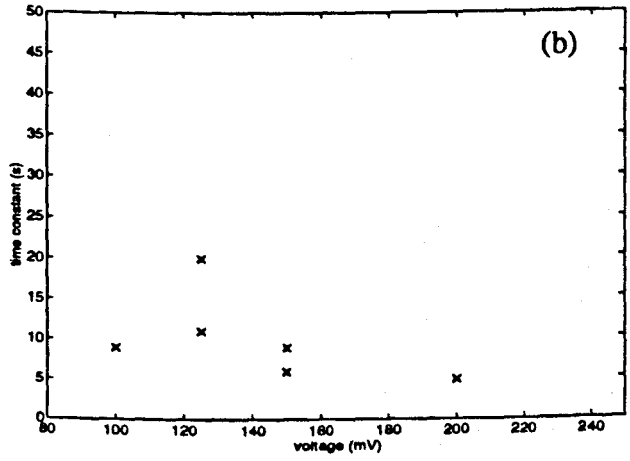

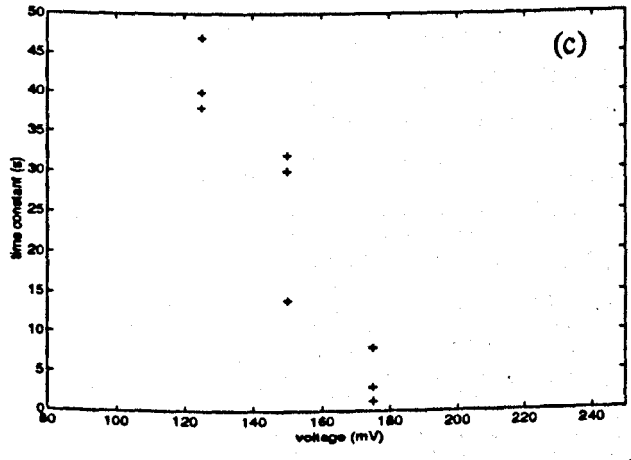

FIGURE 7.10 τ versus voltage behaviour for population n of a) 0111:B4, pH 7.2 b) 0111:B4, pH 5.5 and c) K12, pH 7.2.

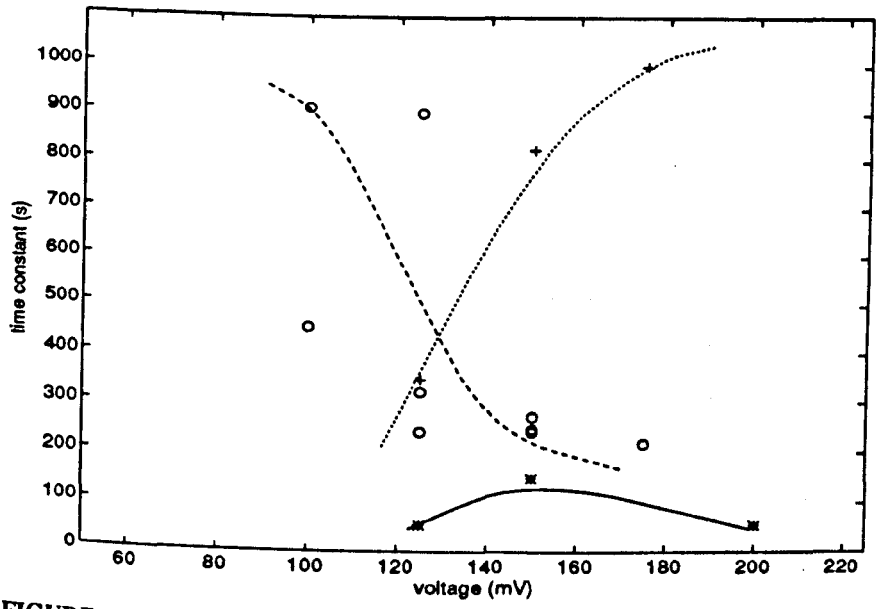

FIGURE 7.11 τ versus voltage relationship for population N of multi-channel membrane containing (*) 0111:B4 porin, pH 5.5 (o) 0111:B4 porin, pH 7.2 and (+) K12 porin, pH 7.2

7.4.3.1 Comparison of 0111:B4 and K12

The data for 0111:B4 and K12 at neutral pH are re-plotted in Figure 7.12 and compared with theoretical curves. The three sets of graphs in the figure correspond to three attempts to fit equation (2.58) to the experimental data. Clearly, with five adjustable parameters, A, B, a, b and V_0 the number of possible 'best-fit' curves to such scattered experimental data is almost limitless. However, some bounds may be placed by noting that the linear plots of $\log(I_\infty/I_j)$ versus voltage in Figure 7.6b, which are based on steady-state populations at the start and end of gating, must be fitted independently by the same parameters.

In Table 7.4 are given the values of the disposable parameters for all the theoretical curves in Figure 7.12. Also tabulated are the gradient, m, and intercept, c, of experimental plots such as those in Figure 7.6b. For comparison are given the predicted gradient and intercept values calculated from equation (2.60) using the appropriate parameter set. Of the three attempts to fit the K12 data in Figure 7.12 only the parameters in (c), where A≠B, come close to satisfying this added constraint (see Table 7.4). The predicted gradient is too high because of the need to use larger values of (a+b) in order to produce a narrower bell shaped curve to pass near the data at 175 mV. Further experimentation would be necessary to determine whether the experimental curve is wider than has been assumed.

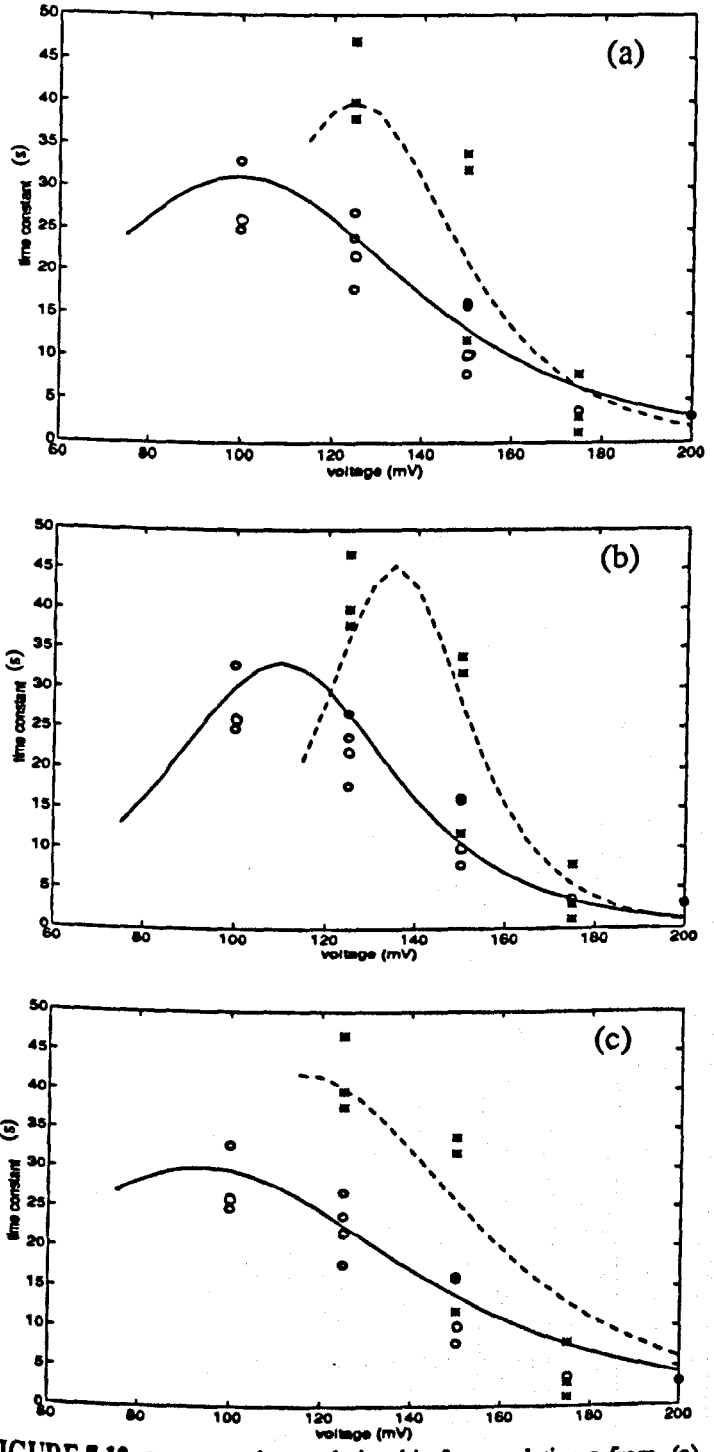

FIGURE 7.12 τ versus voltage relationship for population n from (o) 0111:B4 and (*) K12. The curves have been calculated using equation 7.6 with parameters as given in Table 7.4.

TABLE 7.4 Parameters used for curve fitting to the τ versus voltage data in Figures 7.12 and 7.13. Comparison of calculated values of slope, m, and intercept, c, using equation 2.60 with the experimentally obtained slope and intercept from plots of $\log_e(I_\infty/I_j)$ such as in Figure 7.6.

							predicted using equation (2.60)		$\log_e(I_\infty/I_j)$ versus V Experimental	
Porin	Figure No.	a	b	A	B	Vo (mV)	m	c	m	c
0111:B4	7.12a	1.5	1.5	0.016	0.016	100	60	6	20-60	4.3-10.1
pH 7.2	7.12b	2.25	2.25	0.015	0.015	110	90	9.9		
	7.12c	1.25	1.25	0.00525	0.0525	140	50	4.7		
K12	7.12a	2.5	2.5	0.0125	0.0125	125	100	12.5	25-40	7.0-7.5
pH 7.2	7.12b	3.5	3.5	0.011	0.011	135	140	18.9		
	7.12c	1.55	1.55	0.0019	0.075	175	62	7.15		
0111:B4	7.13	1.5	1.5	0.064	0.016	100	60	7.39	40-70	6.8-10.1
pH 5.5	7.13	1.5	1.5	0.032	0.032	125	60	7.5		

Two of the theoretical curves fitted to the 0111:B4 (pH 7.2) data have parameters consistent with the steady-state data (Figures 7.12a and 7.12c). In Figure 7.12a it has been assumed that $A=B=1/(2\tau_{max})= 0.016\ s^{-1}$, a=b=z=1.5 and V_o = 100 mV. In Figure 7.12c it has been assumed that B=10A, a=b=z=1.25 and Vo, now redefined as the voltage at which the energies of the open and closed states are equal, is 140 mV.

7.4.3.2 Effect of Acidic pH

Earlier experimental evidence in Section 7.4.1.4 suggested a decrease in V_o at acidic pH for the 0111:B4 porin. In Figure 7.13 there is a marked difference in the τ versus voltage relationship for the porin at acidic pH compared to neutral pH. The obvious difference is a reduction in the maximum value of τ in acidic conditions. This cannot be explained simply by a decrease in V_o since this would only shift the curve to lower voltages, while leaving the maximum value of τ unchanged. Measurements show that not only is the maximum value of τ smaller at acidic pH, but the maximum is shifted to higher applied bias. As is the case in Figure 7.12, more than one parameter set will provide equally good fits to the data in Figure 7.13. For example, the two theoretical curves fitting the data at pH 5.5 nearly superimpose over the whole range despite very different values of V_o, A and B. Both of these fitted curves are also consistent with the previous $\log_e I_o/I_j$ data as shown in Table 7.4. It is significant that for both 'best-fit' curves either A=B or A>B, in contrast with neutral pH where A<B (Figure 7.12) provided the best fit. It was not possible to find a reasonable fit to the τ data collected at acidic pH with A<B.

Acidic conditions have been shown by some authors to affect the voltage-gating of porins (Xu *et al.*, 1986, Todt *et al.*, 1992). We have already demonstrated a change in the single channel conductance related to pH, which may be partly due to physical changes in the pore size brought about by pH induced conformation changes in the protein. Lakey *et al.* (1991), studying OmpC mutants in planar lipid bilayers, reported that the mutations studied affected both conductance and gating. These findings indicate that part of the protein structure responsible for the 'size filter' may also be involved in the voltage sensitivity of gating. The constriction zone (Section 3.4.3) with its strong transverse electric field (Cowan *et al.*, 1992) represents the most critical site for permeability and gating properties. It is also known that selectivity of the porin, due to the presence of charged amino acid side groups, is reduced by acidic conditions. It is not unlikely, then, that the part(s) of the protein sensitive to the applied field may have moved and/or be surrounded by a different charged environment in acidic conditions, which, in turn, changes the protein's response to applied voltage. It has also been suggested (Xu *et al.*, 1986) that there is less

interaction between the sub-units at low pH, with the closed conformation being the most favourable.

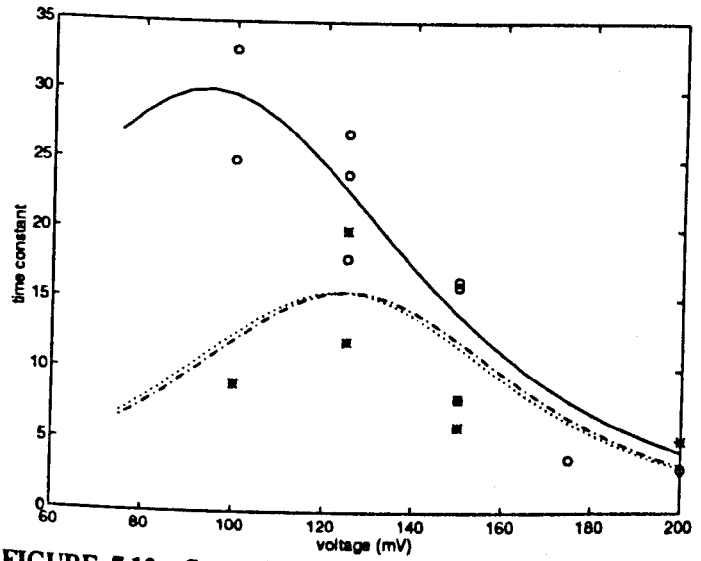

FIGURE 7.13 Comparison of τ versus voltage relationship for population n from 0111:B4 at (o) pH 7.2 and (*) pH 5.5. Parameters for the curves are A=0.00525, B=0.0525, a=b=1.25, V_0 = 140 mV (solid line); A=B=0.032, a=b=1.5, V_0=125 mV (dashed line) and A=0.064, B=0.016, a=b=1.5 and V_0=100 mV (dotted line).

7.4.4. Estimating the Contribution of Each Population to the Steady-State Current

Since the fraction of the steady-state current to apportion to the two populations is not known, then the estimates of z and V_0 in Tables 7.1-7.3 could be significantly in error, thus invalidating the comparison in Table 7.4. Had the time-constant data been more plentiful and less scattered, an alternative approach would have been possible for determining the contributions made to the steady-state current by the two populations. As an example, consider the data points collected for the 0111:B4 porin at neutral pH. These are re-plotted in Figure 7.14, together with 'best fit' plots (as judged by eye) for the two populations.

Figure 7.15 shows the steady-state data for the two populations. Interestingly, although individual experiments followed slightly different linear plots, hence the different values of z and V_0 in Table 7.1, when collected together the data for each population is grouped around a common straight line. When the estimates of z and V_0 from all the best fit curves in Figure 7.14 are used to fit this data, a straight

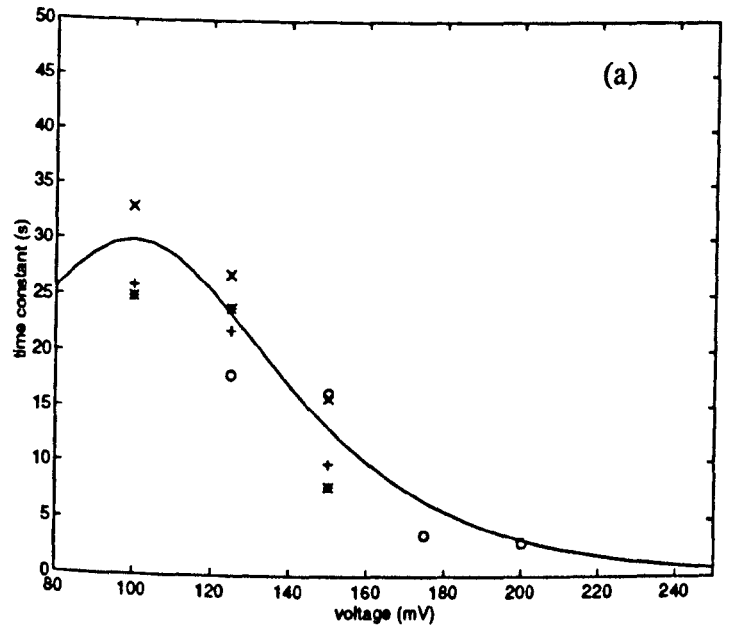

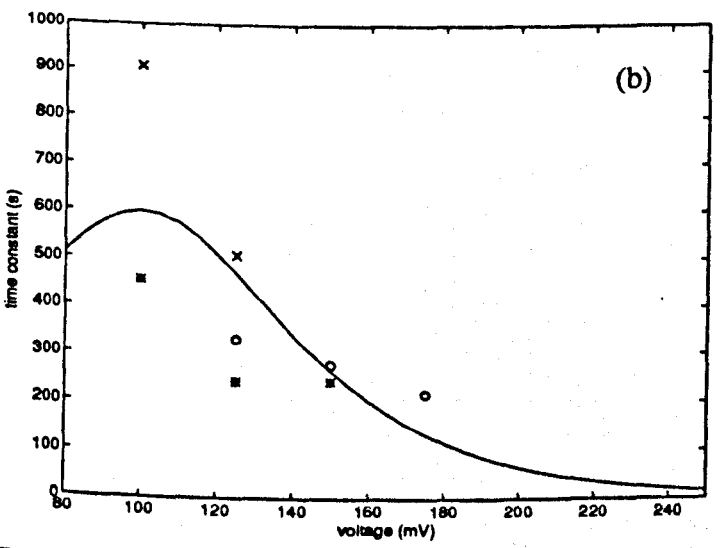

FIGURE 7.14 τ versus voltage relationship for a) population n and b) population N of 0111:B4 porin at pH 7.2. Each symbol type represents a different membrane. The fitted curves both have parameters of V_0 =100 mV and z=1.5. In a) τmax=30s and in b) τmax=600s.

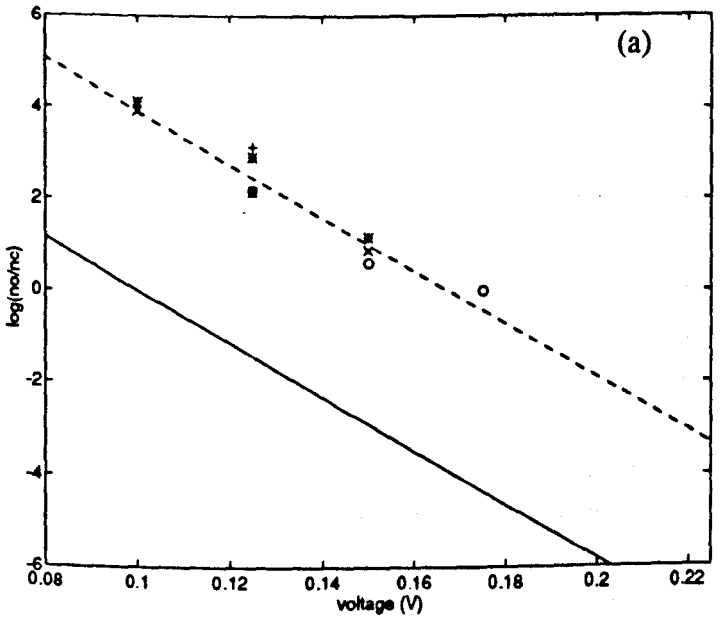

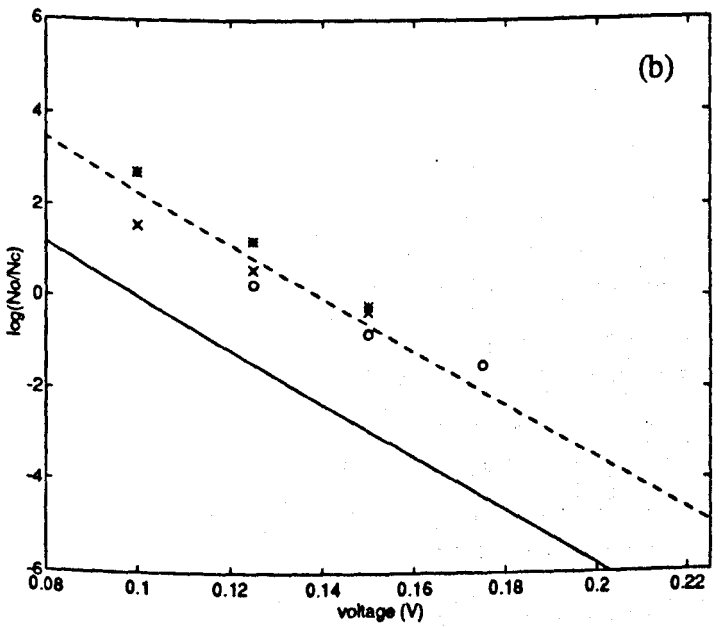

FIGURE 7.15 Log I_∞/I_j versus voltage for (a) population n and (b) population N. The data have been obtained from the same membranes as in Figure 7.14. The solid lines are theoretical lines calculated using the values z and V_0 from Figure 7.14. The dashed lines have been formed by shifting the theoretical lines by (a) log(50) and (b) log(10).

line plot of identical slope is obtained. However, this theoretical plot is well below the data in both cases.

One explanation is that when applying assumptions (i) and (ii) in Section 7.4.1.1 we have grossly overestimated the contribution of each population to the steady-state current. By forcing the data in Figures 7.15a and 7.15b to match the theoretical lines it is concluded that only 2% of the steady-state current arises from the fast (n) population and about 10% is contributed by the slower (N) population. This would indicate the presence of a third population, comprising some 88% of the total, which is not voltage-gated. This contradicts the experimental finding that, at the highest applied voltages, gating can lead to a reduction of 60% or more in the measured current, e.g. curve(c) in Figure 7.6a. This inconsistency is likely to have arisen from the difficulty of fitting the data in Figures 7.14a and 7.14b. For instance both V_o and z are the same for the fast (n) and slow (N) populations in the 'best fit' curves in Figures 7.14a and 7.14b. This is inconsistent with the N_c/n_c data in Figure 7.9a, which suggest different z and V_o values for the two populations.

7.5 CONCLUSIONS

Evidence from both single channel and multi-channel membranes has established unequivocally that OmpF and OmpC porins from *E. coli* undergo voltage-gating. Previously, where voltage-gating had been observed, the authors seemed only concerned as to whether voltage-gating was present or not. Consequently, little quantitative information on the voltage-gating process in porins has been published. Detailed studies carried out here on multi-channel membranes has revealed the presence of several different types of current relaxation in response to sustained application of voltage. In approximately 1/3 of the experiments the current relaxation was only partially reversible following the first application of high transmembrane voltage, but was reversible thereafter. In a small number of experiments, some with the applied voltage as low as 25 mV, most or all of the channels closed irreversibly. If the voltage application was sustained for up to 1 hour, some experiments showed a series of current relaxations. In addition, a change in voltage sensitivity and in the asymmetry of the voltage-gating behaviour was seen over time with some membranes. This is the first time that a single study has revealed such widely differing behaviour in nominally identical channels.

Furthermore, the most commonly observed type of current relaxation, which was studied in detail, was seen to be composed of two exponential decays, indicating the presence of two distinct closing populations, i.e. one fast (n) and one slow (N). The fast population closed with a time constant between 3s and 25s while the slow

population closed with a time constant between 40s and 900s. Such behaviour has not been reported previously for porins incorporated in lipid bilayer membranes.

A few authors have studied the manner in which the ratio of open to closed channels at steady-state depends on the applied voltage. Upon applying the two-state model of Ehrenstein and Lecar (1977) to such data, an estimate of the magnitude of the gating charge, z, as well as V_0, the voltage at which half the channels are closed, can be made. In this study, the presence of two populations in the current relaxation makes such an estimate difficult since the fraction of the steady-state current, I_∞, arising from the individual populations is not known. Nevertheless, by assuming that the whole of the current arises solely from one or the other population, upper limits for V_0 and a reasonable estimate for z can be made. In addition, so as to enable easier comparison with other workers, it has also been assumed that the whole relaxation arises from a single population.

Despite the assumptions made about the origin of the d.c. level, all values of z (0.45-1.6) and V_0 (89-267 mV) were reasonable. This was in part due to the logarithmic dependence of the open to closed ratio on applied voltage. Average values of z, approximately 1 unit for both populations and for both sources of porin, were approximately half that reported by Morgan *et al.* (1990). The unusually low value of 65 mV for V_0 reported by Morgan *et al.* (1990) was not confirmed in this research either.

The ratio of the two closing populations, N_c/n_c, was not constant but appeared to vary systematically with applied voltage. It was demonstrated that relatively small differences in z and V_0 between the two populations could be responsible for this variation.

The τ versus voltage data fell into three distinct groups corresponding to the 0111:B4 porin at pH 7.2 and at pH 5.5 and the K12 porin at pH 7.2. Each group of data points fell on part of a bell-shaped curve as predicted by the two-state model (Ehrenstein and Lecar, 1977). Theoretical curves for τ were compared with the experimental data. Steady-state measurements had indicated that lowering the pH decreased V_0 whilst leaving z unchanged. The change in the τ versus voltage relationship of 0111:B4 when the pH was lowered could not, however, simply be explained by a change in V_0. The τ data indicated that changes were also occurring in the opening and closing rates of the porin channels.

An attempt was also made to estimate the contribution of each population to the steady-state current. The results of this analysis, which relied on the accuracy of the τ data, were conflicting. Population n was estimated to contribute only 20% of the d.c. level whilst population N, which was expected therefore to contribute the majority of the d.c. level, was estimated to contribute only 10%. This unsatisfactory result was

due in part to the lack of suitable quality data. Despite these contradictory findings the multi-channel membranes which exhibited reversible voltage-gating followed the general behaviour predicted by the two-state model.

CHAPTER 8

CONCLUSIONS

8.1 CONCLUSIONS

The motivation for this work was two-fold. Firstly, our interest stemmed from reports in the literature that porin was voltage-gated. Such a channel, situated in a lipid bilayer, provides an environment which confines and controls the flow of ions and, as such, has similar properties to solid-state devices which control and confine the flow of electronic charges. It was thought that knowledge gained from such a system could possibly be useful in future electronic devices based on organic molecules. Secondly, in enteric bacteria such as *E. coli* the outer membrane acts as a very effective permeability barrier to some antibiotics and high levels of resistance have been established by some bacterial strains. Porins are the main route of antibiotic flow from the outside of the cell to the target site. An understanding of the mechanisms which control the flow of molecules, such as antibiotics, through porin channels is therefore of great importance to the pharmaceutical industry.

A study was, therefore, made of ion flow through porin channels. At the onset of the research project the intention was to concentrate on voltage-gating. Initial experiments, however, which were carried out simply to confirm some of the properties of porin already reported in the literature, revealed some previously unreported porin behaviour. In consequence this work evolved into a more general study of the biophysics of porin channels.

To extract porin from whole cells of *E. coli* 0111:B4 and K12 (a 'rough' mutant) the high level of detergent resistance of native porin trimers and their tight non-covalent association with peptidoglycan was successfully exploited. Final porin preparations from both strains contained a mixture of OmpF and OmpC porins, 0111:B4 being OmpF rich and K12 being OmpC rich. When examined using SDS polyacrylamide gel electrophoresis the two porins did not run in the order expected from their molecular weights as deduced from amino acid sequences. The two porins are very close in molecular weight and a possible explanation is that heating uncoils the proteins to different degrees such that the slightly heavier protein migrates further on the gel than the lighter protein. The detergent solubilised porin was then studied by incorporating it into lipid bilayer membranes formed by the Montal-Mueller method.

In common with other researchers porin was found to form slightly cation selective channels (Benz, 1985 and Benz and Bauer, 1988) with single channel conductances related to the specific conductance of the aqueous phase. A previously

unreported finding for porin channels in lipid bilayer membranes, but demonstrated consistently in this research, was an asymmetrical and non-linear I/V characteristic. The degree of asymmetry and of non-linearity were dependent upon the pH and the salt concentration of the bathing medium. Electrostatic models by Levitt (1985) and Sancho and Martinez (1991) suggest that such behaviour could be produced by fixed charges or dipoles located at one end of the channel. Relating the above models to the experimental evidence, it is proposed that there is a net negative charge at the LPS end of the porin LPS complex which may be the negative poles of dipoles associated with amino acid and/or sugar residues. The dependence of the asymmetry in the I/V characteristic on the aqueous compartment to which porin is added is evidence that porin inserts into the bilayer in a specific orientation. Application of positive applied potentials to the compartment in which porin has been added resulted in greatly enhanced porin incorporation. An orientation of the porin such that the bulky hydrophilic sugars on the LPS were facing away from the bilayer would be favourable for porin incorporation. The notion that a net negative charge exists at the LPS end of the porin would be consistent with the observed polarity dependence of insertion.

The models above show that conductance is sensitive to the magnitude and the location of charges and dipoles within the channel. The broad distribution of single channel conductances typical for porin channels, often thought to represent a range of channel 'sizes', could be due to statistical fluctuations in the degree of ionisation of charged residues and slight differences in the relative positions of fixed charges and dipoles. Similarly, the decrease in channel conductance with low pH, which would change the degree of ionisation of fixed charges within the channel, cannot all be attributed to physical changes in the size of the aqueous channel as suggested by Todt *et al.* (1992). The sensitivity of channel conductance may account for the variability in measured single channel conductances of OmpF and OmpC porins between different laboratories. Estimates of pore diameter from single channel conductance measurements, based on the assumption that porin is a cylinder filled with bulk electrolyte, have been made by some authors (Morgan *et al.*, 1990; Benz and Bauer, 1988). In the present work, estimates for the diameter of an individual pore within the porin trimer were 0.9 nm for 0111:B4 and 0.83nm for K12, assuming a length of 6 nm for the channel. It is clear, however, that these estimates are not particularly meaningful, not only because the geometry of porin has been shown to be more complex but also because the channel conductance is non-linear. It should be noted, though, that the values for pore diameter in the present work are much closer to the estimates using liposome permeability rates and liposome swelling assays (1.0-1.6 nm) than those obtained by previous authors.

Another phenomenon not previously reported in the literature is a possible interaction between channels within the bilayer. For 0111:B4 the degree of asymmetry of the I/V relationship was reduced as the number of incorporated channels was increased. It is proposed that the channels form aggregates or 'clusters'. Modelling a cluster as a large diameter channel shows that the current density in the cluster decreases as the cluster grows because of the increasing influence of the access resistance. Thus the asymmetrical behaviour of individual porin channels becomes reduced. This may also be partly responsible for the spread of conductances observed during porin incorporation. The observed conductance will depend on whether a porin enters a remote portion of the bilayer, a cluster or indeed even the centre or periphery of a cluster.

Voltage-gating was demonstrated in multi-channel membranes and also in single channels. Reversible channel closure was seen which occurred in three well defined steps consistent with the known trimeric structure of porin. These findings make electrical breakdown of the protein an unlikely explanation for the observed channel closure. In addition, recent evidence of voltage-gating in porin channels provided by patch clamp experiments on outer membrane extracts (Berrier *et al.*, 1989 and Delcour *et al.*, 1989) show that voltage-gating is not merely an artefact of the lipid bilayer technique.

The detailed study in this research has revealed the presence of several different types of current relaxation in the porin extracts. This variation in behaviour, occurring during the course of a single study, has not previously been reported. The most common type of current relaxation was composed of two exponential decays which suggested the presence of more than one population of closing channels. Within a single experiment the time constants of each decay function were repeatable for a given voltage. Between different membranes, however, there was great variability with the shorter time constant ranging from 3-25s and the longer time constant from 40-900s. Estimates of the ratio of the two closing populations, Nc/nc, indicated that the mixture of OmpF and OmpC in the samples was not responsible for the appearance of more than one population. The non-independence of the monomers making up the porin trimer could, however, be responsible. Support for this view comes from recent patch clamp experiments which indicate that porin channel kinetics are more complicated than was thought previously (Berrier *et al.*, 1992) and that monomers cannot be regarded as independent (Delcour *et al.*, 1991). The present research provides evidence that porin channels incorporated in lipid bilayer membranes also show gating behaviour that is more complicated than previously reported. This finding, coupled with the observed asymmetrical I/V relationship, again only previously observed using

patch clamp techniques, indicates that the behaviour of porin *in vitro* may truly reflect its behaviour *in vivo*.

pH has been shown to influence the single channel conductance of open channels and it also appears to influence the porin's response to applied voltage. pH was demonstrated to have a marked effect on the time constant of the current relaxation, as well as influencing the ratio of open to closed channels at steady-state. The traditional view of porin channels as static, open pores in the outer membrane of bacteria can certainly be dismissed.

8.2 FURTHER WORK

Any future work with the system investigated here must of necessity reduce the variability in the experimental results. This could possibly be achieved by:

(i) Extracting porin from mutants which produce only one type of porin so that the resulting sample is purer.

(ii) Removing some of the associated LPS so that the porin/LPS complexes are more homogeneous. In the present work this was not successfully achieved because of the lack of available time.

(iii) The use of a synthetic lipid for bilayer formation to provide a more highly defined environment.

(iv) Construction of a suitable fluid exchange system to reduce the concentration of dissolved porin in the bathing medium when the required number of porin channels have been incorporated. This may solve the problem of continuing porin incorporation at high voltages and could be achieved by the coupling of two syringes, one removing electrolyte and one adding electrolyte to the bath. This would need to be achieved very slowly and very smoothly to be successful.

Bilayers in this research were made exclusively with the zwitterionic phospholipid phosphatidylcholine from egg yolk. The lipid composition is complex and the physical and chemical properties of bilayers formed with this lipid are not fully understood. It may be instructive to study both the rate of insertion and the I/V characteristic of the porin in different lipid environments, including those formed with synthetic lipids which have been more fully characterised. Phospholipids with charged head groups such as phosphatidylserine and phosphatidylglycerol (negative) and 1,2 dihexadecylphoshpatidylcholine (DHPDC) (positive) could also be used in bilayer formation. In addition the Montal-Mueller method allows the formation of asymmetrical bilayers. Thus, it may be possible to mimic more closely the bacterial

outer membrane by forming bilayers with LPS in one leaflet and phosphatidylethanolamine in the other.

Electrostatic models of channel systems have been shown to reliably predict some of the experimental observations of gramicidin channels, thus emphasising their applicability to real systems. The development of a model for porin-like channels incorporating some of the known structural information about this protein, has already begun. The comparison of model calculations with experimental results may lead to a deeper understanding of the motion of ions through such channels.

Recently reported results obtained from outer membrane channels (?porins), applying patch-clamp techniques to giant spheroplasts and native membrane extracts, have been demonstrated concurrently in this work, thus indicating the usefulness of the lipid bilayer technique as a model system. In the investigation of voltage-gating, however, a large number of experiments were rejected during this study because of

(i) irreversible gating behaviour

(ii) continuing porin incorporation and

(iii) increased voltage sensitivity over time, possibly due to changes in the bilayer itself.

The patch-clamp technique, by sampling a small area of native membrane and a small number of channels, will overcome at least problems (ii) and (iii). At present the main disadvantage of the patch clamp technique is that the identity of channels within a patch is not always known. If this problem is overcome, then the patch clamp technique must be the preferred method to study voltage-gating in porin channels.

New scanning probe microscopy (SPM) techniques suitable for use with biological materials may offer opportunities to view the surface of the porin containing bilayer. The orientation of the porin and the presence and size of clusters could therefore be determined. Atomic force microscopy (AFM) and scanning near-field microscopy (SNOM) are both suitable for non-conducting samples and enable biological samples to be maintained in physiologically relevant media. The technique of electrochemical scanning tunnelling microscopy (electrochemical STM) is also suitable for use with bilayer membranes, as it operates in the presence of an electrolyte. SNOM combines the high resolution imaging techniques of SPM with the contrast mechanisms inherent to optical microscopy. Resolutions of better than 30 nm have been achieved in the imaging of the Tobacco Mosaic virus (Moyer *et al.*, 1993). Incorporation of porin, under the influence of an applied field, into pre-formed liposomes may provide a suitable medium in which to view the protein. The polarity of the field could be reversed to assist porin incorporation from both sides of the liposomes. A further stage would involve adaptation of the Montal-Mueller apparatus to house a SNOM probe in order to provide an opportunity for viewing the surface of

the bilayer at high resolution. The bilayer is particularly susceptible to disturbance and precautions would need to be taken to reduce vibration and avoid disruption due to convection currents in the region of the probe.

REFERENCES

Archer S.J. and Cafiso D.S. (1991) *Biophys. J.*, 60, 380-388.

Arndt R.A. and Roper L.D. (1975) *J. Theor. Biol.*, 54, 249-283.

Attwell D. and Jack J. (1978) *Prog. Biophys. Molec. Biol.*, 34, 81-107.

Bamberg E. and Laüger P. (1973) *J. Memb. Biol.*, 117-194.

Bauer K., Van der Ley P., Benz R. and Tommassen J. (1988) *J. Biol. Chem.*, 263, 13046-13053.

Benson S.A., Occi J.L.L. and Sampson B.A. (1988) *J. Molec. Biol.*, 203, 961-970.

Benz R., Janko K. and Lauger P. (1979) *Biochim. Biophys. Acta*, 551, 238-247.

Benz R., Ishii J. and Nakae T. (1980) *J. Memb. Biol.*, 56, 19.

Benz R. and Hancock R.E.W. (1981) *Biochim. Biophys. Acta*, 646, 298-308.

Benz R. (1984) *Current Topics in Membranes and Transport*, 21, 199-219.

Benz R., Tokunga H. and Nakae T. (1984) *Biochim. Biophys. Acta*, 769, 348-356.

Benz R. (1985) *CRC Critical Reviews in Biochemistry*, 119, 145-190.

Benz R., Schmid A. and Hancock R.E.W. (1985) *J. Bacteriol.*, 162, 722-727.

Benz R. and Böhme H. (1985) *Biochim. Biophys. Acta*,812, 286-292.

Benz R. (1988) *Ann. Rev. Microbiol.*, 42, 359-393.

Benz R. and Bauer K. (1988) *Eur. J. Biochem.*, 176, 1-19.

Berg H., Förster W. and Jacob H.E. (1987) *In* Milazzo G. and Blanck M. (eds): Bioelectrochemistry II: Membrane Phenomena. Plenum Press. 135-166.

Berrier C., Coulombe A., Houssin C. and Ghazi A. (1989) *FEBS Letters*, 259, 27-32.

Berrier C., Coulombe A., Houssin C. and Ghazi A. (1992) *FEBS Letters*, 306, 251-256.

Blackburn G.F. (1987) *In* Turner A.P.F., Karube I. and Wilson G.S.(eds): Biosensors, Fundamentals and Applications. Oxford University Press, NY.

Bone S. and Zaba B. (1992) Bioelectronics, Wiley and Sons, NY.

Bosch D. and Tommassen J. (1987) *Molec. Gen. Genet.*, 208,485-489.

Bosch D., Scholten M., Verhagen C. and Tommassen J. (1989) *Molec. Gen. Genet.*, 216,144- 148.

Boser B.E., Sackinger E., Bromley J., LeCun Y. and Jackel L.D. (1992) *IEEE Micro*, February 1992, 34-40.

Bowen P.J. and Lewis T.J. (1983) *Thin Solid Films*, 99, 157-163.

Brass J.M. (1986) *Current Topics in Microbiol and Immunology*, vol. 129. Springer Verlag, Berlin and Heidelberg.

Braun V., Rotering H., Ohms J.P. and Hagenmaier H. (1976) *Eur. J. Biochem.*, 70, 601.
Britton H.G. (1966) *Arch. Biochem. Biophys.*, 117, 167-183.
Britton H.G. (1975) *Biochem. J.*, 161, 517-526.
Buechner M., Delcour A.H., Martinac B., Adler J. and Kung C. (1990) *Biochim. Biophys. Acta*, 1024, 111-121.
Buehler L.K., Kusumoto S., Zhang H. and Rosenbusch J.P. (1991) *J. Biol. Chem.*, 266, 24446-24450.
Buehler L.K. and Rosenbusch J.P. (1993) *Biochem. Biophys. Res. Comm.*, 190, 624-629.
Chapman D., Cornell B.A., Eliasz A.W. and Perry A. (1977) *J. Molec. Biol.*, 113, 517-538.
Chen R., Schmidmayer W. and Henning U. (1979) *Proc. Natl. Acad. Sci. USA.*, 76, 5014-5017.
Chen R., Schmidmayer W., Kramer C., Chen-Schmeisser U. and Henning U. (1980) *Proc. Natl. Acad. Sci. USA.*, 77, 4592-4596.
Chen R., Kramer C., Schmidmayer W., Chen-Schmeisser U. and Henning U. (1982) *Biochem. J.*, 203, 33-43.
Colombini M. (1980) *Ann. NY. Acad. Sci.*, 341, 552-563.
Cooper K, Jakobsson E. and Wolynes P. (1985) *Prog. Biophys. Mol. Biol.*, 46, 51-96.
Cowan S.W., Schirmer T., Rummel G., Steiert M., Ghosh R., Pauptit R.A., Jansonius J.N. and Rosenbusch J.P. (1992) *Nature*, 358, 727-733.
Daniellson B., Lundstrom I., Winquist F. and Mosbach K. (1979) *Anal. Lett. B.*,12, 1189-1199.
Dargent B., Hofmann W., Pattus F. and Rosenbusch J.P. (1986) *EMBO J.*, 5, 773-778.
Darveau R.P., Hancock R.E.W. and Benz R. (1984) *Biochim. Biophys. Acta*, 774, 67-74.
Delcour A.H., Martinac B., Adler J. and Kung C. (1989) *Biophys. J.*, 56, 631-636.
Delcour A.H., Adler J. and Kung C. (1991) *J. Memb. Biol.*, 119, 267-275.
Delcour A.H., Adler J., Kung C. and Martinac B. (1992) *FEBS Letters.*, 304, 216-200.
Dorset D.L., Engel A., Massalski A. and Rosenbusch J.P. (1984) *Biophys. J.*, 45, 128-129.
Edmonds D.T. (1990) *Eur. Biophys. J.*, 18, 135-137.
Ehrenstein G., Lecar H. and Nossal R. (1970) *J. Gen. Physiol.*, 55, 119-133.
Ehrenstein G., Blumenthal R., Latorre R. and Lecar H. (1977) *J. Gen. Physiol.*, 63, 707-721.
Ehrenstein G. and Lecar H. (1977) *Quarterly Reviews Biophys.*, 10, 1-34.
Engel A., Massalski A., Schindler H., Dorset D.L. and Rosenbusch J.P. (1985) *Nature*, 317, 643-645.

Esashi M. and Matsuo T. (1978) *IEEE Transactions on Biomedical Engineering*, 25, 184-191.

Fukushima H. (1994) Synthesis of Biotin-substituted Ligands for Molecular Networks. PhD Thesis, University of Wales, Bangor. UK.

Garavito R.M. and Rosenbusch J.P. (1980) *J. Cell. Biol.*, 86, 327-329.

Garavito R.M., Jenkins J., Jansonius J.N., Karlsson R. and Rosenbusch J.P. (1983) *J. Molec. Biol.*, 164, 313-327.

Garavito R.M., Hinz U. and Neuhaus J.M. (1984) *J. Biol. Chem.*, 259, 4254-4257.

Garavito R.M. and Rosenbusch J.P. (1986) *Meth. Enzym.*, 125, 309-328.

Geddes L.A., Baker L.E. and Moore A.G. (1969) *Med. & Biol. Engng*, 7, 49-56.

Gehring K. and Nikaido H. (1989) *J. Biol. Chem.*, 264, 2810-2815.

Glasstone S., Laidler K.J., Eyring H. (1941) The Theory of Rate Processes. McGraw-Hill, New York.

Goldman D.E. (1943) *J. Gen. Physiol.*, 27, 37-60.

Gudmundsson A., Erlendsdottir H., Gotfredsson M. and Gudmundsson S. (1991) *Anitmicrobial Agents and Chemotherapy*, 35, 2617-2624.

Hall J.E. (1975) *J. Gen. Physiol.*, 66, 531-532.

Hall J.E., Vodyanoy I., Balasubramanian T.M. and Marshall G.R. (1984) *Biophys. J.*, 45, 233-245.

Hancock R.E.W. (1986) *In* Inouye M. (ed): Bacterial Outer Membranes as Model Systems. John Wiley and Sons, NY.,188-255.

Hancock R.E.W. (1987) *J. Bacteriol.*, 169, 929-933.

Harris E.L.V. and Angal S. (Editors) (1989) Protein Purification Methods; A Practical Approach. IRL Press.

Hasted J.B. (1973) Aqueous Dielectrics. Chapman and Hall, London.

Henning U., Schmidmayr W. and Hindennach I. (1977) *Mol. Gen. Genet.*, 154, 293-298.

Hille B. (1984) Ionic Channels of Excitable Membranes. Sinauer Ass. Inc.

Hladky S.B. and Haydon D.A. (1984) *In* Stein W.D. (ed): Ion Channels: Molecular and Physiological Aspects. Academic Press, Florida. 327-372.

Hodgkin A.L. and Katz B. (1949) *J. Physiol. (Ldn.).*, 108, 37-77.

Inokuchi K., Norihiro M., Matsuyama S. and Mizushima S. (1982) *Nucleic Acids Res.*, 10, 6957-6968.

Jan L.Y. and Jan Y.N. (1989) *Cell*, 56, 13-25.

Jap B.K. (1989) *J. Molec. Biol.*, 205, 407-419.

Jap B.K. and Walian P.J. (1990) *Quarterly Reviews Biophys.*, 23, 367-403.

Jordan P.C. (1982) *Biophys. J.*, 39, 157-164.

Jordan P.C., Bacquet R.J., McCammon A.J. and Tran P. (1989) *Biophys. J.*, 55, 1041-1052.

Kleffel B., Garavito R.M., Baumeister W. and Rosenbusch J.P. (1985) *EMBO J.*, 4, 1589-1592.

Krull U.J. (1987) *Anal. Chim. Acta*, 197, 203.

Kuan S.S. and Guilbault G.G. (1987) *In* Turner A.P.F., Karube I. and Wilson G.S.: Biosensors, Fundamentals and Applications. Oxford University Press, NY. 135-152.

Kung S.Y. (1988) VLSI Array Processors. Prentice Hall, NY.

Labarca P., Coronado R. and Miller C. (1980) *J. Gen. Physiol.*, 76, 397-424.

Labischinski H., Barnickel G., Bradaczek H., Naumann D., Reitschel E.T. and Giesbrecht P. (1985) *J. Bacteriol.*, 162, 9-20.

Lakey J.H., Watts J.P. and Lea E.J.A. (1985) *Biochim. Biophys. Acta*, 817, 208-216.

Lakey J.H. and Pattus F. (1989) *Eur. J. Biochem.*, 186, 303-308.

Lakey J.H., Lea E.J.A. and Pattus F. (1991) *FEBS Letters*, 278, 31-34.

Lakshminarayanaiah N. (1984) Equations of Membrane Biophysics. Academic Press.

Lambert P.A. (1988) *J. Appl. Bacteriol. Symposium Suppl.*, 21s-34s.

Laüger P. (1980) *J. Memb. Biol.*, 57, 163-168.

Laüger P. (1984) *In* Stein W.D. (ed): Ion Channels: Molecular and Physiological Aspects. Academic Press, Florida. 309-326.

Laüger P. (1985) *Biophys. J.*, 47, 581-591.

Lee W.K. and Jordan P.C. (1984) *Biophys. J.*, 46, 805-819.

Levitt D.G. (1978) *Biophys. J.*, 22, 209-219.

Levitt D.G. (1982) *Biophys. J.*, 37, 575-585.

Levitt D.G. (1985) *Biophys. J.*, 48, 19-31.

Levitt D.G. (1986) *Ann. Rev. Biophys. Biophys. Chem.*, 15, 29-57.

Lugtenberg B., Meyers J., Peters R., Van der Hoek P. and Van Alphen L. (1975) *FEBS Letters*, 58, 254-258.

Lugtenberg B. (1981) *Trends. Biochem. Sci.*, 6, 262-266.

Lugtenberg B. and Van Alphen L. (1983) *Biochim. Biophys. Acta*, 737, 51-115.

Martinac B., Buechner M., Delcour A.H., Adler J. and Kung C. (1987) *Proc. Natl. Acad. Sci. USA.*, 84, 2297-2301.

Martinez G., Sancho M. and Fonseca V. (1992) *In* Allen M.J., Cleary S.J., Sauers A.E. and Shillady D.D. (eds): Charge and Field Effects in Biosystems -3. Birkhauser. 139-151

Mayer H., Bhat U., Masoud H., Radziejewska-Lebrecht J., Widemann C. and Krauss J. (1989) *Pure Appl. Chem.*, 61, 1271-1282.

Misra R. and Benson S.A. (1988) *J. Bacteriol.*, 170, 3611-3617.
Mizuno T., Chou M.Y. and Inouye M. (1983) *J. Biol. Chem.*, 258, 6932-6940.
Montal M. and Mueller P. (1972) *Proc. Natl. Acad. Sci. USA.*, 69, 3561-3566.
Morgan H., Lonsdale J.T. and Adler G. (1990) *Biochim. Biophys. Acta*, 1021, 175-181.
Moyer P., Marchese-Ragona S.P. and Christie B. (1993) *Adv. Scanning Probe Microscopy*, no 2, December 1993.
Mueller P., Rudin D.O., Tien H.T. and Westcott W.C. (1962) *Nature*, 194, 979-980.
Myers D.J. (1992) *BT Technol. J.*, 110, 141-148.
Nabedryk E., Garavito R.M. and Breton J. (1988) *Biophys. J.*, 53, 671-676.
Nakae T. (1976) *Biochem. Biophys. Res. Comm.*, 71, 877-889.
Nakae T., Ishii J. and Tokunagu M. (1979) *J. Biol. Chem.*, 254, 1457-1461.
Nakae T. (1986) *Crit. Rev. Microbiol.*, 1-62.
Nakamura K., Osterovsky D.N., Miyazawa T. and Mizushima S. (1974) *Biochim. Biophys. Acta*, 332, 329-335.
Neher E. and Sakmann B. (1976) *Nature*, 206, 779-802.
Nernst W. (1888) *z. Phys. Chem.*, 613-637.
Nikaido H. and Nakae T. (1979) *Adv. Microb. Physiol.*, 20, 163-250.
Nikaido H. and Rosenberg E.Y. (1983) *J. Bacteriol.*, 153, 241-252.
Nikaido H. and Wu H.C.P. (1984) *Proc. Natl. Acad. Sci. USA.*, 81, 1048-1052.
Nikaido H. and Vaara M. (1985) *Microbiol. Rev.*, 49, 1-32.
Nikaido H. (1992) *Molecular Microbiology*, 6, 435-442.
Niles W.D., Levis R.A. and Cohen F.S. (1988) *Biophys. J.*, 53, 327-335.
Palva E.T. (1979) *Eur. J. Biochem.*, 93, 495-503.
Parr T.R. Jr., Poole K., Crockford G.W.K. and Hancock R.E.W. (1986) *J. Bacteriol.*, 165, 523-526.
Partridge R.H. (1967) *Polym. Letters*, 5, 205-208.
Pauptit R.A., Schirmer T., Jansonius J.N., Rosenbush J.P., Parker M.W., Tucker A.D., Tsernoglou D., Weiss M.S. and Schulz G.E. (1991) *J. Struct. Biol.*, 107, 136-145.
Perskoff A. and Bers D.M. (1988) *Biophys. J.*, 53, 863-875.
Pethig R. (1987) University of Wales Review, Science and Technology 5.
Pullman A. and Etchebest C. (1983) *FEBS Letters*, 163, 199-202.
Reeves P. (1979) *In* Inouye M. (ed): Bacterial Outer Membranes, Biogenesis and Functions. John Wiley and Sons, NY. 256-291.
Roberts G.G. (1990) LB Films, Plenum Press, N.Y.
Rogers C.E. (1965) *In* Physics and Chemistry of the Organic Solid State. N.Y. Interscience, 510-635.

Rosenbusch J.P. (1974) *J. Biol. Chem.*, 249, 8019-8029.

Saint N., De Sylviane J.E., Orange N. and Molle G. (1993) *Biochim. Biophys. Acta*, 1145, 119-123.

Sancho M. and Martinez G. (1991) *Biophys. J.*, 60, 81-88.

Schindler H. (1980) *FEBS Letters*, 122, 77-79.

Schindler H. and Rosenbusch J.P. (1978) *Proc. Natl. Acad. Sci. USA.*, 75, 3751-3755.

Schindler H. and Rosenbusch J.P. (1981) *Proc. Natl. Acad. Sci. USA.*, 78, 2302-2306.

Schindler H. and Rosenbusch J.P. (1984) *FEBS Letters*, 173, 85-89.

Schnaitman C.A. (1974) *J. Bacteriol.*, 118,442-453.

Scotto A.W. and Zakim D. (1988) *J. Biol. Chem.*, 263, 18500-18506.

Sen K., Hellman J. and Nikaido H. (1988) *J. Biol. Chem.*, 263, 1182-1187.

Sigworth F.J. (1993) *Quarterly Reviews of Biophysics*, 27, 1-40.

Singleton P. and Sainsbury D. (1984) Introduction to Bacteria. Wiley and Sons, Ldn.

Smythe W.R. (1950) Static and Dynamic Electricity. McGraw-Hill, NY.

Stein W.D. (1986) Transport and Diffusion Across Cell Memranes, Academic Press.

Steven A.C., Ten Heggeler B., Müller R., Kistler J. and Rosenbusch J.P. (1977) *T. Cell. Biol.*, 72, 292-301.

Sugawara E. and Nikaido H. (1992) *J. Biol. Chem.*, 267, 2507-2511.

Thompson M., Krull U.J. and Bendell-Young L.I. (1983) *In* Seiyama T., Fucki K., Shiokawa J. and Susuki S. (eds): Proc. Int. Meeting on Chemical Sensors. Elsevier-Kodansha

Tien H.T. (1974) Bilayer Lipid Membranes (BLM) Theory and Practice. Marcel Dekker Inc., N.Y.

Tien H.T., Salamon Z., Kochev V., Ottova A. and Zviman M. (1989) *In* Hong F.T (ed): 'Molecular Electronics' Biosensors and Biocomputers. Plenum Press, NY. 259-268.

Todt J.C., Rocque W.J. and McGroarty E.J. (1992) *Biochem.*, 31, 10471-10478.

Todt J.C. and McGroarty E.J. (1992) *Biochem. Biophys. Res. Comm.*, 189,

Tommassen J. (1988) *In* Op den Kamp J.A.F. (ed): Membrane Biogenesis, NATO ASI series, 16, 351-373. Springer, Berlin, Heidelberg.

Tredgold R.H. and Hole P.N. (1976) *Biochim. Biophys. Acta*, 443, 137-142.

Unwin N. (1989) *Neuron*, 3, 665-676.

Urry D.W., Ventatachalam C.M., Spisni C.M., Laüger P. and Abu Khaled M. (1980) *Proc. Natl. Acad. Sci. USA.*, 77, 2028-2032.

Urry D.W., Prascad K.U. and Trapane T.L. (1982) *Proc. Natl. Acad. Sci. USA.*, 79, 390-394.

Ussing H.H. (1949) *Acta Physiol. Scand.*, 19, 43-56.

Vachon V., Laprade R. and Coulton J.W. (1986) *Biochim. Biophys. Acta*, 861, 74-82.

Van Alphen W. and Lugtenberg B. (1977) *J. Bacteriol.*, 131, 623-630.

Van der Ley P., Bekkers A., Van Meersbergen J. and Tommassen J. (1987) *Eur. J. Biochem.*, 164, 469-475.

Vogel H. and Jähnig F. (1986) *J. Molec. Biol.*, 190, 191-199.

Weiss M.S., Wacker T., Nestel U., Woitzik D., Weckesser J., Kreutz W., Welte W. and Schulz G.E. (1989) *FEBS Letters*, 256, 143-146.

Weiss M.S., Kreusch A., Schlitz E., Nestel U., Welte W, Weckesser J. and Schulz G.E. (1991) *FEBS Letters*, 280, 379-382.

White S.H. (1986) *In* Miller C. (ed): Ion Channel Reconstitiution. The Physical Nature of Planar Bilayer Membranes. Plenum Press. 3-32.

Xu G.Z., Shi B., McGroarty E.J. and Tien H.T. (1986) *Biochim. Biophys. Acta*, 57-64.

Young J.D.E., Blake M., Maura A. and Cohn Z. (1983) *Proc. Natl. Acad. Sci. USA.*, 80, 3831-3835.

APPENDIX A

DERIVATION OF GOLDMAN-HODGKIN-KATZ EQUATIONS

1 VOLTAGE EQUATION

1.1 Current carried by positive ions

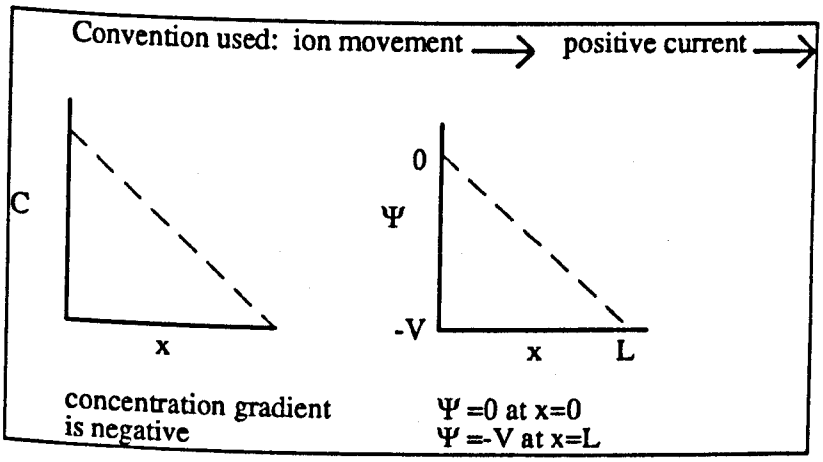

FIGURE 1 Conventions used in the derivation of the GHK equations

Using the Nernst-Planck differential equation for fluxes, the current carried by an ion depends on the concentration gradient and electric field. The equation for a positive ion is written as

$$J_+ = -zFD\left[\frac{dc}{dx} + \frac{Fzc}{RT}\frac{d\Psi}{dx}\right] \tag{1}$$

where z is the valence of the ion, F is Faraday's constant, R is the gas constant, T is the absolute temperature, c is the ion concentration and Ψ is the potential. By letting

$$\Psi_0 = \frac{RT}{Fz}$$

and multiplying both sides of equation (1) by

$$\exp\frac{\Psi}{\Psi_0}dx$$

equation (1) becomes

$$J_+ \exp\frac{\Psi}{\Psi_0} dx = -zFD\left[\exp\frac{\Psi}{\Psi_0} dc + \frac{c}{\Psi_0}\exp\frac{\Psi}{\Psi_0} d\Psi\right].$$

(2)

Noting that the terms in the square brackets of equation (2) are the differential of the product below

$$d\left[c\exp\frac{\Psi}{\Psi_0}\right]$$

and substituting the above into equation (2) results in

$$J_+ \exp\frac{\Psi}{\Psi_0} dx = -zFD\, d\left[c\exp\frac{\Psi}{\Psi_0}\right].$$

(3)

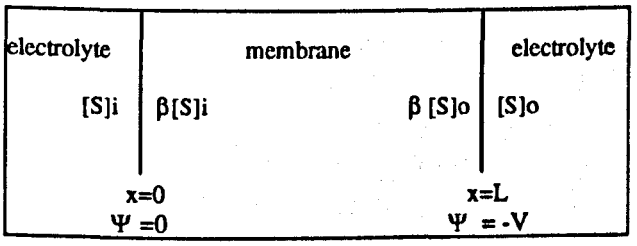

FIGURE 2 Boundary conditions. [S]i and [S]o are the ion concentrations on the two sides of the membrane and β is the electrolyte-membrane partition coefficient.

Equation (3) can now be integrated with the boundary conditions above to yield

$$J_+ \int_0^L \exp\frac{\Psi}{\Psi_0} dx = -zFD \int_{\beta[S]i,0}^{\beta[S]o,-\Psi} d\left[c\exp\frac{\Psi}{\Psi_0}\right].$$

(4)

Assuming that Ψ varies as -Vx/L i.e. is linear and substituting into equation (4) gives

$$J_+ \int_0^L \exp\frac{Vx}{L\Psi_0}\,dx = -zFD \int_{\beta[S]i,0}^{\beta[S]o,-V} d\left[c\exp\frac{V}{\Psi_0}\right].$$

(5)

Equation (5) can now be integrated and if limits are taken becomes

$$J_+\left(\frac{-L\Psi_o}{V}\right)\left(\exp\frac{-V}{\Psi_o}-1\right) = -zFD\beta\left[[S]o\exp\frac{-V}{\Psi_o}-[S]i\right]$$

(6)

which on rearrangement can be written as

$$J_+ = \frac{zFD\beta\Psi}{L\Psi_0}\left[\frac{[S]o\exp\frac{-V}{\Psi_o}-[S]i}{\exp\frac{-V}{\Psi_o}-1}\right].$$

(7)

The membrane permeability to the cation, P_+, is given by $D_+\beta/L$ and remembering that $\Psi_0=RT/Fz$ we can write the current density due to positive ion movement as

$$J_+ = \frac{z^2F^2P_+V}{RT}\left[\frac{[S]o\exp\frac{-zFV}{RT}-[S]i}{\exp\frac{-zFV}{RT}-1}\right].$$

(8)

1.2 Current carried by negative ions.

The starting point for negative ions is

$$J_- = zFD\left[\frac{dc}{dx}-\frac{Fzc}{RT}\frac{d\Psi}{dx}\right]$$

which if integrated using the boundary conditions as for positive ions becomes

$$J_{-} = \frac{z^2F^2P_{-}V}{RT}\left[\frac{[S]o\exp\frac{+zFV}{RT} - [S]i}{\exp\frac{+zFV}{RT} - 1}\right]. \tag{9}$$

Multiplying the numerator and denominator of equation (9) by exp(-zFV/RT) gives

$$J_{-} = \frac{z^2F^2P_{-}V}{RT}\left[\frac{[S]o - [S]i\exp\frac{-zFV}{RT}}{1 - \exp\frac{-zFV}{RT}}\right]. \tag{10}$$

When the zero-current potential is applied the sum of the two currents is zero i.e. $J_+ + J_-=0$. If the two ion species are K^+ and Cl^- the resulting equation is

$$0 = \frac{JRT}{z^2F^2V} = P_K\left[[K^+]_o\exp(-V) - [K]_i\right] - P_{Cl}\left[[Cl]_o - [Cl]_i\exp(-V)\right]$$

which can be rearranged to give the familiar GHK voltage equation as shown below

$$\exp\frac{zFV}{RT} = \frac{P_K[K]_o + P_{Cl}[Cl]_i}{P_K[K]_i + P_{Cl}[Cl]_o} \tag{11}$$

where P_K and P_{Cl} are the permeabilities of the potassium and chloride ions respectively and $[K]_o$, $[K]_i$ and $[Cl]_o$, $[Cl]_i$ are the ion concentrations on the two sides of the membrane.

2 CURRENT EQUATIONS

The current equations in (8) and (10) can be considered to be made up of two independent fluxes as shown below.

$$\vec{J}_+ = \frac{z^2F^2P_+V}{RT}\left[\frac{[S]i}{1-\exp\frac{-zFV}{RT}}\right]$$

$$\overleftarrow{J}_+ = \frac{z^2F^2P_+V}{RT}\left[\frac{[S]_o}{1-\exp\frac{+zFV}{RT}}\right]$$

$$\vec{J}_- = \frac{z^2F^2P_-V}{RT}\left[\frac{[S]i}{1-\exp\frac{+zFV}{RT}}\right]$$

$$\overleftarrow{J}_- = \frac{z^2F^2P_-V}{RT}\left[\frac{[S]_o}{1-\exp\frac{-zFV}{RT}}\right]$$

For V>>0 positive current approximates to

$$\vec{J}_+ + \overleftarrow{J} = \frac{z^2F^2P_+V}{RT}[S]i_- + \frac{z^2F^2P_-V}{RT}[S]_o$$

and for V<<0 negative current approximates to

$$\overleftarrow{J}_+ + \vec{J}_- = \frac{z^2F^2P_+V}{RT}[S]_o + \frac{z^2F^2P_-V}{RT}[S]_i.$$

If we let $z^2F^2V/RT=K$ then for V>>0

$$\vec{J}_{total} = K\left(P_+[S]_i + P_-[S]_o\right)$$

and for V<<0

$$\overleftarrow{J}_{total} = K\left(P_+[S]_o + P_-[S]_i\right)$$

APPENDIX B

ABBREVIATIONS FOR AMINO ACIDS

Amino Acid	Abbreviation	
	Single letter	Three letter
Alanine	A	Ala
Aspartic acid	D	Asp
Glutamic acid	E	Glu
Phenylalanine	F	Phe
Glycine	G	Gly
Histidine	H	His
Isoleucine	I	Ile
Lysine	K	Lys
Leucine	L	Leu
Methionine	M	Met
Asparagine	N	Asn
Proline	P	Pro
Glutamine	Q	Gln
Arginine	R	Arg
Serine	S	Ser
Threonine	T	Thr
Valine	V	Val
Tryptophan	W	Trp
Tyrosine	Y	Tyr